

**INTEGRATED SURFACE WATER –
GROUNDWATER MODELLING
LINKING SURFACE WATER AND GROUNDWATER
USING DIVAST-SG**

By Tim Sparks

**A thesis submitted to Cardiff University as
partial fulfilment of the requirements for a PhD**



**NATURAL
ENVIRONMENT
RESEARCH COUNCIL**

UMI Number: U585006

All rights reserved

INFORMATION TO ALL USERS

The quality of this reproduction is dependent upon the quality of the copy submitted.

In the unlikely event that the author did not send a complete manuscript and there are missing pages, these will be noted. Also, if material had to be removed, a note will indicate the deletion.



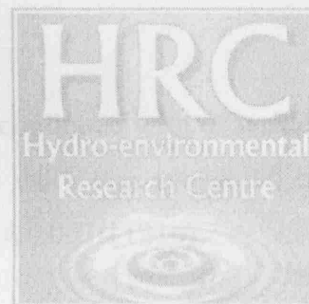
UMI U585006

Published by ProQuest LLC 2013. Copyright in the Dissertation held by the Author.
Microform Edition © ProQuest LLC.

All rights reserved. This work is protected against
unauthorized copying under Title 17, United States Code.



ProQuest LLC
789 East Eisenhower Parkway
P.O. Box 1346
Ann Arbor, MI 48106-1346



DECLARATION

This work has not previously been accepted in substance for any degree and is not concurrently submitted in candidature for any degree.

Signed.....*T D Sparks*..... (candidate)

Date: ..*2/2/08*.....

STATEMENT 1

This thesis is being submitted in partial fulfilment of the requirements for the degree of PhD.

Signed.....*T D Sparks*..... (candidate)

Date: ..*2/2/08*.....

STATEMENT 2

This thesis is the result of my own independent work/investigation, except where otherwise stated. Other sources are acknowledged by explicit references.

Signed.....*T D Sparks*..... (candidate)

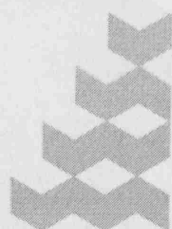
Date: ..*2/2/08*.....

STATEMENT 3

I hereby give consent for my thesis, if accepted, to be available for photocopying and for inter-library loan, and for the title and summary to be made available to outside organisations.

Signed.....*T D Sparks*..... (candidate)

Date: ..*2/2/08*.....



**NATURAL
ENVIRONMENT
RESEARCH COUNCIL**

ACKNOWLEDGEMENTS

This thesis, like all others I know of, would not have been started, continued with or written; let alone finished, without the help of a large number of people. The work was sponsored by the Natural Environment Research Council (NERC studentship NER/S/A/2003/11216).

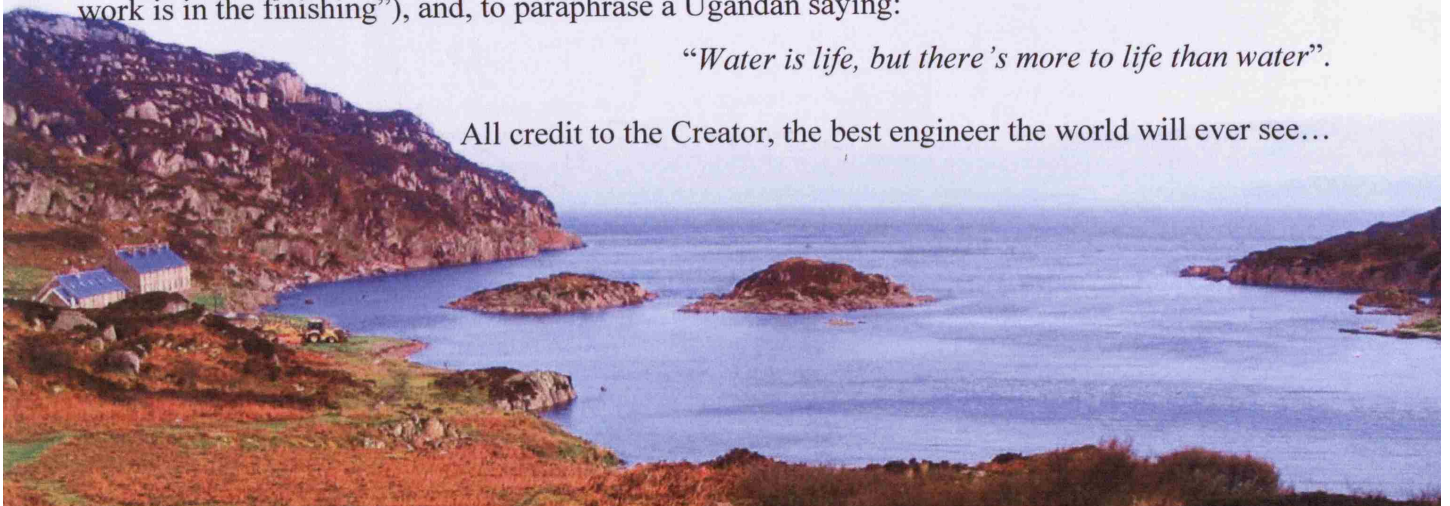
Firstly, my thanks go to my supervisors **Dr. Bettina Bockelmann**, and **Professor Roger Falconer**, without whose support and work this thesis would never have reached its finished state. A number of other colleagues' help was invaluable along the way: **Dr. Ingo Schnauder** for continual encouragement and help with measuring the properties of the foam, **Katerina Spanoudaki** (NTUA, Greece) and **Diana Kountcheva** for help with the initial experimental work, **Florian Schaeffer**, **Anthony Osei-Twumasi**, and **Fathia Abdulgawad** assisted in the subsequent experimental work and **Dr. Masoud Namin** helped with the initial ideas for the new numerical scheme; my sincere thanks go to all of them.

On technical matters in the laboratory, the help of **Paul Leach** was absolutely indispensable. **Chris Joseph**, **Rami Malki**, **Reza Ahmadian**, **Mofazzal Syed**, **Pat Xavier**, **Ingo Schnauder**, **Koji Kawasaki** and **William Rauen** all helped me through the days at work when it seemed like the project would never end – many thanks! Proof-reading was heroically performed under a tight schedule by my supervisors. **Bill and Rachel Taylor-Beales** are semi-responsible for my decision to start the PhD, and together with **Dai and Michelle Hankey**, and **Chris and Rhian Horn**, have suffered the inevitable consequences – many thanks for your support and prayers. **Dot Stewart**, **Jenny Howard** and **Isabel Hands** from the Camas Centre (see below) carried my computer over the Sound of Iona to the hut where I write this, and allowed me time off to finish the last bits of the thesis – many thanks! My **mum (Cilla)**, **dad (Steve)** and **twin brother (Ben)**, and **Sarah Fry** have all been a great support over this time; without their love and encouragement this would never have been written – thanks for putting up with me!

Lastly, in the words of a debatable school motto: "*Finis Opus Coronat*" ("The crowning of the work is in the finishing"), and, to paraphrase a Ugandan saying:

"Water is life, but there's more to life than water".

All credit to the Creator, the best engineer the world will ever see...



SUMMARY OF THESIS

Surface-water and groundwater are two resources both requiring careful management and protection. Computer modelling of both has long been used as an aid to their management. Historically they have been modelled separately, as their behaviour is represented by different mathematical equations. However, in reality, they are a linked resource; each affects the other.

DIVAST is a two-dimensional hydrodynamic and water quality numerical model developed for estuarine and coastal modelling. The original model enables the simulation of problems such as pollution and flooding in surface waters. In this study the existing model is extended to allow the modelling of groundwater as well as surface water in the same model.

Chapters 1-5 introduce the problem, review some existing models, and then derive, discretise, and implement the equations for surface water and groundwater flow into the new model. Chapters 6-10 test the new model against analytical solutions, laboratory data, field data, and an existing groundwater model (MODFLOW).

The outcome is a new version of the DIVAST model, known as DIVAST-SG (Depth Integrated Velocities And Solute Transport in Surface water and Groundwater). It simulates interactions between two-dimensional surface water and groundwater, in addition to the facilities of the original code. The equations are solved within one model, avoiding coupling problems. It is successfully tested against analytical solutions, laboratory studies and field data, and compared to an existing groundwater code, where it successfully models a gravel aquifer adjacent to tidal surface water. A framework is laid for continuing this work to produce a pseudo 3-D surface-water / groundwater code. In addition, novel techniques are pioneered in the laboratory, where open cell foam is used in a tidal flume to represent a porous aquifer adjacent to a river, and a highly detailed dataset of groundwater field data is compiled in the course of the work.

Integrated Surface Water – Groundwater Modelling

Linking Surface Water and Groundwater using DIVAST-SG

CONTENTS

CHAPTER 1	Introduction	9
1.1	Introduction	9
1.2	Hydrodynamic modelling.....	11
1.3	Aims and Objectives.....	12
1.4	Outline of Thesis	12
CHAPTER 2	Review of Existing Models	14
2.1	Review of Existing Models	14
2.1.1	Field Data on Bank Storage and River-Aquifer interactions.....	32
2.2	Summary of existing models and studies.....	33
CHAPTER 3	Governing Model Equations.....	35
3.1	Introduction	35
3.2	Conservation of Mass – Surface Water.....	35
3.2.1	Groundwater term in Surface Water equations.	39
3.3	Conservation of Mass - Groundwater.....	40
3.3.1	Unconfined Aquifer	40
3.3.2	Confined Aquifer	42
3.4	Calculating Seepage Terms	43
3.4.1	Surface Water to Groundwater.....	44
3.4.2	Groundwater to Groundwater.....	45
3.4.3	Summary	47
3.5	Conservation of Momentum – Surface Water	47
3.6	Conservation of Momentum – Groundwater – Darcy's Law	50
3.6.1	Unconfined Aquifer	50
3.6.2	Confined Aquifer	52
3.7	Summary	54
CHAPTER 4	Finite Difference Scheme and Equation Discretisation.....	55
4.1	Model Overview.....	55
4.2	Equation Discretisation	56
4.2.1	Mass Conservation Equations	59
4.2.2	Momentum Conservation.....	61
4.2.3	Recurrence Relationships.....	69
4.3	Iteration of seepage terms.....	70
4.4	Summary	72
CHAPTER 5	Model Implementation.....	73
5.1	Introduction	73
5.2	Modifications to existing 2-D Model.....	73
5.2.1	Sequential running of input files	73
5.2.2	Hot-start	74
5.2.3	Point Data collection	74

5.2.4	Outfall Discharge Variation	74
5.2.5	Defining boundary conditions velocity/flow and elevation.....	74
5.2.6	Defined new coefficients to allow inclusion of groundwater.....	74
5.3	<i>Input file</i>	74
5.3.1	General Variables.....	75
5.3.2	Hotstart Info	75
5.3.3	Point Data Collections.....	75
5.3.4	Open Boundary Conditions.....	75
5.3.5	Model Data.....	77
5.3.6	Outfalls and Solute Prediction.....	77
5.3.7	Tidal Boundary Data.....	79
5.3.8	Velocity or Flow Boundary.....	79
5.3.9	Layer Domain Specification.....	80
5.3.10	Elevation Data for surface and Groundwater Layers	80
5.3.11	Aquifer Data.....	81
5.4	<i>Code Structure</i>	82
5.5	<i>Modifying to include Groundwater equations</i>	85
5.5.1	INITL subroutine	85
5.5.2	HYDMOD subroutines	87
5.6	<i>Hotstart Model</i>	88
5.7	<i>Summary</i>	90
CHAPTER 6	Analytical Verification	91
6.1	<i>Introduction</i>	91
6.2	<i>Derivation of the equation</i>	92
6.3	<i>Evaluating the Equations</i>	96
6.4	<i>Comparison with DIVAST-SG</i>	99
6.4.1	Scenario 1.....	99
6.4.2	Scenario 2.....	102
6.5	<i>Summary of Analytical Verification</i>	104
CHAPTER 7	Laboratory Validation	105
7.1	<i>Introduction</i>	105
7.2	<i>Flume Design and Construction</i>	105
7.3	<i>Testing the properties of the Foam</i>	109
7.3.1	Permeability Testing	109
7.3.2	Constant Head Test (pre-construction).....	109
7.3.3	In Situ Permeability Test (post-construction).....	112
7.3.4	Porosity	116
7.4	<i>Initial Experimental Work</i>	118
7.4.1	Choice of Tracer.....	118
7.4.2	Flume construction.....	118
7.4.3	Instruments.....	120
7.4.4	Experiments.....	120
7.4.5	Numerical Modelling	121
7.4.6	Discussion	121
7.4.7	Problems and Solutions.....	123
7.5	<i>Adapting the Flume</i>	125
7.6	<i>New flume setup</i>	127
7.7	<i>Water Level Measurements and Modelling</i>	128
7.7.1	Collecting the data.....	128
7.7.2	Setting up the model.....	131
7.7.3	Adjusting the model	132
7.7.4	Dicussion of Water Level Experiments.....	137

7.8	<i>Tracer Experiments</i>	140
7.8.1	Experimental Set-up.....	140
7.8.2	Model set-up.....	143
7.8.3	Exit point of tracer from foam.....	143
7.8.4	Fluorometer Data	156
7.8.5	Discussion of Tracer Experiments	158
7.9	<i>Summary of Laboratory Validation</i>	160
CHAPTER 8	Visual MODFLOW – Modelling Cardiff Bay	162
8.1	<i>Cardiff Bay Background and Geology</i>	162
8.2	<i>Preparing the Data</i>	163
8.3	<i>Modelling Groundwater Levels in Cardiff Bay using Visual MODFLOW</i>	167
8.3.1	Visual MODFLOW.....	167
8.3.2	Premodelling using DIVAST	167
8.3.3	Setting up Visual MODFLOW.....	171
8.4	<i>Results</i>	177
8.4.1	Model Run 1.....	179
8.4.2	Manual Calibration.....	179
8.5	<i>PEST</i>	181
8.5.1	PEST Run.....	181
8.5.2	Comparison	184
8.5.3	PEST run with confining layer.....	186
8.6	<i>Discussion</i>	189
8.6.1	Estimated Parameters	189
8.6.2	Comparing the model with field data	191
8.7	<i>Summary</i>	194
CHAPTER 9	DIVAST-SG - Modelling Cardiff Bay	196
9.1	<i>Introduction</i>	196
9.2	<i>Creating the input file</i>	196
9.2.1	Surface elevations	198
9.2.2	Subsurface Elevations	199
9.2.3	Boreholes	199
9.2.4	Boundary Conditions	199
9.2.5	Inactive cells at north of domain.	200
9.3	<i>Running the model</i>	203
9.3.1	Initial Conditions.....	203
9.4	<i>Parameter estimation</i>	204
9.4.1	Initial Run	205
9.4.2	R ² value.....	207
9.4.3	Average Error.....	212
9.4.4	Optimum parameters	216
9.5	<i>Summary</i>	222
CHAPTER 10	Discussion and Conclusions	223
10.1	<i>Introduction</i>	223
10.2	<i>Analytical Validation</i>	223
10.3	<i>Laboratory Verification</i>	224
10.3.1	Water Level Experiments.....	224
10.3.2	Tracer Experiments	225
10.4	<i>Modelling of Cardiff Bay</i>	227
10.4.1	MODFLOW modelling.....	228
10.4.2	DIVAST-SG modelling.....	228
10.4.3	Comparison	230

10.5	<i>Further Work</i>	231
10.5.1	3-D layered model.....	231
10.5.2	Laboratory Foam	233
10.5.3	3-D Visualisation	233
10.5.4	Further Analytical Verification	233
10.5.5	Unsaturated Flow, Seepage Faces and Recharge	233
10.5.6	Solute Transport in Groundwater	234
10.5.7	Grid size and timestep.....	234
10.5.8	Visual Interface	234
10.6	<i>Conclusion</i>	236
References	237	
Index Of Figures	241	
Index of Tables	246	
APPENDIX A Sample Input Files	247	
APPENDIX B Detailed Discretisations	264	
APPENDIX C Individual Borehole Plots	267	
APPENDIX D Appendix CD	268	

CHAPTER 1 INTRODUCTION

1.1 Introduction

Surface Water and Groundwater - two different resources, but both require careful management and protection. Computer modelling of both resources has long been used as an aid to the management of water resources. Historically groundwater and surface water have been modelled separately, as their behaviour is represented by different mathematical equations. However, they are a linked resource; one depends on and impacts on the other.

Groundwater provides a third of our drinking water in the UK, and in some areas of southern England up to 80% of drinking water comes from groundwater resources. Usually it requires little or no treatment before it is drinkable. However, if contaminated, these resources are expensive and difficult to restore, so groundwater needs to be protected. Surface water in rivers, lakes, estuaries and coastal systems is more visibly abundant but no less important – its behaviour affects our everyday lives through flooding, leisure activities, transport, drinking water etc. These two resources are integral; the baseflow in streams and rivers comes from the contributing groundwater; agricultural chemicals may seep into groundwater, which subsequently may flow into streams. Accurate modelling of surface water should recognise that groundwater plays a significant part in how surface waters behave (Figure 1.1). This research project aims to provide a modelling tool that allows simultaneous modelling of groundwater adjacent to surface water.

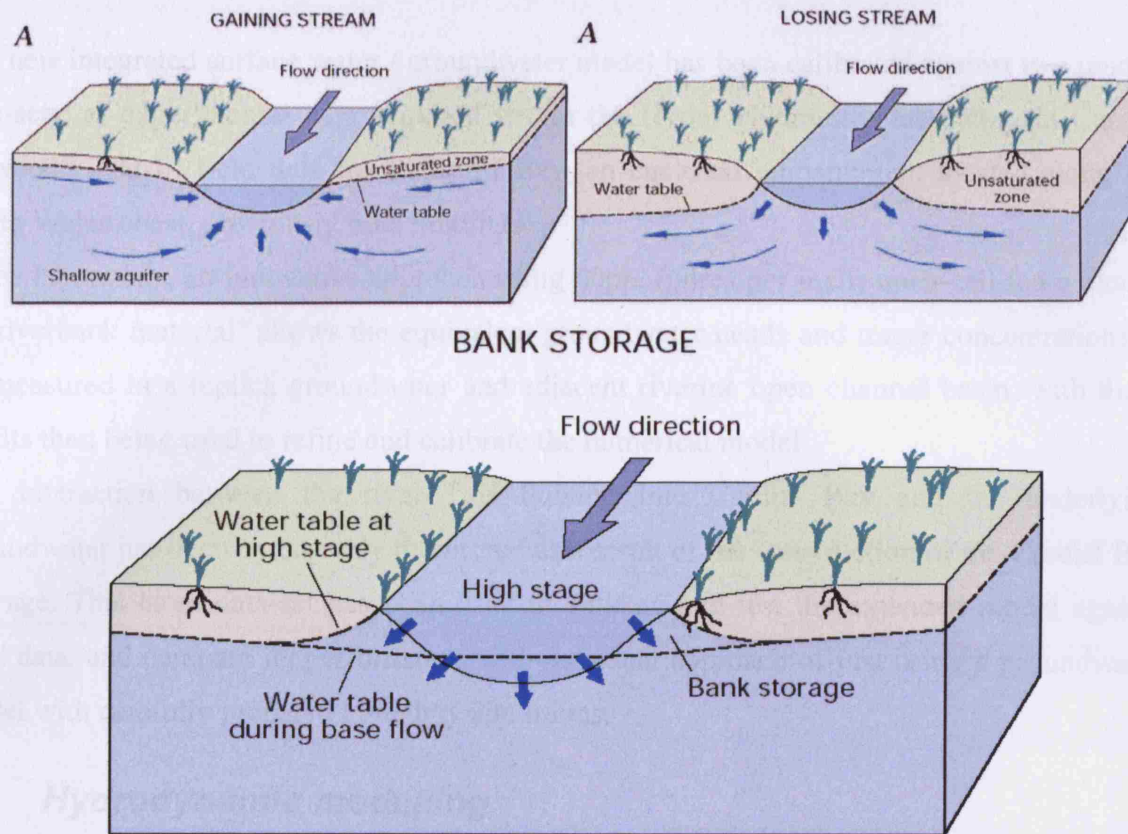


Figure 1.1: - Gaining and Losing streams, and illustration of bank storage. (from Winter et al 1998)

DIVAST (Depth Integrated Velocities And Solute Transport) is a two-dimensional hydrodynamic and water quality numerical model which has been developed for estuarine and coastal modelling by researchers at Cardiff University. The original model simulates two-dimensional distributions of surface water currents, elevations and various water quality parameters as functions of time thereby enabling the prediction and simulation of such water management issues as pollution and flooding in surface waters. In this study the existing model will be extended to allow for the modelling of groundwater as well as surface water in the same model. This can provide a valuable decision support tool for predicting how contaminated groundwater will affect surface water resources such as estuaries, rivers and lakes, and vice-versa, and to include the groundwater flow in flooding simulations.

Extending a surface water model to include groundwater allows the river and the water in the ground it flows over to be modelled simultaneously. This is more suited to the 'integrated river basin management' approach stipulated in the new EU Water Framework Directive (EC 2000), which requires that rivers are now managed as a whole river basin, rather than dividing up a watershed into territorial boundaries.

The new integrated surface water / groundwater model has been calibrated against two unique data-sets: a) experimental data acquired within the Hyder Hydraulics laboratory at Cardiff University and b) field data from Cardiff Bay, an enclosed embankment located along the South Wales coast, previously tidal mudflats.

In the laboratory, an innovative approach using 60ppi (pores per inch) open-cell foam blocks as ‘riverbank material’ allows the equivalent groundwater heads and tracer concentrations to be measured in a replica groundwater and adjacent riverine open channel basin, with these results then being used to refine and calibrate the numerical model.

The interaction between the river Taff flowing into Cardiff Bay and the underlying groundwater has been extensively monitored as a result of the construction of the Cardiff Bay Barrage. This large data-set has been used to validate and test the extended model against field data, and compare its performance with the usual approach of just using a groundwater model with carefully prepared boundary conditions.

1.2 *Hydrodynamic modelling*

Traditionally hydrodynamic modelling has generally concentrated on specific problems, for instance a dam break scenario, flooding of a lowland river, or groundwater pollution of an abstraction zone. This type of modelling requires specific, accurate models of a particular hydrological/hydraulic regime, e.g. 1-D modelling of surface water channels, 3-D modelling of air-water interaction, 3-D groundwater simulation, or 2-D estuarine modelling etc. However, hydrologists are increasingly finding that many water resources problems cannot be addressed by such specific models. Increasingly, there is an interest in combining several models together and modelling at a whole system level.

Environmental awareness has increased enormously in the past few decades, together with a realisation that the planet (and its water) must be treated as a whole, rather than as discrete systems. Pollution of groundwater will certainly influence surface water resources, and vice versa. Flooded rivers are almost certainly influenced by the surrounding groundwater regime, and also by rainfall-runoff characteristics often some distance from the flooding zone. European legislation is reflecting this in its holistic ‘catchment’ approach to river management, aimed at managing a river basin as a whole, rather than in sections. In order to model these situations, modellers must combine the existing methods of modelling each regime separately into integrated hydrological models.

1.3 Aims and Objectives

From the review of models in Chapter 2 it is clear that integrating surface water and groundwater modelling is an important part of hydrodynamic modelling. There are many different models that attempt to include this interaction, but the non-commercial codes are mostly limited to 1-D surface water. There are very few 2-D surface water codes that allow simultaneous modelling of groundwater. The objectives of this research were to extend the existing non-commercial surface water model DIVAST, to simultaneously model groundwater. The model is a 2-D model, thus it can be used for modelling complex surface water situations such as those occurring in large rivers and estuaries – the addition of a groundwater modelling option would be a valuable addition to the model's capabilities. If possible, the model should be self-contained, i.e. not consist of a separate groundwater and surface water model, but an integrated code that can move from groundwater to surface water easily. The model is not needed to be a stand-alone groundwater model, rather an extended surface water model that could model bank-storage and solute transport from groundwater to surface water. Thus problems like local flooding caused by bank-storage release, and diffuse source pollution from adjacent groundwater, can be simulated in one integrated model. For example, in Cardiff Bay, when a barrage across the mouth of the estuary (that would create a large freshwater lagoon and significantly raise the mean water level) was proposed, there were concerns that the rise in surface water elevations would create groundwater flooding problems. A joint surface water-groundwater model would have been ideal for the modelling of this situation. The aim of this study is to take DIVAST and take it closer to this holistic integrated ideal.

1.4 Outline of Thesis

The first part of this thesis (Chapters 2, 3, 4 and 5) outlines the development of the model itself. Chapter 2 is devoted to a review of the existing models in the public domain that deal with surface water and groundwater and summarises the state of the integrated modelling problem. Chapter 3 then derives the governing model equations for 2-D surface water flow and 2-D subsurface flow. Equations describing seepage between model layers are also described here, allowing the model to be taken to a pseudo 3-D level. Chapter 4 takes these equations and applies them to the specific finite difference scheme used in the model by discretising them in time and space. An overview of how the model solves the equations is included here. Chapter 5 deals with specific adaptations to the existing DIVAST model and how the input file is used to define the problem being modelled.

The remainder of the thesis (Chapters 6, 7, 8 and 9) tests this extended numerical model against various challenges. Chapter 6 then tests the model against an analytical solution to a groundwater wave induced by surface water variation. Chapter 7 details the construction of a laboratory scale tidal flume in Cardiff University, and how this was used to simulate the interaction of surface water and groundwater. The new model is set-up and then compared to the experimental results. Chapters 8 and 9 describe extensive field data collected in Cardiff Bay before the impoundment of the bay in 1999 – a brief history of this is given in Chapter 8. Chapter 8 then takes this data and sets-up a MODFLOW model of the area and compares the model results to the field data. Chapter 9 details how the new DIVAST-SG model is set-up for the same area and the model results are again compared to the field data and the MODFLOW model. Detailed discussions of results from each test are included in each chapter.

Chapter 10 then discusses more broadly all the different aspects of the thesis in turn and draws conclusions based on the work, and suggests further work that could be carried out using the model and data collected. The appendices contain example input files for the model and the full source code for the model itself (on the CD). Also included are additional detailed discretisations unnecessary in the main text, and additional borehole plots from Cardiff Bay for completeness. The appendix CD contains the full source code, several spreadsheets used in the analysis, a number of animations of model results that clarify points made in the text and other relevant items. Where an item on the Appendix CD is relevant a footnote gives the location on the CD.

CHAPTER 2 REVIEW OF EXISTING MODELS

2.1 Review of Existing Models

Since the first half of this century, both open channel and groundwater flow have been considered for solution by numerical methods. Where the two ‘zones’ meet, the problem was usually approached by calculating the response of the groundwater system to changes in the river elevation (Cooper and Rorabaugh 1963; Pinder and Sauer 1971) (Figure 2.1). Cooper and Rorabaugh (1963) derived an analytical solution for the changes in groundwater heads, groundwater flow and bank storage that occurred as the result of a flood-wave stage oscillation. These analyses assumed that the stream elevation changes only as a function of time and that horizontal groundwater flow occurred only normal to the stream. Pinder and Sauer (1971) pointed out the limitations in this approach and described a more complex modelling approach to simulating flood wave modification due to bank storage effects. This model used one-dimensional unsteady channel flow to describe the stream elevation, and a two-dimensional groundwater model to describe the aquifer flow. Darcy’s law was used to couple the two models in an iterative manner. Since the two zones were treated separately, the model was capable of calculating flow underneath the river. Pinder and Sauer used the model to simulate a flood wave travelling down an extensive river reach (130,000 feet), and showed that bank storage played a significant role, but was largely dependent on the properties of the aquifer (conductivity, porosity etc).

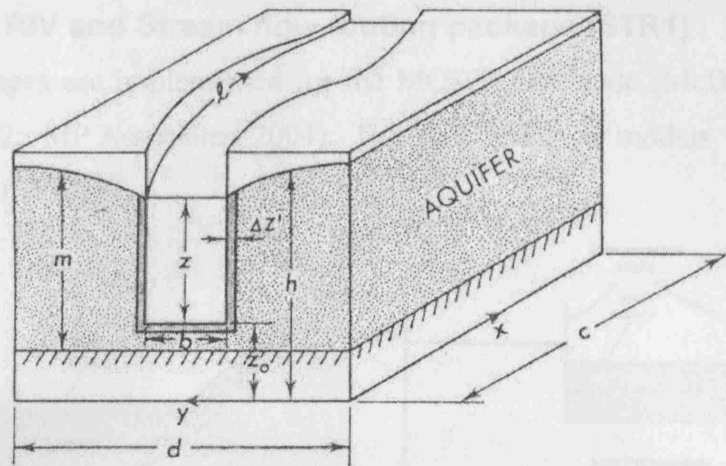


Figure 2.1 – Pinder and Sauer (1971) model of aquifer-stream interaction.

Smith and Woolhiser (1971) developed a model describing infiltration and overland flow based on the soil moisture properties. Freeze (1972) took this approach a stage further and described numerical solutions to the coupled boundary problems representing 3-D, transient, saturated-unsaturated subsurface flow, and 1-D, gradually varied, unsteady channel flow. The entry velocity of the subsurface flow was assumed to be negligible compared to the stream velocity. Outflow from the subsurface to the stream via baseflow was obtained either for a constant or fluctuating head boundary. Seepage from the stream bank (above the stream elevation) was from a freely fluctuating seepage face. This model allowed rainfall events to be predicted, together with their effects on a stream via the baseflow input.

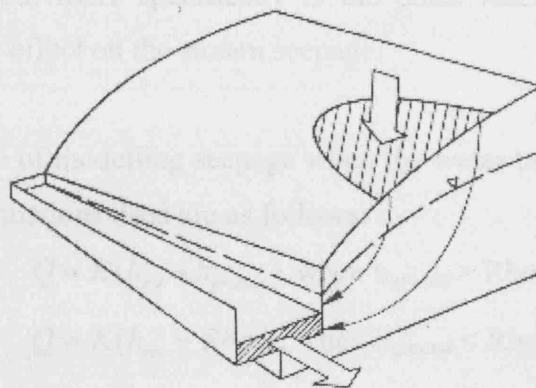


Figure 2.2 – Freeze model. “A 3-D, saturated-unsaturated subsurface flow system with rainfall input, which delivers base flow to a one-dimensional stream channel.” (Freeze 1972)

River package RIV and Stream flow routing package (STR1)

Both these packages are implemented for the MODFLOW code (McDonald and Harbaugh 1988; EMS 2002; MP Associates 2004). The RIV package models basic stream-aquifer interaction in MODFLOW.

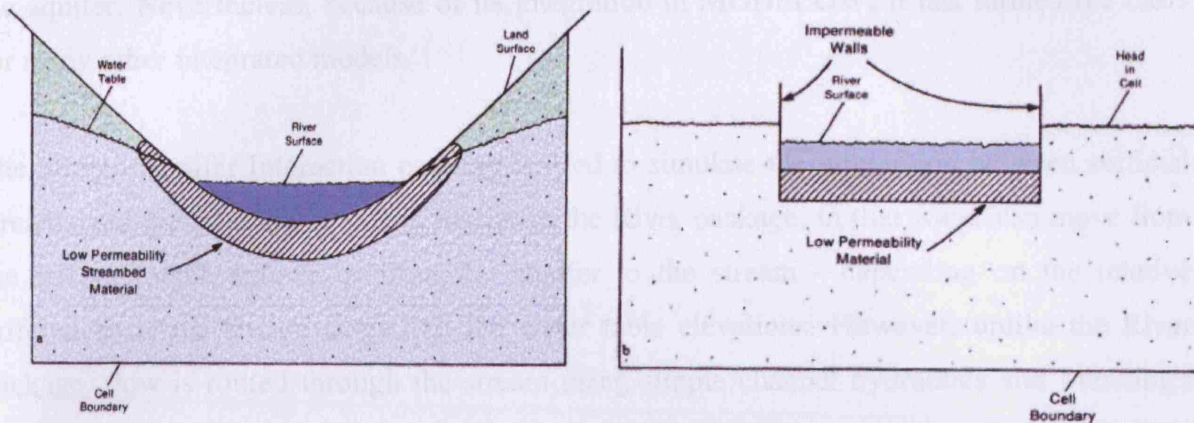


Figure 2.3: - a) Cross-section of an aquifer containing a stream, and b) conceptual representation. (McDonald and Harbaugh 1988)

Figure 2.3 shows the basic situation that the river package deals with, and also the conceptual representation that the program uses to solve the problem. The river is divided into reaches; in which the reaches are contained within each grid cell, so there is a reach for each model cell. Three parameters are defined for each reach, the river stage, the conductance of the stream-aquifer interconnection, and the level at which the 'limiting value of stream seepage' is obtained. This limiting value is usually the base of the low permeability material in the streambed (if present), but more specifically is the point where a further decline in the groundwater level has no effect on the stream seepage.

The simulation is capable of modelling seepage when the water table drops below the base of the riverbed. The basic equations used are as follows:

$$Q = K(h_{riv} - h_{ground}) \text{ when } h_{ground} > R_{bot}$$

$$Q = K(h_{riv} - R_{bot}), \text{ when } h_{ground} < R_{bot}$$

Where Q is the seepage rate from the river to the aquifer, K is a conductance value for the river-aquifer interconnection, h_{riv} is the stage in the river, h_{ground} is the head in the groundwater and R_{bot} is the base of the river bed, or the limiting elevation beyond which further decline of the water table has no effect on the seepage rate.

This simplified model used takes no account of where the river reach is in the cell, and assumes that the water level in the reach is uniform and constant for each stress period. These

assumptions are valid so long as the conditions of flow do not vary significantly along the reach and the flow is near steady; events such as flooding, drying or surges cannot therefore be modelled accurately. This is less of an integrated surface water-groundwater package, and more a river seepage package, as it does not model the surface water directly, just seepage to the aquifer. Nevertheless, because of its integration in MODFLOW, it has formed the basis for many other integrated models.

The Stream/Aquifer Interaction package is used to simulate the interaction between surficial streams and the groundwater. It is similar to the River package, in that water can move from the stream to the aquifer or from the aquifer to the stream - depending on the relative differences in the stream stage and the water table elevations. However, unlike the River package, flow is routed through the stream using simple channel hydraulics and Manning's equation is used to compute the stage in the stream. (EMS 2002)

The Stream Package (STR1) permits representation of intermittent streams in MODFLOW. It is especially useful in systems in the headwaters of small streams. The program limits the amount of ground-water recharge to the available streamflow. It permits two or more streams to merge into one, with flow in the merged stream equal to the sum of the tributary flows. The program also permits diversions from streams. (MP Associates 2004)

MODBRANCH (Swain and Wexler 1996)

This coupled code combines two USGS models, namely BRANCH and MODFLOW. Branch is a one-dimensional numerical model commonly used to simulate unsteady flow in open-channel networks. The coupled code basically replaces the old river package (known as RIV) in MODFLOW with an adapted version of the BRANCH code.

A common problem faced when integrating surface water and groundwater in modelling systems is that of timescale. The timestep used for the simulation of surface water is usually of the order of seconds, minutes or hours, but groundwater is generally modelled in hours, days, months or years. In MODBRANCH, multiple steps of the surface water code are carried out for each timestep in the groundwater code. Leakage terms calculated from the surface water are interpolated linearly to estimate the aquifer head in between each groundwater timestep; this maintains the mass balance between the two models. The average leakage for the surface water steps is then used as the leakage in the groundwater step. The resulting new

groundwater heads are then fed back into the surface water code and the process is repeated until the heads from the surface and groundwater code converge. The river is divided into reaches, as in the River package, and no reach can span an aquifer model cell. Multiple reaches can occur within a cell, but leakage from any reach in a cell is considered to occur at the centre of the aquifer cell. Cross-sections are defined at each node (i.e. the end of a reach). The original Branch model had no leakage term in the equations, so leakage terms were added. These follow a similar fashion to those described above in the original River (RIV) package. The surface water equations are solved using a finite difference method, with the leakage terms passing to the finite difference groundwater equations in MODFLOW.

Drying of river channels is allowed for in the coupled model. The momentum equation in the finite difference form contains a cross-sectional area term in the denominator of many terms, making the equation unstable for small flow areas. This leads to instability at low or dry flows. To get round this problem, when a river dries out a small flow is retained in the channel and the frictional resistance is increased to allow as little discharge as possible. All leakage to the aquifer is eliminated. Flow continuity is retained by this scheme, and re-wetting is easily accomplished by raising the stage again. The cross-section of the river is altered to provide a small area below the actual river bed where this 'retaining' flow can occur. This procedure is similar in concept to the Priessman Slot technique (which allows pressurised pipe flow to be modelled by free-surface equations by the inclusion of a hypothetical 'slot' at the top of a pipe) (Butler and Davies 2000) but should not be confused with it as in this model the slot is simply a storage tool to allow the river to re-wet without breaking flow continuity. The friction is varied gradually with time as the channel wets and dries to avoid jumps in stage.

A steady-state option was added to the Branch model to allow steady-state modelling of aquifers. This was done by removing the time dependent terms in the continuity and momentum equations (effectively setting Δt to infinity).

MOGROW - (Querner 1997)

This model was developed in Denmark by combining the two models SIMGRO (SIMulation of GROundwater flow and surface water levels) and SIMWAT (SIMulation of flow in surface WATER networks). The combined model is known as MOGROW (MOdelling GROundwater flow and the flow in surface Water systems).

Simgro

The groundwater code in MOGRO is simulated by the SIMGRO module. The saturated zone is modelled using the finite element method, and the unsaturated zone is modelled according to land use and soil characteristics. Sub-regions are defined in the catchment, such that the hydrological conditions and soil properties are relatively homogenous in each sub-region (Figure 2.4). Each type of land-use must be known as a percentage of the sub-region (i.e. geometric position is not necessary); the key different types of land-use are: agricultural, urban, nature reserve and woodland. The groundwater system is layered, with horizontal flow in aquifers, and the vertical flow in less-permeable layers (aquitards).

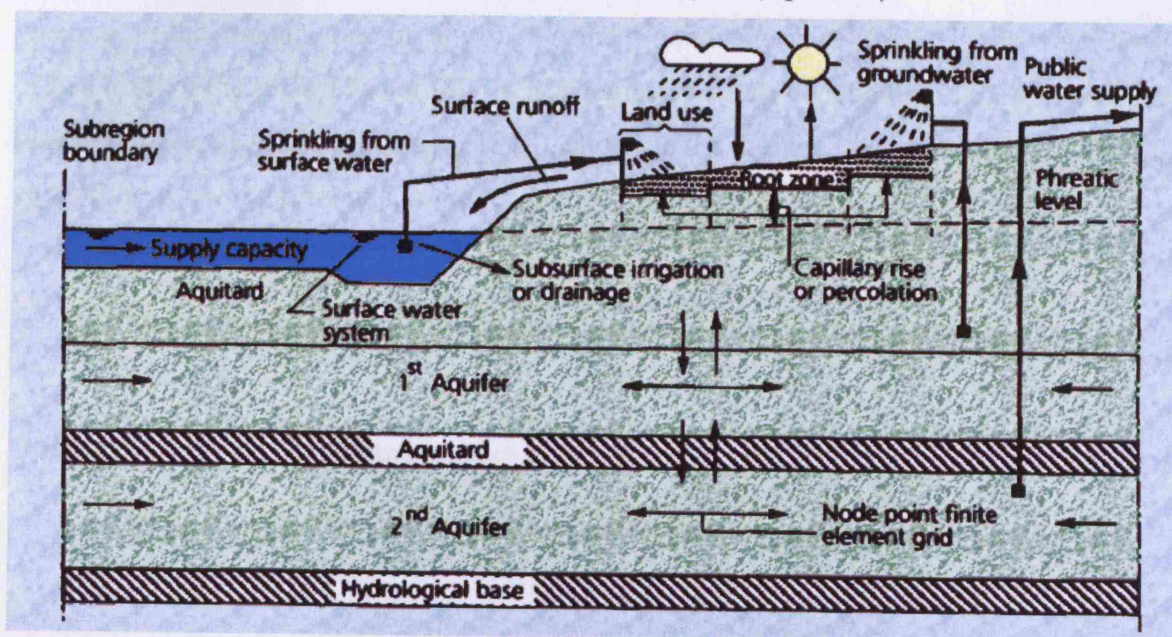


Figure 2.4: -Schematization in SIMGRO of the hydrological system within a sub-region (modified from Querner 1997)

Surface water systems are modelled in four ways: a primary network of channels (modelled by SIMWAT, see below), secondary water courses, tertiary water courses and shallow trenches (considered to be spread evenly over a finite element or sub-region) (see Figure 2.5). SIMGRO and SIMWAT were originally produced for the Netherlands region, where the surface water system consists of a dense network of water courses.

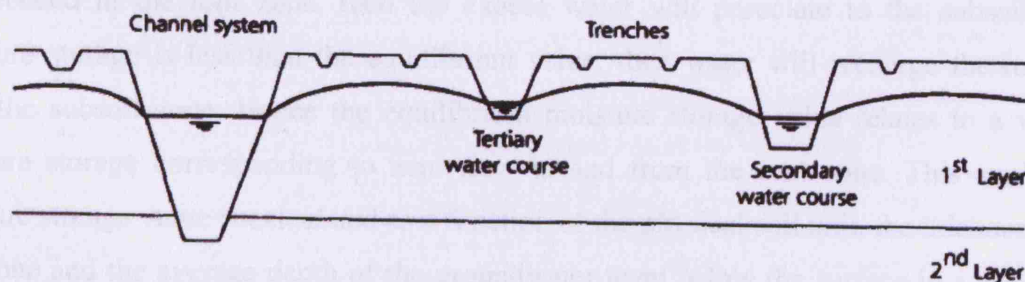


Figure 2.5: - Interaction between surface and groundwater in four categories. (Querner 1997)

The primary network is present only in specific nodes of the finite element mesh.

Drainage to secondary, tertiary and trench water systems is described per unit area using the difference in head and a drainage resistance term (estimated from field measurements and formulas). Drainage to the primary network is considered per unit length of the channel, again using the difference between the heads and drainage resistance parameters.

The interaction between these systems and the groundwater can be described per unit area as (Ernst, 1978)

$$q_w = \frac{(h_i - h)}{\alpha_s T_s} \quad 2.1$$

where q_w is the drainage rate (m day^{-1}), h_i is the groundwater level (m), h is the water level or bed level of the surface water (m), α_s is a geometry factor depending on the shape of the water table (range 0.65-0.85; Ernst, 1978), and T_s is the drainage resistance (day) which is the sum of the vertical, horizontal, radial and entry resistances (Querner 1997, Ernst 1978).

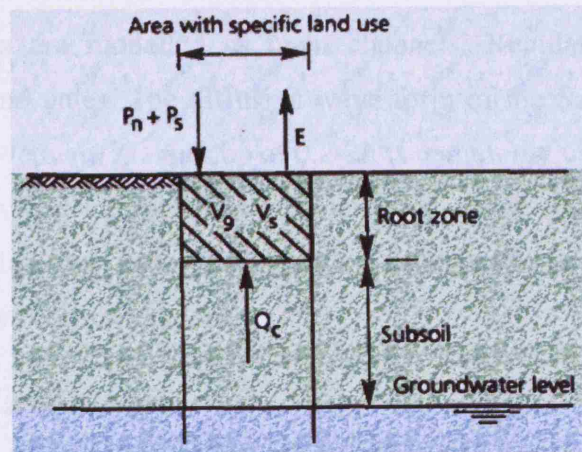


Figure 2.6: - Unsaturated zone per land use. P_n , net precipitation; P_s , sprinkling (watering); E , evapotranspiration; V , moisture storage; Q_c , upward flux.

The unsaturated zone is modelled in two ‘reservoirs’, one for the root zone and one for the subsoil (Figure 2.6). The thickness of the root zone is defined by land-use and the physical soil unit, and is assumed to remain constant over time. If a set ‘equilibrium moisture storage’ is exceeded in the root zone, then the excess water will percolate to the subsoil. If the moisture storage is less than the equilibrium value, then water will recharge the root zone from the subsoil zone. Hence the equilibrium moisture storage value relates to a value of moisture storage corresponding to zero flow to and from the root zone. This equilibrium moisture storage value is calculated as a function of the physical soil unit, the thickness of the root zone and the average depth of the groundwater level below the surface in a sub-region. The groundwater level (or phreatic surface) is calculated using the water balance of the

subsoil zone, using a storage coefficient dependent on the depth of the groundwater below the soil surface. The change in moisture storage in the root zone includes inputs from precipitation and irrigation (sprinkling), and outputs from evapotranspiration. These inputs are corrected for the varying interception patterns of different land-use.

Additional features of SIMGRO include the ability to model perched water tables, hysteresis (i.e. the variation of soil moisture characteristics after wetting and drying conditions), preferential flow in the unsaturated zone, and evapotranspiration from various vegetation types (including effect of wilting and water logging),

Simwat

The surface water module, known as SIMWAT, models major water courses explicitly as a network of sections. As the model was originally designed for use in the Netherlands, where water courses are often small but densely scattered, the model also takes into account the smaller secondary and tertiary water courses, modelling them as reservoirs connected to the main network.

The major water courses are modelled as open channels. Regulating structures can be included, such as weirs and gates. The diffusive wave form of the Saint Venant equation is used to describe water movement. A timestep of 0.2-2h is commonly used in practice.

The water courses are divided into sections with nodes at either end, and where the water level and discharge are calculated. A set of equations is obtained from the nodes and solved in a matrix form by successive approximations.

Integration of Simwat and Simgro

During one groundwater timestep several surface water timesteps are performed, thereby recognising the rapidly varying nature of surface water when in comparison to groundwater. The groundwater level is assumed to remain constant during its time step. Nodal points of the groundwater module are assigned to a nodal point of the surface water module, ensuring that these linkages do not cross sub-region boundaries unrealistically. The bed levels from the surface water system are transferred to the ground water module, followed by the fluxes and water levels as the timesteps proceed.

Wetland simulation module for MODFLOW (Restrepo et al. 1998)

This module attempts to model wetland hydrodynamics and the interaction with the underlying aquifer. Developed by the South Florida Water Management District, the module package is incorporated into the MODFLOW code, and enables the top layer of the grid

system to contain overland flow and channel flow simulations, representing surface flow through vegetation and flow in slough channels respectively. Instead of the Darcy equation used for groundwater flow, a semi-empirical Manning-type equation is used to represent surface water movement, known as the Kadlec equation (Kadlec 1990). This is used to derive the differential equation of overland flow (without sources or sinks) shown in equation 2.2:

$$\frac{\partial}{\partial x} \left(T_x \frac{\partial h}{\partial x} \right) + \frac{\partial}{\partial y} \left(T_y \frac{\partial h}{\partial y} \right) = S_y \frac{\partial h}{\partial t} \quad 2.2$$

where h (m) is the hydraulic head, T_i is the transmissivity component in the i direction, S_y is the specific yield, and is set close to 1.0. The transmissivity is derived from the Kadlec equation by defining the conductance coefficient (of the Kadlec equation) as the inverse of an equivalent roughness coefficient

The model allows for wetting and drying of the wetland, evapotranspiration and vertical and horizontal flux components of the wetland-aquifer interaction. The flow through dense vegetation is treated mathematically as flow through porous media, with a porosity close to 1.0. The slough channels are modelled using cell-by-cell anisotropy factors (i.e. ratio of hydraulic conductivity along a row, to hydraulic conductivity along a column). These factors were originally defined in MODFLOW per layer, but a modified cell-by-cell approach has been added here to allow indirect simulation of slough channels.

The module has a number of options, allowing it to be applied in a variety of situations. It is particularly suited to modelling sheet flow through dense vegetation and channel flow through a slough network, such as is found in wetlands and vegetated saltmarshes.

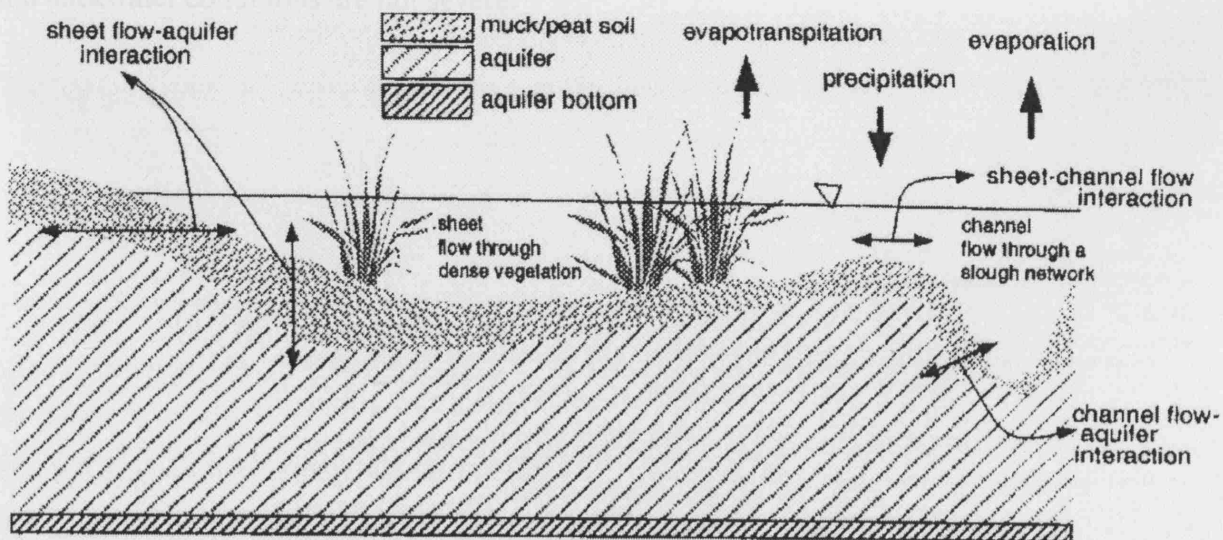


Figure 2.7: Vertical Schematic of surface water pathways in wetlands (Restrepo et al. 1998).

Analytical Solution for channel-aquifer interactions - (Ostfeld et al. 1999)

Ostfeld et al. (1999) documented a new approach to the analytical solution of channel-groundwater interactions. Rather than use the separation of variables, the equations are solved using Laplace transforms. The problem considered is one-dimensional, and consists of 1-D flow between two drainage canals bounding an unconfined aquifer undergoing recharge and evapotranspiration.

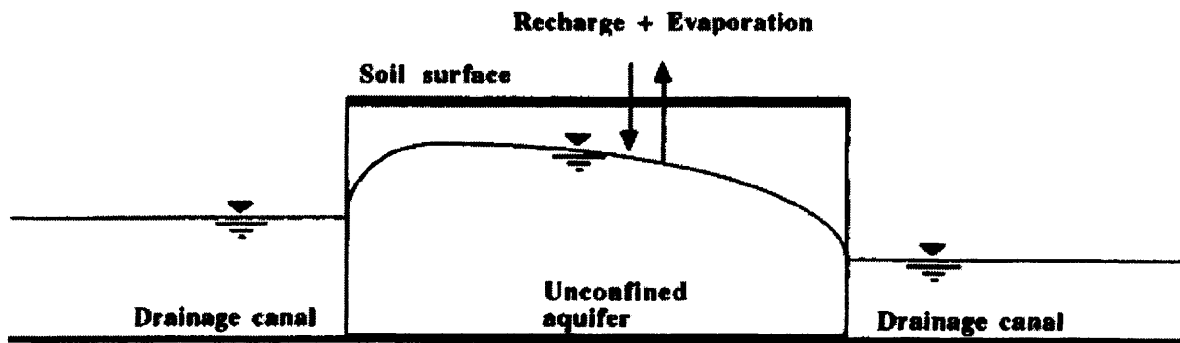


Figure 2.8: - Schematic of problem solved by Ostfeld (1999).

The solution simply considers the groundwater, and uses head boundaries at the surface water interface. The solution was tested against MODFLOW, and favourable results were obtained. The solution does not take seepage faces into account.

DAFLOW – MODFLOW: US Geological Survey (Jobson and Harbaugh 1999)

DAFLOW (Diffusion Analogy Surface-Water Flow model) is a one-dimensional channel flow model that simulates flow using the diffusive wave form of the flow equations. Rivers (or channels) are divided into branches, with each branch divided into a set of sub-reaches. It is designed for simulating flow in upland stream systems where flow-reversals do not occur and backwater conditions are not severe.

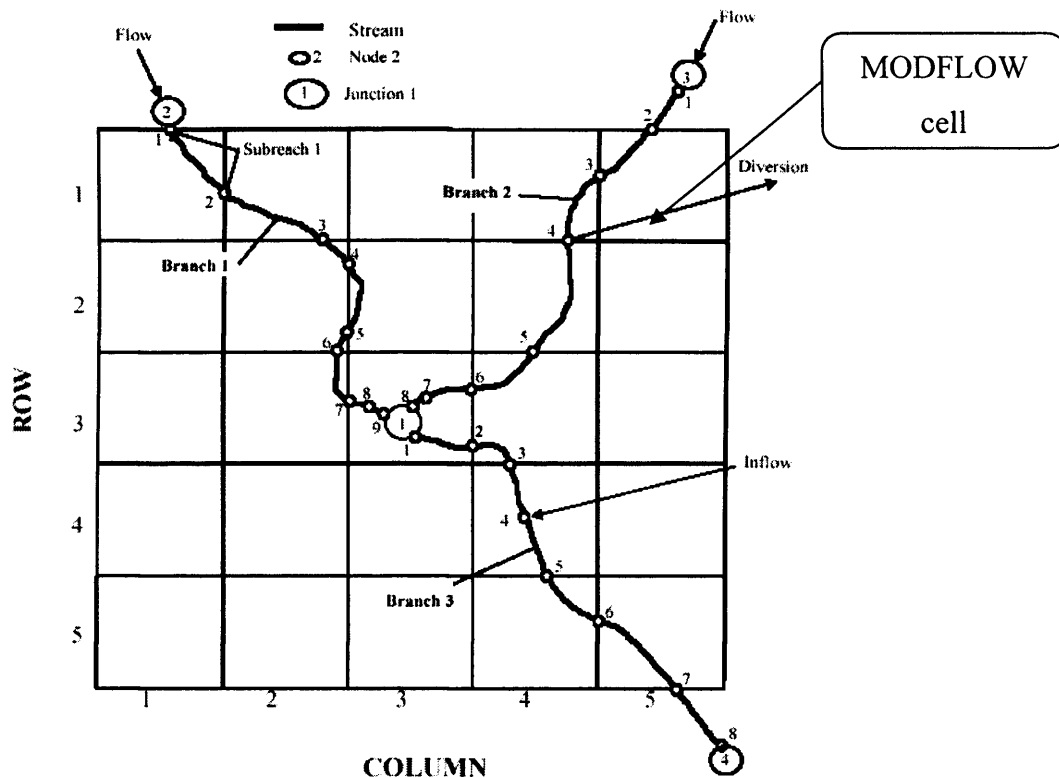


Figure 2.9: - Schematic of DAFLOW-MODFLOW stream layout, showing numbered nodes and branches (Jobson and Harbaugh 1999).

The coupling of the two models was carried out at the USGS (developers of MODFLOW etc), and acknowledges the previous work on coupling of models (e.g. MODBRANCH Swain and Wexler 1996), but makes no attempt to compare this later model with the earlier work.

The coupled model allows multiple time-steps of DAFLOW within a MODFLOW timestep, acknowledging the fact that appropriate time-steps for groundwater and surface water calculations may differ greatly. The model arranges the surface water channels in a similar scheme to the MODBRANCH model. The branches are divided into sub-reaches; as a minimum, a node (i.e. a joint between sub-reaches) is placed where the stream intersects the groundwater cell boundary. Like MODBRANCH, seepage associated with each sub-reach is assumed to flow into the aquifer below at the centre of the relevant cell.

Seepage from the river is calculated in a similar procedure to that outlined in the original RIV module described above, based on Darcy's Law. The seepage is calculated at each surface water timestep, and summed during the GW timestep to compute the total exchange with the aquifer.

The DAFLOW model can only be applied to channels having a fixed-channel geometry and no backwater. One-dimensional, un-stratified flow is assumed. Flow splitting into multiple branches is possible, but constant percentages of flow must be assigned to each branch. The

model allows the drying out of stream reaches, which the original DAFLOW model did not, but the review does not state exactly flow continuity is maintained – although the source code is included in an appendix. If the seepage demands exceed the streamflow, the flow in the stream is set to zero and the seepage term is set equal to the available water in the stream.

Because of the nature of the simplification of the dynamic wave equations, the surface water model accuracy increases with the slope of the stream. Hence, this approach is excellent for modelling upland streams with a unique relationship between stage and discharge.

Since each stream sub-reach is assigned to a single cell in MODFLOW, this places certain limitations on the cell-size / stream size. If the stream is wider than the cell, then accuracy will be lost as the seepage is assigned to a single cell rather than spread across multiple cells across the width of the stream. Similarly, and perhaps more significantly, in the vertical direction, the channel depth should remain in a single MODFLOW layer. The model will operate if this is violated, but again, seepage will only be assigned to one layer. If the MODFLOW cells are much larger than the stream width, the head around the stream may not be accurately represented.

Lake-Aquifer interaction package (LAK3) for MODFLOW (Meritt and Konikow 2000)

This is another module from the USGS for its MODFLOW program. The original version of MODFLOW contained the River package, as described above. Lake-aquifer interactions could be approximated by generalising this river package to represent the lake as a constant-head source of fixed areal extent, implying that the stage of the lake was fixed. This concept was extended by the development of the Reservoir package (Fenske et al. 1996), which allowed the stage of the reservoir (lake) to vary linearly over a stress-period, and the extent of the reservoir to vary accordingly. In both cases, the lake stage had to be entered as a prior specification, and was assumed to be independent of leakage to the aquifer.

Meritt and Konikow (2000) used a different approach based on a generic lake package, designed to handle the many different requirements of the problem. The lake is described within the MODFLOW grid as a volume composed of inactive cells extending downwards from the upper surface. Active model cells bordering this space represent the adjacent aquifer. The seepage is calculated using Darcy's law, based on the difference between the head in the lake, and the head in the adjoining aquifer. Where the head in the aquifer drops below the lakebed, the seepage is maintained at the same rate as if the aquifer head was at the lakebed elevation. In effect, the aquifer immediately below the water body is forced to remain

saturated below the lake, as in the River package.

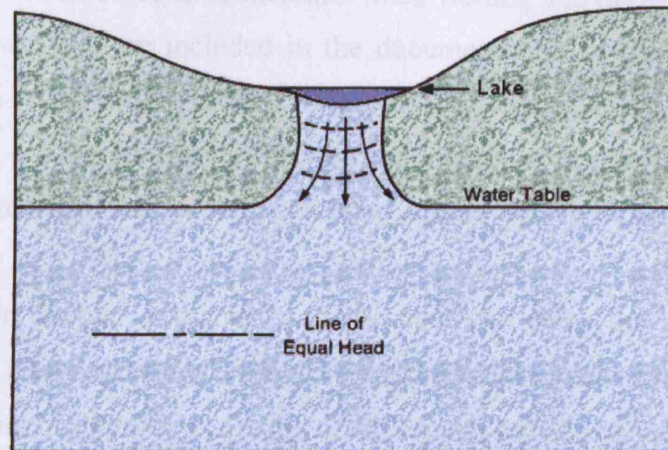


Figure 2.10: - Seepage when aquifer head drops below lake bed, assuming full saturation. (Modified from McDonald and Harbaugh 1988)

Seepage is calculated both laterally and vertically, and modelled as flowing through two distinct materials: the lakebed and the aquifer. Thus the lakebed can be simulated as having a much lower conductivity than the aquifer. The conductance term is calculated by treating the lakebed and the aquifer in series after McDonald and Harbaugh (1988). The seepages calculated are added to the appropriate terms in the MODFLOW matrices.

The timesteps used for the lake and groundwater calculations are identical; indeed the lake is modelled more as an extension of the groundwater than as a standalone water body. Hence, the package focuses on predicting seepage, water levels and the surface area of the lakes, rather than complete surface water modelling. The lake package includes a water budget procedure that is independent of the groundwater budget, and uses estimates of gains from rainfall, overland run-off, inflowing streams, and losses to evaporation, outflowing streams, and anthropogenic gains and losses. Using this budgeting procedure, the lake stage and volume can be calculated explicitly, semi-implicitly, or fully implicitly.

Drying and rewetting is included in the model. As the lake stage drops below the lowest defined 'lake cell' in a column, then the lake volume cells in that column become dry, and the lake volume and surface area are adjusted accordingly. Lakes are allowed to dry out completely, and a semi-empirical method is employed to re-wet the lake after a dry event. Obviously, lake budget calculations cannot continue when the lake is dry, so the program simply checks to see if the average aquifer head is above the lowest elevation of the lake. If this is the case, then the lake stage is set equal to the aquifer head, and the lake budget calculations are resumed from this point. However, this does not account for any retardation of the inflow from the aquifer through the less permeable lakebed. A logical procedure to

allow for separation and coalescence of lakes and sub-lakes has been developed, to allow the irregular bathymetry of most lakes to be included when wetting and drying.

Stream-lake interconnections are included in the documentation of the package, but in the initial release version (with MODFLOW-2000), only seepage lakes (i.e. with no inputs or outputs - Hunt 2003) can be modelled, although the USGS have recently developed a new stream-routing package (SFR1, see section below) to address this deficiency.

Solute concentration in the lake and aquifer can be modelled using the lake package, but as the model is primarily a seepage model, various assumptions are made, including:

- complete and instantaneous mixing of all volume inflows to the lake,
- that the timescale of changes in the groundwater system is substantially longer than the timescale of changes in the surface water and
- that there are no reactions in the lake that affect the solute concentration.

Using these assumptions a simple mixing equation is used to calculate the solute concentration. The model does not attempt to model flow dynamics or spatial variation of water quality in the lake.

When using the explicit method of updating lake stages, the timestep size must be limited to avoid lake stage oscillations, and to provide good estimates for the concurrent timestep. However, the semi and fully-implicit methods require more iterations, more run-time and tighter convergence criteria to avoid significant discrepancies in the water budget.

Ecomag - MODFLOW: ECOFLOW (Sokrut et al. 2001) (Sokrut 2001)

This combined model was developed as part of a licentiate thesis by Nikolay Sokrut, in Sweden. The ECOMAG model (ECOLOGical Model for Applied Geophysics.) is a distributed catchment model, rather than a specific open channel flow model. This makes it relatively straightforward to link to a catchment wide groundwater model, simply by introducing a special sink term into the governing equations. This sink term is generated by the surface model and implemented into the groundwater and solute transport equations.

The ECOMAG surface model was developed for boreal conditions, and describes the processes of infiltration, evapotranspiration, thermal and water regimes of the soil, surface and subsurface flow, groundwater and river flow, and snow accumulation and snowmelt. The drainage basin was originally approximated by triangular elements, but is now (in the second version) mapped by a 2km x 2km rectangular grid network.

The model simulates the infiltration of rainwater and the subsequent run-off when the soil

becomes saturated, and surface depressions are filled. Rivers are modelled in reaches (called links), characterised by length, width, slope, and Manning's roughness coefficient. Water movement in run-off is assumed to take place in the direction of the prevailing slope towards the river. Subsurface flow is modelled in two 'horizons', A and B. Horizon A simulates shallow subsurface flow just below the soil surface (high porosity and conductivity); Horizon B is a deeper layer with a much lower porosity and conductivity, (see Figure 2.11).

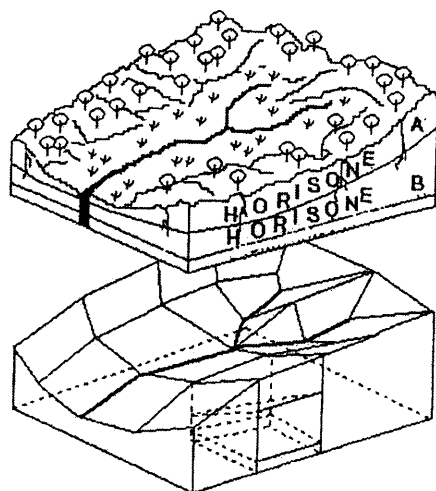


Figure 2.11: - ECOFLOW layers schematisation.

The ECOMAG model also had a bottom layer called the 'groundwater-zone'. In the coupled model this has been replaced with MODFLOW (McDonald and Harbaugh 1988). At present the model must be run with identical grid-sizes and time-steps for both ECOMAG and MODFLOW, and the code is not fully integrated.

FTSTREAM - (Hussein and Schwartz 2003)

Hussein and Schwartz (2003) extended an existing groundwater flow and contaminant model called FTWORK, to incorporate the fate of chemicals and transport in streams. Transport in the stream is based on a one-dimensional advection-dispersion equation. The model also incorporates volatilisation, settling, and decay in the surface water transport. The two zones are linked by a leakage term based on Darcy's law. The equations for the stream and groundwater zones are solved simultaneously in order to provide the head in the aquifer and the depth of flow in the stream that are required for estimating the flow velocities (and subsequently solute transport). The transport between the groundwater and surface water is assumed to be predominantly due to advection, i.e. dispersive transport is neglected.

3D Bank Storage - (Chen and Chen 2003)

Chen and Chen (2003) carried out a study to investigate at the bank storage around a river in a

similar fashion to Cooper and Rorabaugh (1963), but also considering the ‘bank’ storage *beneath* the river. No actual river model was used, rather, MODFLOW was set up with a varying head boundary where the aquifer meets the river. A ‘flood wave’ (change in head) was modelled using the same equations as Cooper and Rorabaugh (1963) and parameters such as duration, time to peak and height of the flood wave were varied. Porosity was kept constant, while conductivity was varied for homogeneous and heterogeneous (layered) aquifers. Anisotropy was also investigated, as well as the effects of a layer of streambed sediment. The initial groundwater level was assumed to be the same as the initial stream stage. Further simulations carried out with initial groundwater levels above (gaining stream) and below (losing stream) the stream stage.

The flow rate between the river and groundwater, and the volume of river water stored (i.e. integral of the flow rate over time) are plotted for each simulation, and also the storage zone. This storage zone is created by using MODPATH (Particle tracking software for MODFLOW, Pollock 1994) to track the pathline of particles beginning in the stream bed. The positions of the particles at a specific time can be joined to form a ‘front’, showing the extent of the infiltrated stream water (Figure 2.12).

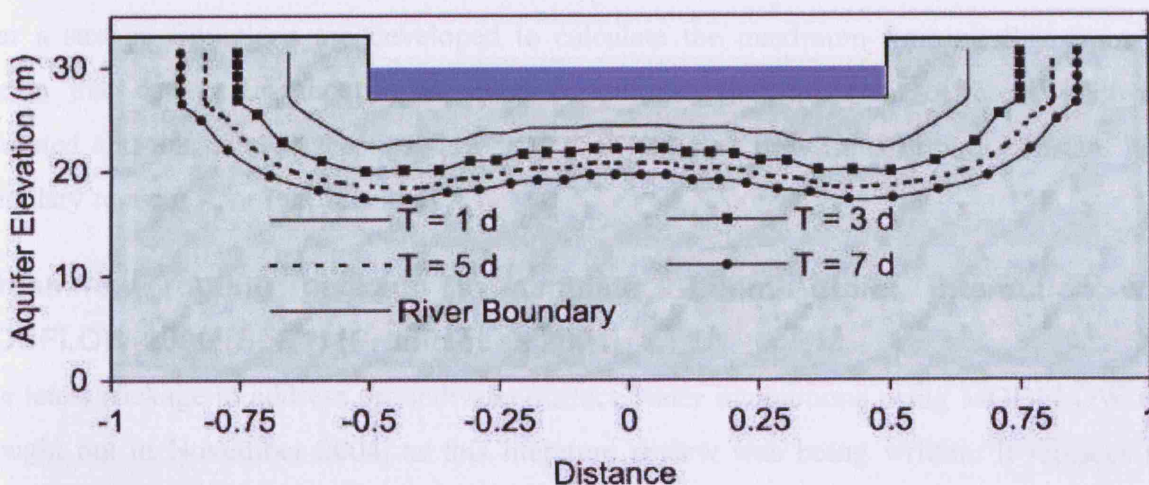


Figure 2.12: - Adapted from Chen and Chen (2003) - illustrating the concept of maximum storage zone with varying flood durations (T = flood duration).

The particles are considered to be transported in the groundwater by advection only (i.e. diffusion and dispersion are assumed to be negligible)

In a study by Squillace (1996) (see below) it was shown that for wide and shallow rivers, the primary interactions with the groundwater occur in the vertical direction. Also included is a brief look at the effect of rainfall recharge during flood waves and evapotranspiration (ET) from the groundwater.

(DAFLOW-MODFLOW-MOC3D) (Lin and Medina Jr 2003)

This study takes the DAFLOW-MODFLOW one stage further and includes MOC3D (3D 'method-of-characteristics' model for solute transport, Konikow et al. 1996). The three models represent a conjunctive stream-aquifer solute transport model. It incorporates transient storage in the streamflow model, setting this model apart from other similar models, by attempting to simulate transient surface storage (i.e. pools, eddies and stagnant zones) and subsurface storage (i.e. hyporheic exchange) within a conjunctive stream-aquifer model. In addition to the transient storage equations, the surface water includes the more general stream-aquifer interactions by way of a groundwater input term. A note in the conclusion mentions that it might be reasonable to treat stream-aquifer interaction not as an independent source/sink to the stream, but rather to combine it with the 'storage zone' equation.

Unsaturated Hyporheic Flow (Fox and Durnford 2003)

Most of the models mentioned in this summary assume saturated flow for seepage from a stream to an aquifer (e.g. Figure 2.10). However, when the water table drops sufficiently below the stream-bed, the region beneath the stream can become unsaturated. This paper attempts to analyse this behaviour and derive equations for use in predicting the effect this has on groundwater levels, e.g. when a pumping well induces drawdown of groundwater levels near a stream. Equations are developed to calculate the maximum limiting flux from the stream that can occur under unsaturated conditions. The important difference between saturated and unsaturated seepage flow is that unsaturated flow transforms a constant head boundary to a constant flux boundary.

Streamflow routing package to simulate Stream-Aquifer interaction with MODFLOW-2000 (SFR1) (Prudic et al. 2004)

The latest package to address groundwater-surface water interactions using MODFLOW was brought out in November 2004, as this literature review was being written. It replaces the older Stream Package (STR1) (Prudic 1989). It is capable of modelling solute transport through interconnected lakes, streams and aquifers and the model is designed to be used with the LAK3 package, for lake-aquifer interactions and as described above. However, the SFR1 package is best suited for modelling long-term changes (months to years) in ground-water flow and solute concentrations using average flows in streams. It is not recommended for modelling the transient exchange of water between streams and aquifers when the objective is to examine short-term (minutes to days) effects caused by rapidly changing streamflows (Prudic et al. 2004).

MODHMS - (Panday and Huyakorn 2004)

The model described by Panday and Huyakorn (Panday and Huyakorn 2004) incorporates 3D saturated and unsaturated flow for the subsurface zone, coupled with the diffusion wave equation for 2-D overland flow, both of which are coupled with the diffusion wave equation for flow through a network of channels, including hydraulic structures. The flow domains are fully-coupled, i.e. not sequentially/iteratively or time-lag coupled (these approaches are compared in a previous paper by the authors) (Fairbanks et al. 2001). The flow between domains is determined by the head difference between each of the domains. Overland/subsurface interaction uses the vertical hydraulic conductivity of the subsurface nodes, and can also include a 'skin later' effect at the surface. Channel/subsurface interaction utilises the conductivity of the channel sediments, and channel/overland interactions are calculated using various weir formulas.

Conceptually, all surface-water bodies (i.e. rivers, lakes, wetlands etc) could be included in the 2D overland domain by using appropriate topography and bathymetry, but problems arise when the water bodies are smaller than the grid discretisation used in the 2-D domain. To avoid over discretisation, these small surface water features may be included in the 1-D channel domain, by including a depth-area relationship. These 1-D water bodies interact with the subsurface over all of their area, and can be connected to channels and other surface water bodies. Provision is also made for interception of precipitation before reaching the ground surface, and also for evapotranspiration. See (Panday and Huyakorn 2004) for more details.

(Gunduz and Aral 2005)

Gundaz and Aral (2005) developed a model for 1-D channel flow, coupled with 2-D vertically averaged groundwater flow. The solution strategy innovatively solves the surface water and groundwater equations simultaneously, using a global matrix technique. No unsaturated zone is considered, so the seepage from the river is linked directly to the underlying aquifer (see Figure 2.13).

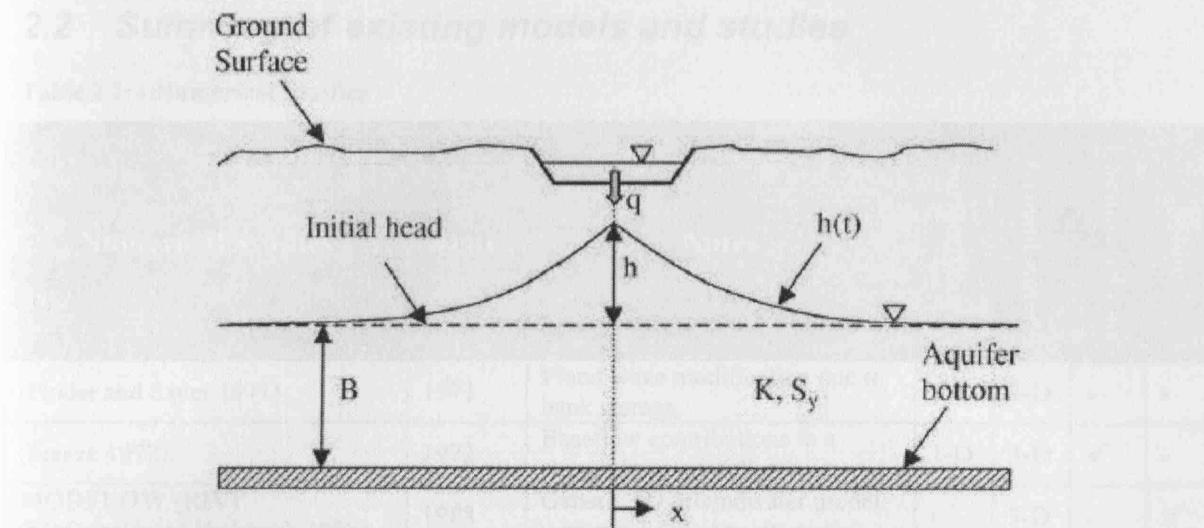


Figure 2.13: - Seepage from the river is linked directly to the 2-D vertically averaged aquifer below. (Gunduz and Aral 2005)

2.1.1 Field Data on Bank Storage and River-Aquifer interactions.

Bank Storage - Cedar River, Iowa, USA

Squillace (1996) measured bank storage at a site on the Cedar River, Iowa, USA, and then modelled the site using MODFLOW. He noted that the flow per unit area through the river bank was about four times greater than the flow through the river bottom, largely due to the higher horizontal conductivity of the medium sand forming the river bank. However, the proportion of bank storage water that had moved through the river bed was about 70%, and only 30% through the bank, as the river bed surface area was at least 10 times larger than that of the river bed. Hence, bank-storage water moving through the river bottom can be a significant portion of the total bank storage when a river is wide and shallow.

PCE groundwater plume – Angus, Ontario, Canada

Conant Jr. et al (2004) monitored a site in Ontario, Canada, where a 60m wide dissolved phase PCE (tetrachloroethene) plume was present in a sand aquifer. The plume concentration, distribution and composition were strongly modified by the near-river zone, prior to discharging to the surface water. The site geology was complex but the study provides a good example of the interaction between groundwater and surface water and solute flux between both systems.

2.2 Summary of existing models and studies

Table 2.1: - Numerical Studies

Numerical Studies	Date	Notes	Surface Water	Ground-water	Unsaturated zone	Solute
(Pinder and Sauer 1971)	1971	Flood wave modification due to bank storage.	1-D	2-D	-	-
(Freeze 1972)	1972	Baseflow contributions to a stream from rainfall events.	1-D	3-D	✓	-
MODFLOW (RIV) (McDonald and Harbaugh 1988)	1988	Generic 3D groundwater model with simple stream interaction	-	3-D	-	✓
MODBRANCH (Swain and Wexler 1996)	1996	Coupled MODFLOW and Branch	1-D	3-D	✓	-
MOGROW (Querner 1997)	1997	Combination of SIMWAT and SIMGRO	1-D+	3-D	✓	-
Wetland module -(MODFLOW) (Restrepo et al. 1998)	1998	Wetland simulation module extension for MODFLOW	2-D	3-D	-	-
DAFLOW-MODFLOW (Jobson and Harbaugh 1999)	1999	Couples DAFLOW and MODFLOW	1-D	3-D	-	-
Lake-Aquifer Module (LAK3) – (MODFLOW) (Meritt and Konikow 2000)	2000	Allows seepage and stage variation in lakes for MODFLOW	-	3-D	-	-
ECOFLOW (Sokrut 2001)	2001		1-D	3-D	✓	-
DAFLOW-MODFLOW-MOC3d (Lin and Medina Jr 2003)	2003	Adds solute transport to previous DAFLOW-MODFLOW model	1-D	3-D	-	✓
Bank storage and Storage Zone changes - (Chen and Chen 2003)	2003	Uses MODFLOW/Modpath to assess bank storage and storage zone from flood wave.	-	3-D	-	-
FTSTREAM (Hussein and Schwartz 2003)	2003	3-D groundwater model extended to 1-D transport in streams.	1-D	3-D	-	✓
Streamflow Routing Module (SFR1) – (MODFLOW) (Prudic et al. 2004)	2004	Allows interconnected streams, lakes and aquifers in MODFLOW	1-D+	3-D	-	-
MODHMS (Panday and Huyakorn 2004)	2004	Stand-alone surface/subsurface model.	1-D channel 2-D areal overland	3-D	✓	-
(Gunduz and Aral 2005)	2005	Simultaneous solution of surface and groundwater equations using global matrix.	1-D	2-D	-	-

Table 2.2 – Analytical Studies

Analytical Studies	Date	Notes
(Cooper and Rorabaugh 1963)	1963	Bank Storage
(Ostfeld et al. 1999)	1999	Flow between surface water bodies via ground, with recharge.
(Workman et al. 1997)	1997	River interaction with alluvial aquifer. One-sided boundary condition.

Table 2.3: - Field Studies

Field Sites	Date	Notes
(Squillace 1996)	1996	Bank storage effects measured and modelled (MODFLOW), Cedar River, Iowa.
(Conant Jr et al. 2004)	2004	PCE groundwater plume measured in Canada

Tables 2.1, 2.2 and 2.3 summarise the existing models and studies reviewed in this chapter. This is not an exhaustive list but represents a significant part of the current integrated modelling situation. For additional references and information on various methods of representing surface water - groundwater interactions readers are pointed to Sophocleous (2002) and especially Rushton (2007). Readers should note that a significant surface water-groundwater model MIKE-SHE has not been included in this review as it is a commercial code – however further info can be found at DHI (2008), Refsgaard and Storm (1995).

A large majority of non-commercial models focus on adding surface water modules to an existing code, usually MODFLOW. Most of these surface water additions are 1-D channel flow models (e.g. DAFLOW-MODFLOW), or simple representations of larger surface water bodies (e.g. LAK3 Lake-aquifer interaction), with the exception of the wetland module by Restrepo et al. (1998). This model allows 2-D overland flow through vegetation by modelling it as a porous media with a high porosity – essentially the top layer of MODFLOW is set to high porosity and treated as vegetated surface water. However, the channel flow is 1-D again. MODHMS is the only non-commercial model found to have a distinct provision for 2-D flow on the surface, but this model is very much designed for large scale modelling, and it was found best to include smaller surface water bodies in the 1-D channel network using a depth-area relationship.

Therefore, in all the models reviewed, no dedicated 2-D surface water code has been adapted to include groundwater. Combinations of two models have been used, but the surface water part is almost exclusively 1-D and unsuitable for estuaries, large rivers or coastal studies. Hence, in this study, a well-documented 2-D surface water model (DIVAST) will be extended to include 2-D and pseudo 3-D groundwater interactions within the same model, allowing smooth transition between the two areas without the common coupling problems.

CHAPTER 3 GOVERNING MODEL EQUATIONS

3.1 Introduction

The models considered in this study simulate the hydrodynamics in surface and subsurface systems. The hydrodynamics of fluid flow is complex, but is governed by fundamental physical processes. Hence water flow can be modelled using relatively simple numerical equations. The basic physics of fluid flow can be described by using the concepts of conservation of mass and momentum. The following sections derive the governing equations for the flow of surface water in two dimensions, and saturated groundwater flow in two dimensions. Unsaturated flow and the equations for solute transport are not considered in this study.

3.2 Conservation of Mass – Surface Water

The concept of conservation of mass can be written as:

3.1

The rate of mass entering a region =

The rate of mass leaving the region + the rate of mass accumulating in the region

Consider first an elemental volume with no free surface, i.e. the space is always full of fluid (Figure 3.1). With this assumption, mass can only accumulate in the volume if the density of the fluid changes. The velocities (m/s) at the centre of the element can be split into components, in the three axes (x, y, z), giving u , v and w vectors respectively. The dimensions of the elemental volume are Δx , Δy and Δz . Hence, the mass flow rate at the centre is equal to velocity \times density \times area of flow, or $\rho u \Delta y \Delta z$ for the x -direction, and similarly for the y and z directions. Taylor's series can be used to obtain the flow rates for the downstream ($x + \frac{1}{2} \Delta x$) and upstream ($x - \frac{1}{2} \Delta x$) faces, see equation 3.2 for x -direction. Assuming the flow is positive in the direction of increasing x , y and z , then flow at the boundaries of the volume can be

described as follows:

3.2

$$\rho u \Delta z \Delta y_{x \pm \frac{\Delta x}{2}} = \rho u \Delta z \Delta y \pm \frac{\partial \rho u \Delta z \Delta y}{\partial x} \left(\frac{\Delta x}{2} \right) \frac{1}{1!} + \frac{\partial^2 \rho u \Delta z \Delta y}{\partial x^2} \left(\frac{\Delta x}{2} \right)^2 \frac{1}{2!} \pm \frac{\partial^3 \rho u \Delta z \Delta y}{\partial x^3} \left(\frac{\Delta x}{2} \right)^3 \frac{1}{3!} \dots$$

The higher order derivatives of density and u are increasingly small, and since Δx is small, the higher derivatives are multiplied by increasingly smaller factors. Therefore the assumption can be made that the results from the third derivatives of u and higher are small enough to be disregarded.

3.3

$$\rho u \Delta z \Delta y_{x \pm \frac{\Delta x}{2}} \approx \rho u \Delta z \Delta y \pm \frac{\partial \rho u \Delta z \Delta y}{\partial x} \left(\frac{\Delta x}{2} \right) + \frac{\partial^2 \rho u \Delta z \Delta y}{\partial x^2} \left(\frac{\Delta x}{2} \right)^2 \frac{1}{2!}$$

and similarly for the y and z directions. Hence the approximate flow at each face of the control volume has been derived. By assuming that the density is constant (thus eliminating the mass accumulation) and by allowing Q_x , Q_y , and Q_z to equal $u \Delta z \Delta y$, $v \Delta z \Delta x$ and $w \Delta x \Delta y$ respectively and substituting into the descriptive form of the continuity equation (3.1) we arrive at equation 3.4.

3.4

$$\begin{aligned} & \rho Q_x - \frac{\partial \rho Q_x}{\partial x} \left(\frac{\Delta x}{2} \right) + \frac{\partial^2 \rho Q_x}{\partial x^2} \left(\frac{\Delta x}{2} \right)^2 \frac{1}{2!} + \rho Q_y - \frac{\partial \rho Q_y}{\partial y} \left(\frac{\Delta y}{2} \right) + \frac{\partial^2 \rho Q_y}{\partial y^2} \left(\frac{\Delta y}{2} \right)^2 \frac{1}{2!} + \rho Q_z - \frac{\partial \rho Q_z}{\partial z} \left(\frac{\Delta z}{2} \right) + \frac{\partial^2 \rho Q_z}{\partial z^2} \left(\frac{\Delta z}{2} \right)^2 \frac{1}{2!} \\ & = \rho Q_x + \frac{\partial \rho Q_x}{\partial x} \left(\frac{\Delta x}{2} \right) + \frac{\partial^2 \rho Q_x}{\partial x^2} \left(\frac{\Delta x}{2} \right)^2 \frac{1}{2!} + \rho Q_y + \frac{\partial \rho Q_y}{\partial y} \left(\frac{\Delta y}{2} \right) + \frac{\partial^2 \rho Q_y}{\partial y^2} \left(\frac{\Delta y}{2} \right)^2 \frac{1}{2!} + \rho Q_z + \frac{\partial \rho Q_z}{\partial z} \left(\frac{\Delta z}{2} \right) + \frac{\partial^2 \rho Q_z}{\partial z^2} \left(\frac{\Delta z}{2} \right)^2 \frac{1}{2!} \end{aligned}$$

mass entering volume per unit time

= mass leaving volume per unit time

The second derivative terms and the ρQ_i terms cancel leaving the first derivatives only as in equation 3.5.

3.5

$$\frac{\partial \rho Q_x}{\partial x} \Delta x + \frac{\partial \rho Q_y}{\partial y} \Delta y + \frac{\partial \rho Q_z}{\partial z} \Delta z = 0$$

Expanding the Q_i terms:

3.6

$$\frac{\partial \rho u}{\partial x} \Delta z \Delta y \Delta x + \frac{\partial \rho v}{\partial y} \Delta z \Delta x \Delta y + \frac{\partial \rho w}{\partial z} \Delta x \Delta y \Delta z = 0$$

And dividing by Δx , Δy , and Δz .

3.7

$$\frac{\partial \rho u}{\partial x} + \frac{\partial \rho v}{\partial y} + \frac{\partial \rho w}{\partial z} = 0$$

Assuming incompressible flow allows density to be cancelled, giving:

3.8

$$\frac{\partial u}{\partial x} + \frac{\partial v}{\partial y} + \frac{\partial w}{\partial z} = 0$$

Where u , v , and w are discharge per unit area or velocities in the x , y , and z directions respectively. Equation 3.8 is the three-dimensional mass conservation equation for an incompressible fluid (often referred to as the continuity equation).

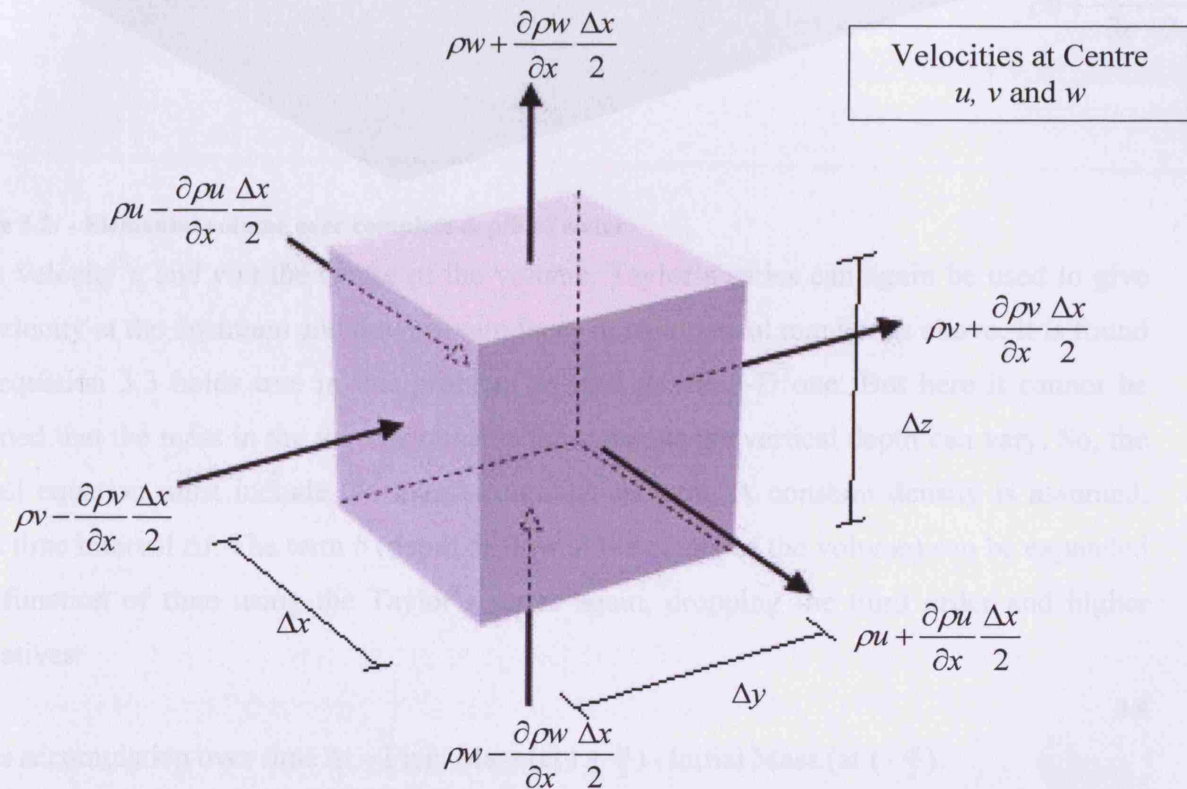


Figure 3.1: - Elemental control volume, surrounded by fluid on all sides.

This equation applies to a small arbitrary 'cube' of fluid surrounded by fluid on all sides, but does not hold when we reach the surface of the water. Here, the vertical dimension is variable, as the depth of water changes and no flow is possible 'upwards' from these elements.

A two-dimensional problem will now be considered, using the whole depth of a surface water body, in order to define an equation that will hold for surface water problems.

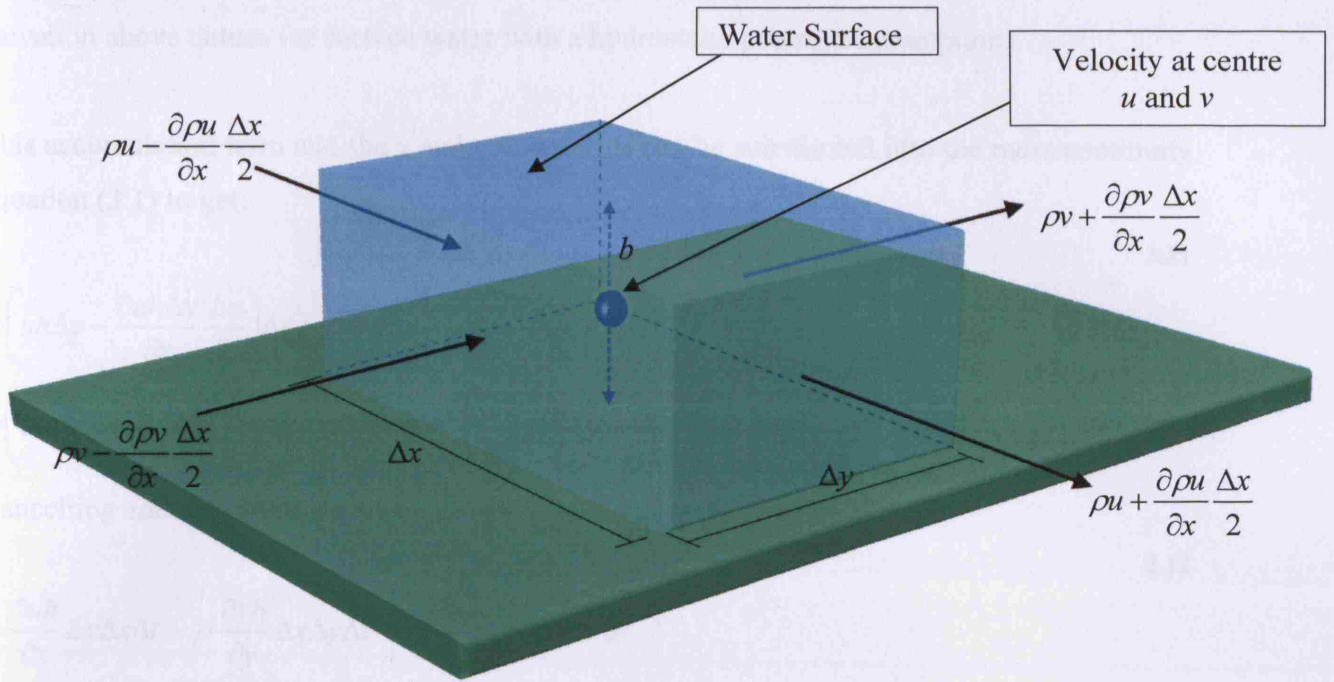


Figure 3.2: - Elemental volume over complete depth of water

For a velocity u and v at the centre of the volume, Taylor's series can again be used to give the velocity at the upstream and downstream faces in an identical manner as above. It is found that equation 3.3 holds true in this problem as well as the 3-D one. But here it cannot be assumed that the mass in the volume remains the same, as the vertical depth can vary. So, the overall equation must include the mass accumulation term. A constant density is assumed, and a time interval Δt . The term b (depth of flow at the centre of the volume) can be expanded as a function of time using the Taylor's series again, dropping the third order and higher derivatives.

3.9

Mass accumulation over time $\Delta t = \text{Final Mass (at } t + \frac{\Delta t}{2}) - \text{Initial Mass (at } t - \frac{\Delta t}{2})$

$$\begin{aligned}
 &= \left[\rho \left(b + \frac{\partial b}{\partial t} \frac{\Delta t}{2} \right) \Delta x \Delta y \right] - \left[\rho \left(b - \frac{\partial b}{\partial t} \frac{\Delta t}{2} \right) \Delta x \Delta y \right] \\
 &= \rho \frac{\partial b}{\partial t} \Delta t \Delta x \Delta y
 \end{aligned}$$

Where b is the depth of water at the centre of the volume, and ρ is density of the fluid.

The rate of change of depth with respect to time is identical to the rate of change of surface elevation with respect to time, so for convenience h (surface elevation) can be substituted for b :

3.10

$$\text{Mass accumulation over time } \Delta t = \rho \frac{\partial h}{\partial t} \Delta t \Delta x \Delta y$$

Where h is the piezometric head elevation above datum (identical to the water surface

elevation above datum for surface water with a hydrostatic pressure assumption).

This accumulation term and the x and y flow terms can be substituted into the mass continuity equation (3.1) to get:

3.11

$$\rho \left(uh\Delta y - \frac{\partial uh\Delta y}{\partial x} \frac{\Delta x}{2} \right) \Delta t + \rho \left(vh\Delta x - \frac{\partial vh\Delta x}{\partial y} \frac{\Delta y}{2} \right) \Delta t =$$

$$\rho \left(uh\Delta y + \frac{\partial uh\Delta y}{\partial x} \frac{\Delta x}{2} \right) \Delta t + \rho \left(vh\Delta x + \frac{\partial vh\Delta x}{\partial y} \frac{\Delta y}{2} \right) \Delta t + \rho \frac{\partial h}{\partial t} \Delta t \Delta x \Delta y$$

Cancelling and rearranging gives:

3.12

$$\rho \frac{\partial uh}{\partial x} \Delta y \Delta x \Delta t + \rho \frac{\partial vh}{\partial y} \Delta x \Delta y \Delta t + \rho \frac{\partial h}{\partial t} \Delta x \Delta y \Delta t = 0$$

Cancelling density, Δt , Δx , and Δy

3.13

$$\frac{\partial uh}{\partial x} + \frac{\partial vh}{\partial y} + \frac{\partial h}{\partial t} = 0$$

$$uh = \frac{Q_x}{\Delta y} = q_x$$

$$vh = \frac{Q_y}{\Delta x} = q_y$$

Where u and v are the velocities in the x and y directions respectively. q_x (or uh) and q_y (or vh) are flow per unit width. Equation 3.13 is the two-dimensional continuity equation for a free surface water body. **From this point on, to avoid overuse of subscripts, q_x and q_y will be referred to as p and q respectively.**

3.14

$$\frac{\partial p}{\partial x} + \frac{\partial q}{\partial y} + \frac{\partial h}{\partial t} = 0$$

$$p = q_x = \frac{Q_x}{\Delta y} = uh$$

$$q = q_y = \frac{Q_y}{\Delta x} = vh$$

3.2.1 Groundwater term in Surface Water equations.

Since the model developed is intended to simulate interactions between the surface water and groundwater, a groundwater seepage term will be added. This will only be used when the

model is extended downwards (a pseudo 3D application), for a 2-D horizontal flow application this is not necessary, as it is assumed that the base of the surface water cell is impermeable. This groundwater seepage can be added by including an additional term in the mass continuity equation (3.11).

Groundwater flow will enter or leave the control volume through the base of the cell. This flow will be called Q_{base} and for purposes of the equation assumed to leave the cell i.e. flow is positive when water flows from the surface water to the groundwater. This term can be positive or negative and represents the flow to or from the groundwater respectively, giving:

3.15

$$\rho \left(uh\Delta y - \frac{\partial uh\Delta y}{\partial x} \frac{\Delta x}{2} \right) \Delta t + \rho \left(vh\Delta x - \frac{\partial vh\Delta x}{\partial y} \frac{\Delta y}{2} \right) \Delta t =$$

$$\rho \left(uh\Delta y + \frac{\partial uh\Delta y}{\partial x} \frac{\Delta x}{2} \right) \Delta t + \rho \left(vh\Delta x + \frac{\partial vh\Delta x}{\partial y} \frac{\Delta y}{2} \right) \Delta t + \rho \cdot Q_{base} \cdot \Delta t + \rho \frac{\partial h}{\partial t} \Delta t \Delta x \Delta y$$

Cancelling terms gives:

3.16

$$\frac{\partial p}{\partial x} + \frac{\partial q}{\partial y} + \frac{\partial h}{\partial t} + q_{base} = 0$$

$$p = \frac{Q_x}{\Delta y} = uh$$

$$q = \frac{Q_y}{\Delta x} = vh$$

$$q_{base} = \frac{Q_{base}}{\Delta x \cdot \Delta y} = \text{velocity of seepage into groundwater}$$

Equation 3.16 is the mass continuity equation for 2-D free surface water including groundwater seepage. The seepage itself is calculated using an application of Darcy's Law as given in Section 3.4.

3.3 Conservation of Mass - Groundwater

A mass continuity equation for the groundwater cells must also be derived and is given below for an unconfined and a confined aquifer.

3.3.1 Unconfined Aquifer

For groundwater 'cells' with a phreatic surface (i.e. an unconfined aquifer), then Figure 3.2 can be considered in much the same way as before, but this time the volume may not contain only water. Some of the control volume will be rock, or sand, whatever the porous media

under consideration is made up of. *Porosity* can be used as a measure of how much space is left for the water to flow through. If the total unit volume V_T of a soil or rock is divided into the volume of the solid portion V_s and the volume of voids V_v , the porosity n is defined as $n = V_v / V_T$ (Freeze and Cherry 1979). A porosity of 1 (100%) would mean the control volume contains only water, a porosity of zero would mean that only solid rock was present. Actual ground material varies greatly in porosity as shown in Table 3.1.

Table 3.1: - Range of values of Porosity (Freeze and Cherry 1979)

n	
Unconsolidated deposits	
Gravel	0.25 - 0.40
Sand	0.25 - 0.50
Silt	0.35 - 0.50
Clay	0.40 - 0.70
Rocks	
Fractured Basalt	0.05 - 0.50
Karst Limestone	0.05 - 0.50
Sandstone	0.05 - 0.30
Limestone, dolomite	0.00 - 0.20
Shale	0.00 - 0.10
Fractured Crystalline Rock	0.00 - 0.10
Dense Crystalline Rock	0.00 - 0.05

This porosity value will affect the mass accumulation term (equation 3.9). As h increases, the mass increase for a geological control volume will be less than that of a surface water control volume, as less water is required to increase the head. The volume of fluid that can fill the total volume has been reduced by a factor of n (known as the total porosity) and hence the mass accumulation term will become:

3.17

$$\text{mass accumulation over time } \Delta t = \rho \frac{\partial h}{\partial t} \Delta x \Delta y \Delta t . n$$

A surface-groundwater seepage term can be included in the same way as before, but this time seepage into the top of the cell must be considered as well as seepage from the base of the cell. These terms are basically provide source/sink terms that can be used to add or remove any mass flux from the cell.

The 2-D continuity equation for groundwater can now be expressed:

3.18

$$\begin{aligned} &\text{mass entering a region per unit time} = \\ &\text{mass leaving the region per unit time} + \\ &\text{mass accumulating in the region per unit time} \end{aligned}$$

3.19

$$\rho \left(uh\Delta y - \frac{\partial uh\Delta y}{\partial x} \frac{\Delta x}{2} \right) \Delta t + \rho \left(vh\Delta x - \frac{\partial vh\Delta x}{\partial y} \frac{\Delta y}{2} \right) \Delta t + \rho Q_{top} \Delta t =$$

$$\rho \left(uh\Delta y + \frac{\partial uh\Delta y}{\partial x} \frac{\Delta x}{2} \right) \Delta t + \rho \left(vh\Delta x + \frac{\partial vh\Delta x}{\partial y} \frac{\Delta y}{2} \right) \Delta t + \rho Q_{base} \Delta t + \rho \frac{\partial h}{\partial t} \Delta x \Delta y \Delta t n$$

3.20

$$\frac{\partial p}{\partial x} + \frac{\partial q}{\partial y} + n \frac{\partial h}{\partial t} - q_{top} + q_{base} = 0$$

where the p , and q terms have the same definitions as in equation 3.16, h is the piezometric head elevation above datum. q_{top} and q_{base} are defined in Section 3.4, and represent of recharge into the top of the aquifer, and seepage from the bottom.

3.3.2 Confined Aquifer

Where the aquifer is unconfined, it has been assumed the water is incompressible, and the porosity remains unchanged with the head of water. The effective porosity is used to describe the change in volume of water in the cell as the head changes, as the water surface level is equivalent to the piezometric head (in a 2-D model). In a confined aquifer another method of description must be used, as the water ‘surface’ level is restricted by a confining layer, while the piezometric head may rise indefinitely. The *specific storage coefficient*, S_s is defined as the volume of water released per unit volume of aquifer, per unit decrease in the head (units of inverse distance) (Rushton and Redshaw 1979, Chap. 2). This term is a function of the density of water, the porosity, the pore volume compressibility, and the compressibility of water (*ibid.*). A physical derivation of this term can be obtained based on these variables (Bras 1990, Appendix B) but it is more usual to determine this parameter through field testing. Cartwright et al (2006) define the specific storage S_s as follows:

3.21

$$S_s = \rho g (\alpha_m + n\beta_w)$$

Where ρ is the density of the fluid, g is acceleration due to gravity, α_m is the compressibility of the aquifer matrix (pore volume compressibility), n is porosity of the aquifer and β_w is compressibility of the fluid (compressibility of water is approx $4.4 \times 10^{-10} \text{ Pa}^{-1}$). The specific storage coefficient is usually in the range 10^{-5} to 10^{-7} m^{-1} (Rushton and Redshaw 1979); i.e. the coefficient is much smaller than the effective porosity. In actual fact, a rigorous application of the equations would require the storage coefficient to be included in equation 3.20 for the unconfined aquifer, but this storage is insignificant when compared to the

porosity term. However, confined aquifers are often much deeper than unconfined aquifers, and this storage term can become significant when b (depth of aquifer) is large.

To include S_s in our continuity equation the mass accumulation term must be modified. Using the definition above we obtain:

3.22

$$\text{mass accumulation over time } \Delta t = \rho \cdot S_s \cdot \Delta x \cdot \Delta y \cdot b \cdot \frac{\partial h}{\partial t} \cdot \Delta t$$

where b is the thickness of the confined aquifer in question (Figure 3.3 – technically semi-confined as the confining layer may be permeable and allow recharge).

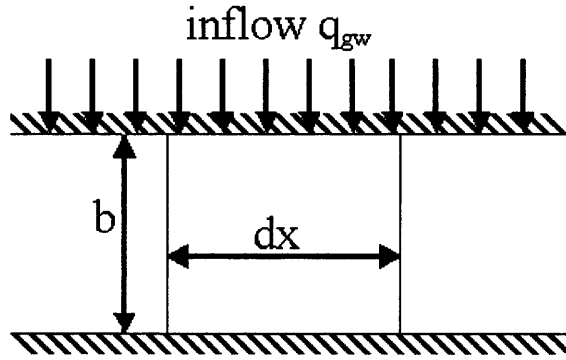


Figure 3.3: - Elemental volume in a semi-confined aquifer

Including equation 3.22 in our mass conservation equation, including a source/sink term and cancelling ρ , Δx , Δy and Δt gives:

3.23

$$\frac{\partial p}{\partial x} + \frac{\partial q}{\partial y} + S_s b \frac{\partial h}{\partial t} - q_{top} + q_{base} = 0$$

where the p , and q terms have the same definitions as in equation 3.16. See Section 3.4 for the full definition of q_{top} and q_{base} in this case.

3.4 Calculating Seepage Terms

Calculating the seepage terms used in the mass continuity equations for both groundwater and surface water needs careful handling. An approach similar to that used by McDonald and Harbaugh (McDonald and Harbaugh 1988) is used herein. It is assumed that the seepage term q_{base} associated with each cell refers to the seepage out of the base of the cell, with q_{top} being therefore identical to q_{base} for the previous layer.

3.4.1 Surface Water to Groundwater

Groundwater flow may be enter or leave the surface water cell through the base of the cell. This flow is termed Q_{base} and it is assumed to be positive when the flow leaves the surface water cell i.e. flowing from the surface water to the groundwater. An expression is needed to represent the q_{base} term in equation 3.16.

Flow between the surface water cell and the underlying groundwater cell is based on the difference between the heads in each cell. Darcy's Law (discussed in section 3.6) is used to obtain an expression for this flow, giving:

3.24

$$Q_{base} = \frac{K \cdot \Delta x \cdot \Delta y \cdot (\xi - h)}{L}$$

$$q_{base} = \frac{K(\xi - h)}{L}$$

where K is the saturated hydraulic conductivity (m/s) (section 3.6 for discussion), ξ and h are heads in the surface water cell and groundwater cell respectively (m), L is the distance over which the seepage is calculated and is taken as the distance from the base of the surface water cell to the centre of elevation of the groundwater cell. In the simplest case, a river is assumed to run directly on top of the underlying aquifer, in which case the K value is simply that of the aquifer at that point, and L is half the thickness of the aquifer layer. See Figure 3.4.

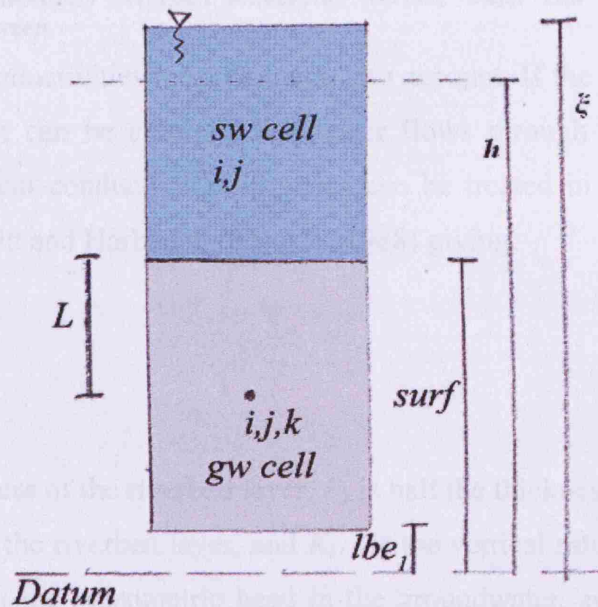


Figure 3.4: - Simple underlying aquifer schematic. A surface water cell is shown above a groundwater cell with no lower conductivity layer between them. lbe_1 is layer base elevation 1, and $surf$ is the ground surface elevation.

A more realistic situation is shown in Figure 3.5. A river bed will often have a conductivity

that is several orders of magnitude less than the underlying aquifer, due to the deposition of clays, silts, organic detritus and other materials deposited by the river. (Sophocleous et al. 1995; Calver 2001; Fox and Durnford 2003). The evaluation of the seepage through this layer to the aquifer below is slightly more complicated (Figure 3.5).

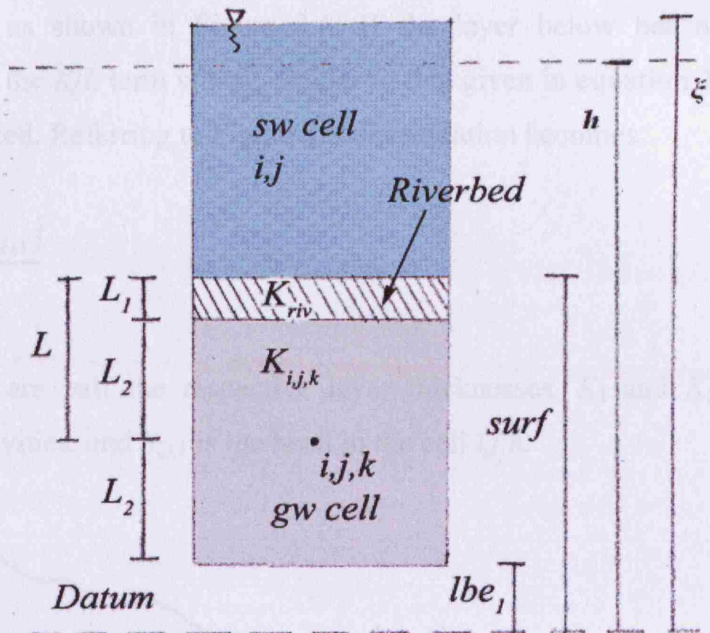


Figure 3.5: - Low permeability riverbed schematic. Surface water cell overlying aquifer with low conductivity layer in between.

Here two different conductivities must be taken into account. If the low conductivity layer is relatively thin, then it can be assumed that water flows through the layer in the vertical direction only. Different conductivities in series can be treated in a fashion similar to that described by McDonald and Harbaugh (Chap. 5, 1988) giving:

3.25

$$q_{base} = \frac{(\xi - h)}{\frac{L_{riv}}{K_{riv}} + \frac{L_2}{K_{i,j,k}}}$$

where L_1 is the thickness of the riverbed layer, L_2 is half the thickness of the aquifer layer, K_{riv} is the conductivity of the riverbed layer, and $K_{i,j,k}$ is the vertical saturated conductivity of the groundwater cell, h is the piezometric head in the groundwater, and ξ is the surface water elevation as shown in Figure 3.5.

3.4.2 Groundwater to Groundwater

The confined aquifer shown in Figure 3.3 has a confining layer of semi-permeable rock,

however, this could equally well be a ‘layer’ of groundwater; as the flow between layers is similarly related to the difference in the head. Using an unconfined aquifer for the top layer, ‘confined aquifer’ layers can be stacked up below, allowing variations in head, and permeability over the depth of the domain. For this situation, a new definition of q_{base} is needed. The L term in 3.24 now refers to the vertical distance between the centre of each groundwater cell as shown in Figure 3.6. If the layer below has a different hydraulic conductivity, then the K/L term will be similar to that given in equation 3.25, as two K values must be incorporated. Referring to Figure 3.6, the equation becomes:

3.26

$$q_{base} = \frac{(h_{i,j,k} - h_{i,j,k+1})}{\frac{L_1}{K_1} + \frac{L_2}{K_2}}$$

where L_1 and L_2 are half the respective layer thicknesses, K_1 and K_2 are the respective hydraulic conductivities, and $h_{i,j,k}$ is the head in the cell i,j,k .

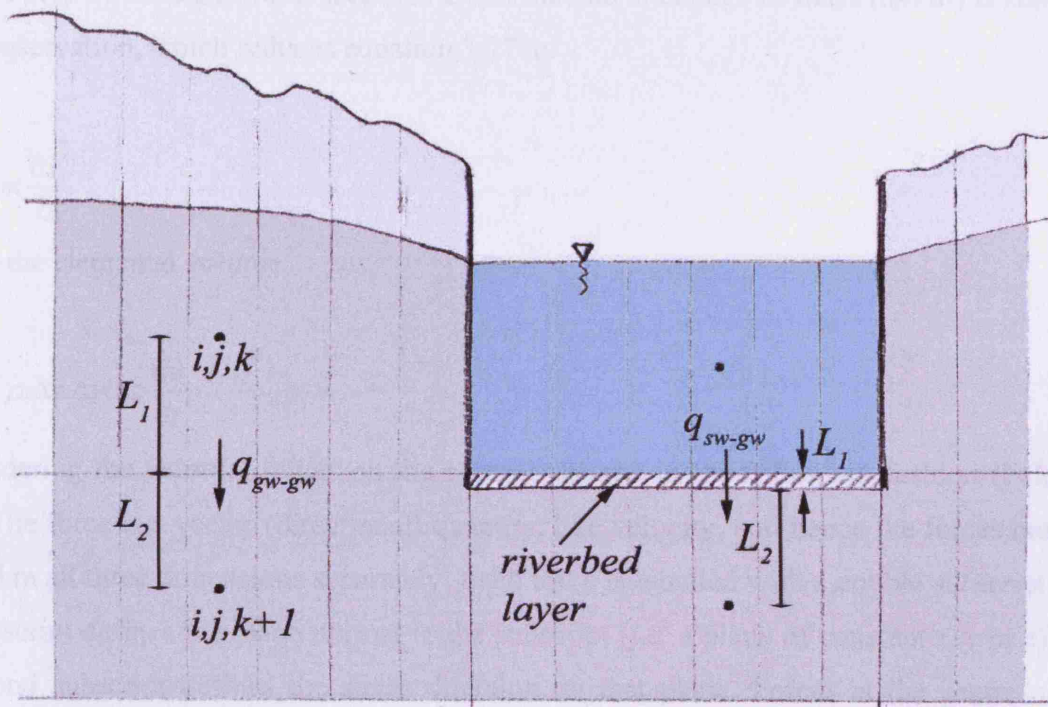


Figure 3.6: - Schematic for seepage between layers.

These terms are defined for the seepage to/from the base of the cell. When terms are included in the mass conservation equation, then seepage to/from the cell above must be included as well. This can be obtained from the seepage term calculated for the cell above. Note that the bottom layer is assumed to have an impermeable base, and so does not have seepage terms associated with it.

3.4.3 Summary

Three different types of seepage flow have been identified.

1. Surface Water straight to an aquifer layer (3.24).
2. Surface Water through a semi-permeable River-bed to an aquifer layer (3.25).
3. Flow from an aquifer layer to another aquifer layer (3.26).

3.5 Conservation of Momentum – Surface Water

Newton's second law of motion states that the sum of the external forces acting on a mass must equal the rate of change of linear momentum. Momentum is defined as mass multiplied by velocity. Therefore: -

3.27

$$\sum \vec{F} = \frac{d(m\vec{V})}{dt} = m \frac{\partial \vec{V}}{\partial t} + \vec{V} \frac{\partial m}{\partial t}$$

where F is a force vector, m is mass and V is velocity. If we consider an elemental volume as in Figure 3.7, we have shown in section 3.2 that the rate of change of mass (dm/dt) is zero, i.e. mass conservation, which reduces equation 3.27 to: -

3.28

$$\sum \vec{F} = m \frac{\partial \vec{V}}{\partial t}$$

And for the elemental volume

3.29

$$m \frac{\partial \vec{V}}{\partial t} = \rho \cdot \Delta x \cdot \Delta y \cdot \Delta z \frac{du}{dt}$$

In considering the external forces on the control volume in the following fashion (Falconer 1993). The force is a vector (directional) quantity, like velocity, and hence the forces must be resolved in all three dimensions separately. Each force is labelled with a double subscript. The first subscript defines the plane normal to the subscript (i.e. a plane of constant x , y or z), and the second subscript defines the stress direction on that plane. Forces at the centre of the volume are assigned as follows:

τ_{yx} , τ_{zx} (x-direction) τ_{xy} , τ_{zy} (y-direction) τ_{xz} , τ_{yz} (z-direction) shear forces

σ_{xx} , σ_{yy} , σ_{zz} tensile fluid stresses (normal stress) in x, y, z directions respectively

X , Y , Z - Body forces (e.g. gravity) per unit mass in x, y, z directions respectively

As with the continuity equation, Taylor's series can be used to expand these terms, in order to

evaluate the terms at the faces of the elemental volume. Figure 3.7 shows three of these expansions, with the other three faces being expanded in a similar manner.

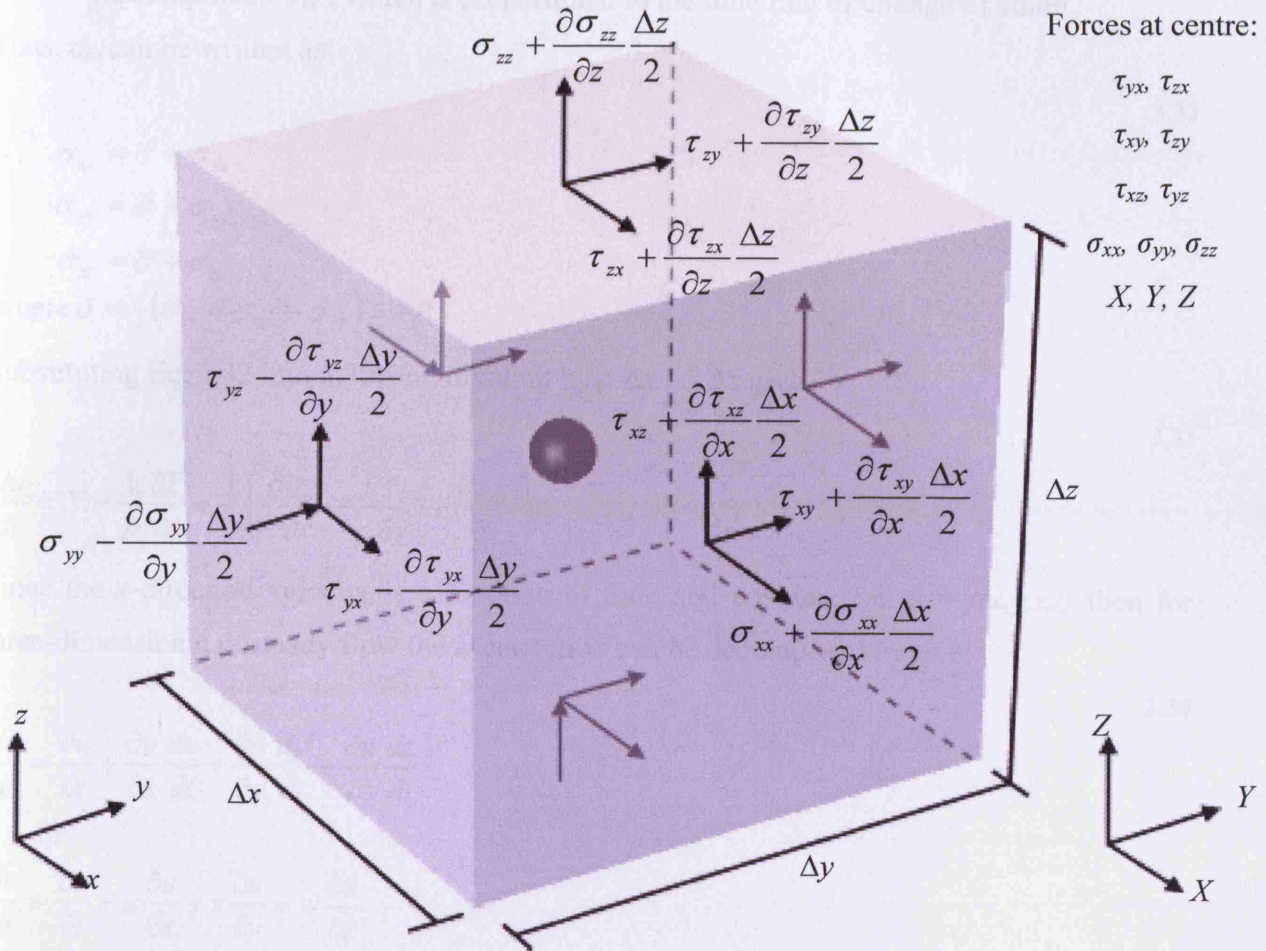


Figure 3.7: - Elemental volume showing forces acting at faces

Hence, the forces in the x -direction can be summed up as follows, using eq. 3.28 to give: -

3.30

$$\begin{aligned} \rho \Delta x \Delta y \Delta z \frac{du}{dt} = & \rho X \Delta x \Delta y \Delta z + \left[\left(\sigma_{xx} - \frac{\partial \sigma_{xx}}{\partial x} \frac{\Delta x}{2} \right) - \left(\sigma_{xx} + \frac{\partial \sigma_{xx}}{\partial x} \frac{\Delta x}{2} \right) \right] \Delta y \Delta z \\ & + \left[\left(\tau_{xy} - \frac{\partial \tau_{xy}}{\partial x} \frac{\Delta x}{2} \right) - \left(\tau_{xy} + \frac{\partial \tau_{xy}}{\partial x} \frac{\Delta x}{2} \right) \right] \Delta y \Delta z \\ & + \left[\left(\tau_{xz} - \frac{\partial \tau_{xz}}{\partial x} \frac{\Delta x}{2} \right) - \left(\tau_{xz} + \frac{\partial \tau_{xz}}{\partial x} \frac{\Delta x}{2} \right) \right] \Delta y \Delta z \end{aligned}$$

Reducing to:

3.31

$$\rho \Delta x \Delta y \Delta z \frac{du}{dt} = \rho X \Delta x \Delta y \Delta z + \frac{\partial \sigma_{xx}}{\partial x} \Delta x \Delta y \Delta z + \frac{\partial \tau_{xy}}{\partial y} \Delta x \Delta y \Delta z + \frac{\partial \tau_{xz}}{\partial z} \Delta x \Delta y \Delta z$$

The tensile fluid stress σ_{xx} is composed of two components:

- the hydrostatic pressure P , and
- the component σ'_{xx} , which is proportional to the time rate of change of strain.

Thus, σ_{xx} can be written as:

3.32

$$\sigma_{xx} = \bar{\sigma} + \sigma'_{xx}$$

$$\sigma_{yy} = \bar{\sigma} + \sigma'_{yy}$$

$$\sigma_{zz} = \bar{\sigma} + \sigma'_{zz}$$

$$\text{where } \bar{\sigma} = \frac{1}{3}(\sigma_{xx} + \sigma_{yy} + \sigma_{zz}) = -P$$

Substituting Eq. 3.32 into 3.30, and dividing by $\rho \cdot \Delta x \cdot \Delta y \cdot \Delta z$ gives: -

3.33

$$\frac{du}{dt} = X - \frac{1}{\rho} \frac{\partial P}{\partial x} + \frac{1}{\rho} \left(\frac{\partial \sigma'_{xx}}{\partial x} + \frac{\partial \tau_{yx}}{\partial y} + \frac{\partial \tau_{zx}}{\partial z} \right)$$

Since the x -direction velocity is a function of time and position, i.e. $u = f(x, y, z, t)$ then for three-dimensional unsteady flow the acceleration can be decomposed to give:

3.34

$$\frac{du}{dt} = \frac{\partial u}{\partial t} + \frac{\partial u}{\partial x} \frac{dx}{dt} + \frac{\partial u}{\partial y} \frac{dy}{dt} + \frac{\partial u}{\partial z} \frac{dz}{dt}$$

or

$$\frac{du}{dt} = \frac{\partial u}{\partial t} + u \frac{\partial u}{\partial x} + v \frac{\partial u}{\partial y} + w \frac{\partial u}{\partial z}$$

Combining Eq. 3.33 and 3.34 gives:

3.35

$$\frac{\partial u}{\partial t} + u \frac{\partial u}{\partial x} + v \frac{\partial u}{\partial y} + w \frac{\partial u}{\partial z} = X - \frac{1}{\rho} \frac{\partial P}{\partial x} + \frac{1}{\rho} \left(\frac{\partial \sigma'_{xx}}{\partial x} + \frac{\partial \tau_{yx}}{\partial y} + \frac{\partial \tau_{zx}}{\partial z} \right)$$

The tensile and shear stress terms can be represented as follows for laminar flow (Schlichting 1979; Falconer 1993).

3.36

$$\frac{\partial u}{\partial t} + u \frac{\partial u}{\partial x} + v \frac{\partial u}{\partial y} + w \frac{\partial u}{\partial z} = X - \frac{1}{\rho} \frac{\partial P}{\partial x} + \nu \left(\frac{\partial^2 u}{\partial x^2} + \frac{\partial^2 u}{\partial y^2} + \frac{\partial^2 u}{\partial z^2} \right)$$

where ν is the kinematic viscosity of the fluid.

For turbulent flow, the velocities can be considered as having a temporal average velocity component and a fluctuating velocity component (Schlichting 1979) and treating the velocities in this way, the instantaneous momentum equation can be time averaged to give:

3.37

$$\frac{\partial \bar{u}}{\partial t} + \bar{u} \frac{\partial \bar{u}}{\partial x} + \bar{v} \frac{\partial \bar{u}}{\partial y} + \bar{w} \frac{\partial \bar{u}}{\partial z} =$$

$$X - \frac{1}{\rho} \frac{\partial P}{\partial x} + \frac{\partial}{\partial x} \left(\nu \frac{\partial \bar{u}}{\partial x} + \varepsilon \left[2 \frac{\partial \bar{u}}{\partial x} \right] \right) + \frac{\partial}{\partial y} \left(\nu \frac{\partial \bar{u}}{\partial y} + \varepsilon \left[\frac{\partial \bar{u}}{\partial y} + \frac{\partial \bar{v}}{\partial x} \right] \right) + \frac{\partial}{\partial z} \left(\nu \frac{\partial \bar{u}}{\partial z} + \varepsilon \left[\frac{\partial \bar{u}}{\partial z} + \frac{\partial \bar{w}}{\partial x} \right] \right)$$

where $\bar{u}, \bar{v}, \bar{w}$ are the time averaged velocity components in the x, y, z directions respectively.

For convenience herein after the overbar will be dropped and the time average velocity components expressed as u, v , and w . ε is the eddy viscosity.

This equation for two dimensional turbulent flow can be integrated over the depth (b).

Assuming that $\varepsilon \gg \nu$ and following Falconer (1993) we can arrive at the following:

3.38

$$\frac{\partial Ub}{\partial t} + \frac{\partial \beta U^2 b}{\partial x} + \frac{\partial \beta UV b}{\partial y} = \Omega V b - gb \frac{\partial \xi}{\partial x} - \frac{b}{\rho} \frac{\partial P_a}{\partial x} + \varepsilon b \left[2 \frac{\partial^2 U}{\partial x^2} + \frac{\partial^2 U}{\partial y^2} + \frac{\partial^2 V}{\partial x \partial y} \right] + fW_x - \frac{gU \sqrt{U^2 + V^2}}{C^2}$$

Recalling that $uh = p$ and $vh = q$, or flow per unit width in the x and y directions respectively, we can arrive at the 2-D momentum equations used in DIVAST.

3.39

i) x - direction

$$\frac{\partial p}{\partial t} + \frac{\partial \beta p U}{\partial x} + \frac{\partial \beta p V}{\partial y} + gb \frac{\partial \xi}{\partial x} + \frac{gp \sqrt{p^2 + q^2}}{C^2 b^2} - \varepsilon \left[2 \frac{\partial^2 p}{\partial x^2} + \frac{\partial^2 p}{\partial y^2} + \frac{\partial^2 q}{\partial x \partial y} \right] - \Omega q - fW_x + \frac{b}{\rho} \frac{\partial P_a}{\partial x} = 0$$

ii) y - direction

$$\frac{\partial q}{\partial t} + \frac{\partial \beta q U}{\partial x} + \frac{\partial \beta q V}{\partial y} + gb \frac{\partial \xi}{\partial y} + \frac{gq \sqrt{p^2 + q^2}}{C^2 b^2} - \varepsilon \left[\frac{\partial^2 q}{\partial x^2} + 2 \frac{\partial^2 q}{\partial y^2} + \frac{\partial^2 p}{\partial x \partial y} \right] - \Omega p - fW_y + \frac{b}{\rho} \frac{\partial P_a}{\partial y} = 0$$

where p is flow in the x direction per unit width or bU , q is flow in the y direction per unit width or bV , β is the momentum correction factor to correct for non-uniform velocity distribution, U is the velocity in the x direction, V is the velocity in the y direction, b is the depth of the water column, g is the acceleration due to gravity, ξ is the elevation of the water surface above datum, C is the Chezy roughness coefficient, ρ is density of the fluid, ε is the eddy viscosity, fW_i is a function of the wind speed in the i -direction, P_a is the atmospheric pressure.

3.6 Conservation of Momentum – Groundwater – Darcy's Law

3.6.1 Unconfined Aquifer

The second equation used to solve the groundwater flow process can be derived

mathematically from first principles (Bear 1972, Chap. 4) as part of the basic governing equation for fluid motion through porous media. The full derivation is detailed and complex, however, a simplified form is known as Darcy's experimental law. Darcy conducted various experiments in 1856 related to the fountains of Dijon, France (Darcy 1856), from which he concluded that the rate of flow through a porous medium is proportional to the gradient of the piezometric head, and the cross-sectional area of flow. The famous Darcy formula summarises this as follows:

3.40

$$Q = -\frac{K.A.(h_2 - h_1)}{\Delta x} \quad \text{or} \quad Q = -K.A.\frac{\partial h}{\partial x}$$

where Q is the rate of flow (L^3T^{-1}), K is a coefficient of proportionality with units of speed (LT^{-1}), A is the cross-sectional area of flow (L^2), h is the piezometric head in the medium (L), and $(h_1 - h_2)$ is the difference in head across a distance Δx (L). Note that Q is positive when h_1 is greater than h_2 , i.e. the hydraulic slope is downward from point 1 to point 2.

K is usually known as the *hydraulic conductivity* or *coefficient of permeability*. This is a function of the properties of the fluid and the solid matrix, and describes "the ease with which a fluid is transported through a porous matrix" (Bear 1972). This is different from *intrinsic permeability* which is solely a function of the properties of the solid matrix. In this study only the saturated hydraulic conductivity is considered i.e. the conductivity when the porous media is fully saturated by the fluid.

Darcy's law can be used to describe the movement of groundwater as shown. Rearranging Eq. 3.40 and using the x -direction as an example gives:

3.41

$$Q_x = -K.A.\frac{\partial h}{\partial x} = -K.\Delta y.b_{av}.\frac{\partial h}{\partial x} \approx -K.\Delta y.b_{av}.\frac{(h_2 - h_1)}{\Delta x}$$

$$A = \Delta y.b_{av}$$

$$q_x = \frac{Q_x}{\Delta y} = -\frac{K.b_{av}.(h_2 - h_1)}{\Delta x}$$

$$q_x + \frac{K.b_{av}.(h_2 - h_1)}{\Delta x} = 0$$

Where q_x is flow per unit width in the x -direction, as before. Δx and Δy are cell dimensions in the x and y directions respectively, b_{av} is the average depth of flow over the distance in question, calculated as $0.5(b_1 + b_2)$, and the other terms have the same meaning as given previously. Figure 3.8 shows the notation used in a diagram. Note: with an unconfined aquifer, h (head) could be used to calculate the gradient just as well as ζ (water surface

elevation). This is **not** true with a confined aquifer, as the depth/water elevation is restricted, but the pressure head can increase above the confining layer as the pressure rises. Care should be taken to avoid confusion of the three terms b (the depth of water considered), h (the piezometric pressure head of the water considered above a datum), and ζ (water surface elevation above a datum). Figure 3.8 and Figure 3.9 illustrate the difference.

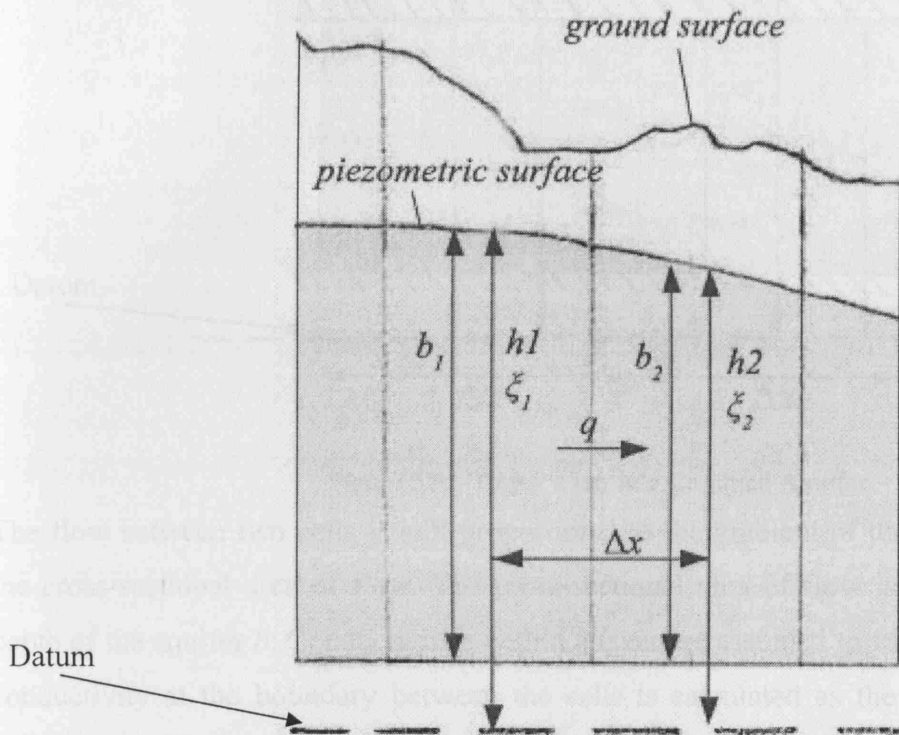


Figure 3.8: - Schematic for Darcy's Law

Eq. 3.41 can be rearranged to a form similar to the surface water momentum equation to give the x and y -direction equations:

3.42

$$\begin{aligned} \text{a) } x\text{-direction} \quad p + K_x b_{av} \frac{(h_2 - h_1)}{\Delta x} &= 0 \\ \text{b) } y\text{-direction} \quad q + K_y b_{av} \frac{(h_2 - h_1)}{\Delta y} &= 0 \end{aligned}$$

Note that these equations assume that the conductivity is the same between the cells. For situations where the conductivity varies over a layer then the formulation is modified as given below.

3.6.2 Confined Aquifer

With a confined aquifer, the water elevation is limited by a confining layer, whereas the head can increase above the aquifer top. Hence, h (head) is **no longer** equivalent to ζ (water surface elevation), as illustrated in Figure 3.9.

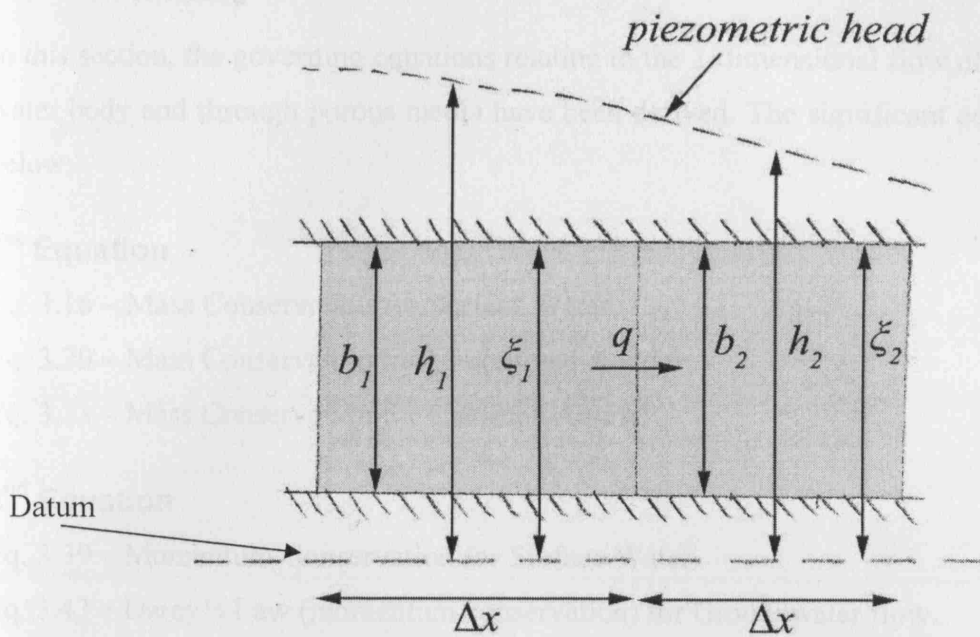


Figure 3.9: - Darcy's law in a Confined Aquifer

The flow between two cells is still proportional to the gradient of the piezometric head, and the cross-sectional area of flow. The cross-sectional area of flow is now dependent on the depth of the aquifer b . Conductivities within a layer are assumed to vary smoothly, so that the conductivity at the boundary between the cells is calculated as the average of each cells' individual conductivity (the conductivity of each cell is defined at its centre) rather than the more complex series conductivity calculation (as used between separate layers).

Thus the corresponding equation for the x -direction flow is given by:

3.43

$$q_x = \frac{Q_x}{\Delta y} = -\frac{K_{av} b_{av} (h_2 - h_1)}{\Delta x}$$

$$K_{av} = \frac{K_1 + K_2}{2} \quad b_{av} = \frac{b_1 + b_2}{2}$$

where b_1 and b_2 are the depths of the aquifer in the respective cells, and K_1 and K_2 are hydraulic conductivities. A similar formulation is given for flow in the y -direction.

3.7 Summary

In this section, the governing equations relating to the 2-dimensional flow of fluids in an open water body and through porous media have been derived. The significant equations are listed below:

1st Equation

Eq. 3.16 – Mass Conservation for Surface Water.

Eq. 3.20 – Mass Conservation for Unconfined Aquifer.

Eq. 3.23 – Mass Conservation for Confined Aquifer.

2nd Equation

Eq. 3.39 – Momentum Conservation for Surface Water.

Eq. 3.43 – Darcy's Law (momentum conservation) for Groundwater flow.

Seepage Flow

Eq. 3.24 - Surface Water straight to the aquifer layer.

Eq. 3.25 - Surface Water through semi-permeable river-bed to aquifer layer.

Eq. 3.26 - Flow from an aquifer layer to another aquifer layer.

CHAPTER 4 FINITE DIFFERENCE SCHEME AND EQUATION DISCRETISATION

4.1 *Model Overview*

In order to model a body of water, the following must be known:

- the size and shape of the region of flow,
- the equation of flow within the region,
- the boundary conditions around the boundaries of the region,
- the initial conditions in the region,
- the spatial distribution of the hydrogeologic or hydrologic parameters that control the flow,
- a numerical method of solution.

(Freeze and Cherry 1979, p67)

The size and shape of the region, the boundary conditions, initial conditions, and hydrologic parameters are all defined in the model input file to the model. The equations of flow have been derived in the previous chapter, but they must now be adapted for use in a computer simulation, using a numerical method of solution. The main equations to be solved are summarised here.

1st Equation (Mass Conservation)

Eq. 3.16 – Mass Conservation for Surface Water.

Eq. 3.20 – Mass Conservation for Unconfined Aquifer.

Eq. 3.23 – Mass Conservation for Confined Aquifer.

2nd Equation

Eq. 3.39 – Momentum Conservation for Surface Water.

Eq. 3.43 – Darcy's Law for Groundwater flow.

Seepage Flow

Eq. 3.24 - Surface Water straight to the aquifer layer.

Eq. 3.25 - Surface Water through semi-permeable river-bed to aquifer layer.

Eq. 3.26 - Flow from an aquifer layer to another aquifer layer.

The numerical model operates by dividing the area to be modelled into a grid, and the above equations are solved for each grid cell. Each cell in the domain is assigned values that represent the conditions at that point. In DIVAST, each grid cell is square, i.e. Δx and Δy are the same. The cell-size must be small enough to allow the model domain to be represented accurately in square cells. The larger the cell-size, the more approximate the values for each cell become, with each cell covering a larger area. Also, the Taylor's series expansion in Eq. 3.3 assumes that Δx is small – the larger the cell size, the less valid this assumption. Smaller cell-sizes make for more accurate models, but this also increases the number of simultaneous equations to be solved, meaning the model will take much longer to run.

In the original 2-D surface water model, each grid cell extends downwards throughout the depth of the water column; parameters calculated for each cell are assumed not to vary over the depth of the water column. This is still true in the extended versions of the model, but additional layers can be used to allow conditions to vary over the depth of the model.

The above equations must therefore be divided up in time and space; this process is called discretisation – taking the continuous equations and forming discrete segments in time (timestep, Δt) and space (grid-size, Δx , Δy). To refer to any point in space in our model we can use the indices i , j , and k to refer to the position in the x , y and z -direction (vertical) respectively. The surface layer of the model is assumed to be $k=1$ and layers are numbered from the top down. The position in time is cited in terms of n .

4.2 Equation Discretisation

There are many different techniques for solving a large grid of equations, and each scheme requires a slightly different discretisation. DIVAST uses the Alternating Direction Implicit (ADI) scheme developed by Peaceman and Rachford (Peaceman and Rachford-Jr. 1955).

This scheme uses a ‘double-sweep’ algorithm to solve efficiently the simultaneous equations. The principle timestep is divided into two, half for the ‘x’ sweep, and half for the ‘y’ sweep. In the first half-timestep, the water elevation ζ^{n+1} and flow in x-direction p^{n+1} are solved, using the previously calculated flow in the y-direction $q^{n+1/2}$. In the second half-timestep, using the value of p^{n+1} , the water elevation $\zeta^{n+3/2}$ and the flow in y-direction $q^{n+3/2}$ are calculated (Figure 4.1).

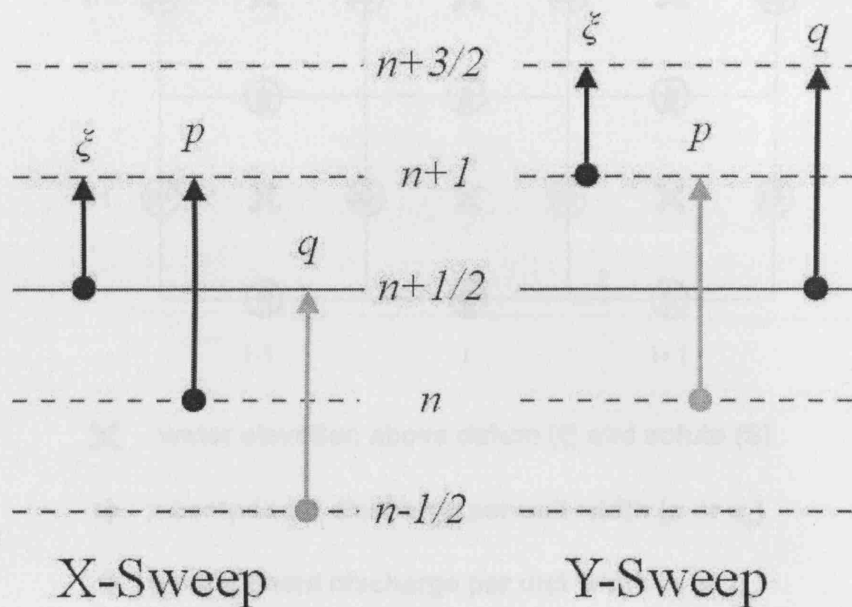


Figure 4.1: - ADI method. The grey variable is known (from previous timestep)

The area to be modelled is divided into cells, with the key variables referencing different parts of each cell as shown in Figure 4.2.

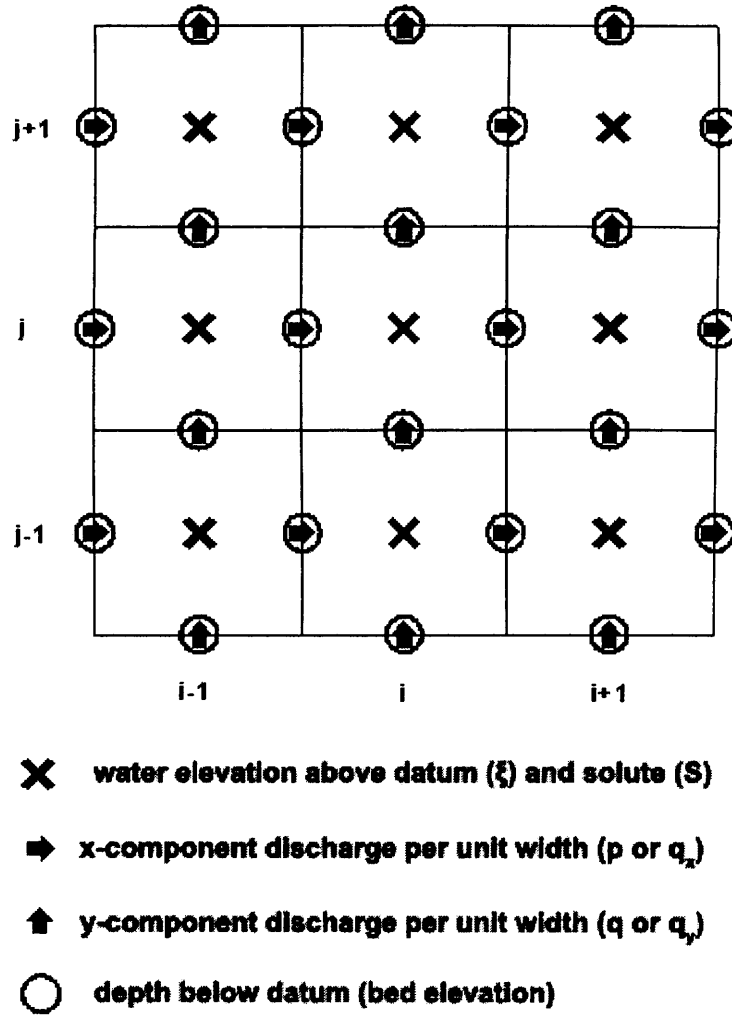


Figure 4.2: - Finite difference staggered grid. Adapted from Falconer et. al (2001a).

The ADI scheme is time-centred and theoretically has no stability constraints. However, to achieve reasonable computational accuracy, the time-step needs to be restricted in relation to the grid-size. A maximum Courant number for the ADI method has been suggested by (Stelling et al. 1986):

4.1

$$C = 2\Delta t \sqrt{gh \left(\frac{1}{\Delta x^2} + \frac{1}{\Delta y^2} \right)} \leq 4\sqrt{2}$$

where g is the acceleration due to gravity (m/s^2), Δx , Δy , and Δt are grid sizes and the time-step, and h is the average depth of flow.

If Δx and Δy are the same (square grid cells) then this equation can be reduced to:

4.2

$$\Delta t \leq \frac{2\Delta x}{\sqrt{gh}}$$

This expression can be used as a guideline for determining an appropriate timestep for a model, given the grid size and average depth of flow. From experience in running the model, timesteps significantly greater than this may be used, but at the risk of unpredictable stability issues, especially at boundaries – these do not always occur, but if so, they can usually be resolved by reducing the timestep to below the suggested number.

4.2.1 Mass Conservation Equations

Surface Water

The surface water mass conservation equation can be discretised as follows, using Eq. 3.16 (the continuity equation) as a starting point. Bold terms are unknown at the current timestep.

4.3:

x-sweep mass conservation equation

$$\frac{\partial \xi}{\partial t} + \frac{\partial p}{\partial x} + \frac{\partial q}{\partial y} + q_{base} = 0$$

$$\left(\frac{\xi_{i,j}^{n+1} - \xi_{i,j}^{n+1/2}}{0.5\Delta t} \right) + \left(\frac{\mathbf{p}_{i+\frac{1}{2},j}^{n+1} - \mathbf{p}_{i-\frac{1}{2},j}^{n+1}}{\Delta x} \right) + \left(\frac{q_{i,j+\frac{1}{2}}^{n+\frac{1}{2}} - q_{i,j-\frac{1}{2}}^{n+\frac{1}{2}}}{\Delta y} \right) + q_{base} = 0$$

$$\xi_{i,j}^{n+1} + \frac{1}{2} \frac{\Delta t}{\Delta x} \mathbf{p}_{i+\frac{1}{2},j}^{n+1} - \frac{1}{2} \frac{\Delta t}{\Delta x} \mathbf{p}_{i-\frac{1}{2},j}^{n+1} = \xi_{i,j}^{n+1/2} - \frac{\Delta t}{2} \left(\frac{q_{i,j+\frac{1}{2}}^{n+\frac{1}{2}} - q_{i,j-\frac{1}{2}}^{n+\frac{1}{2}}}{\Delta y} \right) - \frac{\Delta t}{2} q_{base}$$

4.4

y-sweep mass conservation equation

$$\frac{\partial \xi}{\partial t} + \frac{\partial p}{\partial x} + \frac{\partial q}{\partial y} + q_{base} = 0$$

$$\left(\frac{\xi_{i,j}^{n+3/2} - \xi_{i,j}^{n+1}}{0.5\Delta t} \right) + \left(\frac{p_{i+\frac{1}{2},j}^{n+1} - p_{i-\frac{1}{2},j}^{n+1}}{\Delta x} \right) + \left(\frac{\mathbf{q}_{i,j+\frac{1}{2}}^{n+3/2} - \mathbf{q}_{i,j-\frac{1}{2}}^{n+3/2}}{\Delta y} \right) + q_{base} = 0$$

$$\xi_{i,j}^{n+3/2} + \frac{1}{2} \frac{\Delta t}{\Delta y} \mathbf{q}_{i,j+\frac{1}{2}}^{n+3/2} - \frac{1}{2} \frac{\Delta t}{\Delta y} \mathbf{q}_{i,j-\frac{1}{2}}^{n+3/2} = \xi_{i,j}^{n+1} - \frac{\Delta t}{2} \left(\frac{p_{i+\frac{1}{2},j}^{n+1} - p_{i-\frac{1}{2},j}^{n+1}}{\Delta x} \right) - \frac{\Delta t}{2} q_{base}$$

4.5

Summary of Surface Water Mass Conservation Discretisation

$$\begin{aligned}
A\mathbf{p}_{i-1/2}^{n+1} + B\xi_i^{n+1} + C\mathbf{p}_{i+1/2}^{n+1} &= D_x \\
A\mathbf{q}_{j-1/2}^{n+3/2} + B\xi_j^{n+3/2} + C\mathbf{q}_{j+1/2}^{n+3/2} &= D_y \\
\text{where} \\
A = -C &= -\frac{1}{2} \frac{\Delta t}{\Delta x} \\
B &= 1 \\
D_x &= \xi_{i,j}^{n+1/2} - \frac{\Delta t}{2} \left(\frac{q_{i,j+1/2}^{n+1/2} - q_{i,j-1/2}^{n+1/2}}{\Delta y} \right) - \frac{\Delta t}{2} q_{base} \\
D_y &= \xi_{i,j}^{n+1} - \frac{\Delta t}{2} \left(\frac{p_{i+1/2,j}^{n+1} - p_{i-1/2,j}^{n+1}}{\Delta x} \right) - \frac{\Delta t}{2} q_{base}
\end{aligned}$$

Groundwater Mass Conservation

Starting with Eq. 3.23, then the x -sweep mass conservation equation for groundwater can be written as:

4.6

$$\begin{aligned}
S \cdot \frac{\partial h}{\partial t} + \frac{\partial p}{\partial x} + \frac{\partial q}{\partial y} - q_{top} + q_{base} &= 0 \\
S \cdot \left(\frac{\mathbf{h}_{i,j}^{n+1} - h_{i,j}^{n+1/2}}{0.5\Delta t} \right) + \left(\frac{\mathbf{p}_{i+1/2,j}^{n+1} - \mathbf{p}_{i-1/2,j}^{n+1}}{\Delta x} \right) + \left(\frac{q_{i,j+1/2}^{n+1/2} - q_{i,j-1/2}^{n+1/2}}{\Delta y} \right) - q_{top} + q_{base} &= 0 \\
S \cdot \mathbf{h}_{i,j}^{n+1} + \frac{1}{2} \frac{\Delta t}{\Delta x} \mathbf{p}_{i+1/2,j}^{n+1} - \frac{1}{2} \frac{\Delta t}{\Delta x} \mathbf{p}_{i-1/2,j}^{n+1} &= S \cdot h_{i,j}^{n+1/2} - \frac{\Delta t}{2} \left(\frac{q_{i,j+1/2}^{n+1/2} - q_{i,j-1/2}^{n+1/2}}{\Delta y} \right) + \frac{\Delta t}{2} q_{top} - \frac{\Delta t}{2} q_{base}
\end{aligned}$$

Likewise the y -sweep mass conservation equation for groundwater becomes:

4.7

$$\begin{aligned}
S \cdot \frac{\partial h}{\partial t} + \frac{\partial p}{\partial x} + \frac{\partial q}{\partial y} - q_{gw} &= 0 \\
S \cdot \left(\frac{\mathbf{h}_{i,j}^{n+3/2} - h_{i,j}^{n+1}}{0.5\Delta t} \right) + \left(\frac{p_{i+1/2,j}^{n+1} - p_{i-1/2,j}^{n+1}}{\Delta x} \right) + \left(\frac{\mathbf{q}_{i,j+1/2}^{n+3/2} - \mathbf{q}_{i,j-1/2}^{n+3/2}}{\Delta y} \right) - q_{top} + q_{base} &= 0 \\
S \cdot \mathbf{h}_{i,j}^{n+3/2} + \frac{1}{2} \frac{\Delta t}{\Delta y} \mathbf{q}_{i,j+1/2}^{n+3/2} - \frac{1}{2} \frac{\Delta t}{\Delta y} \mathbf{q}_{i,j-1/2}^{n+3/2} &= S \cdot h_{i,j}^{n+1} - \frac{\Delta t}{2} \left(\frac{p_{i+1/2,j}^{n+1} - p_{i-1/2,j}^{n+1}}{\Delta x} \right) + \frac{\Delta t}{2} q_{top} - \frac{\Delta t}{2} q_{base}
\end{aligned}$$

where S refers to the storage term (n ; porosity for unconfined aquifers, and $S_s \cdot b_{ij}$; specific storage coefficient multiplied by the aquifer depth for confined aquifers. See Eqs. 3.20 and 3.23)

4.8

Summary of Groundwater Mass Conservation Discretisation

$$\begin{aligned}
A^* \mathbf{p}_{i-1/2}^{n+1} + B^* \mathbf{h}_i^{n+1} + C^* \mathbf{p}_{i+1/2}^{n+1} &= D_x^* \\
A^* \mathbf{q}_{j-1/2}^{n+3/2} + B^* \mathbf{h}_j^{n+3/2} + C^* \mathbf{q}_{j+1/2}^{n+3/2} &= D_y^* \\
\text{where} \\
A^* = -C^* &= -\frac{1}{2} \frac{\Delta t}{\Delta x} \\
B^* &= S \\
D_x^* &= S \cdot h_{i,j}^{n+1/2} - \frac{\Delta t}{2} \left(\frac{q_{i,j+1/2}^{n+1/2} - q_{i,j-1/2}^{n+1/2}}{\Delta y} \right) + \frac{\Delta t}{2} q_{top} - \frac{\Delta t}{2} q_{base} \\
D_y^* &= S \cdot h_{i,j}^{n+1} - \frac{\Delta t}{2} \left(\frac{p_{i+1/2,j}^{n+1} - p_{i-1/2,j}^{n+1}}{\Delta x} \right) + \frac{\Delta t}{2} q_{top} - \frac{\Delta t}{2} q_{base}
\end{aligned}$$

where for an unconfined aquifer $S = n_{i,j,k}$ and for a confined aquifer $S = S_{i,j,k} \cdot b_{i,j,k}$

4.2.2 Momentum Conservation**Surface Water**

The momentum equations in the x and y directions are discretised as follows, starting with Eq. 3.39 (see APPENDIX B for detailed discretisation), giving the difference equation (with bold symbols referring to unknown values):

4.9

$$\begin{aligned}
&\left(\frac{\mathbf{p}_{i+1/2,j}^{n+1} - p_{i+1/2,j}^n}{\Delta t} \right) + \frac{\beta}{4\Delta x} \left[(p_{i+3/2}^n + p_{i+1/2}^n)(U_{i+3/2}^n + U_{i+1/2}^n) - (p_{i+1/2}^n + p_{i-1/2}^n)(U_{i+1/2}^n + U_{i-1/2}^n) \right] \\
&+ \frac{\beta}{2\Delta y} \left[(q_{i+1,j+1/2}^{n+1/2} + q_{i,j+1/2}^{n+1/2})U_{i+1/2,j}^n - (q_{i+1,j-1/2}^{n+1/2} + q_{i,j-1/2}^{n+1/2})U_{i+1/2,j}^n \right] \\
&+ \frac{g}{2\Delta x} \cdot (b_{i+1/2,j}^n)(\xi_{i+1}^{n+1} - \xi_i^{n+1} + \xi_{i+1}^{n+1/2} - \xi_i^{n+1/2}) \\
&+ \frac{g(p_{i+1/2,j}^{n+1} + p_{i+1/2,j}^n)}{2} \cdot \frac{\sqrt{(p_{i+1/2,j}^{n+1/2})^2 + (q_{i+1/2,j}^{n+1/2})^2}}{(C_{i+1/2,j}^n)^2 (b_{i+1/2,j}^n)^2} \\
&- \frac{\varepsilon b_{i+1/2,j}^{n+1/2}}{\Delta x^2} \left[2(\hat{U}_{i+3/2,j}^n + \hat{U}_{i-1/2,j}^n) + \hat{U}_{i+1/2,j+1}^n + \hat{U}_{i+1/2,j-1}^n \right. \\
&\left. - 6\hat{U}_{i+1/2,j}^n + V_{i,j-1/2}^n - V_{i,j+1/2}^n - V_{i+1,j-1/2}^n + V_{i+1,j+1/2}^n \right] - \Omega q_{i+1/2,j}^{n+1/2} - \frac{\rho_a}{\rho} C_e W^2 \cos \psi = 0
\end{aligned}$$

Re-arranging to give in terms of the unknown values gives:

4.10

$$\begin{aligned}
& -\xi_i^{n+1} \frac{g \cdot \Delta t \cdot b_{i+1/2,j}^{n+1/2}}{2\Delta x} + \mathbf{p}_{i+1/2,j}^{n+1} \left(1 + \frac{g\Delta t}{2} \cdot \frac{\sqrt{(p_{i+1/2,j}^{n+1/2})^2 + (q_{i+1/2,j}^{n+1/2})^2}}{(C_{i+1/2,j}^n)^2 (b_{i+1/2,j}^n)^2} \right) + \xi_{i+1}^{n+1} \frac{g \cdot \Delta t \cdot b_{i+1/2,j}^{n+1/2}}{2\Delta x} \\
& = p_{i+1/2,j}^n - \frac{\beta \Delta t}{4\Delta x} [(p_{i+3/2}^n + p_{i+1/2}^n)(U_{i+3/2}^n + U_{i+1/2}^n) - (p_{i+1/2}^n + p_{i-1/2}^n)(U_{i+1/2}^n + U_{i-1/2}^n)] - \\
& \quad \frac{\beta \Delta t}{2\Delta y} [(q_{i+1,j+1/2}^{n+1/2} + q_{i,j+1/2}^{n+1/2})U_{i+1/2,j}^n - (q_{i+1,j-1/2}^{n+1/2} + q_{i,j-1/2}^{n+1/2})U_{i+1/2,j}^n] - \\
& \quad \frac{g\Delta t}{2\Delta x} (b_{i+1/2,j}^n)(\xi_{i+1}^{n+1/2} - \xi_i^{n+1/2}) + \frac{\varepsilon \Delta t b_{i+1/2,j}^{n+1/2}}{\Delta x^2} [2(\hat{U}_{i+3/2,j}^n + \hat{U}_{i-1/2,j}^n) + \hat{U}_{i+1/2,j+1}^n + \hat{U}_{i+1/2,j-1}^n \\
& \quad - 6\hat{U}_{i+1/2,j}^n + V_{i,j-1/2}^n - V_{i,j+1/2}^n - V_{i+1,j-1/2}^n + V_{i+1,j+1/2}^n] - \frac{g\Delta t (p_{i+1/2,j}^n)}{2} \cdot \frac{\sqrt{(p_{i+1/2,j}^{n+1/2})^2 + (q_{i+1/2,j}^{n+1/2})^2}}{(C_{i+1/2,j}^n)^2 (b_{i+1/2,j}^n)^2} \\
& \quad + \Omega \Delta t q_{i+1/2,j}^{n+1/2} + \Delta t \frac{\rho_a}{\rho} C_e W^2 \cos \psi
\end{aligned}$$

And for the second sweep in the y-direction:

4.11

$$\begin{aligned}
& \left(\frac{\mathbf{q}_{i,j+1/2}^{n+3/2} - q_{i,j+1/2}^{n+1/2}}{\Delta t} \right) + \frac{\beta}{2\Delta x} [(p_{i+1/2,j+1}^{n+1} + p_{i+1/2,j}^{n+1})V_{i,j+1/2}^{n+1/2} - (p_{i-1/2,j+1}^{n+1} + p_{i-1/2,j}^{n+1})V_{i,j+1/2}^{n+1/2}] \\
& \quad + \frac{\beta}{4\Delta y} [(q_{j+3/2}^{n+1} + q_{j+1/2}^{n+1})(V_{j+3/2}^{n+1} + V_{j+1/2}^{n+1}) - (q_{j+1/2}^{n+1} + q_{j-1/2}^{n+1})(V_{j+1/2}^{n+1} + V_{j-1/2}^{n+1})] \\
& \quad + \frac{g}{2\Delta x} (b_{i,j+1/2}^{n+1})(\mathbf{h}_{j+1}^{n+1} - \mathbf{h}_j^{n+1} + h_{j+1}^{n+1/2} - h_j^{n+1/2}) \\
& \quad + \frac{g(\mathbf{q}_{i,j+1/2}^{n+3/2} + q_{i,j+1/2}^{n+1/2})}{2} \cdot \frac{\sqrt{(p_{i,j+1/2}^{n+1})^2 + (q_{i,j+1/2}^{n+1})^2}}{(C_{i,j+1/2}^{n+1})^2 (b_{i,j+1/2}^{n+1})^2} \\
& \quad - \frac{\varepsilon b_{i,j+1/2}^{n+1}}{\Delta y^2} [2(\hat{V}_{i+3/2,j}^{n+1} + \hat{V}_{i,j-1/2}^{n+1}) + \hat{V}_{i+1,j+1/2}^{n+1} + \hat{V}_{i-1,j+1/2}^{n+1} \\
& \quad - 6\hat{V}_{i,j+1/2}^{n+1} + U_{i-1/2,j}^{n+1} - U_{i+1/2,j}^{n+1} - U_{i-1/2,j+1}^{n+1} + U_{i+1/2,j+1}^{n+1}] - \Omega p_{i,j+1/2}^{n+1} - \frac{\rho_a}{\rho} C_e W^2 \cos \psi = 0
\end{aligned}$$

Isolating the unknown terms again gives:

4.12

$$\begin{aligned}
& -\xi_j^{n+3/2} \frac{g \cdot \Delta t \cdot b_{i,j+1/2}^{n+1}}{2\Delta x} + q_{i,j+1/2}^{n+3/2} \left(1 + \frac{g\Delta t}{2} \cdot \frac{\sqrt{(p_{i,j+1/2}^{n+1})^2 + (q_{i,j+1/2}^{n+1})^2}}{(C_{i,j+1/2}^{n+1})^2 (b_{i,j+1/2}^{n+1})^2} \right) + \xi_{j+1}^{n+3/2} \frac{g \cdot \Delta t \cdot b_{i,j+1/2}^{n+1}}{2\Delta x} \\
& = q_{i,j+1/2}^{n+1/2} - \frac{\beta}{2\Delta x} [(p_{i+1/2,j+1}^{n+1} + p_{i+1/2,j}^{n+1})V_{i,j+1/2}^{n+1/2} - (p_{i-1/2,j+1}^{n+1} + p_{i-1/2,j}^{n+1})V_{i,j+1/2}^{n+1/2}] - \\
& \quad \frac{\beta}{4\Delta y} [(q_{j+3/2}^{n+1} + q_{j+1/2}^{n+1})(V_{j+3/2}^{n+1} + V_{j+1/2}^{n+1}) - (q_{j+1/2}^{n+1} + q_{j-1/2}^{n+1})(V_{j+1/2}^{n+1} + V_{j-1/2}^{n+1})] - \\
& \quad \frac{g\Delta t}{2\Delta x} (b_{i,j+1/2}^{n+1})(\xi_{j+1}^{n+1} - \xi_j^{n+1}) + \frac{\varepsilon\Delta t b_{i,j+1/2}^{n+1}}{\Delta x^2} [2(\hat{V}_{i+3/2,j}^{n+1} + \hat{V}_{i,j-1/2}^{n+1}) + \hat{V}_{i+1,j+1/2}^{n+1} + \hat{V}_{i-1,j+1/2}^{n+1} \\
& \quad - 6\hat{V}_{i,j+1/2}^{n+1} + U_{i-1/2,j}^{n+1} - U_{i+1/2,j}^{n+1} - U_{i-1/2,j+1}^{n+1} + U_{i+1/2,j+1}^{n+1}] - \frac{g\Delta t (q_{i,j+1/2}^{n+1})}{2} \cdot \frac{\sqrt{(p_{i,j+1/2}^{n+1})^2 + (q_{i,j+1/2}^{n+1})^2}}{(C_{i,j+1/2}^{n+1})^2 (b_{i,j+1/2}^{n+1})^2} \\
& \quad + \Omega\Delta t p_{i,j+1/2}^{n+1} + \Delta t \frac{\rho_a}{\rho} C_e W^2 \cos\psi
\end{aligned}$$

Summary of the discretised surface water momentum equation matrix coefficients

$$\begin{aligned}
E\xi_i^{n+1} + Fp_{i+1/2}^{n+1} + G\xi_{i+1}^{n+1} &= H_x \\
E\xi_j^{n+3/2} + Fq_{j+1/2}^{n+3/2} + G\xi_{j+1}^{n+3/2} &= H_y
\end{aligned}$$

where

$$\begin{aligned}
E &= -\frac{g \cdot \Delta t \cdot b}{2\Delta x} = -G \\
F &= \left(1 + \frac{g\Delta t}{2} \cdot \frac{\sqrt{p^2 + q^2}}{C^2 b^2} \right) \\
H_x &= p_{i+1/2,j}^n - \frac{\beta\Delta t}{4\Delta x} \left[(p_{i+3/2}^n + p_{i+1/2}^n)(U_{i+3/2}^n + U_{i+1/2}^n) - (p_{i+1/2}^n + p_{i-1/2}^n)(U_{i+1/2}^n + U_{i-1/2}^n) \right] - \\
&\quad \frac{\beta\Delta t}{2\Delta y} \left[(q_{i+1,j+1/2}^{n+1/2} + q_{i,j+1/2}^{n+1/2})U_{i+1/2,j}^n - (q_{i+1,j-1/2}^{n+1/2} + q_{i,j-1/2}^{n+1/2})U_{i+1/2,j}^n \right] - \\
&\quad \frac{g\Delta t}{2\Delta x} \cdot (b_{i+1/2,j}^n)(\xi_{i+1}^{n+1/2} - \xi_i^{n+1/2}) + \frac{\varepsilon\Delta t b_{i+1/2,j}^{n+1/2}}{\Delta x^2} \left[2(\hat{U}_{i+3/2,j}^n + \hat{U}_{i-1/2,j}^n) + \hat{U}_{i+1/2,j+1}^n + \hat{U}_{i+1/2,j-1}^n \right. \\
&\quad \left. - 6\hat{U}_{i+1/2,j}^n + V_{i,j-1/2}^n - V_{i,j+1/2}^n - V_{i+1,j-1/2}^n + V_{i+1,j+1/2}^n \right] - \frac{g\Delta t(p_{i+1/2,j}^n)}{2} \cdot \frac{\sqrt{(p_{i+1/2,j}^{n+1/2})^2 + (q_{i+1/2,j}^{n+1/2})^2}}{(C_{i+1/2,j}^n)^2 (b_{i+1/2,j}^n)^2} \\
&\quad + \Omega\Delta t q_{i+1/2,j}^{n+1/2} + \Delta t \frac{\rho_a}{\rho} C_e W^2 \cos\psi \\
H_y &= q_{i,j+1/2}^{n+1/2} - \frac{\beta}{2\Delta x} \left[(p_{i+1/2,j+1}^{n+1} + p_{i+1/2,j}^{n+1})V_{i,j+1/2}^{n+1/2} - (p_{i-1/2,j+1}^{n+1} + p_{i-1/2,j}^{n+1})V_{i,j+1/2}^{n+1/2} \right] - \\
&\quad \frac{\beta}{4\Delta y} \left[(q_{j+3/2}^{n+1} + q_{j+1/2}^{n+1})(V_{j+3/2}^{n+1} + V_{j+1/2}^{n+1}) - (q_{j+1/2}^{n+1} + q_{j-1/2}^{n+1})(V_{j+1/2}^{n+1} + V_{j-1/2}^{n+1}) \right] - \\
&\quad \frac{g\Delta t}{2\Delta x} \cdot (b_{i,j+1/2}^{n+1})(\xi_{j+1}^{n+1} - \xi_j^{n+1}) + \frac{\varepsilon\Delta t b_{i,j+1/2}^{n+1}}{\Delta x^2} \left[2(\hat{V}_{i+3/2,j}^{n+1} + \hat{V}_{i,j-1/2}^{n+1}) + \hat{V}_{i+1,j+1/2}^{n+1} + \hat{V}_{i-1,j+1/2}^{n+1} \right. \\
&\quad \left. - 6\hat{V}_{i,j+1/2}^{n+1} + U_{i-1/2,j}^{n+1} - U_{i+1/2,j}^{n+1} - U_{i-1/2,j+1}^{n+1} + U_{i+1/2,j+1}^{n+1} \right] - \frac{g\Delta t(q_{i,j+1/2}^{n+1})}{2} \cdot \frac{\sqrt{(p_{i,j+1/2}^{n+1})^2 + (q_{i,j+1/2}^{n+1})^2}}{(C_{i,j+1/2}^{n+1})^2 (b_{i,j+1/2}^{n+1})^2} \\
&\quad + \Omega\Delta t p_{i,j+1/2}^{n+1} + \Delta t \frac{\rho_a}{\rho} C_e W^2 \cos\psi
\end{aligned}$$

Groundwater

In applying Darcy's Law the differential equations are written as:

4.14

$$p + kb \frac{\partial h}{\partial x} = 0$$

$$q + kb \frac{\partial h}{\partial y} = 0$$

where k is saturated hydraulic conductivity, b is the average depth of the water column and dh/dx is the hydraulic gradient, and h is the piezometric head above a datum.

Reformulating the above equations gives equation 4.15, showing how k and b are calculated from the average of the two cells involved – these terms are subsequently shown as $k_{i+1/2}$ and $b_{i+1/2}$:

4.15

$$\text{a) } x\text{-direction} \quad p + \frac{(K_{1x} + K_{2x})}{2} \cdot \frac{(b_1 + b_2)}{2} \cdot \frac{(h_2 - h_1)}{\Delta x} = 0$$

$$\text{b) } y\text{-direction} \quad q + \frac{(K_{1y} + K_{2y})}{2} \cdot \frac{(b_1 + b_2)}{2} \cdot \frac{(h_2 - h_1)}{\Delta y} = 0$$

Discretisation of the differential equation in the x -direction gives:

4.16

$$p_{i+1/2}^{n+1} + k_{i+1/2} b_{i+1/2}^{n+1/2} \left(\frac{1}{2} \frac{h_{i+1}^{n+1} - h_i^{n+1}}{\Delta x} + \frac{1}{2} \frac{h_{i+1}^{n+1/2} - h_i^{n+1/2}}{\Delta x} \right) = 0$$

$$- \frac{k_{i+1/2} b_{i+1/2}^{n+1/2}}{2\Delta x} \cdot h_i^{n+1} + p_{i+1/2}^{n+1} + \frac{k_{i+1/2} b_{i+1/2}^{n+1/2}}{2\Delta x} \cdot h_{i+1}^{n+1} = - \frac{k_{i+1/2} b_{i+1/2}^{n+1/2}}{2\Delta x} (h_{i+1}^{n+1/2} - h_i^{n+1/2})$$

Likewise, discretisation in the y -direction gives:

4.17

$$q_{j+1/2}^{n+3/2} + k_{j+1/2} b_{j+1/2}^{n+1} \left(\frac{1}{2} \frac{h_{j+1}^{n+3/2} - h_j^{n+3/2}}{\Delta y} + \frac{1}{2} \frac{h_{j+1}^{n+1} - h_j^{n+1}}{\Delta y} \right) = 0$$

$$- \frac{k_{j+1/2} b_{j+1/2}^{n+1}}{2\Delta y} \cdot h_j^{n+3/2} + q_{j+1/2}^{n+3/2} + \frac{k_{j+1/2} b_{j+1/2}^{n+1}}{2\Delta y} \cdot h_{j+1}^{n+3/2} = - \frac{k_{j+1/2} b_{j+1/2}^{n+1}}{2\Delta y} (h_{j+1}^{n+1} - h_j^{n+1})$$

4.18

Summary of groundwater 2nd equation coefficients.

$$\begin{aligned}
E^* h_i^{n+1} + F^* p_{i+1/2}^{n+1} + G^* h_{i+1}^{n+1} &= H_x^* \\
E^* h_j^{n+3/2} + F^* q_{j+1/2}^{n+3/2} + G^* h_{j+1}^{n+3/2} &= H_y^* \\
\text{where} \\
E^* &= -\frac{kb}{2\Delta x} = -G^* \\
F^* &= 1 \\
H_x^* &= -\frac{k_{i+1/2} b_{i+1/2}^{n+1/2}}{2\Delta x} (h_{i+1}^{n+1/2} - h_i^{n+1/2}) \\
H_y^* &= -\frac{k_{j+1/2} b_{j+1/2}^{n+1}}{2\Delta y} (h_{j+1}^{n+1} - h_j^{n+1})
\end{aligned}$$

All the coefficients for surface water and groundwater equations, and x and y directions have now been defined. All of the equations can now be defined using these coefficients (Eq. 4.19) These are summarised for the x and y directions in Table 4.1 and Table 4.2.

4.19

x - sweep

$$\begin{aligned}
A p_{i-1/2}^{n+1} + B \xi_i^{n+1} + C p_{i+1/2}^{n+1} &= D_x \\
E \xi_i^{n+1} + F p_{i+1/2}^{n+1} + G \xi_{i+1}^{n+1} &= H_x
\end{aligned}$$

y - sweep

$$\begin{aligned}
A q_{j-1/2}^{n+3/2} + B \xi_j^{n+3/2} + C q_{j+1/2}^{n+3/2} &= D_y \\
E \xi_j^{n+3/2} + F q_{j+1/2}^{n+3/2} + G \xi_{j+1}^{n+3/2} &= H_y
\end{aligned}$$

Note, when solving the groundwater equations, h (piezometric head) is used instead of ξ (surface water elevation) For convenience and completeness all of the variables are defined here again.

Terms used:

Δt	-	timestep (s)
$\Delta x, \Delta y$	-	grid spacing (m)
S	-	storage coefficient unconfined $S = n_{i,j,k}$, confined aquifer $S = S_{S\ i,j,k} \cdot b_{i,j,k}$
n	-	porosity of aquifer (dimensionless)
S_s	-	Specific storage coefficient, volume of water released per unit volume of aquifer per unit decrease in the head (m^{-1})
b	-	depth of water in cell (m)
h	-	piezometric head of water in groundwater (m)

ξ	-	surface water elevation (m)
p	-	flow in x -direction per unit width ($\text{m}^3/\text{s}/\text{m}$)
q	-	flow in y -direction per unit width ($\text{m}^3/\text{s}/\text{m}$)
q_{top}, q_{base}	-	seepage flows into top and from base of cell per unit area (m/s)
g	-	acceleration due to gravity (m/s^2)
k	-	saturated hydraulic conductivity of the aquifer (m/s)
C	-	Chezy coefficient
i, j, k	-	position in i, j, k indices. If omitted, index is simply i, j or k
$n(+1)$	-	position in time (n = current timestep, $n+1$ = next timestep etc)

Table 4.1: - Summary of Coefficients for x -sweep

Coefficient	x -Sweep	
	Surface Water	Groundwater
A	$-\frac{1}{2} \frac{\Delta t}{\Delta x}$	$-\frac{1}{2} \frac{\Delta t}{\Delta x}$
B	1	S
C	$\frac{1}{2} \frac{\Delta t}{\Delta x}$	$\frac{1}{2} \frac{\Delta t}{\Delta x}$
D	$\xi_{i,j}^{n+1/2} - \frac{\Delta t}{2} \left(\frac{q_{i,j+1/2}^{n+1/2} - q_{i,j-1/2}^{n+1/2}}{\Delta y} \right) - \frac{\Delta t}{2} q_{base}$	$S \cdot h_{i,j}^{n+1/2} - \frac{\Delta t}{2} \left(\frac{q_{i,j+1/2}^{n+1/2} - q_{i,j-1/2}^{n+1/2}}{\Delta y} \right) + \frac{\Delta t}{2} q_{top} - \frac{\Delta t}{2} q_{base}$
E	$-\frac{g \cdot \Delta t \cdot b_{i+1/2}^{n+1/2}}{2\Delta x}$	$-\frac{k_{i+1/2} b_{i+1/2}^{n+1/2}}{2\Delta x}$
F	$1 + \frac{g\Delta t}{2} \cdot \frac{\sqrt{(p_{i+1/2}^n)^2 + (q_{i+1/2}^{n+1/2})^2}}{(C_{i+1/2}^n)^2 (b_{i+1/2}^n)^2}$	1
G	$\frac{g \cdot \Delta t \cdot b_{i+1/2}^{n+1/2}}{2\Delta x}$	$\frac{k_{i+1/2} b_{i+1/2}^{n+1/2}}{2\Delta x}$
H	See 4.13	$-\frac{k_{i+1/2} b_{i+1/2}^{n+1/2}}{2\Delta x} (h_{i+1}^{n+1/2} - h_i^{n+1/2})$

Table 4.2: - Summary of Coefficients for y-sweep

Coefficient	y-Sweep	
	Surface Water	Groundwater
A	$-\frac{1}{2} \frac{\Delta t}{\Delta y}$	$-\frac{1}{2} \frac{\Delta t}{\Delta y}$
B	1	S
C	$\frac{1}{2} \frac{\Delta t}{\Delta y}$	$\frac{1}{2} \frac{\Delta t}{\Delta y}$
D	$\xi_{i,j}^{n+1} - \frac{\Delta t}{2} \left(\frac{p_{i+1/2,j}^{n+1} - p_{i-1/2,j}^{n+1}}{\Delta x} \right) - \frac{\Delta t}{2} q_{base}$	$S.h_{i,j}^{n+1/2} - \frac{\Delta t}{2} \left(\frac{p_{i+1/2,j}^{n+1} - p_{i-1/2,j}^{n+1}}{\Delta x} \right) + \frac{\Delta t}{2} q_{top} - \frac{\Delta t}{2} q_{base}$
E	$-\frac{g.\Delta t.b_{j+1/2}^{n+1/2}}{2\Delta y}$	$-\frac{k_{j+1/2}b_{j+1/2}^{n+1/2}}{2\Delta y}$
F	$1 + \frac{g\Delta t}{2} \cdot \frac{\sqrt{(p_{j+1/2}^{n+1})^2 + (q_{j+1/2}^{n+1/2})^2}}{(C_{j+1/2}^{n+1/2})^2 (b_{j+1/2}^{n+1/2})^2}$	1
G	$\frac{g.\Delta t.b_{j+1/2}^{n+1/2}}{2\Delta y}$	$\frac{k_{j+1/2}b_{j+1/2}^{n+1/2}}{2\Delta y}$
H	See 4.13	$-\frac{k_{j+1/2}b_{j+1/2}^{n+1}}{2\Delta y} (h_{j+1}^{n+1} - h_j^{n+1})$

Table 4.3: - Summary of Seepage Equations

	Seepage Equations between layers
q_{base} surface water (with permeable riverbed)	$\frac{(h_k - h_{k+1})}{\frac{L_{riv}}{k_{riv}} + \frac{0.5b_{k+1}}{k_{k+1}}}$
q_{base} groundwater	$\frac{(h_k - h_{k+1})}{\frac{b_k}{2k_k} + \frac{b_{k+1}}{2k_{k+1}}}$
q_{top} groundwater (not directly underneath surface water cell)	$\frac{(h_{k-1} - h_k)}{\frac{b_{k-1}}{2k_{k-1}} + \frac{b_k}{2k_k}}$

4.2.3 Recurrence Relationships

In order to solve the equations the terms are first re-arranged and then recurrence relationships are defined.

4.20

x - sweep

$$A\mathbf{p}_{i-1/2}^{n+1} + B.h_i^{n+1} + C\mathbf{p}_{i+1/2}^{n+1} = D_x$$

$$E.h_i^{n+1} + F\mathbf{p}_{i+1/2}^{n+1} + G\mathbf{h}_{i+1}^{n+1} = H_x$$

y - sweep

$$A\mathbf{q}_{j-1/2}^{n+3/2} + B.h_j^{n+3/2} + C\mathbf{q}_{j+1/2}^{n+3/2} = D_y$$

$$E.h_j^{n+3/2} + F\mathbf{q}_{j+1/2}^{n+3/2} + G\mathbf{h}_{j+1}^{n+3/2} = H_y$$

Formulating the unknown variables h_i^{n+1} and $p_{i+1/2}^{n+1}$ as follows gives:

4.21

$$a) h_i^{n+1} = -P_i p_{i+1/2}^{n+1} + Q_i$$

$$b) p_{i+1/2}^{n+1} = -R_i h_{i+1}^{n+1} + S_i$$

Using the x-sweep as an example, rearranging Eq. 4.20 to the form of Eq. 4.21, variables P_i , Q_i , R_i , and S_i can be re-written as:

4.22

$$a) h_i^{n+1} = \frac{D_x - C p_{i+1/2}^{n+1} - A p_{i-1/2}^{n+1}}{B}$$

$$= -\frac{C}{B} p_{i+1/2}^{n+1} + \frac{D_x - A p_{i-1/2}^{n+1}}{B}$$

$$b) p_{i+1/2}^{n+1} = \frac{H_x - G h_{i+1}^{n+1} - E h_i^{n+1}}{F}$$

$$= -\frac{G}{F} h_{i+1}^{n+1} + \frac{H_x - E h_i^{n+1}}{F}$$

By formulating Eq. 4.21 b) in an i-1/2 format, it can be shown that:

4.23

$$p_{i-1/2}^{n+1} = -\frac{G}{F} h_i^{n+1} + \frac{H_x - E h_{i-1}^{n+1}}{F}$$

$$\therefore -\frac{G}{F} = R_{i-1}$$

$$\frac{H_x - E}{F} h_{i-1}^{n+1} = S_{i-1}$$

Substituting this into Eq. 4.22 a):

4.24

$$h_i^{n+1} = -\frac{C}{B} p_{i+1/2}^{n+1} + \frac{D_x - A(-R_{i-1}h_i^{n+1} + S_{i-1})}{B}$$

rearranging :

$$\begin{aligned} Bh_i^{n+1} &= -Cp_{i+1/2}^{n+1} + D_x + AR_{i-1}h_i^{n+1} - AS_{i-1} \\ h_i^{n+1}(B - AR_{i-1}) &= -Cp_{i+1/2}^{n+1} + D_x - AS_{i-1} \\ h_i^{n+1} &= -\frac{C}{B - AR_{i-1}} p_{i+1/2}^{n+1} + \frac{D_x - AS_{i-1}}{B - AR_{i-1}} \end{aligned}$$

Similarly the same formulations can be performed with Eqs. 4.21a and 4.22b giving:

4.25

$$\begin{aligned} p_{i+1/2}^{n+1} &= -\frac{G}{F} h_{i+1}^{n+1} + \frac{H_x - E(-P_i p_{i+1/2}^{n+1} + Q_i)}{F} \\ p_{i+1/2}^{n+1} &= -\frac{G}{F - EP_i} h_{i+1}^{n+1} + \frac{H_x - EQ_i}{F - EP_i} \end{aligned}$$

From Eqs. 4.21, 4.24 and 4.25 the following recurrence relationships can be obtained.

4.26

$$\begin{aligned} P_i &= \frac{C}{B - AR_{i-1}} & R_i &= \frac{G}{F - EP_i} \\ Q_i &= \frac{D_x - AS_{i-1}}{B - AR_{i-1}} & S_i &= \frac{H_x - EQ_i}{F - EP_i} \end{aligned}$$

From Table 4.1 it is known that $A = -C$ and $E = -G$, giving:

4.27

$$\begin{aligned} P_i &= \frac{C_i}{B_i + C_i R_{i-1}} & R_i &= \frac{G_i}{F_i + G_i P_i} \\ Q_i &= \frac{D_{xi} + C_i S_{i-1}}{B_i + C_i R_{i-1}} & S_i &= \frac{H_{xi} + G_i Q_i}{F_i + G_i P_i} \end{aligned}$$

Eq. 4.27 gives the recurrence relationships. The same relationships can be used for the y -direction variables by using the following equations:

4.28

$$\begin{aligned} h_j^{n+3/2} &= -P_j q_{j+1/2}^{n+3/2} + Q_j \\ q_{j+1/2}^{n+3/2} &= -R_j h_{j+1}^{n+3/2} + S_j \end{aligned}$$

4.3 Iteration of seepage terms

Cells i,j,k and $i,j,k+1$ (i.e. cells immediately above/below one another) will share one of the seepage expressions, as the flow leaving one cell will equate to the flow entering the other cell. Since the seepage depends on the head in each of these cells, and the head depends on

the seepage, then the solution is an implicit problem. For each timestep the previous heads (or initial heads at the start) can be used to estimate the seepage and calculate the new heads. The heads can then be recalculated with the new seepage values based on the previous calculation. A convergence criterion can be set to ensure that this process is repeated enough to ensure the iteration is accurate. Figure 4.3 shows a schematic of the way in which these seepage flows are calculated in the model.

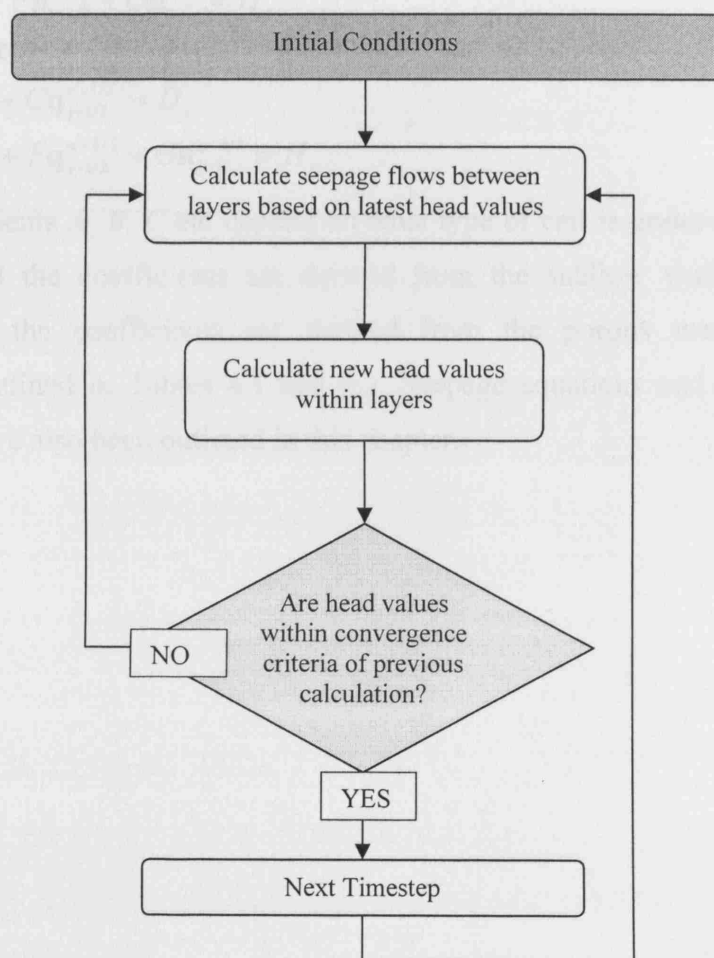


Figure 4.3: - Flowchart for iteration of seepage and head values.

4.4 Summary

The key governing equations were derived in Chapter 3 . These governing equations have been discretised in time and space in order to be used in the Alternating Difference Implicit method, which allows the governing equations to be broken down to numerous simultaneous equations. The equations take the format of the following equations:

x - sweep

$$A\mathbf{p}_{i-1/2}^{n+1} + B.\mathbf{h}_i^{n+1} + C\mathbf{p}_{i+1/2}^{n+1} = D_x$$

$$E.\mathbf{h}_i^{n+1} + F\mathbf{p}_{i+1/2}^{n+1} + G\mathbf{h}_{i+1}^{n+1} = H_x$$

y - sweep

$$A\mathbf{q}_{j-1/2}^{n+3/2} + B.\mathbf{h}_j^{n+3/2} + C\mathbf{q}_{j+1/2}^{n+3/2} = D_y$$

$$E.\mathbf{h}_j^{n+3/2} + F\mathbf{q}_{j+1/2}^{n+3/2} + G\mathbf{h}_{j+1}^{n+3/2} = H_y$$

Where the coefficients A , B , C etc depend on what type of cell is under consideration. For a surface water cell the coefficients are derived from the shallow water equations. For a groundwater cell the coefficients are derived from the porous media equations. The coefficients are defined in Tables 4.1 and 4.2. Seepage equations and method of iteration between layers have also been outlined in this chapter.

CHAPTER 5 MODEL IMPLEMENTATION

5.1 *Introduction*

In the preceding chapters, the basic governing equations have been formulated, both for surface water and groundwater. The equations are stated in a depth integrated form, i.e. in the two horizontal dimensions and assuming no variation in the variables over depth. A framework has been suggested in Chapter 3 that allows the numerical model to include variations in the vertical dimension by means of additional model layers. Chapter 4 shows how these equations can be discretised in time and space in the format that has been used in this study. This chapter aims to show conceptually how these equations are used in the existing DIVAST model, and how this model has been extended to include the groundwater equations.

The traditional version of DIVAST, has been well documented, so a brief section is included which summarises the modifications to the original model, together with a step by step summary of how the input file is used to set-up a model. The original model has an extensive user and reference manual (Falconer et al. 2001b; Falconer et al. 2001a) which should be referred to for further details. In this chapter focus will be made on areas where the new model differs from the original.

5.2 *Modifications to existing 2-D Model*

5.2.1 *Sequential running of input files*

The entire code is now enclosed within a loop, allowing multiple input files to be run in sequence. Variations on a scenario can be set up in separate input files, and then run back to back. This is ideal for undertaking long runs of large models.

5.2.2 Hot-start

Models can create a snapshot of the simulation at any particular time, and then the model can be restarted from such a time if required; this is known as a ‘hot-start’. Parameters can be changed in the subsequent runs, allowing branched variations of a model with a common run up. The domain size should be the same for subsequent runs.

5.2.3 Point Data collection

Data (i-index, j-index, depth, elevation, u-velocity, v-velocity, w-velocity, porosity, permeability, solute concentration) can now be collected at specific points and the output sent to a .csv file to allow easy access to data for particular monitoring points.

5.2.4 Outfall Discharge Variation

Outfalls can have a varying discharge over time.

5.2.5 Defining boundary conditions velocity/flow and elevation.

These sections have been completely re-written in the model subroutines BOUND and HYDBND. See the input file description below.

5.2.6 Defined new coefficients to allow inclusion of groundwater.

This is the major modification wherein new recursion coefficients have been included to take account of the groundwater cells. It allows the code to switch between solving the groundwater equations and the shallow water equations, as required.

5.3 Input file

The input file for the model should ideally contain all of the details of the scenario being modelled. The code itself should be as generic as possible, so that the model can be fully set-up with the input file alone, i.e. without needing to modify the source code itself. This was not the case for the original model at the start of this project, so several additional modifications have been made to the structure of the input file and code to allow more generality. This section summarises the input file, and shows how the model is set-up. A sample input file is included in Appendix A and several more are on the Appendix CD. These should be referred to, to aid understanding of this chapter. The sections are dealt with in the order that they appear in the input file itself.

5.3.1 General Variables

The first section of the input file outlines the basic size of the model, some formats for data input and flags to allow various aspects of the model to be switched on and off as appropriate. Significant variables include:

- IMAX and JMAX, give the size of the domain in the I and J direction respectively. KMAX gives the number of layers if required.
- TECOUT switches output to a Tecplot format file on and off
- TECTIM gives the interval that Tecplot and point data is collected.
- N**PRN switch the old style text output files on and off.
- NFL*** switch wind stress, flooding and drying, solute predictions, and surface water-groundwater interactions on and off.

5.3.2 Hotstart Info

Here the model can be 'hotstarted', i.e. started using the conditions of a previous run, allowing a model run to be continued where it left off before.

HOTSTART sets whether the current model is a continuation of a previous model.

HSTOUT and HSTTIME specify if a 'hotstart point' for the current model is to be saved, and when it refers to.

5.3.3 Point Data Collections

This section sets up monitoring locations in the domain so that data can be collected specifically for points of interest. The number of points is first specified, then the i and j coordinates are specified for each point. Data collected is i, j, depth, elevation, u-velocity, v-velocity, w-velocity, porosity, permeability, and solute concentrations.

5.3.4 Open Boundary Conditions

This section defines the type and location of the open boundary conditions. The details of these are set-up later in the input file.

IENDOB defines how many open boundaries perpendicular to the i-direction are present in the model, i.e. flow from these boundaries will emerge or leave in the i-direction.

JENDOB does the same for the j-direction.

IOBDx is a 4 (or 5) part array, defining the type and location of the i-boundary x as follows:

IOBD(x) = (type) (i-index) (start j-value) (end j-value) (k-value)

e.g.

IOBD(1) = 3 40 10 15 (1)

The above statement defines i-boundary 1 as type ‘3’, on i-index 40, stretching from j-index 10 to j-index 15. If the 3-D code is being used, the layer (k-value) must also be specified.

The types are defined as follows:

- 0 - flow or velocity at lower boundary;
- 1 - flow or velocity at upper boundary;
- 2 - water elevation at lower boundary;
- 3 - water elevation at upper boundary.

Note that upper and lower do not refer to upstream or downstream, but simply which direction the boundary faces. A ‘lower’ boundary faces the direction of increasing i or j, an ‘upper’ boundary faces the direction of decreasing i or j. So the example above defines an upper water elevation boundary that would look like Figure 5.1. The i direction is shown vertically, as this is how the domain is presented in the input file later.

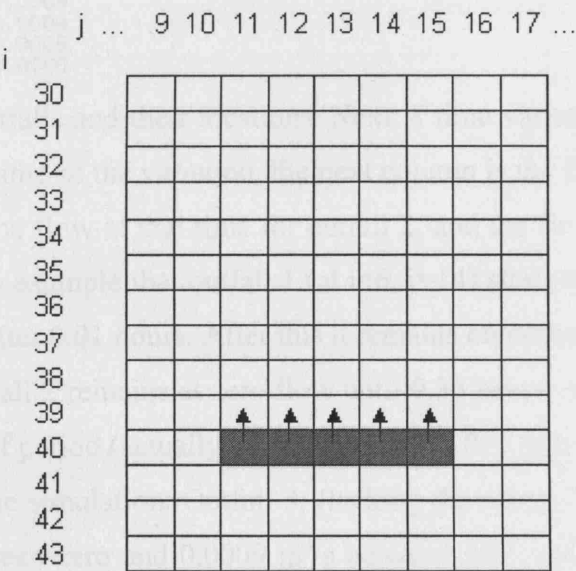


Figure 5.1: - example boundary condition.

This process is repeated for the JOBBD (j open boundaries).

5.3.5 Model Data

This section defines physical data specific to the scenario. Key variables are:

- **TIMESM** The duration of the simulation (hours)
- **HFDT** The half timestep used in the solution (ADI method) (seconds)
- **DELX** The grid spacing (metres)

Also defined here are roughness of the bed, viscosity, alpha and beta (velocity and momentum correction factors), eddy viscosity coefficient, dispersion and diffusion coefficients, latitude of domain and north direction for coriolis effect, wind speed (if any) and water temperature.

5.3.6 Outfalls and Solute Prediction

Here the outfalls (point boundary conditions) are defined. First NUMOUT, the number of outfalls present, is defined. Then each outfall is given an i,j co-ordinate. Next, the number of variations in the outfall flow is defined, and followed by a list of those variations for each outfall. The code will interpolate linearly between the defined time variations. For example:

```
NUMOUT = 3          NUMBER OF OUTFALLS
OUTFALL1 = 6 14      river flow
OUTFALL2 = 29 77     dye injection point
OUTFALL3 = 9 36      varied flow
NUMTME = 8          NUMBER OF TIME VARIATIONS OF OUTFALL DISCHARGE
OUTFALL DISCHARGES m^3/s (time,discharge for outfall 1, discharge for outfall 2 etc)
0.0000 0.0000 0.0000 0.0000
0.0100 0.0005 0.0000 0.0000
0.2000 0.0005 0.0000 0.0009
0.3499 0.0005 0.0000 0.0009
0.3500 0.0005 0.0010 0.0009
0.3650 0.0005 0.0010 0.0009
0.3651 0.0005 0.0000 0.0009
0.5000 0.0005 0.0000 0.0000
```

This code defines 3 outfalls and their locations. Next, 8 time variations are defined. The first column represents the time of the variation, the next column is the flow at that time for outfall 1, the next column is the flow at that time for outfall 2, and the final column refers to outfall 3. It can be seen in this example that outfall 1 (at i=6, j=14) starts at zero flow, but is quickly raised to 0.0005 m³/s after 0.01 hours. After this it remains constant at 0.0005 m³/s for the rest of the simulation. Outfall 2 remains at zero flow until 0.35 hours, when it suddenly increases to 0.001 m³/s for a brief period (actually 1min 30secs, or 0.015 hrs) and then falls back to zero for the remainder of the simulation. Outfall 3, (lacking the sharp time definitions for Outfall 2) varies linearly between zero and 0.0009 m³/s between 0.01 and 0.2 hrs, and back to zero between 0.3651 and 0.5 hrs. If plotted on a graph the outfall flows would look like Figure 5.2. In this way, any desired flow can be defined, constant flows (1), short injections (2), or slowly varying flows. Curves can be approximated by defining enough points.

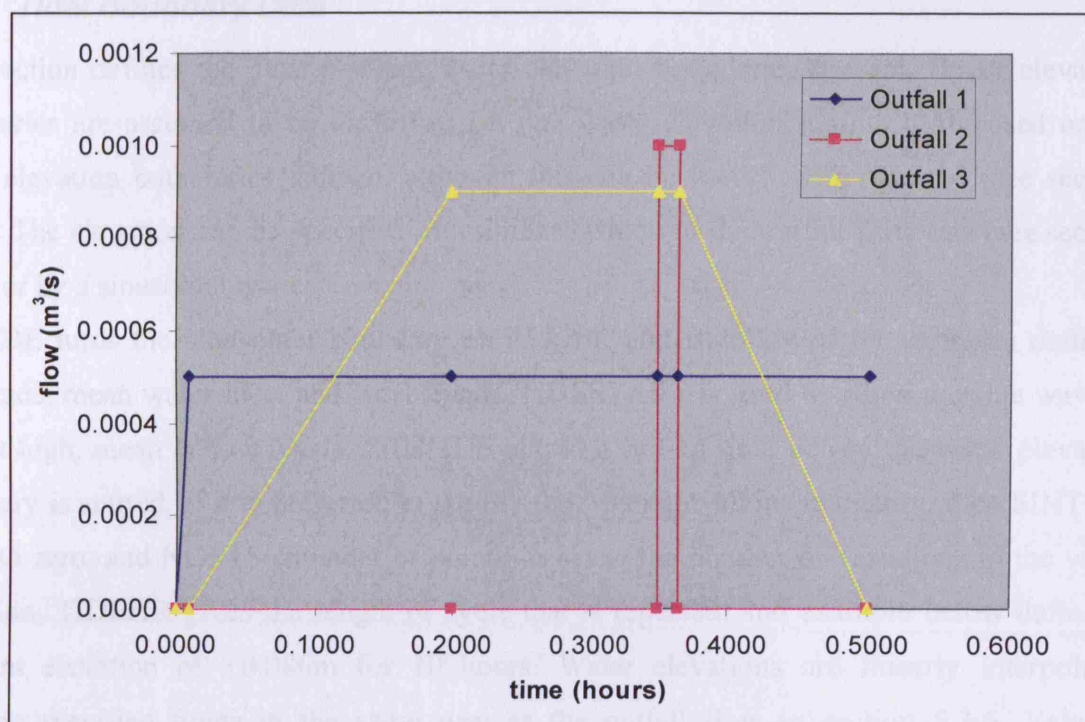


Figure 5.2: - Example outfall flows

Also in this section of the input file, flags for various solute types are set. Solute types are salinity, temperature, total coliforms, faecal coliforms, B.O.D., organic N, ammonia N, nitrate N, D.O., algal biomass, and phosphorus.

After these flags are defined scaling factors for the printout of the solute prediction. These are largely redundant if using the Tecplot output.

Next, initial and outfall levels are defined for each solute. The initial level is the starting concentration of that solute throughout the domain. The outfall level is the concentration of the solute in each outfall in turn. For example, to define salinity concentrations for the 3 example outfalls above the following would be used:

```
SAL OUTS:-      0.00    100.00    1.00    OUTFALL SALINITY LEVELS (PPT)
```

This would result in outfall 1 having no salinity, making it just a flow input to the domain. Outfall 2 has a high concentration of 100 ppt (parts per thousand) (appropriate to short injection of solute). Outfall 3 has a low level of 1ppt.

After this, the input file defines multiple other sediment and solute related parameters, including sediment diameters, decay rates, and temperature corrections. Interested readers are referred to other references on DIVAST's solute modelling capabilities (Falconer et al. 2001a).

5.3.7 Tidal Boundary Data

This section defines the details of any water elevation boundaries present. Water elevation boundaries are assumed to be universal, i.e. one water elevation regime is imposed on all water elevation boundaries defined, although this can be modified if required (see section 7.7.2). The elevation can be specified in a similar fashion to the outfall flow rate (see section 5.3.6) or by a sinusoidal wave.

SINTIDE turns the sinusoidal boundary on and off, and is followed by variables defining amplitude, mean water level and wavelength. TIDESTART is used to allow the sine wave to start at high, mean or low levels. PRETIDE allows a run-up time before the water elevation boundary is started. If it is preferred to specify the water elevations manually, then SINTIDE is set to zero, and NOPTS (number of points) is set to the number of variations in the water elevation. TIDEHR gives the length of cycle that is repeated, and example below defines a constant elevation of +0.086m for 10 hours. Water elevations are linearly interpolated between specified times in the same way as the outfall flow in section 5.3.6. Velocity information is not required at the water level boundary, as this is calculated from the water surface slope.

```
-----Tidal boundary (water elevation) Data-----
SINTIDE = 0 I6 Sinusoidal tide, 1= yes, 0= no
TIDEAMP = 0.0700 F10.4 Tidal Amplitude (only used NUMTDS gives the number of
times it is repeated. Then the water elevation is defined as
follows. The first column is the time, the second column is the
elevation at that time. The example in APPENDIX A ('bar.dsg')
produces a sinusoidal tide of 1 metre amplitude and 0.5 hour
wavelength, oscillating around 0.0 metres. The if SINTIDE=1)
TIDEMWL = 0.2000 F10.4 Tidal Mean Water Level (only used if SINTIDE=1)
TIDEHR = 10.0000 F10.4 Tidal period (wavelength for sinusoidal tide, length of cycle to
repeat for non-sinusoidal tide) (hours)
TIDESTART=HIGH A4 Start sinusoidal tidal cycle at: high tide (HIGH), Rising Mean
Water Level (MWL+), Falling Mean Water Level (MWL-) or low tide (LOW )
PRETIDE = 0.0000 F10.4 Time before tidal boundary cycle is started. (hours)
NOPTS = 2 I6 Number of points specified for non-sinusoidal tide
NUMTDS = 10.0000 F10.4 Number of tidal cycles
time elevation (non-sinusoidal tide points on NOPTS lines below here F6.3 F8.3)
0.000 +0.086
10.000 +0.086
```

5.3.8 Velocity or Flow Boundary

Here any flow boundaries are defined. FLOWTYPE allows a flow or velocity to be specified, and the value is defined in a similar way to the water elevation and outfall flow. Each flow boundary has its own setup. The example below defines two flow boundaries, the first with a constant flow and the second with a varied flow.


```

-----Flow or velocity boundary data:-----
FLOWTYPE =      0      I6      Type of Boundaries (0=Flow 1=velocity )
FPHASE   =    0.0500    F10.4    Time over which flow at boundary is introduced
CDWEIR   =    0.6100    F10.4    weir coefficient
-----First flow Boundary-----
IBNDPTS 1=      2      I4      Number of flow changes for flow boundary 1 - (minimum 2)
time(F10.4) flow/velocity(F10.4) (flow change points on NOFPTS lines below here)
           0.000      0.0300
           3.000      0.0300
-----Second flow Boundary-----
IBNDPTS 1=      3      I4      Number of flow changes for flow boundary 2 - (minimum 2)
time(F10.4) flow/velocity(F10.4) (flow change points on NOFPTS lines below here)
           0.000      0.1000
           2.000      0.5000
           3.000      0.0300

```

5.3.9 Layer Domain Specification

Here the domain is set-up in a grid. Each cell is assigned an index (stored in the code as the IWET array). Basic values defined here are as follows.

0 – no flow. The cell is not part of the hydraulic model and acts as a solid wall.

1 – surface water cell. The cell is treated as a surface water cell and solved using the shallow water equations.

7 – groundwater cell. The cell is treated as part of an aquifer, and solved using the porous media equations.

The i-direction is assumed to be vertical in this input file. An example is included in Appendix A as 'bar.dsg' and elaborated in the next section. The digit '7' is used, because during the running of the program, numbers 1 through to 6 are used to define other types of cells, such as temporarily dry cells, outfall locations, or open boundaries.

5.3.10 Elevation Data for surface and Groundwater Layers

The elevations of the domain are defined in a grid like the domain cells. Because groundwater flow is being considered, both surface elevations and base of the groundwater elevations need to be specified. First, the surface elevations are defined, either at the corner of each cell, or at the centre of the sides of each cell. The latter gives a better resolution, but requires twice as much data. The side of the cell referred to as i or j is the positive side of the cell (see Figure 5.3).

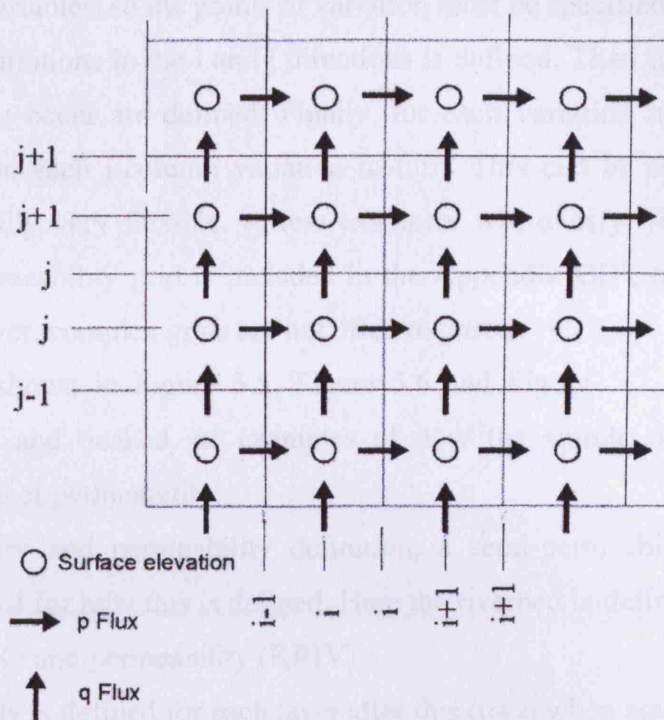


Figure 5.3: - layout of grid cells. i refers to cell and positive side of cell.

The 'bar.dsg' example in Appendix A would produce a model like that in Figure 5.4.

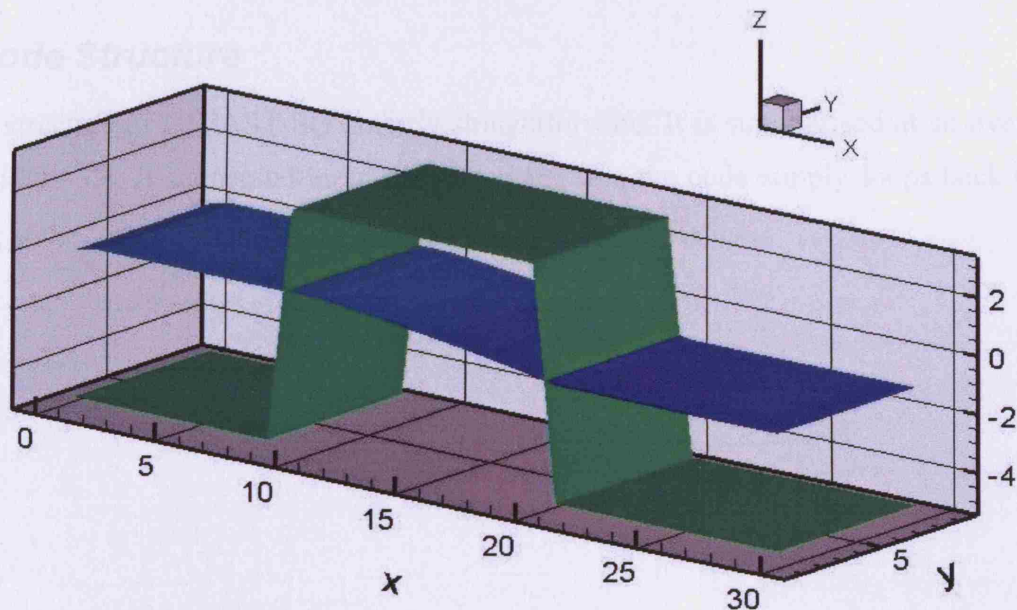


Figure 5.4: - Visualisation of 'bar.dsg' model from Appendix A (green for land surface, blue for water surface).

5.3.11 Aquifer Data

Following the domain and depths, details are given about the aquifers. Porosity and permeability are defined in the same fashion. A 2-D linear interpolation routine is used in the

code to assign these variables, so the points of variation must be specified.

First the number of variations in the i and j directions is defined. Then the j-column numbers where these variations occur are defined. Finally, for each variation in the i-direction, the variable is specified at each j-column variation in turn. This can be somewhat difficult to visualise, but is actually very flexible. A few examples will clarify. A spreadsheet with a macro to plot the permeability grid is included in the Appendix CD^a, to aid the creation of complex grids. However, complex grids are not often required.

Three examples are shown in Figure 5.5, Figure 5.6 and Figure 5.7, defining a constant porosity grid, sloped and peaked, as examples of how the simple definition can set-up complex arrangements of permeability.

Following the porosity and permeability definition, a semi-permeable river bed can be defined. See section 3.4 for how this is defined. Here the riverbed is defined as present or not, its thickness (RIVTHK) and permeability (KRIV).

Aquifer compressibility is defined for each layer after this (used when aquifer is confined).

Finally, the surface water-groundwater head convergence criteria is set; used when more than one layer is present and seepage changes the heads. The seepage and heads are repeatedly calculated until repeat calculations differ by less than this criteria.

5.4 Code Structure

The code structure of DIVAST-SG is fairly straightforward. It is summarised at an overview level in Figure 5.8. If sequential input files are being run, the code simply loops back to the beginning at the 'end program' and runs the next input file in the list.

^a Spreadsheet file: D:\DIVAST-SG General Model and Input Files\permeability grid sheet.xls

```

imax  jmax
20    20

ivar  jvar
2     2

jvars
1     20

ivars
1     0.5  0.5
20    0.5  0.5

```

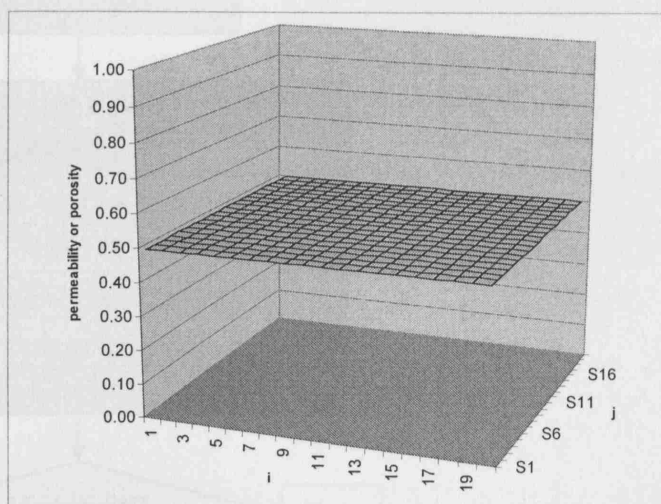


Figure 5.5: - Defining a constant permeability over the domain. The commands used are in the top left corner, the grid and surface plot show what the code interpolates these commands as.

```

imax  jmax
20    20

ivar  jvar
2     2

jvars
1     20

ivars
1     0.5  0.5
20    1    0.5

```

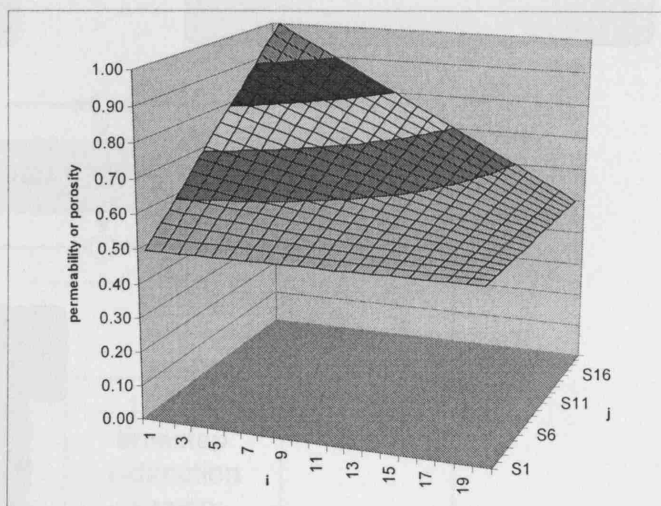


Figure 5.6: - Defining a permeability that changes in a slope. Definition in top left and surface plot shows the result.

```

imax  jmax
20    20

ivar  jvar
5     5

jvars
1     3    10    17    20

ivars
1     0.5  0.5  0.5  0.5  0.5
3     0.5  0.5  0.5  0.5  0.5
10    0.5  0.5  1    0.5  0.5
17    0.5  0.5  0.5  0.5  0.5
20    0.5  0.5  0.5  0.5  0.5

```

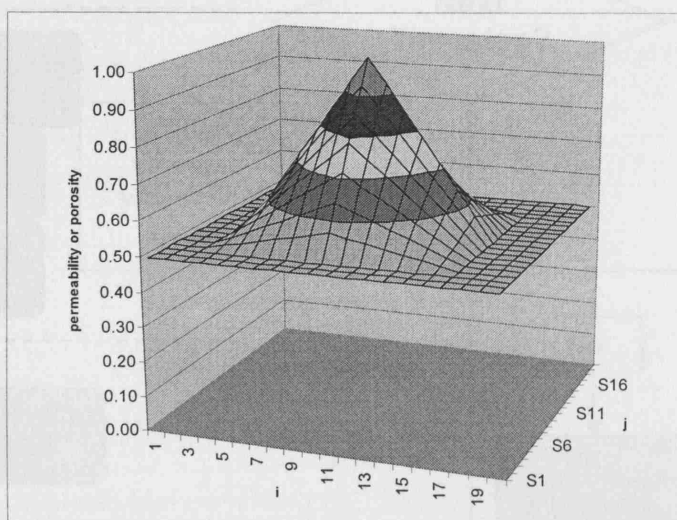


Figure 5.7: - Defining a permeability grid with a peak or similar. Definition at top left; grid and surface plot show result.

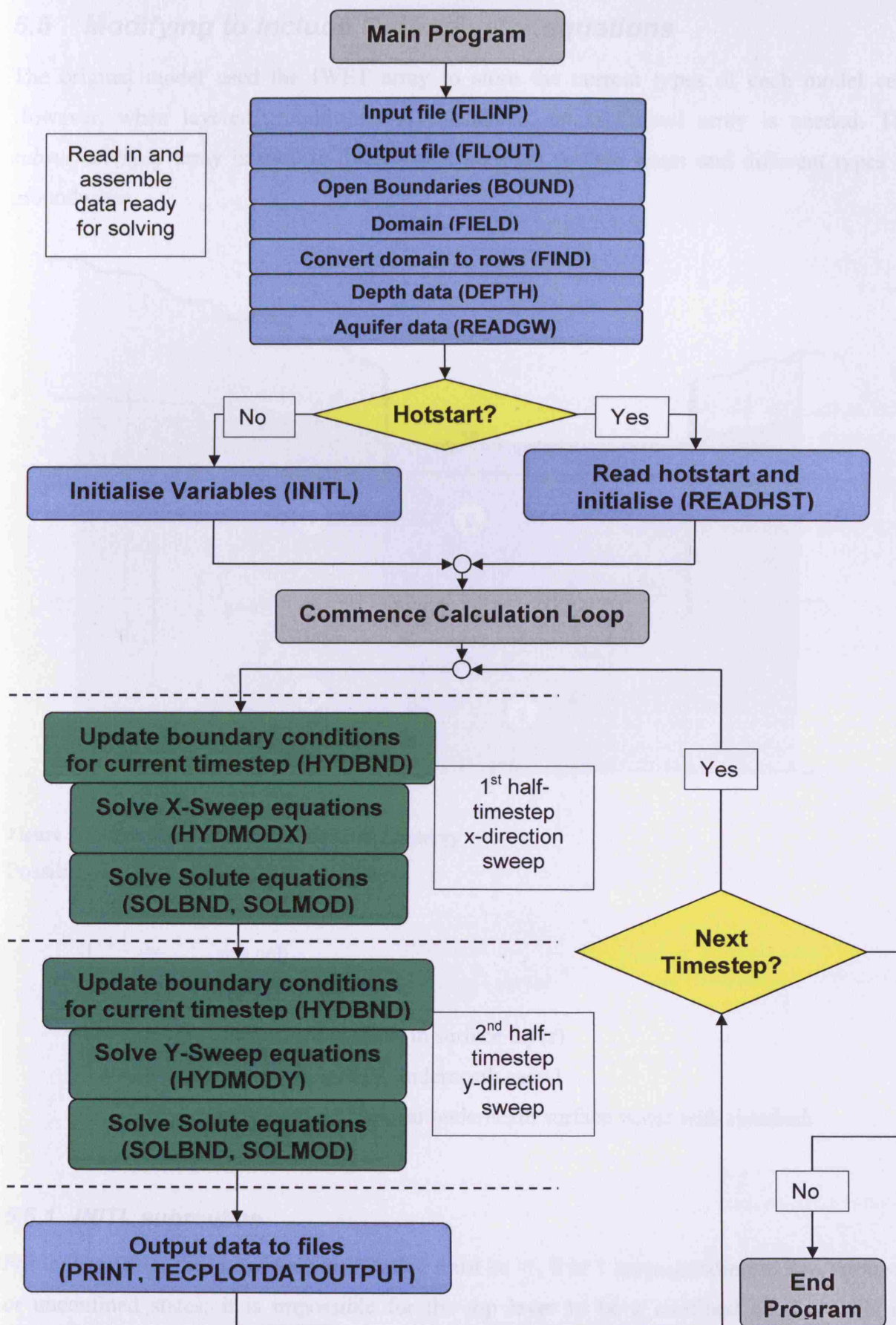


Figure 5.8: - Schematic Structure of DIVAST-SG code

5.5 Modifying to include Groundwater equations

The original model used the IWET array to store the current types of each model cell. However, when layered groundwater is considered, an additional array is needed. The $subsurface(i,j,k)$ array is used to differentiate between surface water and different types of groundwater.

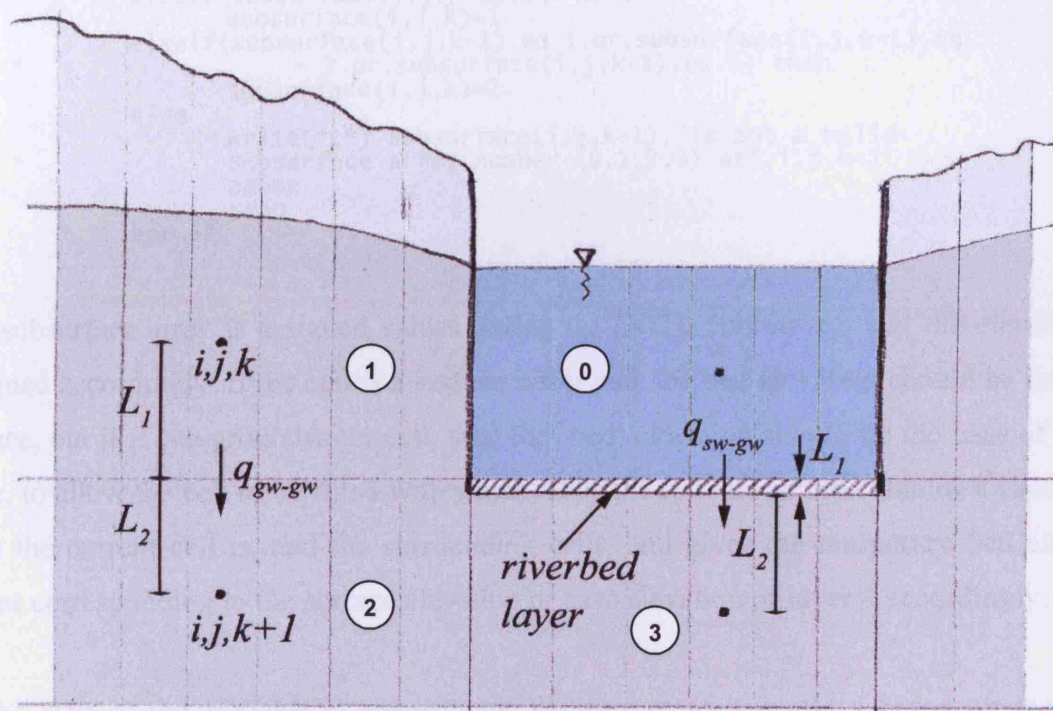


Figure 5.9: - Possible values for $subsurface(i,j,k)$ array

Possible values of $subsurface(i,j,k)$ array.

-1	=	dry cell
0	=	surface water
1	=	unconfined aquifer (in surface layer)
2	=	'confined' aquifer underneath case 1
3	=	semi-confined aquifer underneath surface water with riverbed.

5.5.1 INITL subroutine

For the top layer, the $subsurface$ array value must be -1, 0 or 1 corresponding to dry, surface, or unconfined states; it is impossible for the top layer to be a confined aquifer. This is distinguished using the IWET values 0 or 9 (permanently dry or temporarily dry), 1-6

(various surface water states), and 7 (groundwater).

For underlying layers, the code simply looks at the cell immediately above and determines the subsurface value accordingly: 1, 2 or 3 corresponding to unconfined, confined, or semi-confined aquifers.

Code Extract 5.A (INITL subroutine)

```

      if(subsurface(i,j,k-1).eq.0) then
        subsurface(i,j,k)=3
      elseif(subsurface(i,j,k-1).eq.-1) then
        subsurface(i,j,k)=1
      elseif(subsurface(i,j,k-1).eq.1.or.subsurface(i,j,k-1).eq.
*         2.or.subsurface(i,j,k-1).eq.3) then
        subsurface(i,j,k)=2
      else
*         write(*,*) subsurface(i,j,k-1),"is not a valid
        subsurface array number (0,1,2,3) at",i,j,k-1
        pause
        stop
      end if

```

The subsurface array is assigned values during the INITL subroutine, and the elevations are assigned accordingly. If the cell is a surface water cell, the bed elevation should be that of the surface, but if it is a groundwater cell, then the ‘bed’ elevation should be the base of the first layer, to allow the cell to be filled with water. Thus the INITL routine contains a check to see what the current cell is, and the surrounding cells, and gives the temporary bed elevations values corresponding to the surface elevation or base elevation of layer 1 accordingly.

At the start of the HYDMOD subroutines, the current seepage rates based on the current groundwater heads are calculated using the equations in 3.24 to 3.26. Code Extract 5.B shows the section of code that implements these equations.

3.24

$$Q_{base} = \frac{K \cdot \Delta x \cdot \Delta y \cdot (\xi - h)}{L}$$

$$q_{base} = \frac{K(\xi - h)}{L}$$

Seepage from surface water to groundwater

3.25

$$q_{base} = \frac{(\xi - h)}{\frac{L_{riv}}{K_{riv}} + \frac{L_2}{K_{i,j,k}}}$$

Seepage from surface water through riverbed

3.26

$$q_{base} = \frac{(h_{i,j,k} - h_{i,j,k+1})}{\frac{L_1}{K_1} + \frac{L_2}{K_2}}$$

Seepage from groundwater to groundwater

Code Extract 5.B Calculating seepage in HYDMOD subroutines.

```

      headdiff=eu(i,j,k)-eu(i,j,k+1)
      select case(subsurface(i,j,k))
      case(-1)
C       Dry cell
      case(0)
C       Surface Water Cell
        if(riverbed) then
          L=0.5 * (HCEN(i,j,k+1)-RIVTHK-HCEN(i,j,k))
          wm(i,j,k)=(headdiff)/((RIVTHK/KRIV)+(L/permab(i,j,k)))
        else
          L = 0.5 * (HCEN(i,j,k+1)-HCEN(i,j,k))
          wm(i,j,k)= permab(i,j,k+1)*(headdiff/L)
        endif
      case(1)
C       Unconfined Aquifer Cell
          L1 = 0.5 * (eu(i,j,k)+HCEN(i,j,k))
          L2 = 0.5 * (HCEN(i,j,k+1)-HCEN(i,j,k))
          perm1 = permab(i,j,k)
          perm2 = permab(i,j,k+1)
          wm(i,j,k)=(headdiff)/((L1/perm1)+(L2/perm2))
      case(2)
C       Aquifer Cell with groundwater above (pseudo-confined)
          L1 = 0.5 * (HCEN(i,j,k)-HCEN(i,j,k-1))
          L2 = 0.5 * (HCEN(i,j,k+1)-HCEN(i,j,k))
          perm1 = permab(i,j,k)
          perm2 = permab(i,j,k+1)
          wm(i,j,k)=headdiff/((L1/perm1)+(L2/perm2))
      case(3)
C       Aquifer Cell with Surface water above
        if(riverbed) then
          L1 = 0.5 * (HCEN(i,j,k)-RIVTHK-HCEN(i,j,k-1))
        else
          L1 = 0.5 * (HCEN(i,j,k)-HCEN(i,j,k-1))
        endif
          L2 = 0.5 * (HCEN(i,j,k+1)-HCEN(i,j,k))
          perm1 = permab(i,j,k)
          perm2 = permab(i,j,k+1)
          wm(i,j,k)=headdiff/((L1/perm1)+(L2/perm2))
      end select

```

5.5.2 HYDMOD subroutines

In 3.21 S_s is defined as $S_s = \rho g(\alpha_m + n\beta_w)$ where beta (compressibility of the fluid) is approximately 4.4×10^{-10} for water. This has been used in the calculation of coefficient B (storage term for groundwater cells). Equations for all the coefficients are defined in Table 4.1 and Table 4.2. Recursion coefficients are defined in 4.27. Code Extract 5.C shows this section of the HYDMOD routine, with slight modifications for clarity. Significant coefficients are in bold. Most variables are self-explanatory, but for detailed definitions of some (particularly those in Htemp definition) see the full source code on the Appendix CD^a.

^a Source code stored in D:\DIVAST-SG General Model and Input Files\Source Code\

Code Extract 5.C Calculating Coefficients in HYDMOD subroutines

```

C -----Chooses correct Storage term-----
C
      if(subsurf.eq.0) then
        Btemp = 1.0
      elseif(subsurf.eq.1) then
        Btemp = porosit(i,j,k)
      elseif(subsurf.eq.2.or.subsurf.eq.3) then
        Btemp = 1000*9.81*(pvc(k)+porosit(i,j,k)*4.4E-10)
        *      *(HCEN(i,j,k)-HCEN(i,j,k-1))
      elseif(subsurf.eq.-1) then
        Btemp = 1.0
      else
        write(*,*) "Invalid subsurface value"
      end if

C-----Assigns qtop and qbase seepage-----
      if(subsurf.eq.1.or.subsurf.eq.0) then
        qtop = 0
      else
        qtop = wm(i,j,k-1)
      endif
      qbase = wm(i,j,k)

C-----Set-up coefficients-----
      Ctemp = HFDT/DELX
      Dtemp = Btemp*em(i,j,k)-Ctemp*(qyl(i,j,k)-qyl(i,jm1,k))
      *      +HFDT*(qtop - qbase)

      if(subsurf.gt.0) then
        Ftemp = 1.0
        perm = 0.5 * (permab(i+1,j,k)+permab(i,j,k))
        Gtemp = (perm * depx(i,j,k)) / (2*delx)
        Htemp = -Gtemp * (EL(IP1,J,k) - EL(i,j,k))
      Else
        Ftemp = ONE+D4BDFR
        Gtemp = D1DPC
        Htemp = QXL(I,J,K)-D2BETA*(DUUHDY+DUVHDY)+D3CORI*QYMAV
        *      -D4BDFR*QXL(I,J,K)+WSTRESS-D1DPC*(EL(IP1,J,K)
        *      -EL(I,J,K))+D5EDDY*(UM(IP1,J,K)+UM(IM1,J,K)
        *      +UMR+UML-FOUR*UMC)
      End if

C-----Recursion Coefficients-----
      P(I) = Ctemp / (Btemp + Ctemp*R(IM1))
      Q(I) = (Dtemp + Ctemp*S(IM1)) / (Btemp + Ctemp*R(IM1))
      R(I) = Gtemp / (Ftemp + Gtemp*P(I))
      S(I) = (Htemp + Gtemp*Q(I)) / (Ftemp + Gtemp*P(I))

```

The recursion coefficients are then used to determine the elevation and velocity by using.

4.21

$$a) h_i^{n+1} = -P_i p_{i+1/2}^{n+1} + Q_i$$

$$b) p_{i+1/2}^{n+1} = -R_i h_{i+1}^{n+1} + S_i$$

5.6 Hotstart Model

The addition of a hotstart function allows a model to be run, stopped and then continued from where it left off. In order for this to work, a 'snapshot' of the model at the required timestep is taken. The data required is shown in Table 5.1 and Table 5.2

Table 5.1: - i, j and k data required for Hotstart file

Variable	Description
QXL(I, J, k)	Flow per unit width in x-direction - lower timestep (n-1/2)
QXM(I, J, k)	Flow per unit width in x-direction - middle timestep (n)
QXU(I, J, k)	Flow per unit width in x-direction - upper timestep (n+1/2)
QYL(I, J, k)	Flow per unit width in y-direction - lower timestep (n-1/2)
QYM(I, J, k)	Flow per unit width in y-direction - middle timestep (n)
QYU(I, J, k)	Flow per unit width in y-direction - upper timestep (n+1/2)
EL(I, J, k)	Water elevation above datum - lower timestep
EM(I, J, k)	Water elevation above datum - middle timestep
EU(I, J, k)	Water elevation above datum - upper timestep
UM(I, J, k)	Velocity in x-direction at centre of grid side
UMAV(I, j, k)	Velocity in x-direction at centre of cell
VM(I, J, k)	Velocity in y-direction at centre of grid side
VMAV(I, J, k)	Velocity in y-direction at centre of cell
wm(i, j, k)	Vertical Velocity (seepage) at centre of cell
DXX(I, J, k)	Dispersion Coefficient X
DYY(I, J, k)	Dispersion Coefficient Y
lyrbasex(i, j, k)	Elevation of base of layer k at centre of cell x sides
lyrbasey(i, j, k)	Elevation of base of layer k at centre of cell y sides
DEPX(I, J, k)	Depth of water in cell at centre of cell x sides
DEPY(I, J, k)	Depth of water in cell at centre of cell y sides
IWET(I, J, k)	IWET array defines type of each grid cell
HCEN(I, J, k)	Depth at centre of cells
SM(I, J, K, NS)	Solute concentration - lower timestep
SU(I, J, K, NS)	Solute concentration - upper timestep

Table 5.2: - i, and j data (surface water layer only) required for Hotstart file.

surfx(i, j)	Surface Elevation at cell sides - x
surfy(i, j)	Surface Elevation at cell sides - y
C(I, J)	Chezy values at surface
EDDY(I, J)	Eddy viscosity
URES(I, J)	Residual velocity x direction
VRES(I, J)	Residual velocity y direction
TAU(I, J)	Shear stress at surface
TAURES(I, J)	Residual shear stress

5.7 Summary

This chapter is a practical explanation of what modifications have been made to the surface water model in order to allow integrated surface-water – groundwater modelling. The method by which the equations derived in Chapter 3 and discretised in Chapter 4 have been implemented into the FORTRAN code have been shown. The input file has been described step-by-step to allow users to modify the model as required. The overall structure of the code is outlined and the hotstart facility is defined.

CHAPTER 6 ANALYTICAL VERIFICATION

6.1 *Introduction*

The preceding chapters describe mathematically and conceptually how the existing DIVAST numerical model simulates the behaviour of surface water, and how this model has been extended to include the behaviour of groundwater, and its interactions with surface water. In order for this extended model to be used as a predictive tool, it must first be ensured that the model is numerically accurate, i.e. the behaviour it predicts is that which is known to occur in reality. Differences in the numerical model results from natural situations will be due to two broad areas: incorrect derivation and implementation of the equations (mathematical error) and incorrect assumptions or simplifications in the equations themselves (conceptual error). Some errors could be classed as both, e.g. too large timestep or too coarse grid discretisation. The mathematical errors could also be caused by human error in coding, incorrect mathematical procedure in the discretisation or derivation, or simply a missed coefficient. It is important to iron out these mathematical errors before assessing the conceptual validity of the numerical model. Unfortunately, the errors may not be obvious. The model may produce results that look superficially correct, but with, for example, velocities twice as large as they should be, or with elevations changing slower than they should. An independent solution to the problem is required.

Analytical solutions to mathematical equations offer a very useful method of checking for the numerical accuracy of the model. An analytical solution uses pure mathematical techniques applied to the governing equations. The problem is not discretised in time or space as for a numerical solution, however, the governing equations are simplified and solved as directly as possible. This means that, provided the mathematics is valid, there is no issue of conceptual error (at least, so long as the governing equations are correct), and provided the solution is

evaluated carefully, there should be no mathematical error. This gives a definite answer to which the numerical solution can be compared. Unfortunately, analytical solutions have to be simple in terms of equation formulation - there is no question of solving the complex geometries found in actual estuaries or rivers. Analytical models tend to use idealised geometries and generalised boundary conditions that can be described by simple formulae. Numerical models which are, almost by definition, simplifications of the situation in reality, are used to simulate real situations because by discretising in time and space highly complex problems can be broken down and modelled relatively easily.

This chapter aims to use analytical solutions to simplified surface water / groundwater problems to assess the mathematical validity of the extended DIVAST-SG model. The surface water component of the model has been tried and tested over many years, so this study focuses on the extended portion – the groundwater itself, and the surface water / groundwater interface.

6.2 Derivation of the equation

The analytical validation carried out in this section is based on the equations suggested by Cooper and Rorabaugh (1963). They are derived for a number of scenarios. An aquifer of finite length l will be considered here. The groundwater-surface water interaction is based on a flood wave in a fully-penetrating river, adjacent to an aquifer of the same depth as the river. The river has vertical banks and cannot overflow. Variations in the water table are assumed to be small in comparison with the depth of the aquifer, which means that the transmissivity is assumed to be constant in time and space. No recharge is assumed over the aquifer, thus the groundwater variations are due solely to the flood wave in the river.

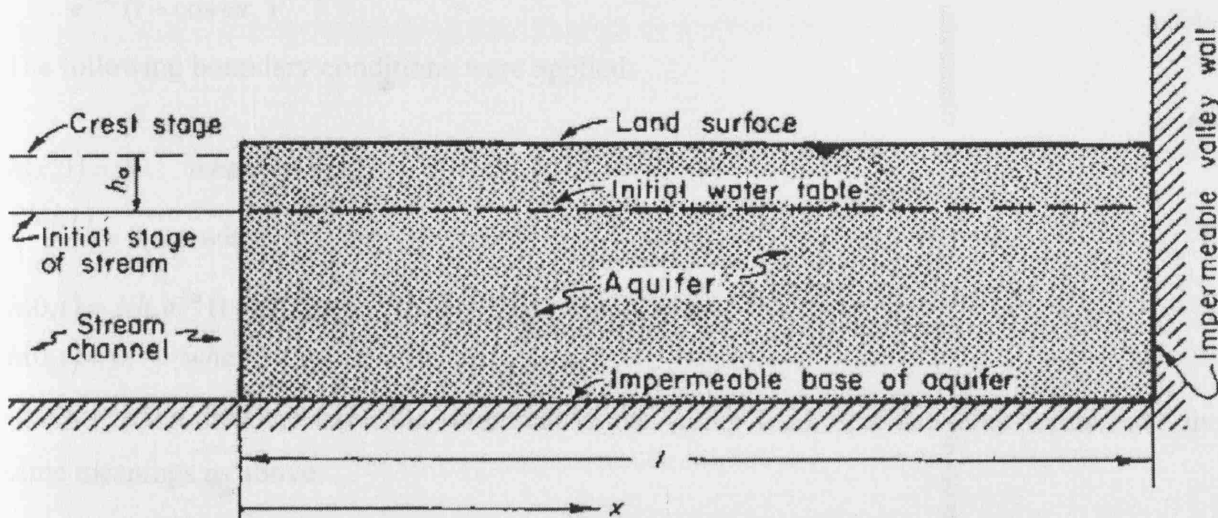


Figure 6.1: - Schematic illustration of aquifer (from Cooper and Rorabaugh 1963)

The differential equation governing non-steady flow of *confined* groundwater in one dimension is as follows (See, for example, Bras 1990 p. 299):

6.1

$$\frac{\partial^2 h}{\partial x^2} - \frac{1}{\sigma} \frac{\partial h}{\partial t} = 0$$

where σ is T/S , or diffusivity of the aquifer. T is the transmissivity of the aquifer (kb , i.e. permeability multiplied by aquifer depth), and S is the coefficient of storage of the aquifer (i.e. n porosity, for an unconfined aquifer). For the purpose of this study this equation was applied to the flow of *unconfined* groundwater, making the assumption that changes in the height of the water table are small in relation to the average depth of flow. Equation 6.1 can be obtained by substituting Darcy's Law into the mass conservation equation in one dimension.

The flood wave is approximated by the equation:

6.2

$$\psi(t) = \begin{cases} Nh_0 e^{-\delta} (1 - \cos \omega t), & \text{when } 0 \leq t \leq \tau \\ 0, & \text{when } t > \tau \end{cases}$$

where h_0 is the maximum rise in height of the flood wave (m), t is the time since the start of the wave, τ is the duration of the wave, ω is the wave frequency $2\pi/\tau$, δ is a constant that defines the degree of asymmetry $\delta = \omega \cot(\omega t_c/2)$, t_c is the time of the flood crest, and N is a constant that serves to make the curves of the family peak at the same height h_0 .

N is given by:

6.3

$$N = \frac{1}{e^{-\delta} (1 - \cos \omega t_c)}$$

The following boundary conditions were applied:

6.4

$$\begin{aligned} h(x,0) &= 0, & \text{when } 0 \leq x \leq l \\ \frac{\partial h(l,t)}{\partial x} &= 0, & \text{when } t \geq 0 \\ h(0,t) &= Nh_0 e^{-\delta} (1 - \cos \omega t), & \text{when } 0 \leq t \leq \tau \\ h(0,t) &= 0, & \text{when } t \geq \tau \end{aligned}$$

where l is the distance from the riverbank to the valley wall, and the other terms have the same meanings as above.

Cooper and Rorabaugh solve this equation by applying the Laplace transformation with respect to time (i.e. variable t (time) becomes p (frequency)). The solution to the Laplace transform is found, and the inverse transform provides the equation in the time domain. It is found that the solution involves summing the residues of the function $f(p) = e^{pt} h(p)$ to give

6.5

$$h = Nh_0 \Sigma [\text{Res } f(p)]$$

Finding equations for all the residues at the poles of $f(p)$ and adding them together by superposition, results in the following equations:

Solution for $t \leq \tau$

6.6

$$h_{t \leq \tau} = Nh_0 \left\{ e^{-\delta t} \left[\frac{\cos[(l-x)\sqrt{\delta/\sigma}]}{\cos[l\sqrt{\eta/\sigma}]} - A \cos(\omega t + \theta) \right] + \frac{4}{\pi} \sum_{n=1}^{\infty} \sin[(2n-1)\pi x / 2l] \frac{(2n-1)e^{-(2n-1)^2 \beta \omega t}}{[\eta - (2n-1)^2] + [\eta - (2n-1)^2]^{\frac{3}{2}} \beta^2} \right\}$$

Solution for $t \geq \tau$

6.7

$$h_{t \geq \tau} = \frac{4Nh_0}{\pi} \sum_{n=1}^{\infty} \sin[(2n-1)\pi x / 2l] \cdot \frac{(2n-1) \left[1 - e^{-[\eta - (2n-1)^2] \frac{1}{2} \pi \beta} \right] e^{-(2n-1)^2 \beta \omega t}}{[\eta - (2n-1)^2] + [\eta - (2n-1)^2]^{\frac{3}{2}} \beta^2}$$

where A , η , β and θ are defined as:

$$A = \left[\frac{\cos^2 a \xi + \sinh^2 b \xi}{\cos^2 a + \sinh^2 b} \right]^{1/2} \quad a = l \left[\frac{(\delta^2 + \omega^2)^{1/2} + \delta}{2\sigma} \right]^{1/2} = \pi \left[\frac{(\eta^2 + 1/\beta^2)^{1/2} + \eta}{8} \right]^{1/2}$$

$$b = l \left[\frac{(\delta^2 + \omega^2)^{1/2} - \delta}{2\sigma} \right]^{1/2} = \pi \left[\frac{(\eta^2 + 1/\beta^2)^{1/2} - \eta}{8} \right]^{1/2}$$

$$\xi = \frac{l-x}{l}$$

$$\eta = \frac{\delta}{\beta \omega}$$

$$\beta = \frac{\pi \sigma \tau}{8l^2} = \frac{\pi \tau T}{8l^2 S} = \frac{kb \pi \tau}{8l^2 S}$$

$$\theta = \arctan \left[\frac{\sin a \xi \sinh b \xi \cos a \cosh b - \cos a \xi \cosh b \xi \sin a \sinh b}{\cos a \xi \cosh b \xi \cos a \cosh b + \sin a \xi \sinh b \xi \sin a \sinh b} \right]$$

Equations 6.6 and 6.7 give the groundwater head at any point x and time t .

The flow in groundwater is proportional to dh/dx , as stated in Darcy's Law (see Section 3.6). Equations 6.6 and 6.7 can now be differentiated to obtain the flow per unit length of river. Setting $x = 0$ will give the flow at the riverbank, i.e. the flow entering the river from the aquifer, as:

$$Q = kA \frac{\partial h}{\partial x} = \frac{k}{b} \cdot 1 \cdot \frac{\partial h(x, t)}{\partial x} = T \frac{\partial h(x, t)}{\partial x} \quad 6.8$$

$$Q_{t \leq \tau} = Nh_0 \sqrt{\omega TS} \left\{ e^{-\eta \beta \omega t} \left[\sqrt{\eta \beta} \tan \frac{\pi \sqrt{\eta}}{2} + B \cos(\omega t + \varphi) \right] + \frac{4\sqrt{\beta}}{\pi} \sum_{n=1}^{\infty} \frac{(2n-1)^2 e^{-(2n-1)^2 \beta \omega t}}{[\eta - (2n-1)^2] + [\eta - (2n-1)^2]^3 \beta^2} \right\} \quad 6.9$$

$$Q_{t \geq \tau} = Nh_0 \sqrt{\omega TS} \cdot \frac{4\sqrt{\beta}}{\pi} \sum_{n=1}^{\infty} \frac{(2n-1)^2 [1 - e^{-[\eta - (2n-1)^2] 2\pi\beta}] e^{-(2n-1)^2 \beta \omega t}}{[\eta - (2n-1)^2] + [\eta - (2n-1)^2]^3 \beta^2} \quad 6.10$$

$$\text{where } B = (\eta^2 \beta^2 + 1)^{1/4} \left[\frac{\cosh 2b - \cos 2a}{\cosh 2b + \cos 2a} \right]^{1/2} \text{ and } \varphi = \arctan \left[\frac{a \sinh 2b + b \sin 2a}{b \sinh 2a - a \sin 2a} \right].$$

The bank storage, or the total amount of water stored in the bank in addition to the starting volume, can be found by integrating the flow with respect to time, but this is unnecessary for the current task.

When $\delta = 0$, the equations simplify slightly as the flood wave takes on a simple symmetrical sinusoidal shape. β is the dimensionless parameter that defines the aquifer; as it gets smaller the aquifer tends towards the limiting value of $\beta = 0$ (a semi-infinite aquifer), i.e. an aquifer that is large enough or 'slow' enough that the fluctuations due to the river stage variation do not reach the valley wall, and hence the valley wall has no effect on the groundwater heads. When $\beta < 1 \times 10^{-5}$ the finite aquifer equations become impractical to evaluate numerically, (i.e. they contain coefficients greater than $1 \times 10^{+999}$) and the semi-infinite equations should be used instead. Full derivations of these equations can be found in Cooper and Rorabaugh (1963). Once β drops below approximately 0.01, the finite and semi-finite equations produce similar results (for groundwater head).



Groundwater head for semi-infinite aquifer when $t \leq \tau$:

6.11

$$h_{t \leq \tau} = \frac{h_0}{2} \left\{ \operatorname{erfc} \left[\frac{x}{2\sqrt{\sigma t}} \right] - e^{-x\sqrt{\omega/2\sigma}} \cos \left[\omega t - x\sqrt{\frac{\omega}{2\sigma}} \right] + \frac{1}{\pi} \int_0^\infty e^{-u^2} \sin \left[x\sqrt{\frac{u}{\sigma}} \right] \frac{u}{u^2 + \omega^2} du \right\}$$

Groundwater head for semi-infinite aquifer when $t > \tau$

6.12

$$h_{t > \tau} = \frac{h_0}{2} \left\{ \operatorname{erfc} \left[\frac{x}{2\sqrt{\sigma t}} \right] - \operatorname{erfc} \left[\frac{x}{2\sqrt{\sigma(t-\tau)}} \right] + \frac{1}{\pi} \int_0^\infty [e^{-u^2} - e^{-u^2(t-\tau)}] \sin \left[x\sqrt{\frac{u}{\sigma}} \right] \frac{u}{u^2 + \omega^2} du \right\}$$

6.3 Evaluating the Equations

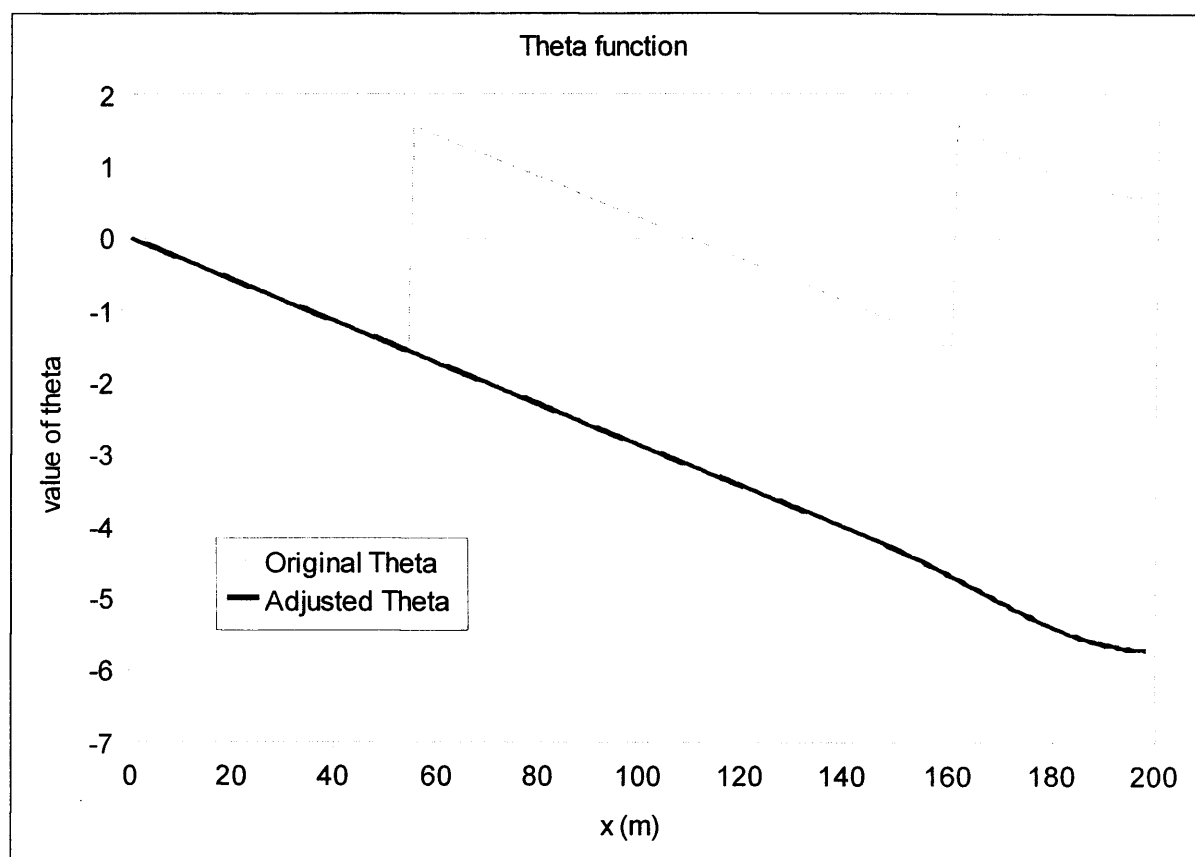
A specific scenario for these equations can be defined by setting the following parameters:

1. t time at which equation is solved (T)
2. τ duration of flood wave, (T)
3. t_c time to crest of flood wave, (T)
4. h_0 height of flood peak above starting level, (L)
5. S storage coefficient (porosity), (dimensionless)
6. k aquifer permeability, (LT^{-1})
7. b aquifer depth, (L)
8. l distance to valley wall from riverbank, (L)

Care must be taken when solving these equations for specific scenarios. If calculated using a spreadsheet such as Excel, for example, then the arctangent function (a.k.a. arctan, inverse tan or \tan^{-1}) in θ and ϕ (equations 6.7 and 6.10), will only give principle values in the range $-\pi/2$ to $+\pi/2$, whereas the required value may be any multiple of π of this value. If this principle value behaviour is used to calculate θ (Eq. 6.7), then the function will by jump up to $+\pi/2$ each time the expression in the brackets changes sign. The function should be adjusted by an integer multiple of π each time the term in brackets in θ changes sign moving along the x -axis; until it forms a continuous expression as shown in Figure 6.2. If this adjustment is not performed then the groundwater head becomes inaccurate and jumps as shown in Figure 6.3. These figures were produced using the scenario variables in Table 6.1.

Table 6.1: - variables used in Figures 6.2 and 6.3.

τ (s)	28800
t_c (s)	14400
h_0 (m)	1
S (-)	0.3
k (m/s)	2.00E-03
b (m)	20
l (m)	200
t (s)	24000

**Figure 6.2: - original and adjusted value of theta function**

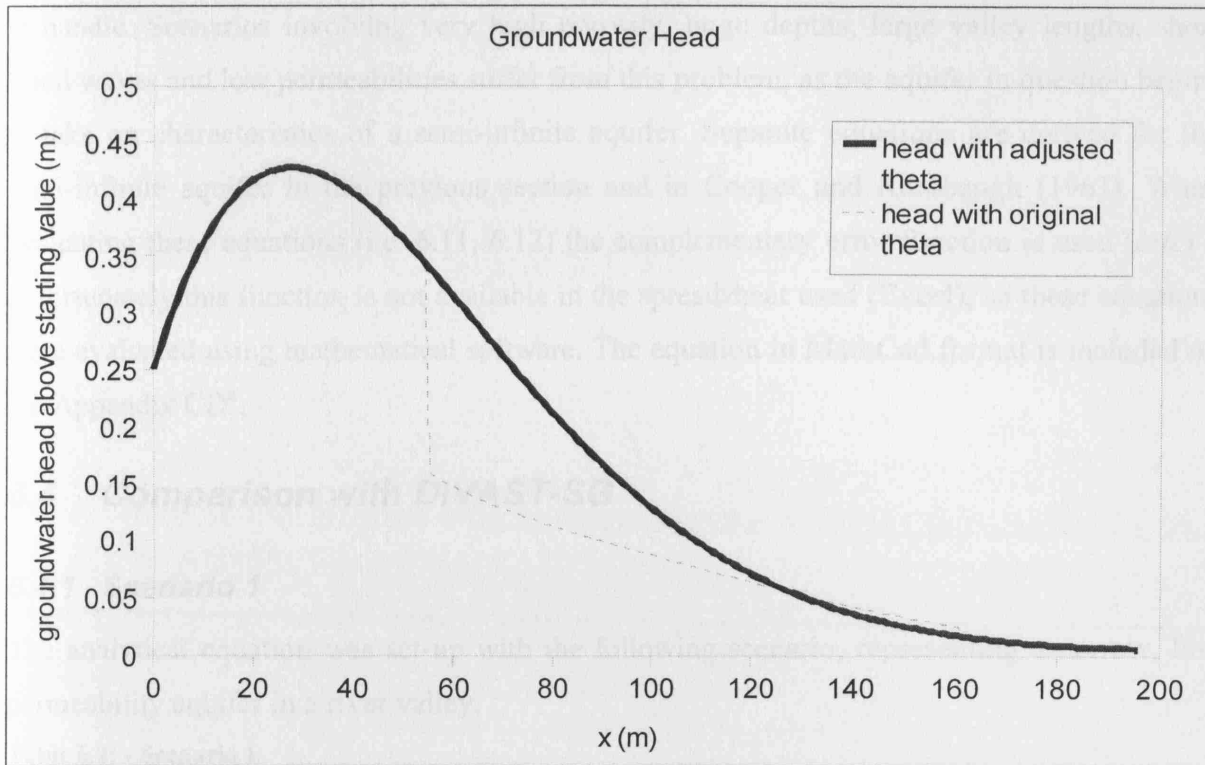


Figure 6.3: - Groundwater head using original and adjusted value of phi

This jump occurs when:

$$\cos a\xi \cosh b\xi \cos a \cosh b = -\sin a\xi \sinh b\xi \sin a \sinh b \quad 6.13$$

Or if $\delta = 0$, when:

$$\cos \frac{\pi\xi}{\sqrt{8\beta}} \cosh \frac{\pi\xi}{\sqrt{8\beta}} \cos \frac{\pi}{\sqrt{8\beta}} \cosh \frac{\pi}{\sqrt{8\beta}} = -\sin \frac{\pi\xi}{\sqrt{8\beta}} \sinh \frac{\pi\xi}{\sqrt{8\beta}} \sin \frac{\pi}{\sqrt{8\beta}} \sinh \frac{\pi}{\sqrt{8\beta}} \quad 6.14$$

Each time this condition occurs in the range $0 < x < l$, an additional π must be subtracted from the original θ function. This makes the equation hard to plot using mathematical software, so instead a spreadsheet is used here. See the spreadsheet on the Appendix CD^a for more information.

In addition, although final values produced by the formula are relatively small, sometimes very large numbers are produced which are then cancelled out. Most spreadsheets will not allow values greater than $1 \times 10^{+999}$ to be utilised in a calculation. As β gets smaller, the numbers produced by the sinh and cosh expressions get larger, until they become unmanageable. When β drops below 1×10^{-5} the expressions tend to produce results too large

^a Spreadsheet file: D:\Analytical Validation\Analytical Equation - Cooper - Spreadsheet Solver.xls

to handle. Scenarios involving very high porosity, large depths, large valley lengths, short flood waves and low permeabilities suffer from this problem, as the aquifer in question begins to take on characteristics of a semi-infinite aquifer. Separate equations are derived for the semi-infinite aquifer in the previous section and in Cooper and Rorabaugh (1963). When evaluating these equations (i.e. 6.11, 6.12) the complementary error function is used (*erfc*) – unfortunately this function is not available in the spreadsheet used (Excel), so these equations were evaluated using mathematical software. The equation in MathCad format is included on the Appendix CD^a.

6.4 Comparison with DIVAST-SG

6.4.1 Scenario 1

The analytical equation was set-up with the following scenario, representing a narrow, low permeability aquifer in a river valley.

Table 6.2: - Scenario 1

Parameter	Symbol	Value
Length of flood wave	T	8 hours (28800 seconds)
Time to crest	T_c	4 hours (14400 seconds)
Height of Flood Wave	h_0	1 metre
Storage Coefficient	S or n	0.2
Aquifer Permeability	K	5×10^{-5} m/s
Aquifer Depth	B	10 m
Distance to Valley Wall	L	100 m

The numerical model was set up to model this scenario. The input file can be found on the Appendix CD^b and also in Appendix A. A 106 x 18 grid was used with a grid spacing of 1m. The aquifer was exactly 100 cells long, with an open water area 4 cells wide at the end. The open boundary was defined as in Eq. 6.2 at 50 specific times during the flood wave. The model was run for 20 hours model time, with a half timestep of 0.5 seconds. Figure 6.4 shows the results for both the analytical solution and the numerical model at 4, 6, 8, 12, 16 and 19.5 hours. The flood wave is 8 hours long, the peak of the flood wave occurs at 4 hours and 6 hours is on the falling limb. The other times are all after the wave has passed and show the bank storage falling. The solid lines show the analytical solution, and the discrete points are from the numerical model, $x = 0$ marks the riverbank.

^a Mathcad file: D:\Analytical Validation\infinite.mcd

^b Input file: D:\Analytical Validation\cooper100.dsg

Comparison of model and analytical results for $l=100\text{m}$, $k=5\text{E-}5$, $n=0.2$, 8hr flood wave, wave height= 1m , aquifer depth= 10m , Grid Spacing = 1m

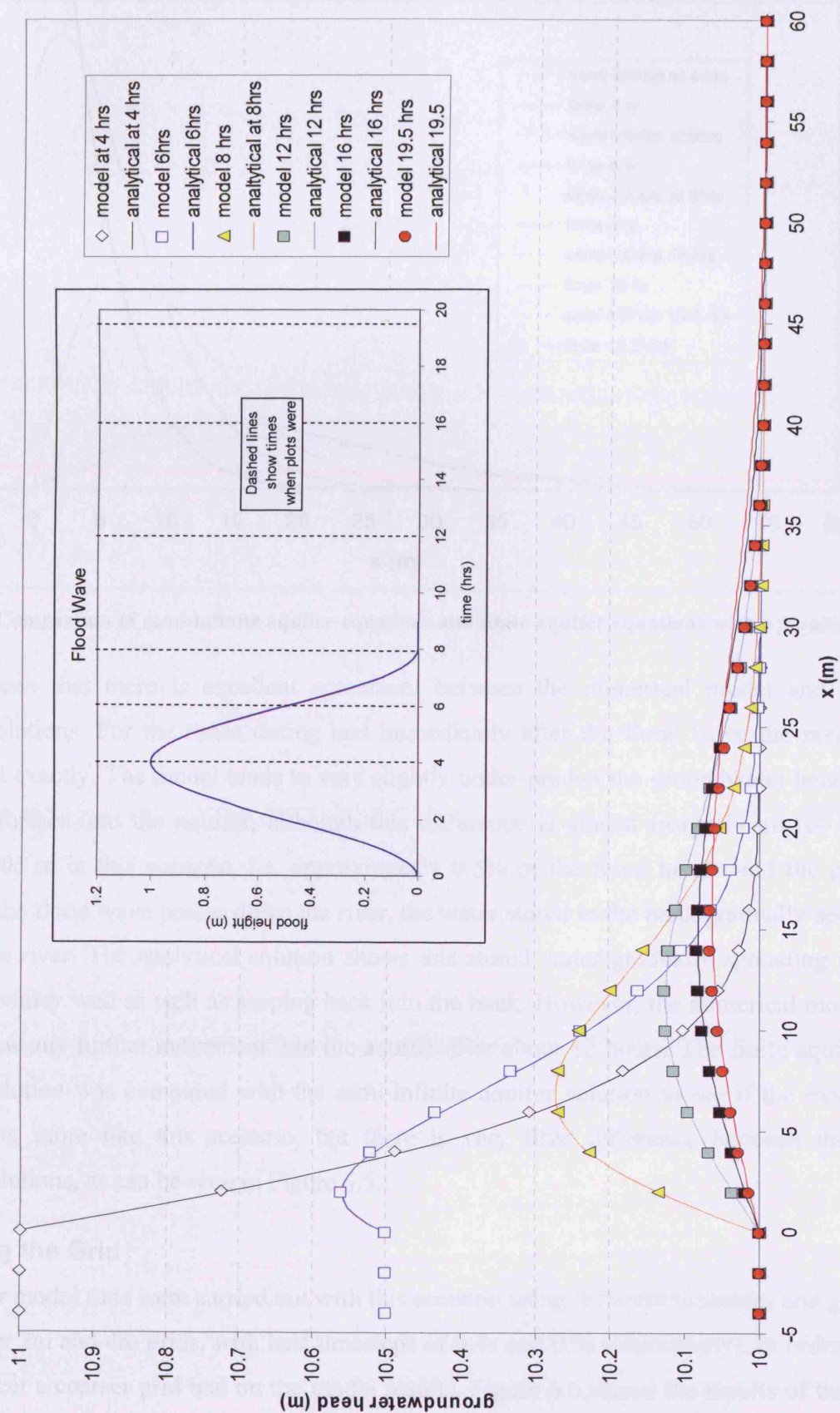


Figure 6.4: - Comparison of analytical result and numerical model - scenario 1

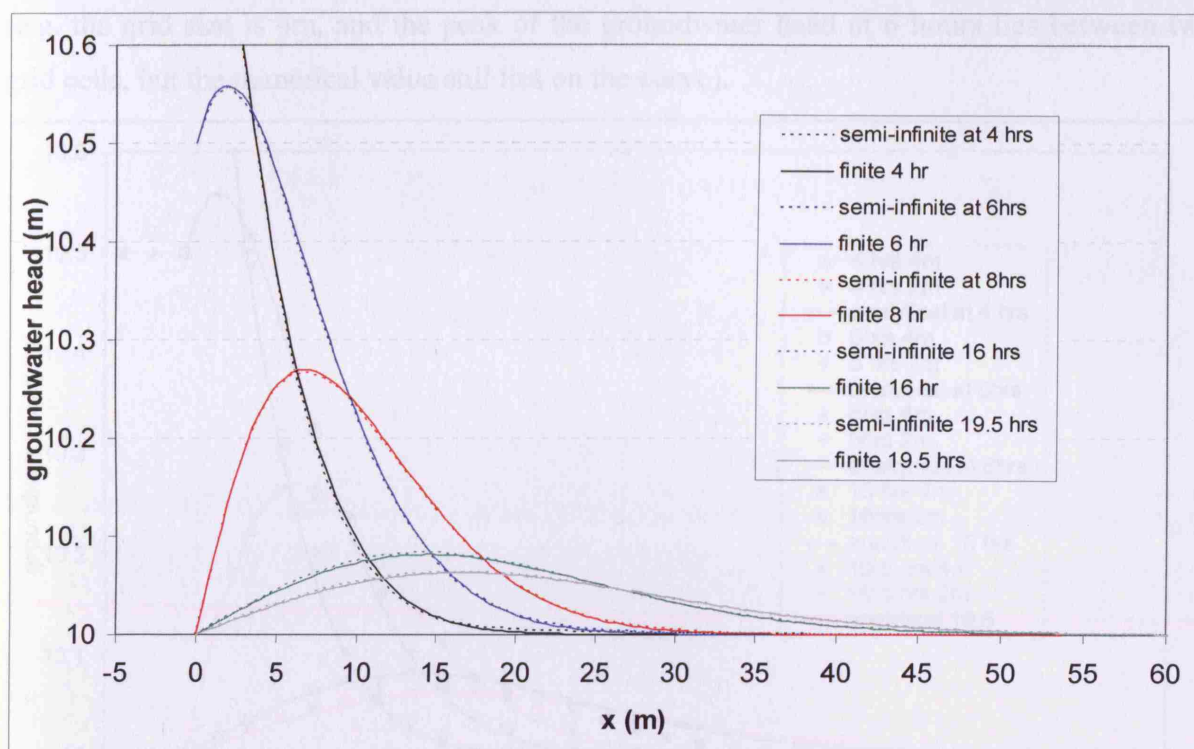


Figure 6.5: - Comparison of semi-infinite aquifer equations and finite aquifer equations with a β value of 0.0028.

It can be seen that there is excellent agreement between the numerical model and the analytical solutions. For the times during and immediately after the flood wave the results agree almost exactly. The model tends to very slightly under-predict the groundwater head at later times further into the aquifer, although this difference is almost insignificant (of the order of 0.005 m in this scenario, i.e. approximately 0.5% of the flood height and the grid size). After the flood wave passes down the river, the water stored in the bank gradually seeps back into the river. The analytical solution shows this stored water gradually spreading out towards the valley wall as well as seeping back into the bank. However, the numerical model does not show any further movement into the aquifer after about 12 hours. The finite aquifer analytical solution was compared with the semi-infinite aquifer solution to see if the model was behaving more like this scenario, but there is very little difference between these analytical solutions, as can be seen in Figure 6.5.

Coarsening the Grid

Several other model runs were carried out with this scenario using different timesteps and grid sizes (namely 2m and 4m grids, with half timesteps of 0.4s and 0.5s respectively), in order to see what effect a coarser grid had on the model results. Figure 6.6 shows the results of these runs, together with the analytical solutions. It can be seen that the numerical solution is quite robust, even at relatively coarse grid sizes compared to the curve of the groundwater head

(e.g. the grid size is 4m, and the peak of the groundwater head at 6 hours lies between two grid cells, but the numerical value still lies on the curve).

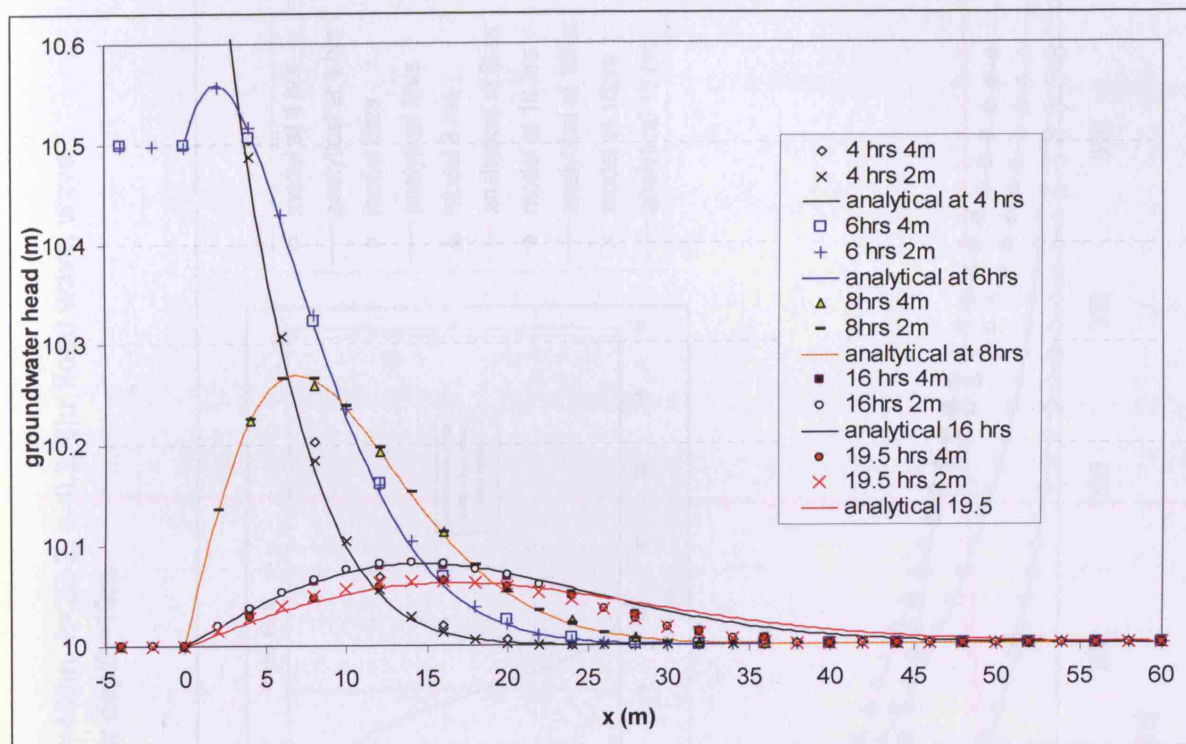


Figure 6.6: - Effect of changing the grid size on the model.

6.4.2 Scenario 2

A scenario with higher permeability and porosity, and a longer distance to the valley wall was tested. This represents a wider river valley adjacent to a highly permeable aquifer. The variables are shown in Table 6.3. The same grid 106 x 18 was used in the numerical model, with a grid-size of 4m.

Table 6.3: - Scenario 2

Parameter	Symbol	Value
Length of flood wave	τ	8 hrs (28800 secs)
Time to crest	t_c	4 hrs (14400 secs)
Height of Flood Wave	h_0	1 m
Storage Coefficient	S or n	0.3
Aquifer Permeability	k	2×10^{-2} m/s
Aquifer Depth	b	10 m
Distance to Valley Wall	l	400 m

Figure 6.7 shows comparisons at 4, 6, 8, 10, and 16 hours, β for this scenario being 0.047. In this scenario the numerical model consistently predicted the analytical solution – the largest deviation being about 1.3 cm (i.e. 1.3 % of the flood height) at 120m into the aquifer after 6 hours – the numerical model tended to overestimate the groundwater head very slightly here.

Comparison of model and analytical results for $l=400\text{m}$, $k=2\text{E-}2$, $n=0.3$, 8hr flood wave, wave height=1m, aquifer depth=10m

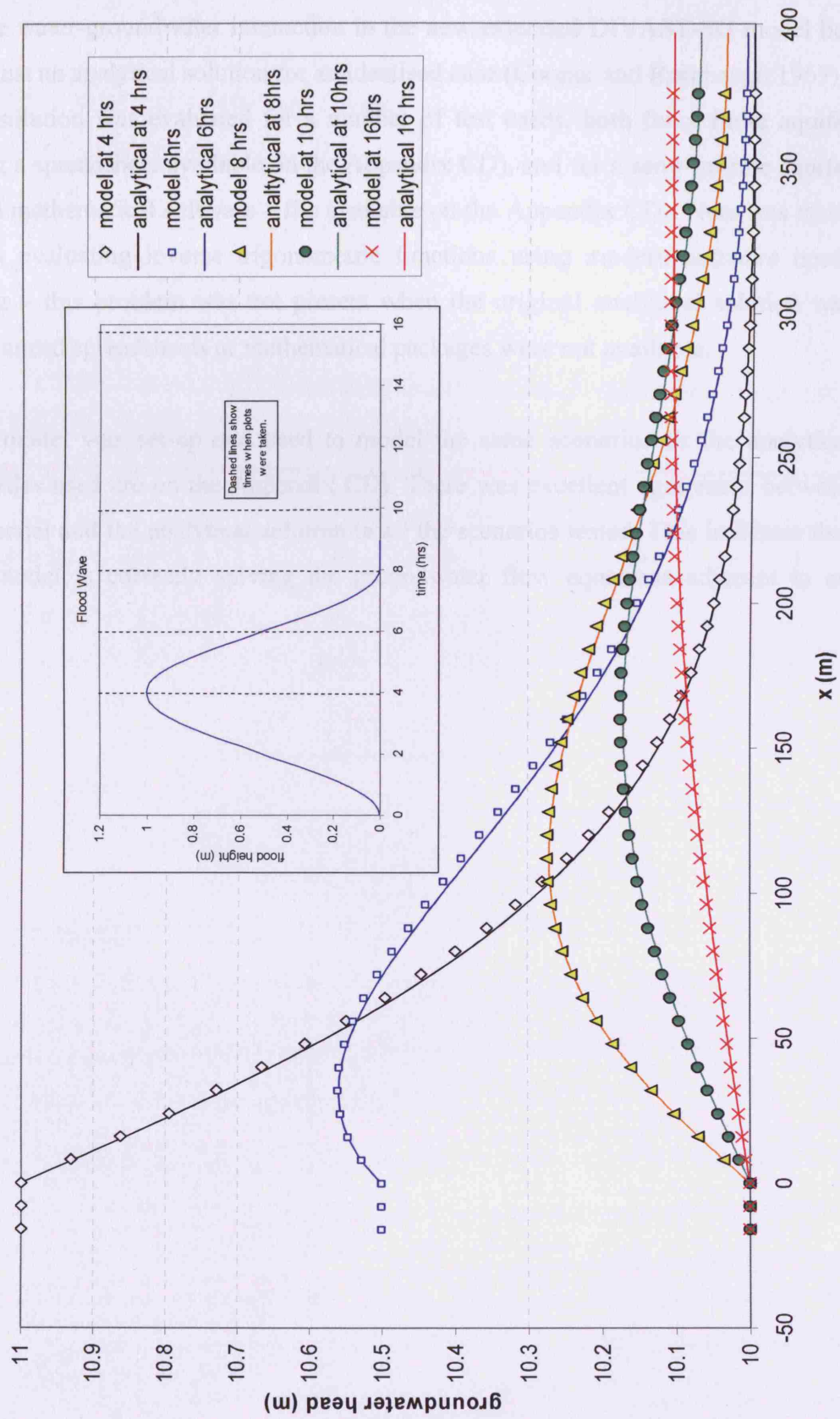


Figure 6.7: - Comparison of analytical solution and numerical model – scenario 2

6.5 Summary of Analytical Verification

The 2-D surface water-groundwater interaction in the new extended DIVAST-SG model has been tested against an analytical solution for an idealised case (Cooper and Rorabaugh 1963). The analytical solution was evaluated for a number of test cases, both for a finite aquifer (evaluated using a spreadsheet available on the Appendix CD), and for a semi-infinite aquifer (using MathCad mathematical software – file available on the Appendix CD). Note was taken of the fact that evaluating inverse trigonometric functions using modern software needs careful handling – this problem was not present when the original analytical solution was proposed as advanced spreadsheets or mathematical packages were not available.

The numerical model was set-up and used to model the same scenarios as the analytical solution (input files used are on the Appendix CD). There was excellent agreement between the numerical model and the analytical solution in all the scenarios tested. This indicates that the numerical model is correctly solving the groundwater flow equations adjacent to an idealised river.

CHAPTER 7 LABORATORY VALIDATION

7.1 *Introduction*

The Hyder Hydraulics Laboratory at Cardiff University has a large tidal basin that has been previously used for physical models of Cardiff Bay and artificial sand bars (Ebrahimi 2004). It was decided that the tidal basin could be adapted to simulate a surface water – groundwater scenario, and used to validate the model for this project. The flume was constructed (section 7.2) and initial experiments carried out. The properties of the laboratory set-up were measured in several ways (section 7.3).

However, several problems with the design and the construction of the flume meant that only limited conclusions could be drawn from these experiments. These initial experiments were carried out with the help of Diana Kountcheva. Section 7.4 is a summary of this work; further details can be found in Sparks (2006).

Lessons learnt in this initial experimentation were used to modify the flume construction and improve the experimental procedure (section 7.5 and 7.6) and further experimentation was carried out on both water levels (section 7.7) and tracer movement (section 7.8).

7.2 *Flume Design and Construction*

Figure 7.1 shows the flume prior to the start of the study reported here. A rectangular tank with a suspended base was used for the tidal basin. Water was supplied from pipes connected to the main re-circulation tank. Water enters the basin through a large perforated pipe seen in Figure 7.2, and accumulates underneath the suspended base of the model. Holes in the suspended floor of the basin allowed the water level to rise to a predefined point within the flume. The water level in the main area of the flume is controlled by a movable weir on the right hand side of the figure. Water is pumped into the area between the baffle and the weir, to ensure that the water level is always the same as the weir elevation. The weir can then be

raised or lowered manually or via a computer program and the water levels in the flume follow the movement of the weir. The first baffle after the weir prevents turbulence from the pumped water from entering the flume area, thus ensuring that water levels in the flume area change smoothly.

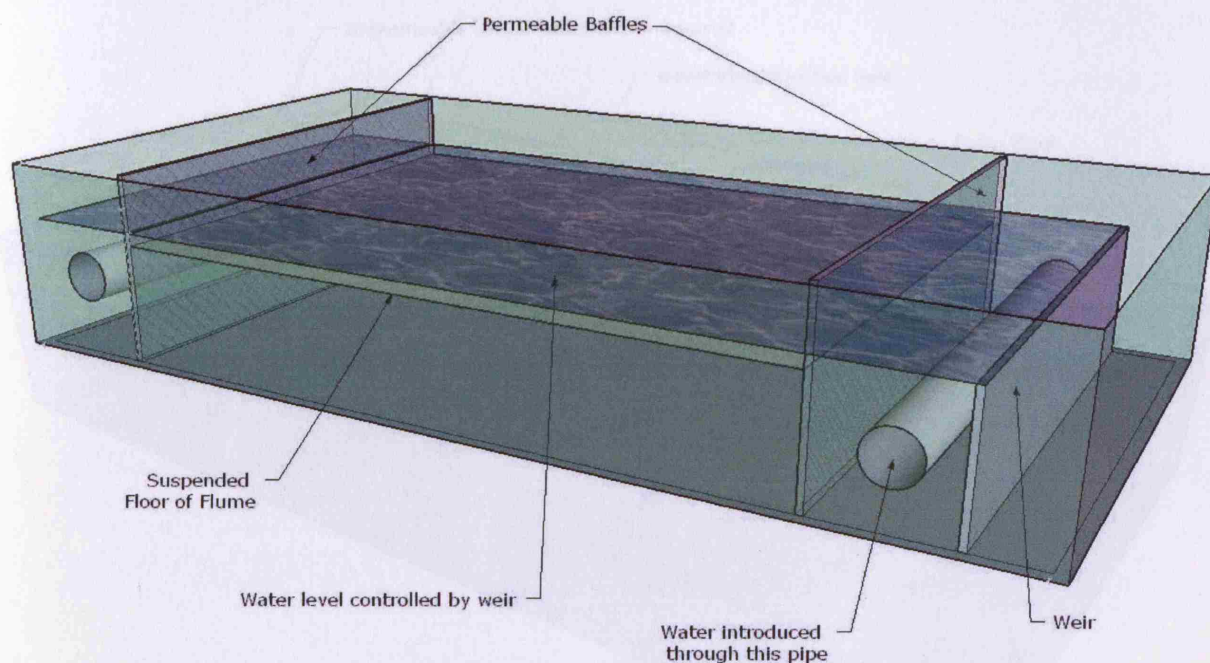


Figure 7.1: - Construction of Tidal Basin at Hyder Hydraulics Laboratory, Cardiff University

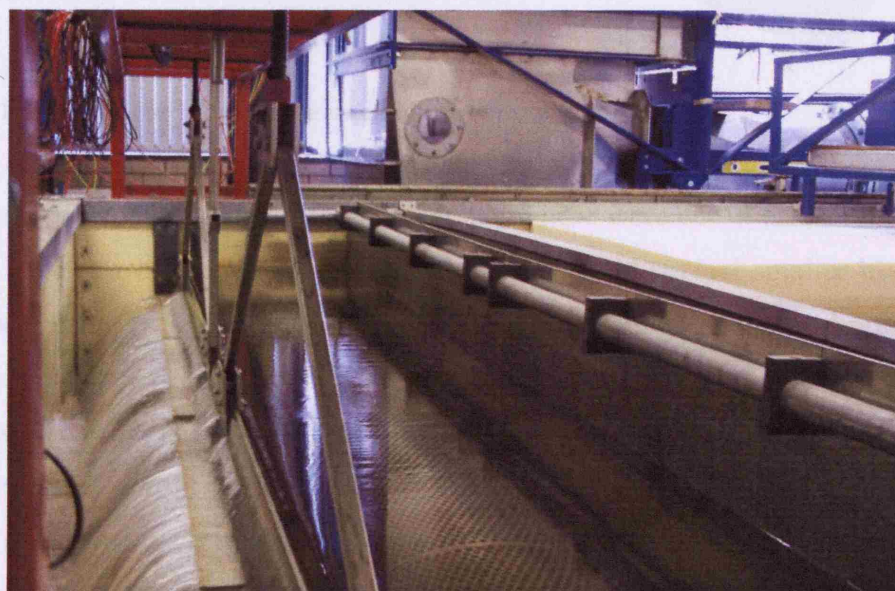


Figure 7.2: - Movable weir on left, perforated inflow pipe, and baffle screen.

It was proposed that foam blocks were used to construct a 'river-bank', and allow water and tracer to move through the idealised groundwater. Several samples of foam were obtained and tests performed to determine the approximate permeability. These and subsequent tests are

detailed in Section 7.3 below. The foam was found to be relatively permeable compared to sand, which is normally used in physical modelling of groundwater. See section 7.3 for more details.

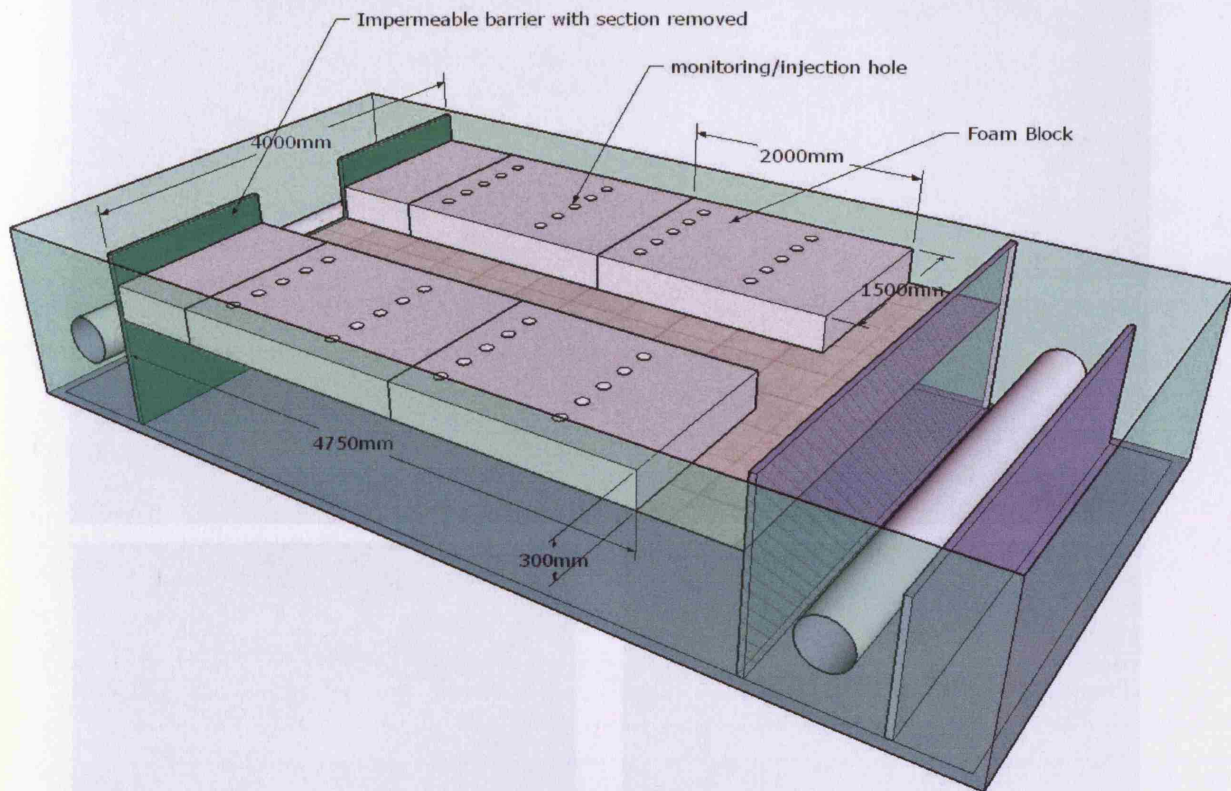


Figure 7.3: - Layout of foam blocks in flume and initial set-up of channel.

The foam was provided as 3m x 2m x 0.5m blocks. These were cut in half and trimmed using an adapted band saw to give 1.5m x 2m x 0.3m blocks, and several smaller blocks. Initially the blocks were simply placed into the flume in the arrangement shown in Figure 7.3. A few monitoring holes were drilled in the foam using a sharpened piece of copper pipe 100 mm in diameter, as seen in Figure 7.4. Initially only a few holes were drilled, more were added later when further monitoring locations were required. Using this set-up, initial experiments were carried out using fluorescent dye Rhodamine WT. These initial experiments are summarised in the next section.

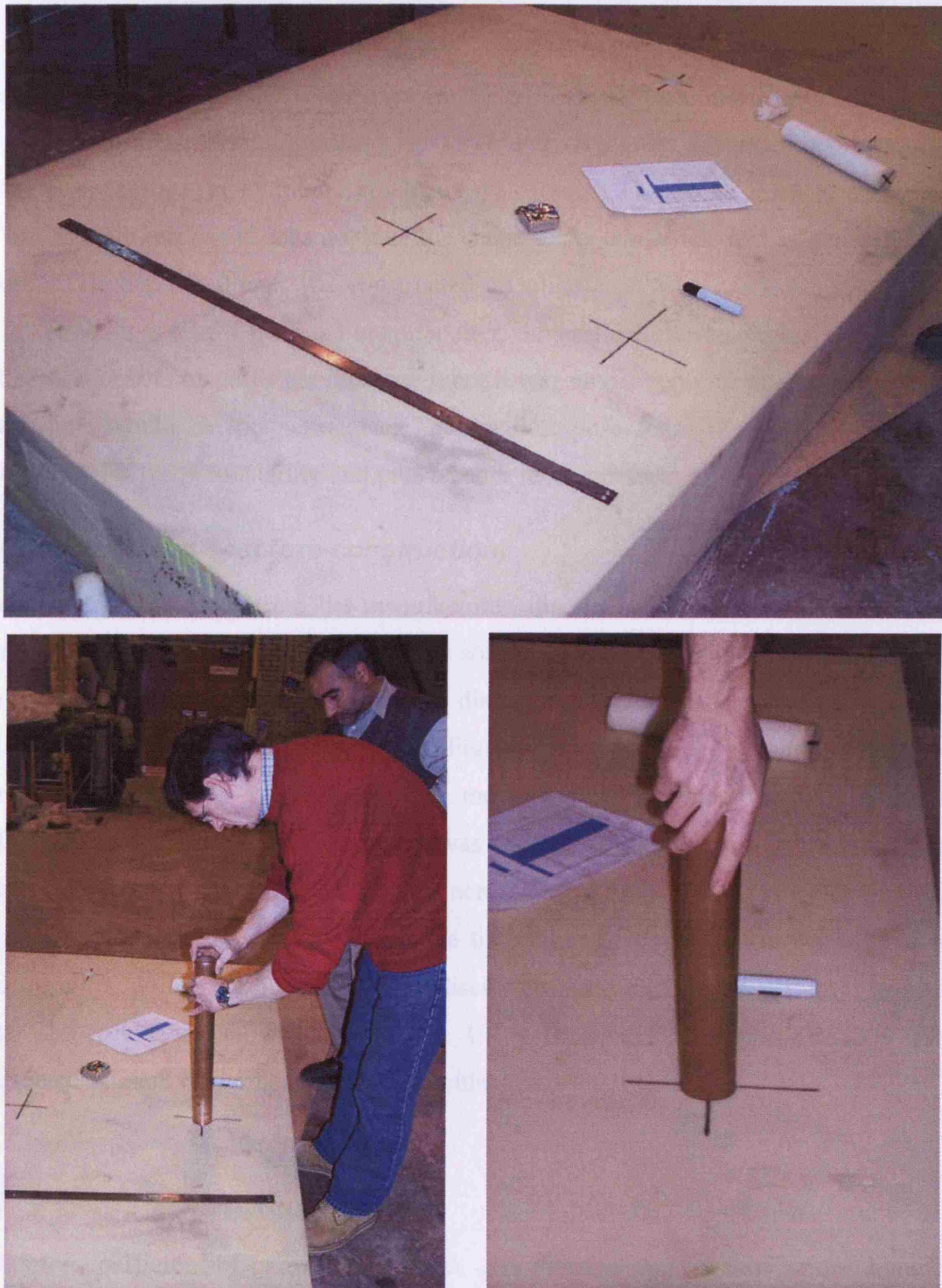


Figure 7.4: - Foam block after cutting (top), and monitoring/injection holes being drilled (bottom)

7.3 Testing the properties of the Foam

7.3.1 Permeability Testing

In order to correctly model the foam used in the laboratory, its conductivity and porosity needed to be measured. British Standard BS 1377: Part 5 : 1990 describes a procedure for testing the permeability (or hydraulic conductivity) of soils. However, foam is not quite so easy to test as soil, because it does not take the shape of its container, and is generally much more porous. Before the flume was constructed an initial test was carried out on a small sample of the foam obtained from the manufacturer. Several different samples were obtained with different numbers of pores per inch (ppi), but it was envisaged that the larger pore foam (i.e. fewer ppi) would be too permeable. The smallest pore foam available (60 ppi) was chosen to minimise the permeability and give a better representation of soil.

7.3.2 Constant Head Test (pre-construction)

Using a sample of the foam from the manufacturer, discs were cut from the foam using a borer, as shown in Figure 7.5. These discs were soaked in water first, and then stacked inside a measuring cylinder of approximately the same diameter as the discs. The cylinder had a hole drilled in the base to allow water to be added. Figure 7.6 shows how the measuring cylinder was then clamped upside down. Another, larger, measuring cylinder was placed underneath to collect the water as it flowed through. Water was added to the top of the first cylinder, and maintained at a constant head by reducing or increasing the flow as necessary (Figure 7.7). When a stable constant head was achieved, the time taken to collect a known volume was recorded from that point. Various numbers of discs were used to measure different hydraulic gradients. The results are shown in Table 7.2. Using the British Standard (BS1377 1990) formula, the coefficient of permeability was calculated as:

7.1

$$k = \left(\frac{q}{i} \right) \left(\frac{R_t}{A} \right)$$

where k is the coefficient of permeability (m/s), q is average rate of flow at one hydraulic gradient (m^3/s), i is the hydraulic gradient h/L , h is the difference between the head on either side of the foam (m), L is the thickness of the foam (m), R_t is a temperature correction factor for the viscosity of water, standardised to 20 °C, and A is the area of the cross-section of the sample (m^2)



Figure 7.5: Discs cut from foam.

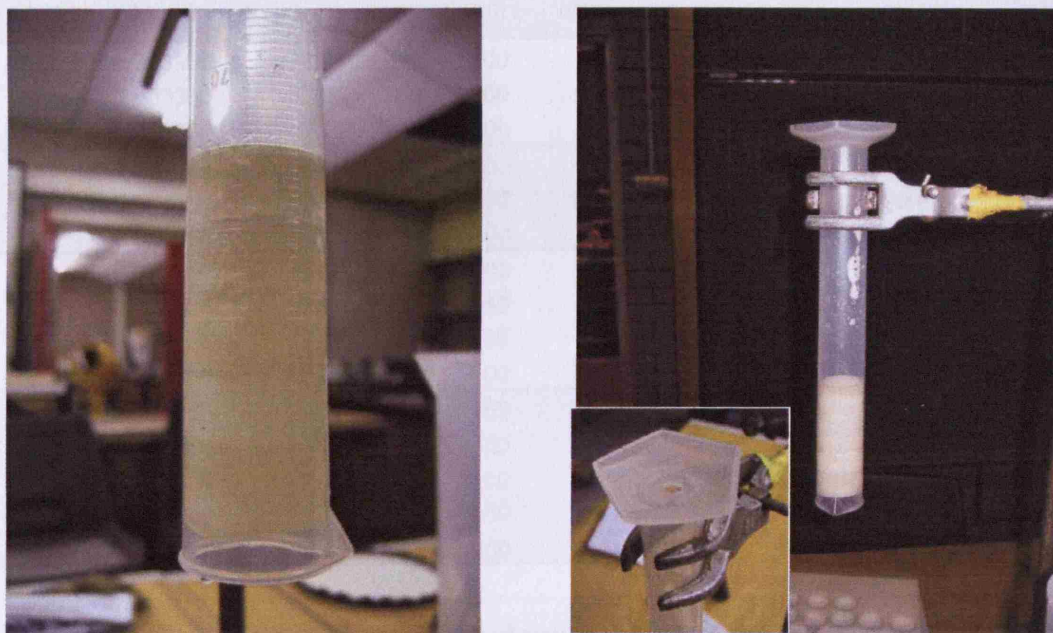


Figure 7.6: - Saturated discs stacked in variable thicknesses in measuring tube (hole drilled in base).

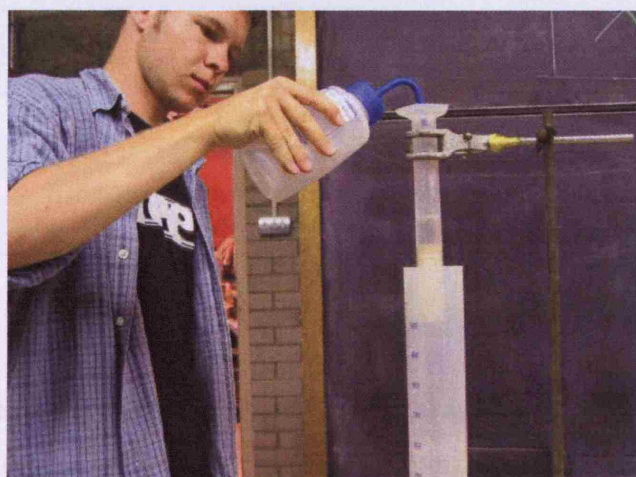


Figure 7.7: Constant head maintained above foam, and flow rate recorded in measuring cylinder below.

Table 7.1: Details of the equipment - Constant Head Test

Detail				
tube diameter	27.63	mm	0.02763	metres
disc diameter	31.78	mm	0.03178	metres
disc thickness	15	mm	0.015	metres
tube area	600	mm ²	6.00E-4	m ²

Table 7.2: Results from Constant Head Test

vol. above foam (ml)	head (m)	time taken (s)	volume passed (ml)	no. of discs	thickness (m)	Flow (ml/s)	Flow (m ³ /s)
20	0.033356	7.97	100	2	0.030	12.5470	1.25E-05
20	0.033356	7.66	100	2	0.030	13.0550	1.31E-05
20	0.033356	7.71	100	2	0.030	12.9700	1.30E-05
20	0.033356	9.89	100	3	0.045	10.1110	1.01E-05
20	0.033356	9.73	100	3	0.045	10.2770	1.03E-05
20	0.033356	9.66	100	3	0.045	10.3520	1.04E-05
20	0.033356	11.90	100	4	0.060	8.4034	8.40E-06
20	0.033356	17.95	150	4	0.060	8.3565	8.36E-06
20	0.033356	17.16	150	4	0.060	8.7413	8.74E-06
20	0.033356	12.09	100	4	0.060	8.2713	8.27E-06
20	0.033356	24.74	150	5	0.075	6.0631	6.06E-06
20	0.033356	25.77	150	5	0.075	5.8207	5.82E-06
20	0.033356	27.89	150	5	0.075	5.3783	5.38E-06
20	0.033356	23.90	150	5	0.075	6.2762	6.28E-06
20	0.033356	22.81	150	5	0.075	6.5761	6.58E-06

Table 7.3: Summary of results and calculations

No. of discs	h (head) (m)	L (thickness) (m)	average flow (m ³ /s)	dh / dL	cross section area (m ²)	dh/dL*area	k (m/s)
2	0.033	0.030	1.29E-05	1.111852	0.0005996	0.000667	1.93E-02
3	0.033	0.045	1.02E-05	0.741235	0.0005996	0.000444	2.31E-02
4	0.033	0.060	8.44E-06	0.555926	0.0005996	0.000333	2.53E-02
5	0.033	0.075	6.02E-06	0.444741	0.0005996	0.000267	2.26E-02
Average							2.26E-02
Standard Deviation							2.16E-03

The average permeability calculated from the results was 0.026 ± 0.002 m/s (Table 7.1 to Table 7.3). By plotting the average flow against the hydraulic gradient multiplied by the area (Figure 7.8) the line of best fit that passes through zero was found – the gradient of this line is approximate to the conductivity. This method gave a value of approximately 0.0213 m/s.

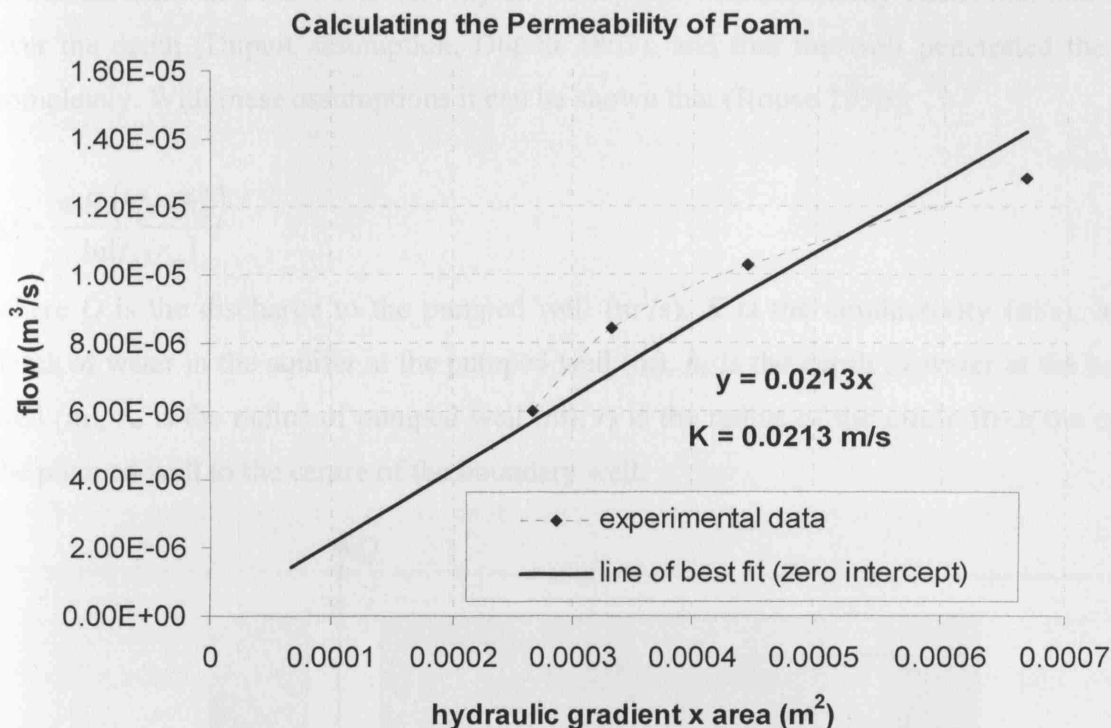


Figure 7.8: Hydraulic Gradient x area, against flow, enabling the permeability to be calculated from the gradient of the line.

7.3.3 In Situ Permeability Test (post-construction)

After the foam was glued into position, further tests on the permeability were carried out. The auger-hole method is a classic field test for permeability, ideally suited to testing permeability of surface aquifers. It was planned to use this method to check the permeability of the foam once in place. However, this proved impossible as the portable pump used for the test was unable to remove water from the hole fast enough – the foam was too permeable for the hole to be pumped dry. A new pumping method was devised to allow the permeability to be measured.

Water was pumped out from one of the monitoring holes at a constant rate. The pumping maintained a constant head difference between the pumped hole and the adjacent hole. The pump flow rate was measured by collecting a measured volume of water over 30 seconds. The hole depths were measured by the use of narrow glass tubes in the hole. When a reading was taken, the experimenter's thumb was placed over the end of the tube, and the tube lifted out of the hole. The water level in the tube was then quickly measured. This was repeated to verify the depth obtained.

It was assumed that the water velocity in the aquifer was essentially horizontal and uniform over the depth (Dupuit assumption, Dupuit 1863), and that the well penetrated the aquifer completely. With these assumptions it can be shown that (Rouse 1950):

7.2

$$Q = \frac{\pi \cdot K \cdot (h_b^2 - h_w^2)}{\ln(r_b / r_w)}$$

where Q is the discharge to the pumped well (m^3/s), K is the conductivity (m/s), h_w is the depth of water in the aquifer at the pumped well (m), h_b is the depth of water at the boundary well (m), r_w is the radius of pumped well (m), r_b is the radius of the circle from the centre of the pumped well to the centre of the boundary well.

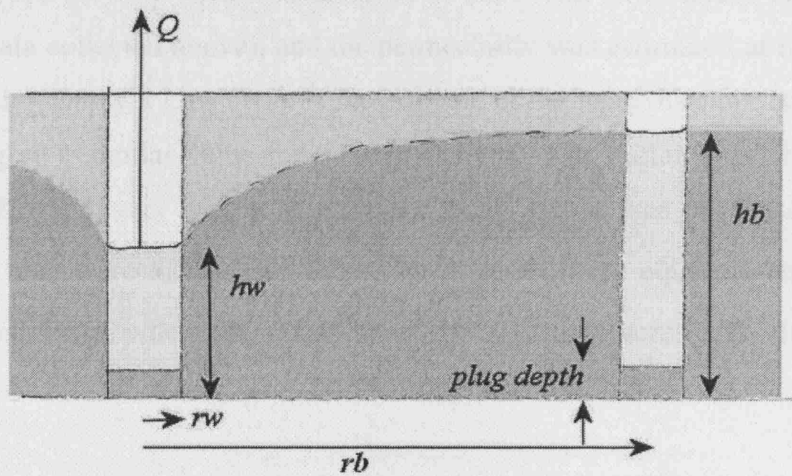


Figure 7.9: - Schematic for permeability test. The depths in two wells in the foam aquifer are measured, while pumping water at a constant rate from one well.

Rearranging Eq. 7.2 in terms of K gives:

7.3

$$K = \frac{Q \cdot \ln\left(\frac{r_b}{r_w}\right)}{\pi \cdot (h_b^2 - h_w^2)}$$

This equation can be used to approximate the permeability of the foam. The experimental results and calculated permeabilities are shown in Table 7.4.

Table 7.4 - Pumping Test to determine Conductivity

Pumped Well				Boundary Well				Q (m ³ /s)	boundary radius (m)	well radius (m)	K (m/s)
Well No.	Measured Water Depth (m)	Plug Depth (m)	Actual water depth (m)	Well No.	Measured Water Depth (m)	Plug Depth (m)	Actual water depth (m)				
14	0.171	0.0540	0.2250	13	0.212	0.0395	0.2515	0.0004	0.5	0.025	0.0302
5	0.230	0.0255	0.2555	6	0.265	0.0290	0.2940	0.0002857	0.5	0.025	0.0129
7	0.155	0.0410	0.1960	8	0.215	0.0405	0.2555	0.000333	0.5	0.025	0.0118
16	0.153	0.0415	0.1945	15	0.213	0.0435	0.2565	0.0002857	0.5	0.025	0.0097
5	0.183	0.0255	0.2085	6	0.206	0.0290	0.2350	0.000333	0.5	0.025	0.0270
1	0.140	0.0525	0.1925	2	0.163	0.0425	0.2055	0.0001975	0.5	0.025	0.0364
Average											0.0213

This can be confirmed by an iterative method carried out as follows. A linear head distribution between the two wells was assumed to start with (with heads at the wells being taken from the data collected above), and the permeability was estimated at intervals between the two wells, using Darcy's Law (7.1). If the estimate of the head distribution is correct, each interval should give a similar value for the conductivity. The initial linear head distribution gave values for K which vary widely between the wells, and so was obviously incorrect. The heads across the area were then varied according to an arbitrary equation based on $y = \sqrt{x}$, and iteration was halted when the variation of the K values across the domain was at a minimum.

The head distribution obtained by this method was confirmed visually to be close to the expected distribution (Figure 7.10). Therefore the stable value of K was used as an estimate of the conductivity. Values obtained are shown in Table 7.5.

Iterated Head Distribution and Conductivity

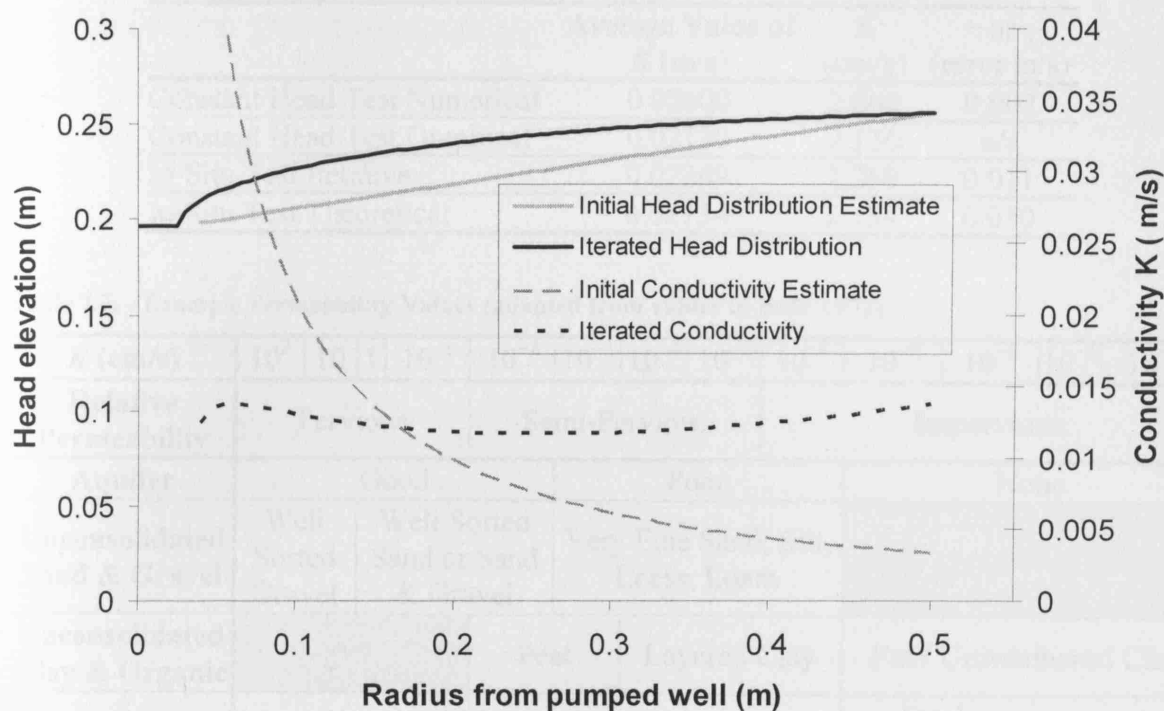


Figure 7.10 - Example of iterative predictions of conductivity (Test number 3). Head distribution is varied until the variation in K (dotted line) is a minimum.

Table 7.5 - Iterative K values compared to theoretical K values from theoretical equation.

	Iterative K	Theoretical K	Difference
Test 1	0.03276	0.03021	0.0026
Test 2	0.01359	0.01288	0.0007
Test 3	0.01233	0.01182	0.0005
Test 4	0.01015	0.00974	0.0004
Test 5	0.02858	0.02702	0.0016
Test 6	0.03870	0.03640	0.0023
AVERAGE	0.02269	0.02134	
Stdev	0.01110	0.01028	
Max	0.03870	0.03640	
Min	0.01015	0.00974	

The iterative values agree closely with the equation values for conductivity, showing that the assumptions made when using the equation were valid. Also, the in-situ results agree well with the previous constant head experiment. It was therefore concluded that the conductivity of the foam was approximately 0.021 ± 0.01 m/s, i.e. it lies between 0.03 and 0.01 m/s. Table 7.6 shows the values of conductivity of the foam found by the different methods. Table 7.7 shows example permeability values to put the foam in context.

Table 7.6 – Conductivity Values for the laboratory foam.

	Average Value of K (m/s)	K (cm/s)	+ or – (error m/s)
Constant Head Test Numerical	0.02600	2.600	0.002
Constant Head Test Graphical	0.02130	2.130	n/a
In-Situ Test Iterative	0.02269	2.269	0.011
In-Situ Test Theoretical	0.02134	2.134	0.010

Table 7.7: - Example Permeability Values (adapted from values in Bear 1972)

K (cm/s)	10^2	10	1	10^{-1}	10^{-2}	10^{-3}	10^{-4}	10^{-5}	10^{-6}	10^{-7}	10^{-8}	10^{-9}	10^{-10}
Relative Permeability	Pervious				Semi-Pervious				Impervious				
Aquifer	Good				Poor				None				
Unconsolidated Sand & Gravel	Well Sorted Gravel	Well Sorted Sand or Sand & Gravel			Very Fine Sand, Silt, Loess, Loam								
Unconsolidated Clay & Organic					Peat		Layered Clay		Fat / Unweathered Clay				
Consolidated Rocks	Highly Fractured Rocks				Oil Reservoir Rocks		Fresh Sandstone		Fresh Limestone, Dolomite		Fresh Granite		

7.3.4 Porosity

Porosity tests were carried out on a cylinder of foam cut from the main block (as seen in Figure 7.4). The cylinder was measured and weighed while dry. It was then completely saturated by submersion and squeezing. When no more air bubbles were produced it was quickly transferred above a measuring cylinder and allowed to drain under gravity. The amount of water drained was recorded. Then, the small portion still saturated at the base of the cylinder was gently squeezed to release the water held. The total amount drained was recorded again. Then the cylinder was squeezed completely to remove as much water as possible by hand. This final amount was also recorded. Finally, the damp cylinder was re-weighed to measure the amount of water retained in the pores. From these measurements several different porosities can be calculated. The results are shown in Table 7.8.

Table 7.8: - Calculating the porosity of the foam

Cylinder of foam Details	Measurement	Porosities
Dimensions		
Diameter	50 mm	
Height	272 mm	
Dry Mass (A)		
	12.395 g	
Gravity Drained (B)	260 ml	0.486827 48.68%
Remaining saturated portion squeezed out (C)	375 ml	0.702154 70.22%
Cylinder squeezed - as much water removed as possible (D)	400 ml	0.748964 74.90%
Final Mass of cylinder (E)		
	31.41 g	
Water remaining in cylinder (E-A) = (F)		
	19.015 g	
Total water held in foam (D+F)	419.015 ml	0.784568 78.46%
Volume of cylinder (G) $= \pi \times (d/2)^2 \times \text{height}$		
	534.0708 cm ³	

The total porosity of the foam was found to be nearly 80%, the effective porosity was estimated at approximately 75%. Therefore the foam is much more porous than an equivalent sand or soil.

Table 7.9: - Approximate porosity values found in nature (Freeze and Cherry 1979).

	N (porosity)
Unconsolidated deposits	
Gravel	0.25 - 0.40
Sand	0.25 - 0.50
Silt	0.35 - 0.50
Clay	0.40 - 0.70
Rocks	
Fractured Basalt	0.05 - 0.50
Karst Limestone	0.05 - 0.50
Sandstone	0.05 - 0.30
Limestone, dolomite	0.00 - 0.20
Shale	0.00 - 0.10
Fractured Crystalline Rock	0.00 - 0.10
Dense Crystalline Rock	0.00 - 0.05

7.4 Initial Experimental Work

This section of the study comprises experimental work done relatively early on in the project. This initial work laid the groundwork for the subsequent experiments (sections 7.7 and 7.8), but encountered several problems which are summarised at the end of this section, along with the solutions that were proposed to solve them. The numerical modelling in this section is only sparingly referred to, because the model set-up is described in detail in later sections (7.7 and 7.8).

The set-up reflected an idealised tidal river basin that could be easily modelled numerically and physically. The tide at one end was varied sinusoidally via the computer controlled weir. The concentrations of dye used in the experiment, the settings of the measuring equipment, and the amount of dye solute used in the model were predetermined with the help of the computer model. The results obtained were then corrected for delays and background concentration, and subsequently compared to the computer model output.

7.4.1 Choice of Tracer

The ideal tracer is non-toxic, usable in small quantities, cost-effective, easy to measure at very low concentrations, and stable during the course of the study. Rhodamine WT, the fluorescent tracer used in these experiments, meets these requirements and is approved for use by the Environmental Protection Agency in the USA (Turner_Designs 2006b). In addition, it is known to adsorb to material less than Rhodamine B, and is comparable to fluoroescien (Kasnavia et al. 1999; Turner_Designs 2006a). Rhodamine WT is a highly fluorescent material with the unique ability to absorb green light and emit red light. Very few compounds have this property, so interferences from other substances are very rare. This makes Rhodamine WT a highly specific tracer (Turner_Designs 2006c).

7.4.2 Flume construction

The channel was constructed out of 60ppi foam blocks with dimensions as shown in Figure 7.11. The foam is intended as porous media through which water and solute can flow as if through a river bank. The foam was glued to the base of the flume, but very quickly after the water was introduced the glue failed and the foam floated. In order to keep the foam attached to the base of the flume weighted boards were used on top of the foam (see Figure 7.13).

Monitoring/injection points were cut out of the foam with a copper tube of 100 mm diameter. The holes went through the entire depth of the foam, and the extracted core was retained for

reinsertion if needed. The position of the injection point was selected so that it was some distance from the top and side boundaries to reduce interference with contaminant accumulating by the walls. This allowed the migration of tracer along the channel and the bank to be investigated, while minimising unwanted effects of conducting the experiments in the laboratory with walls, rather than in a real river. The flume and monitoring/injection points are shown in Figure 7.12. Two monitoring points were selected both from the practical and analytical point of view to enable detection of the tracer plume. Point 'A' was selected along the perpendicular line from the outfall location to the channel. Point 'B' was selected to help investigate the spread of contaminant due to diffusion along the foam (see Figure 7.11 and Figure 7.12).

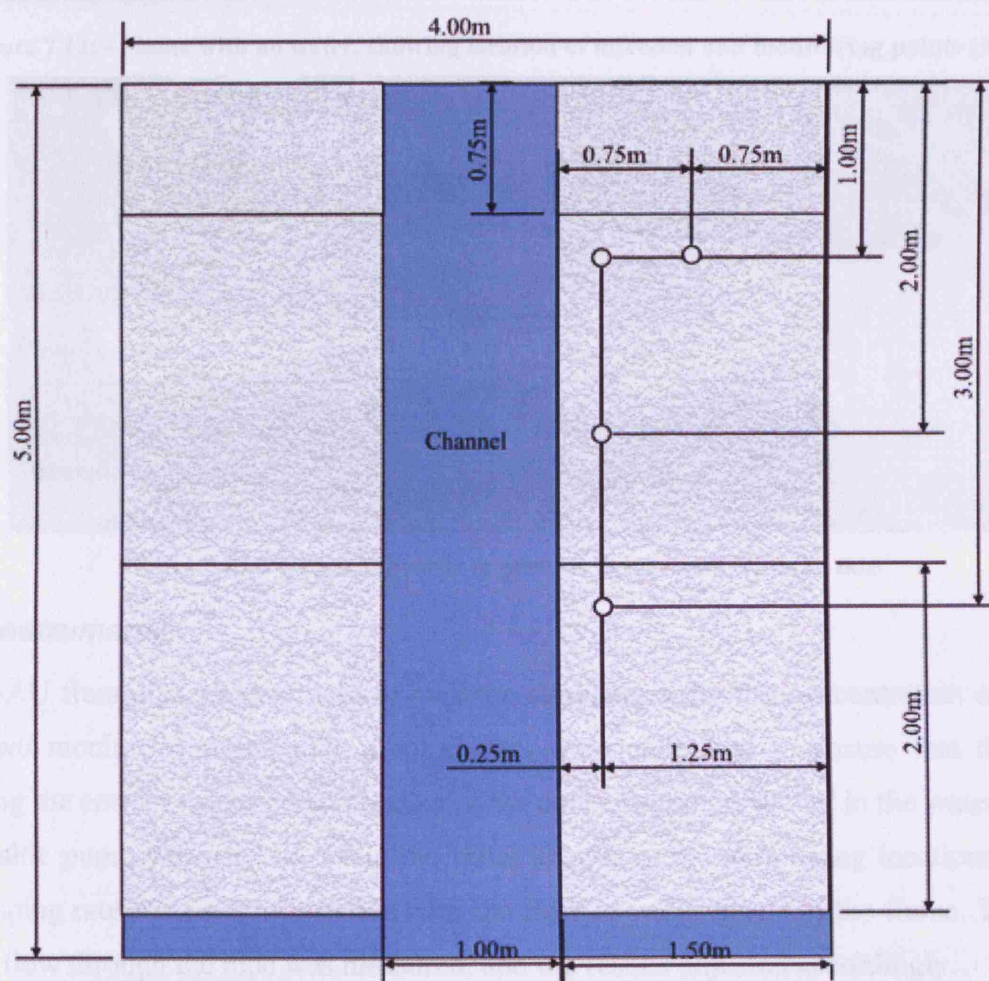


Figure 7.11: - Flume Design

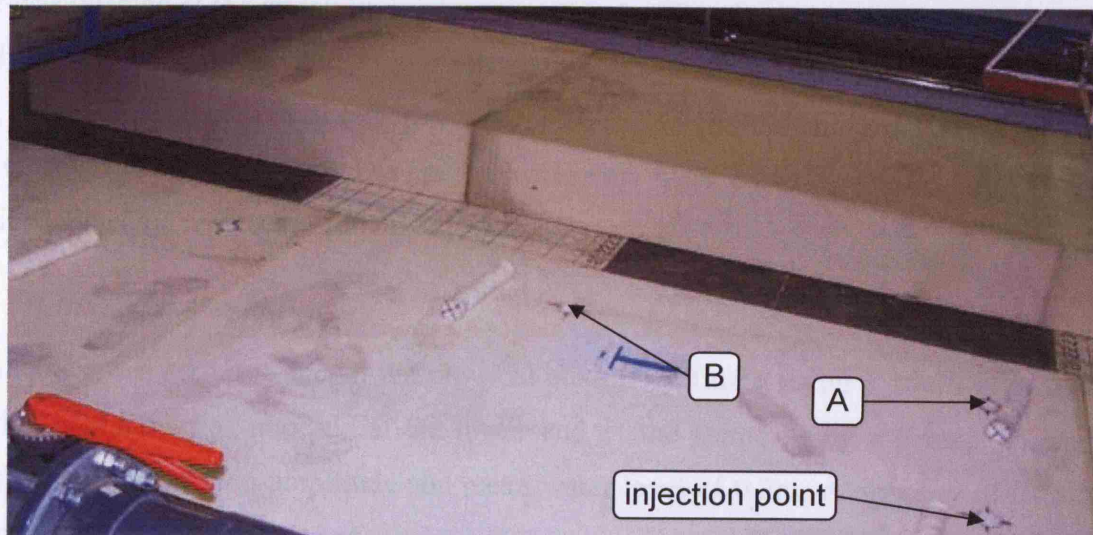


Figure 7.12: - Flume with no water, showing location of injection and monitoring points (A+B).

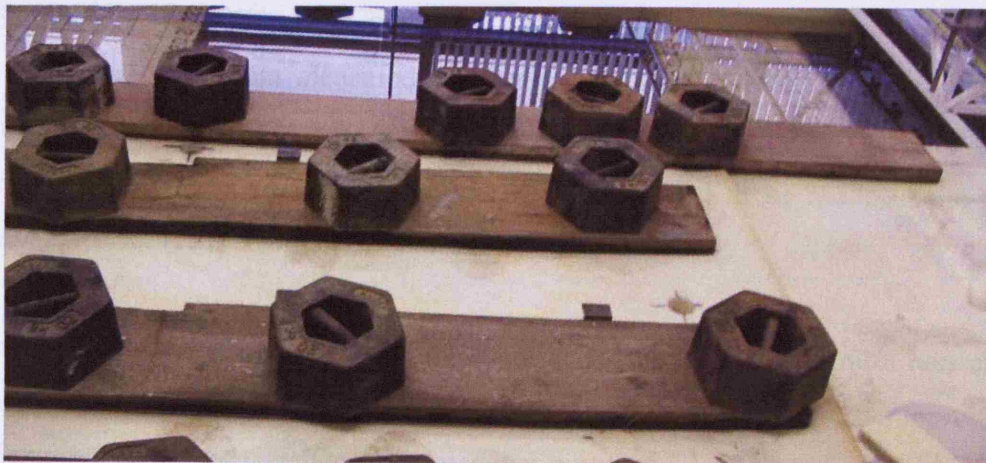


Figure 7.13: - weighted boards to prevent foam rising with the tide

7.4.3 Instruments

Two 10-AU fluorometers were used to measure simultaneously the concentration of the dye at the two monitoring points. The fluorometers were calibrated to ensure that they were measuring the correct values corresponding to the concentration of tracer in the water column. A peristaltic pump was used to obtain the water sample at the monitoring locations, set to a low pumping rate so as not to interfere with the flow or water levels in the flume. The travel time for flow through the pipe was measured, and the results adjusted accordingly.

The sampling point was positioned at an elevation just below the lowest water surface elevation (100mm from the floor of the flume) in order to keep it submerged even at low tide.

7.4.4 Experiments

The flume was driven by a sinusoidal water elevation boundary, varying from 290mm to 110mm and back over a 30 minute period, to simulate a tidal boundary. Rhodamine WT

tracer was injected at the injection point over a period of 2 minutes at a concentration of 1 g/l. The dye was injected at $t=1800s$, i.e. at the peak of a tidal cycle. The volumes injected were 50ml, 75ml and 100ml. Initial experiments for 100ml injections showed the concentrations were too high to measure, so subsequent experiments were performed with 75ml and 50ml injections. Selected results are shown below in Figure 7.14.

7.4.5 Numerical Modelling

DIVAST-SG was set-up to model the physical laboratory flume using a 10cm grid. A water elevation boundary was imposed at the lower end of the flume using a sinusoidal wave of 30min wavelength, 0.09m amplitude and mean water level of 0.2m. A porosity of 0.75 and a permeability of 0.02 m/s was used.

7.4.6 Discussion

Figure 7.14 shows typical data measured at monitoring point A. The data showed a good correlation for the timing of the peaks between the numerical and physical models, although there were a few points that indicate that improvements needed to be made in the physical model. These are discussed in sequence.

The predicted peaks are much higher than the measured peaks. The maximum concentration in the numerical model is 7.5×10^{-4} g/l, (or 750 ppb). The values observed are approximately an order of magnitude below this. This indicates that much of the dye has been ‘lost’ from the foam. Some of the dye has probably been lost due to adsorption to the foam, but it seems likely that for the effect to be this large, a lot of the dye has probably entered the surface water via a short-circuit underneath the foam. The initial experiments conducted support this theory; these were done while the foam was still firmly attached to the base of the flume (before the buoyancy of the foam defeated the glue) and when the concentrations were measurable they were much closer to the predicted order of magnitude. (i.e. time 9000-9900s, predicted range of 250-300ppb, measured range of 175-450ppb).

The peak shown in Figure 7.14 at about 1000 seconds occurred before the dye injection, and so is probably due to background dye from previous tests. The similar shape of the peaks from 6300s to the end of the test may point to a similar source, rather than a gradual dispersion from the injection point. The peaks occur during the rising of the tide, when the rising water re-enters from the channel into the foam and towards the monitoring points. This

suggests that after $t=7200s$ most of the dye detected originated from the channel, with small amounts from the foam. It is not clear as to what extent the peaks are caused by water flowing through the foam, along the suspended floor of the basin, or rising from the larger basin underneath the suspended floor. The sharp peaks occur at a particular level of the rising tide, which could be associated with the critical amount of water necessary to cause enough buoyancy within the foam to lift it enough to allow water flow underneath. In contrast, the numerical model predicted a decrease in concentration as the tide rose, as the cleaner water from the channel entered the foam.

The flow of water within the foam is slow and facilitates tortuosity of the flow paths of particles, which aids diffusion and dispersion of the dye, causing more scattering of the particles. Therefore the shape of a peak is a significant indication of its origin. A round peak indicates that the contaminant is more scattered within the water and it is likely that this reflects dye flowing through the foam. A sharp spiked peak is more characteristic of a source where the dye remains as a well defined “slug”, indicating a short-circuit from the injection point or other dye-rich area. Hence, it was regarded as likely that the rounded peaks which occurred just after low water were from a diffuse source (i.e. had travelled through the foam). The timing of these rounded peaks matched up well with the predicted peaks in the numerical model. In between these peaks the concentration dropped back down almost to the background level very quickly. Again, this indicates that the monitoring holes were connected to the main channel by short-circuiting. If the dye was leaving through the foam then the concentration would reduce much more gradually.

The numerical model predicted that the concentration at point ‘B’ would slowly increase with time as the dye diffused longitudinally through the foam, but the measured values showed no sign of this prediction, only the same increasing background peaks as seen in Figure 7.14. The dye did not reach this second monitoring point as expected; another sign of short-circuiting of the tracer.

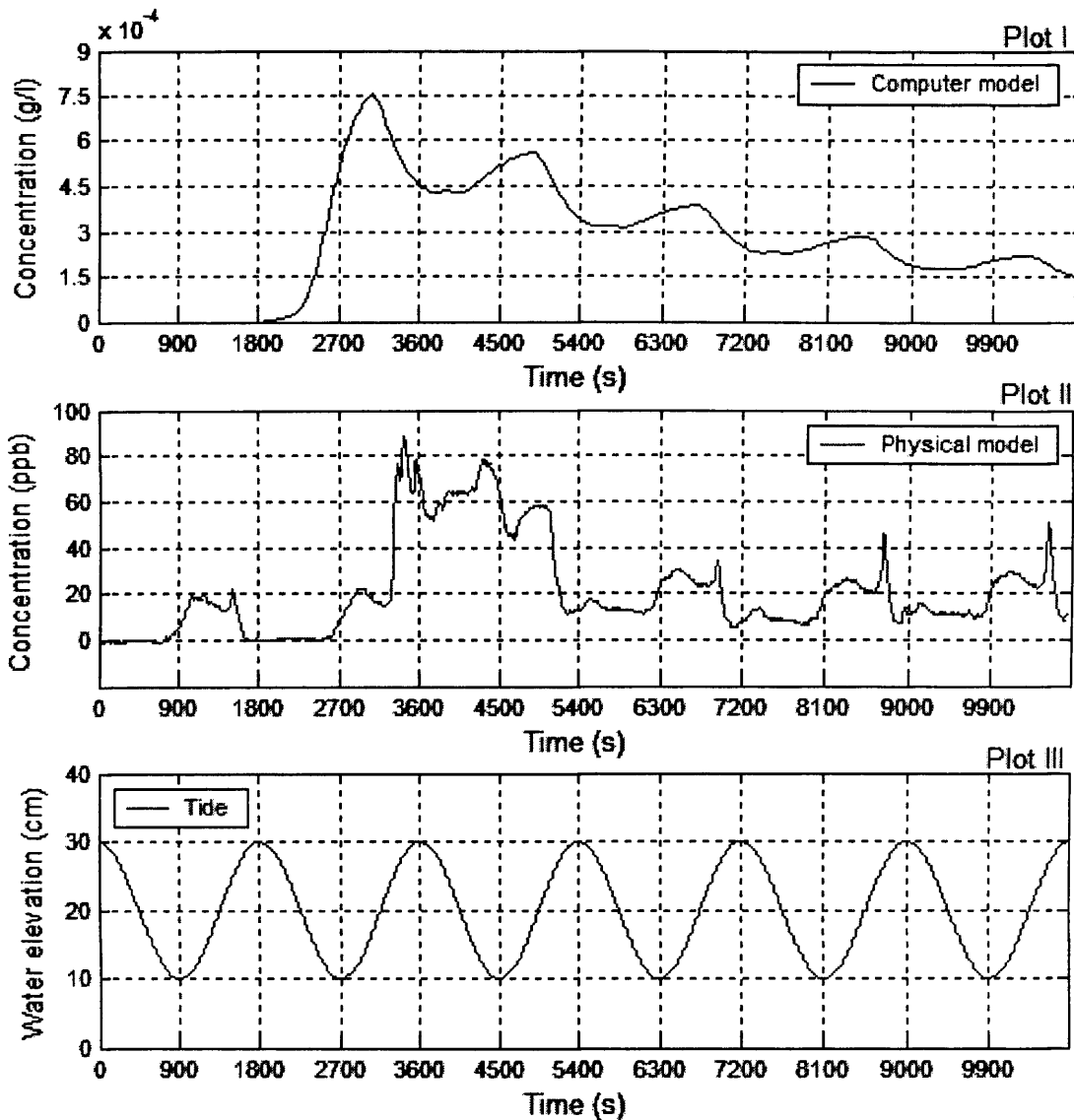


Figure 7.14: - Plot I – Graph of the numerical prediction of change of concentration of Rhodamine WT with time at point A for 75ml of 1g/l dye injected over two minutes. Plot II – the concentration of Rhodamine WT recorded at point A during physical experiment 4. Plot III – the respective tidal phase.

7.4.7 Problems and Solutions.

The foam is buoyant, so in order to stop it rising it was glued to the base of the flume. However, after the first experiment, sections of the foam had lifted away from the flume base. Weighted boards were placed across the foam but from the results it seemed they were insufficient to prevent short-circuiting of the water underneath the foam.

Proposed solutions

After these problems became apparent, several solution methods were proposed.

- Use stronger adhesive to re-attach the foam to the base of the flume.

- Reinsert a small section of foam into the base of the monitoring holes, to prevent direct flow out of the base of the foam layer.
- Seal joints between the blocks with glue, preferably in sections to allow flow to and from separate blocks, but limit seepage along the joint itself.

These solutions were proposed to prevent water flowing along undesirable pathways. While it caused some difficulties, the block structure of the foam makes it easy to rearrange the flume to simulate different scenarios, and to restructure the flume incorporating the above solutions.

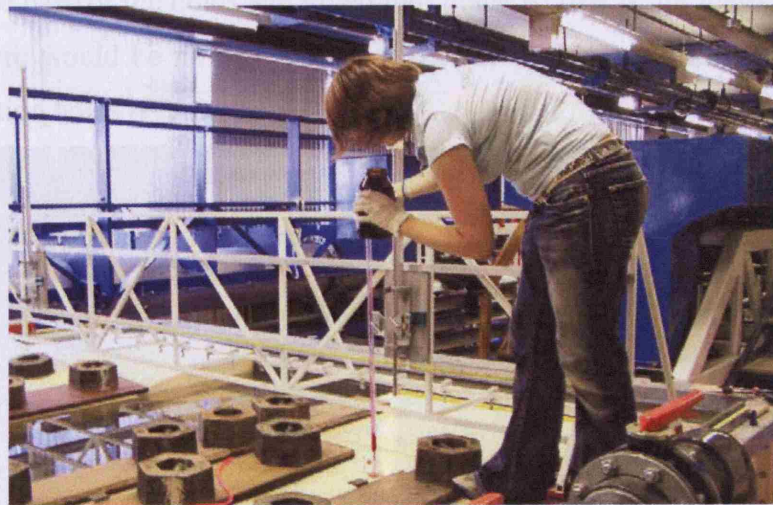


Figure 7.15: - Injecting the dye

7.5 Adapting the Flume

The initial experiments highlighted numerous problems with the physical setup, mostly involving short-circuiting water under the foam. In order to solve these problems the following steps were taken. A stronger water-activated glue was sourced and tested on small samples of the foam. The new glue proved to be much stronger than the previous glue used.

More monitoring holes were drilled in the same way as before. Small discs of foam were reinserted into the base of the holes and glued into place so that if the foam did lift off the bed of the flume, there would be no direct contact between the water beneath the foam and the monitoring/injection holes (Figure 7.16).

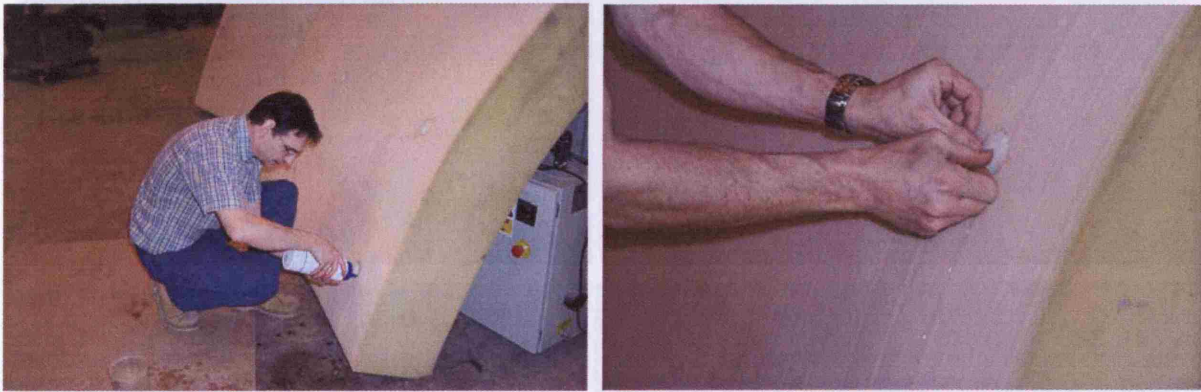


Figure 7.16: - Inserting and glueing small discs of foam in base of holes

The foam blocks were reattached to the bed of the flume using the water-activated glue, see Figure 7.17. The foam blocks, once in the flume, were glued in strips at the joints, in an attempt to limit seepage along the cracks but still allow flow between blocks (Figure 7.18).

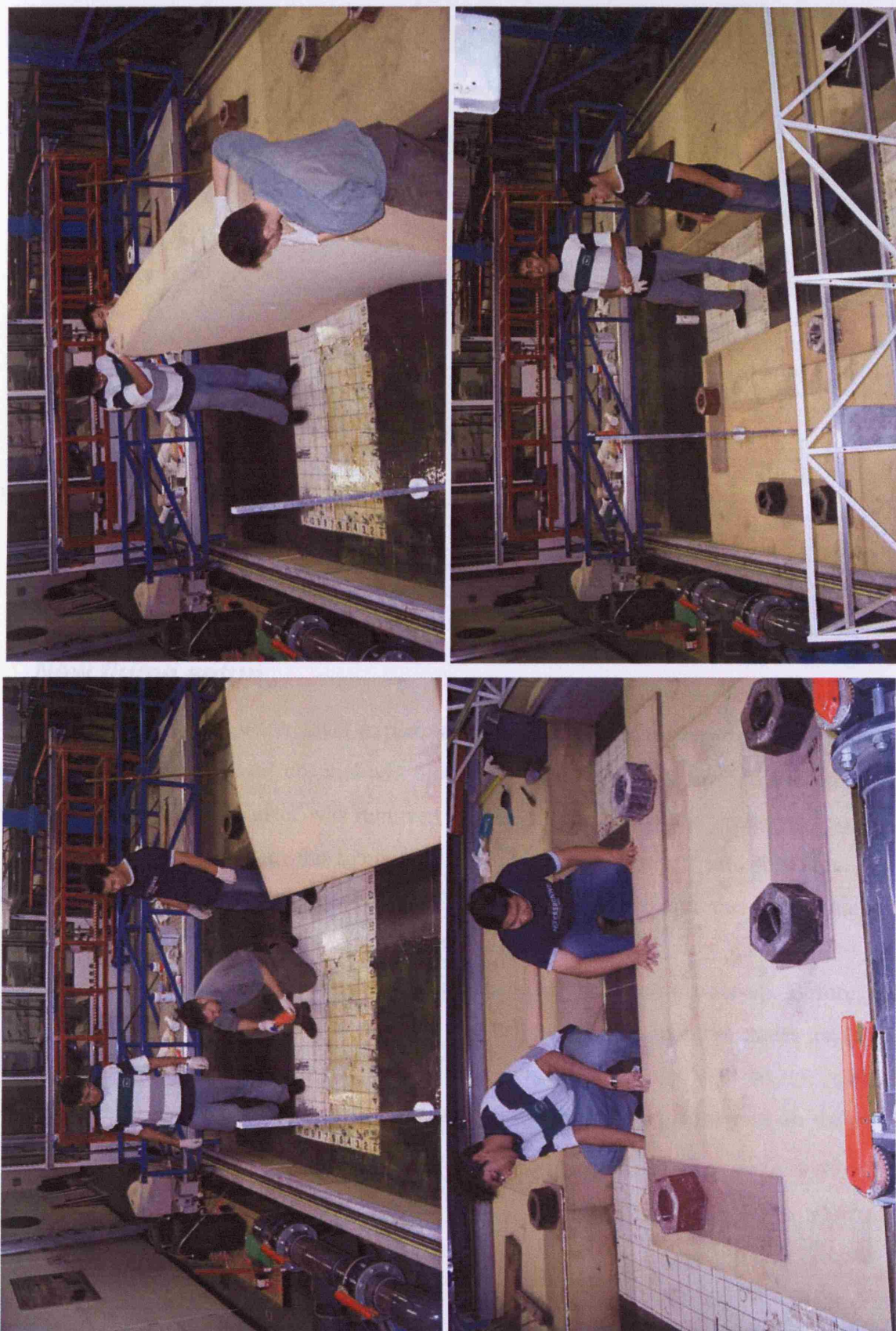


Figure 7.17: - Glueing a foam block in place.

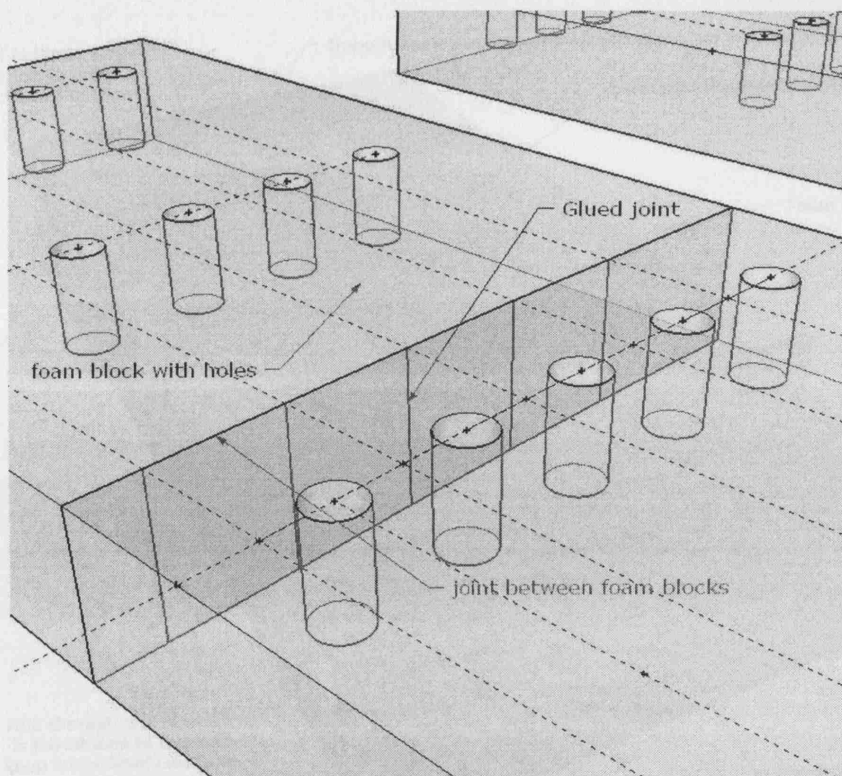


Figure 7.18: - Diagram showing how foam blocks were glued at joints.

7.6 New flume setup

After the initial tracer and water level experiments proved inconclusive, the flume features were changed. The main 'river' channel was blocked off with a wall at the end furthest from the weir. A section of this barrier was removed on one side to allow the upstream reservoir area to be in direct contact with the foam, and water was then pumped into this area. This created a permanent head difference between the upper reservoir and the main channel, causing a constant flow through the foam connected to the reservoir.

This setup provided a constant flow, which was missing in the previous set-up. Before, the flow in the groundwater oscillated with the tide, and as a result, the injected tracer tended to remain in the groundwater, shifting side to side with the tide. With the new set-up, injected tracer flowed from the foam into the main channel, allowing it to be measured on the way, and also when it reaches the channel.

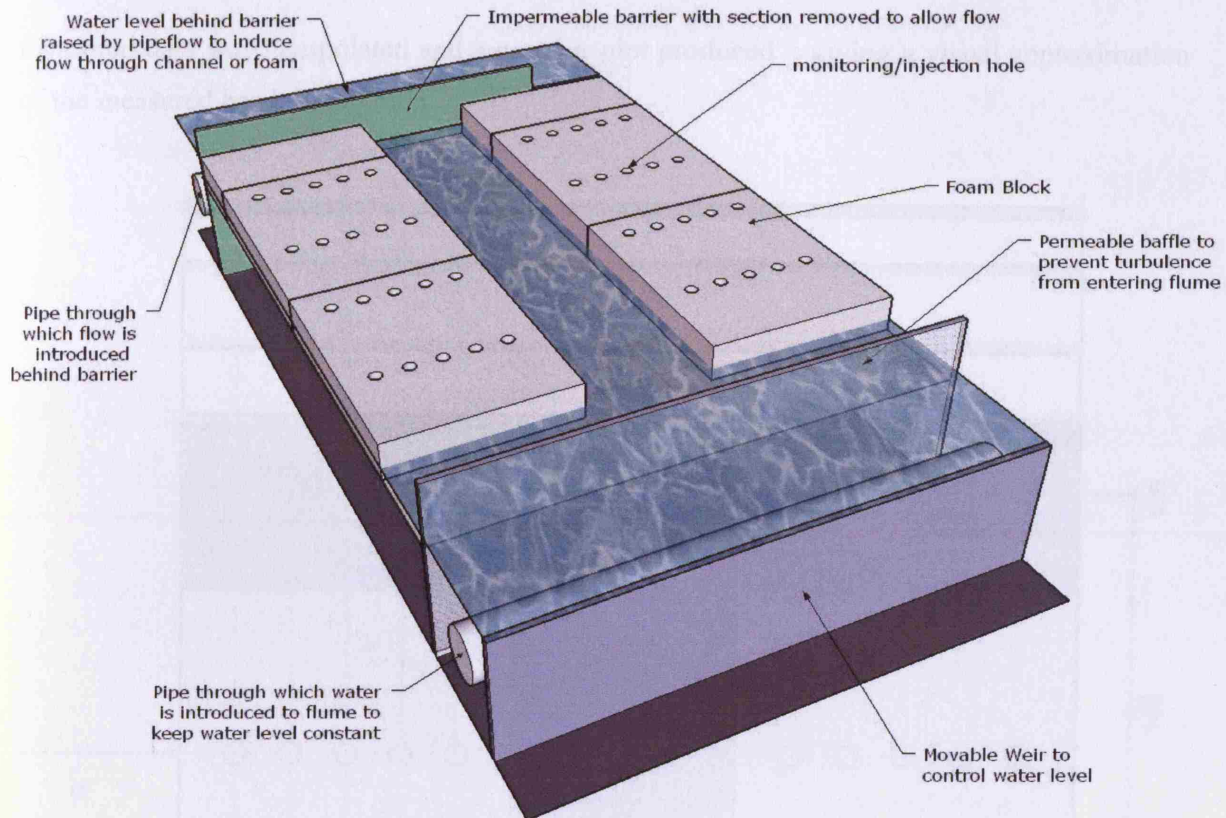


Figure 7.19: - New flume setup with water pumped to upper reservoir.

7.7 Water Level Measurements and Modelling

7.7.1 Collecting the data

Water level data was collected in the monitoring holes using two wave probes. These devices consist of two parallel stainless steel wires which are immersed in the water. The electrical conductivity between the wires varies depending how deeply the probe is immersed. Therefore, by calibrating the probes at known depths, a real-time measure of water levels can be obtained. Unfortunately the probes are quite fragile and require calibrating at regular intervals. The probes were used during the initial phase of experimentation when a sinusoidal tide was imposed at the weir boundary, but inaccuracies in the measured data were impossible to quantify. The scenario described in the previous section (7.6) creates a steady-state situation where the water levels in the flume are not changing. The calibration can be checked *in-situ* by measuring with a ruler and then the wave-probes used with confidence for a number of scenarios, without time-consuming ruler measurement. The monitoring holes are referred to in the scheme shown in Figure 7.20. The measured data is shown in Table 7.10. The

measured data was interpolated and a contour plot produced – giving a visual approximation of the measured head distribution.

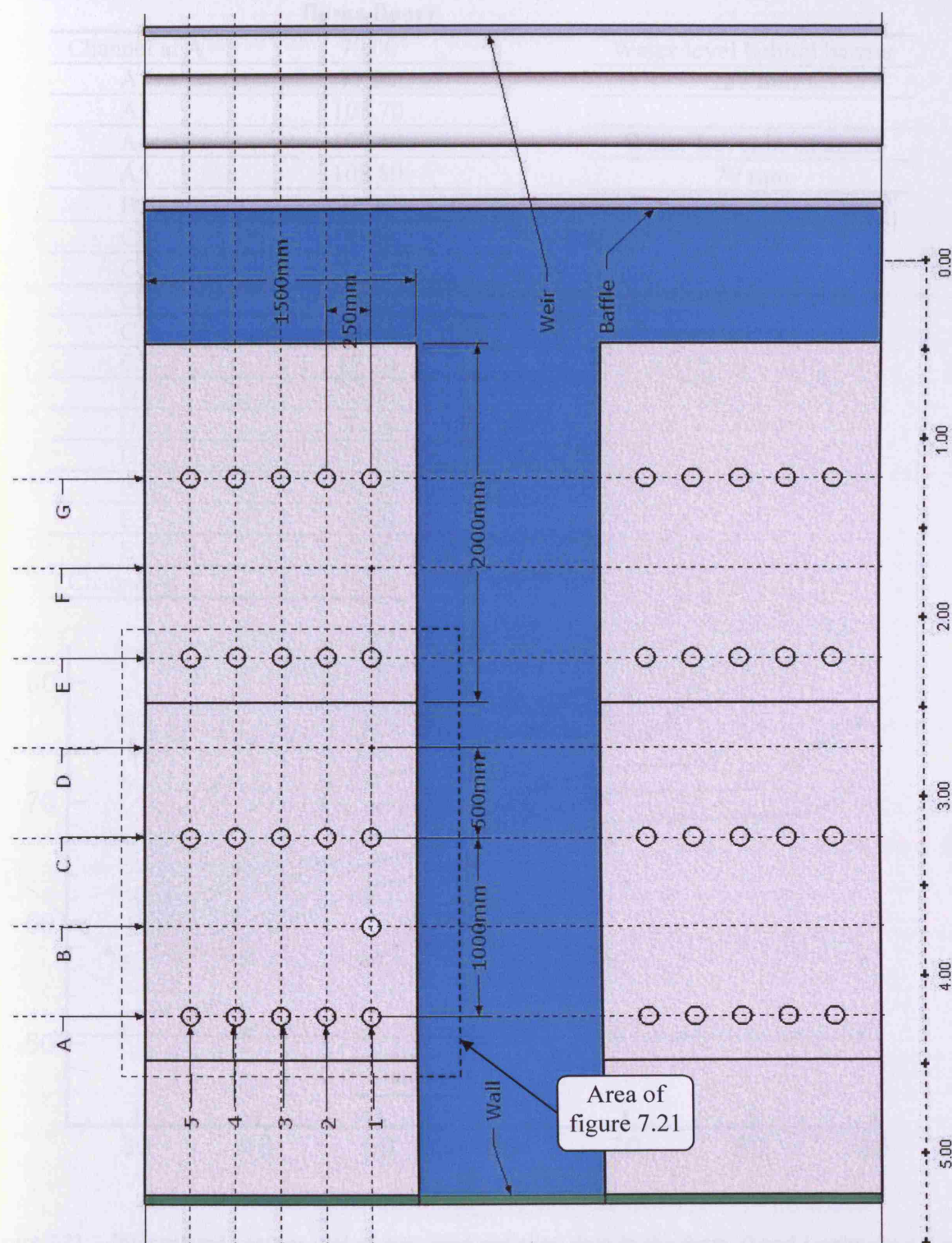


Figure 7.20: - schematic diagram of the tidal flume showing labelling of monitoring holes and reference ruler.

Table 7.10: - Measured Water elevations at steady state.

Location	Measured Water Elevation (mm above flume floor)	Details
Channel at A	70.00	Water level behind barrier
A1	77.00	227 mm
A3	103.70	
A4	109.40	Water Level in Channel
A5	108.80	70 mm
B1	70.30	
C1	70.00	
C2	71.00	
C3	76.00	
C4	80.10	
C5	82.20	
D1	70.00	
D3	70.60	
D5	79.40	
E1	70.00	
E3	70.00	
E5	73.90	
Channel at E	70.00	

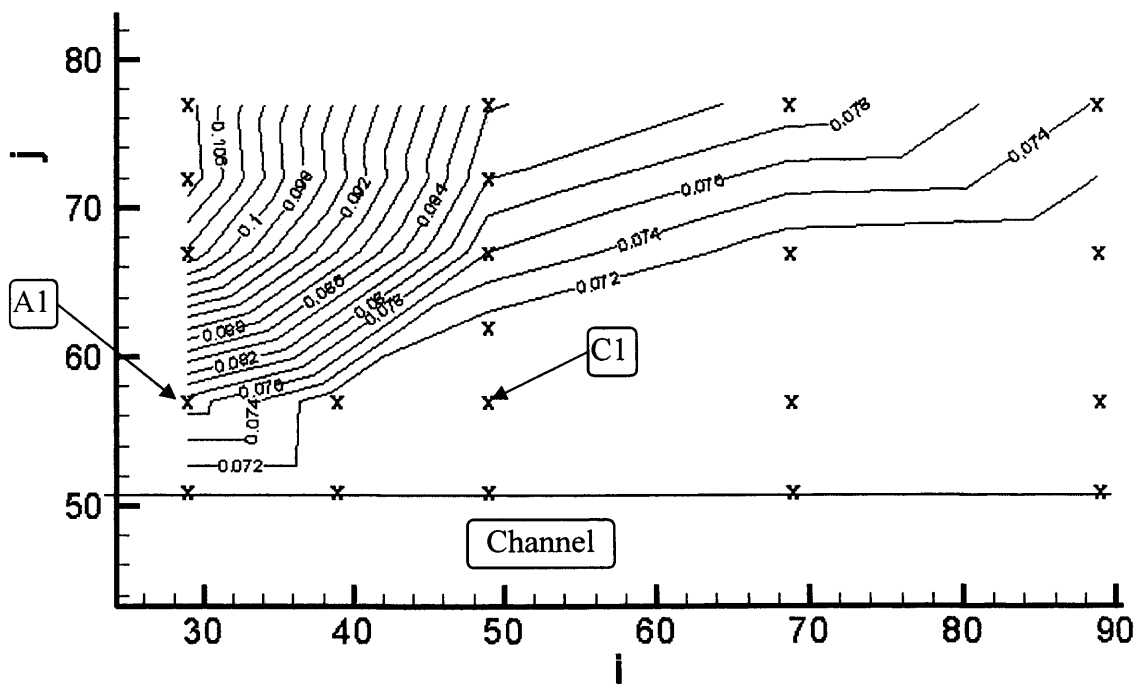


Figure 7.21: - Interpolated contour plot of measured elevation data in the foam. (i and j units are x 5 cm: the grid size used in the model)

7.7.2 Setting up the model

DIVAST-SG was set-up to simulate the situation in the flume described in the section above. The code was modified from the original single elevation boundary version to allow multiple water elevation boundaries to be specified. The modified code is included on the Appendix CD^a. Boundary conditions were specified as two water elevation boundaries. Monitoring points were created at the locations of the monitoring holes in the foam. Permeability was set to 0.02 m/s, and porosity to 0.75 (see section 7.3). The initial model run results are shown in Figure 7.22 and compared to the measured elevations in Figure 7.23.

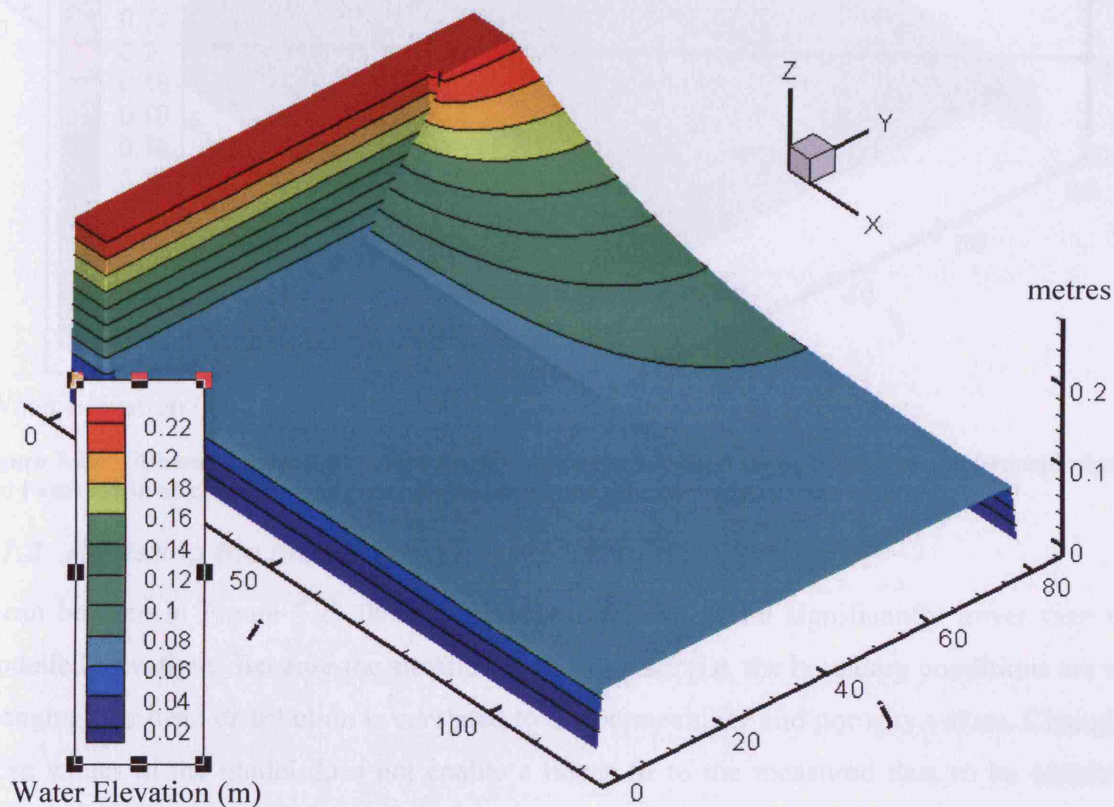


Figure 7.22: - Model results of water elevations for initial run of physical scenario. i and j axes are x5 cm from edge of the model, or grid cell reference.

^a Executable file D:\DIVAST-SG Laboratory Model\Water Level Experiments\sgchannel_mod.exe

Source code: D:\DIVAST-SG Laboratory Model\Source Code\sgchannel_mod.for and divastsg.cmn

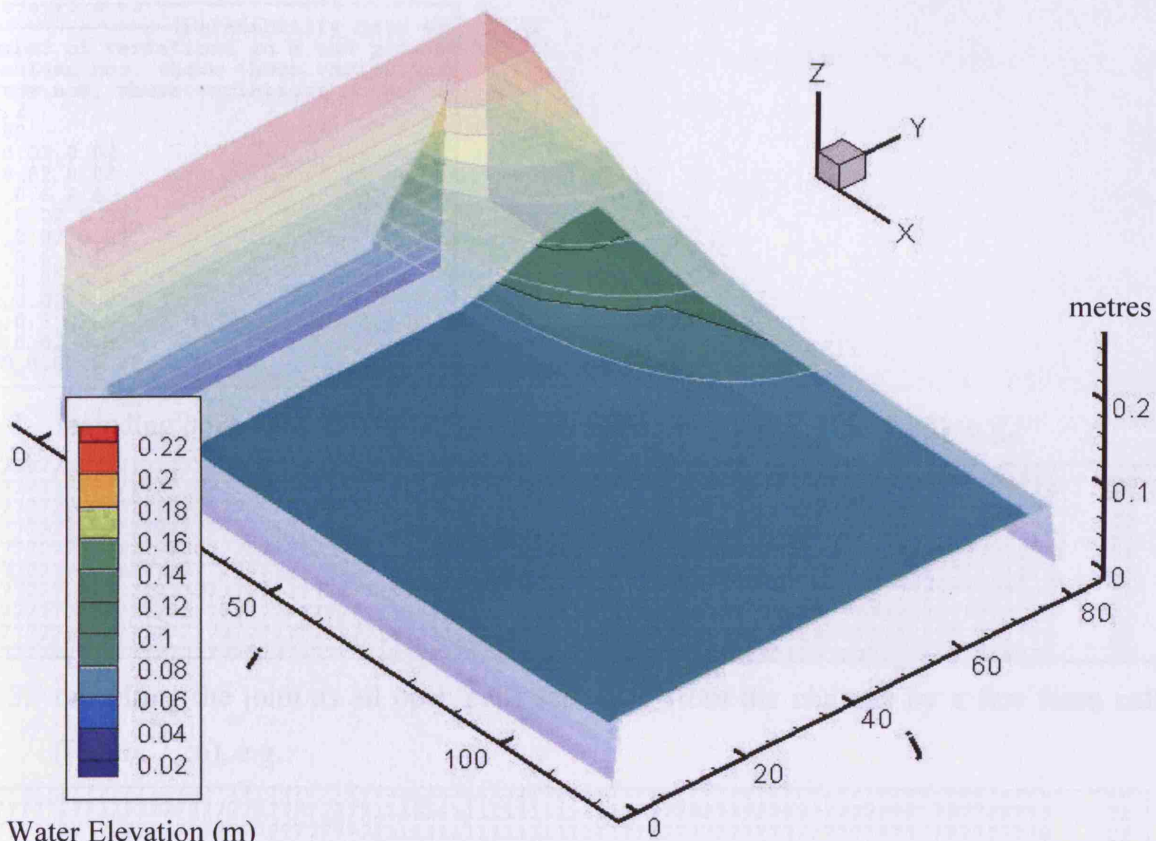


Figure 7.23: - Measured water elevations (solid) compared to initial modelled elevations (transparent). i and j axes are in $x5$ cm from edge of the model, or in grid cell reference coordinates.

7.7.3 Adjusting the model

It can be seen in Figure 7.23 that the measured elevations are significantly lower than the modelled elevations. Because the situation is steady-state (i.e. the boundary conditions are not changing) the head distribution is unrelated to the permeability and porosity values. Changing these values in the model does not enable a better fit to the measured data to be obtained. Therefore, the model was not correctly simulating the head distribution in the flume, which were much lower than the model predicted.

The most likely cause of this was thought to be the structure of the laboratory foam. The blocks of foam were originally glued together in strips in an attempt to reduce the possibility of water finding preferential pathways between the separate blocks, but from the measured data, it appeared that the water was escaping along the joints between the blocks, and therefore lowering the measured elevations. To test this, the model domain was altered, and several methods of including the joints between the foam in the model were tested, as listed below:

1. increasing permeability along the joints (Figure 7.24), e.g.:

```

120,0.75,0.75
-----Permeability data:-----
number of variations in x and y direc
) column nos. where those variations
i row nos. where variations occur, an
11,2
1,82
1,0.02,0.02
9,0.02,0.02
10,0.6,0.6
11,0.02,0.02
24,0.02,0.02
25,0.6,0.6
26,0.02,0.02
64,0.02,0.02
65,0.6,0.6
66,0.02,0.02
120,0.02,0.02

```

- including open cells in between glued areas on the joint (Figure 7.25), e.g.:

[illegible]

3. modelling the joint as all open cells separated from the channel by a few foam cells (Figure 7.26), e.g.:

[illegible]

4. Combinations of the above methods (listed in Table 7.11).

Table 7.11: - Methods of joint modelling

Run number	Method of joint modelling
1a	Permeability of joint 0.1 m/s
1b	Permeability of joint 0.6 m/s (Figure 7.24)
2	Glued joints (no permeability change) (Figure 7.25)
3a	Open cells - 1 cell of foam between channel and joint (no permeability change)
3b	Open cells - 3 cells of foam between channel and joint (no permeability change) (Figure 7.26)
4a	Glued joints (permeability 0.1 m/s)
4b	Glued joints (permeability 0.6 m/s)
4c	Open cells - 3 cells of foam between channel and joint (permeability 0.1 m/s)
4d	Half open cells (permeability 0.1 m/s)
4e	Half open cells (permeability 0.6 m/s) (Figure 7.27)

A summary of the various methods of modelling the joints is shown in Table 7.11, together with references to figures showing the visualised results of the model runs.

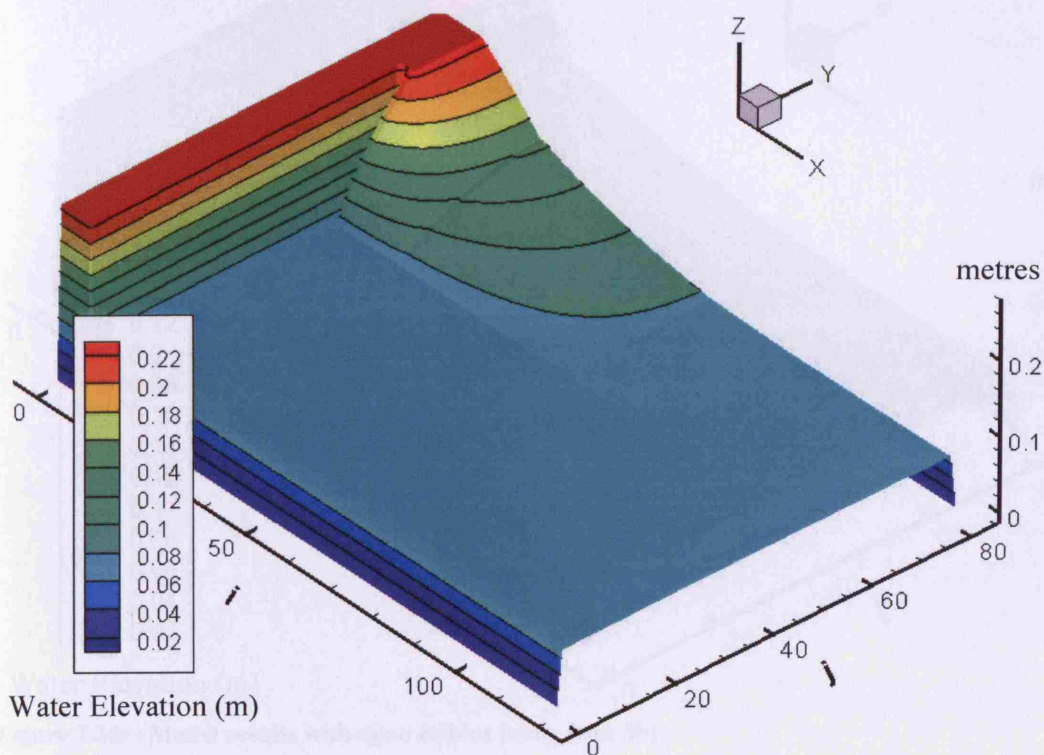


Figure 7.24: - Modelling joints by increased permeability along joints (run 1b)

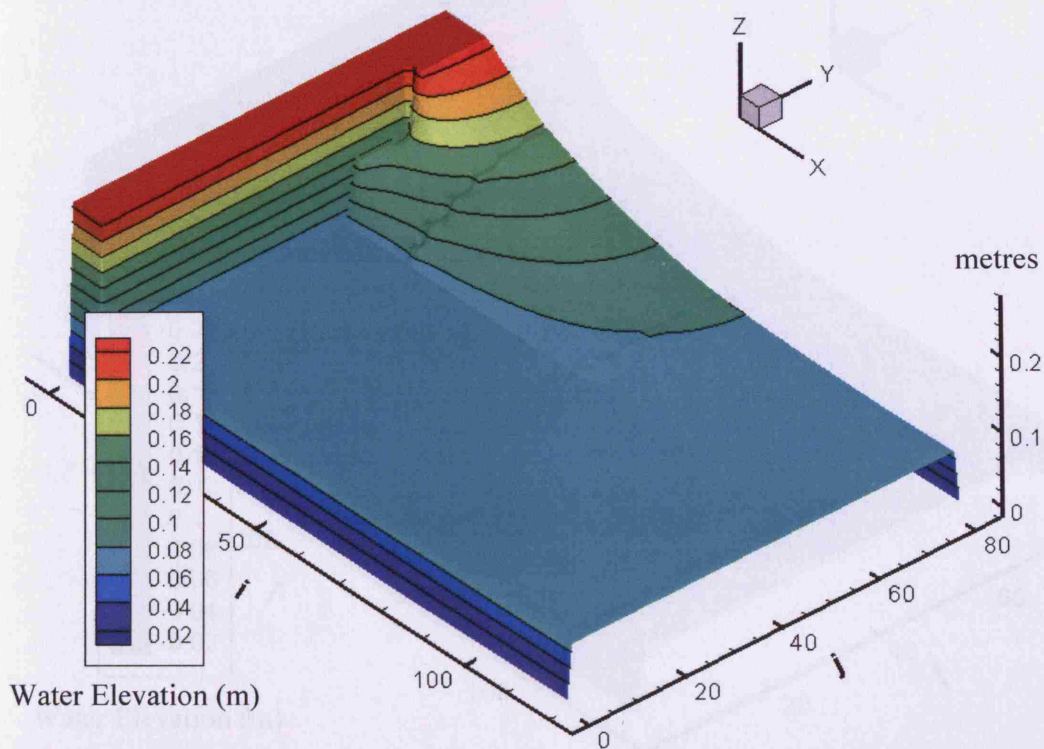


Figure 7.25: - Modelling joints as combination of open cells and foam (run 2)

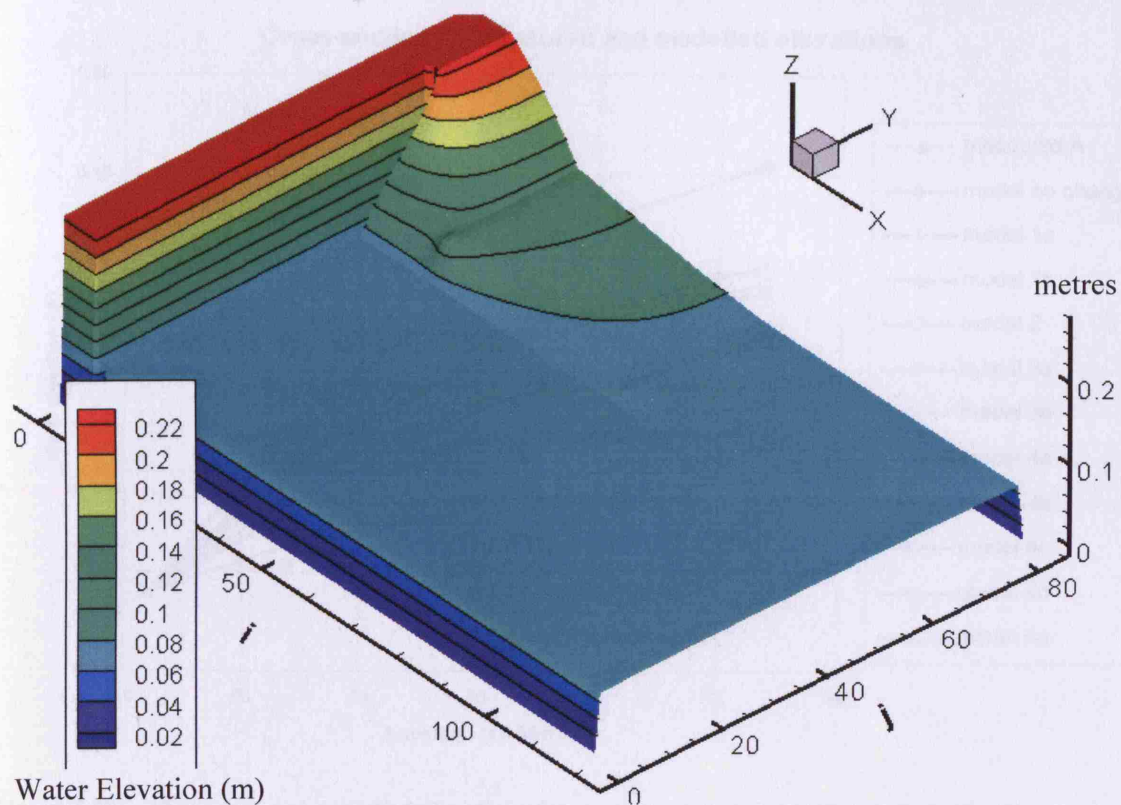


Figure 7.26: - Model results with open cells at joints (run 3b)

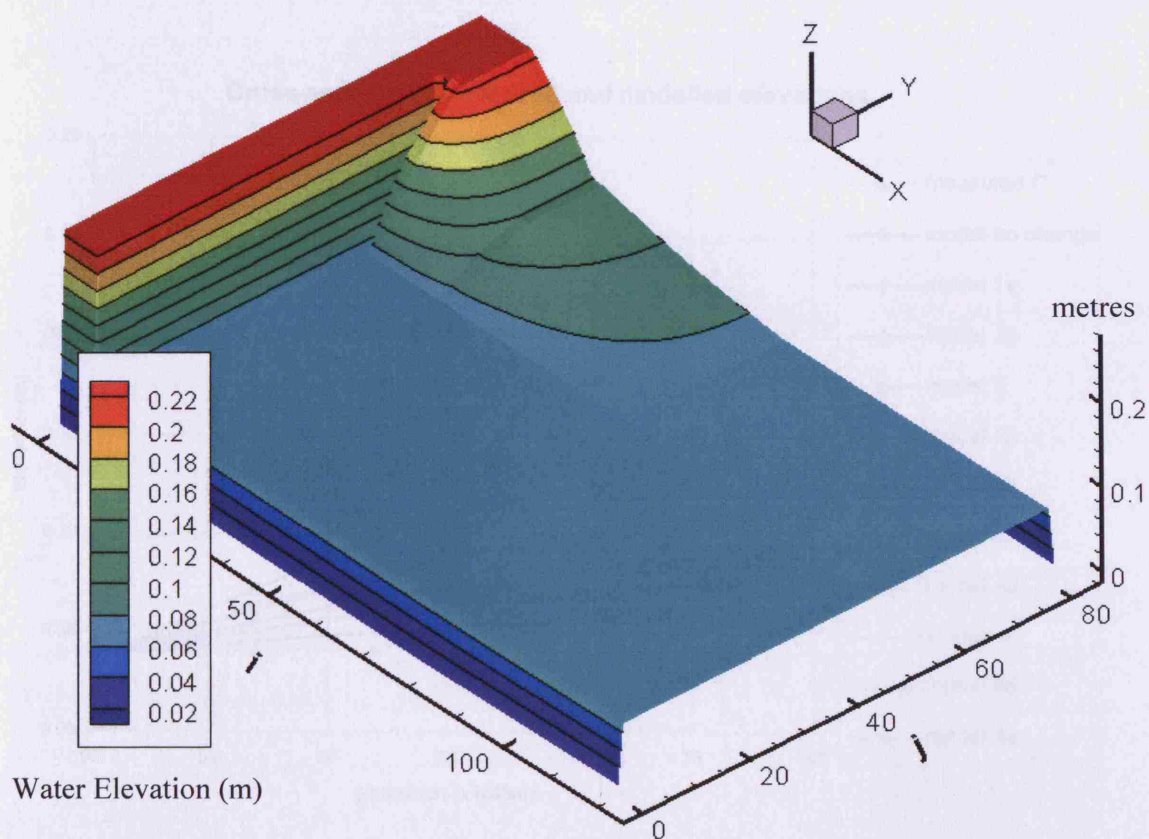


Figure 7.27: - Model results for increased permeability and half open cells (run 4e).

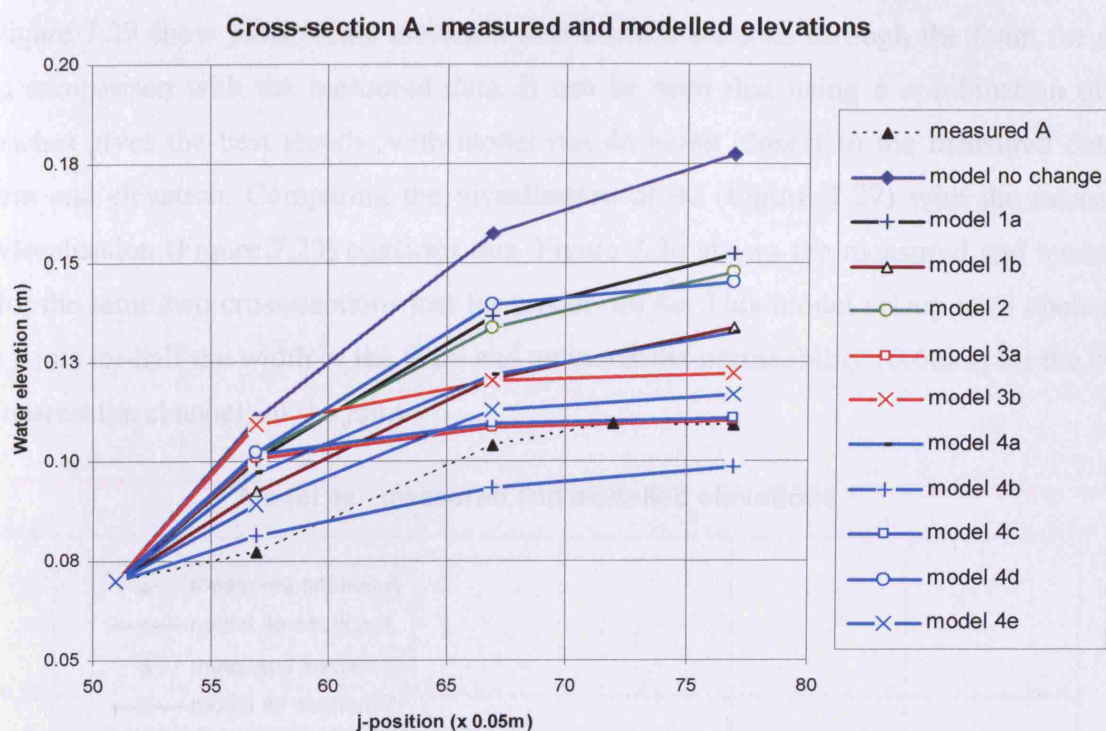


Figure 7.28: - Measured and modelled elevations for cross-section A. j-position is in grid cell reference or x 0.05m from the edge of the model

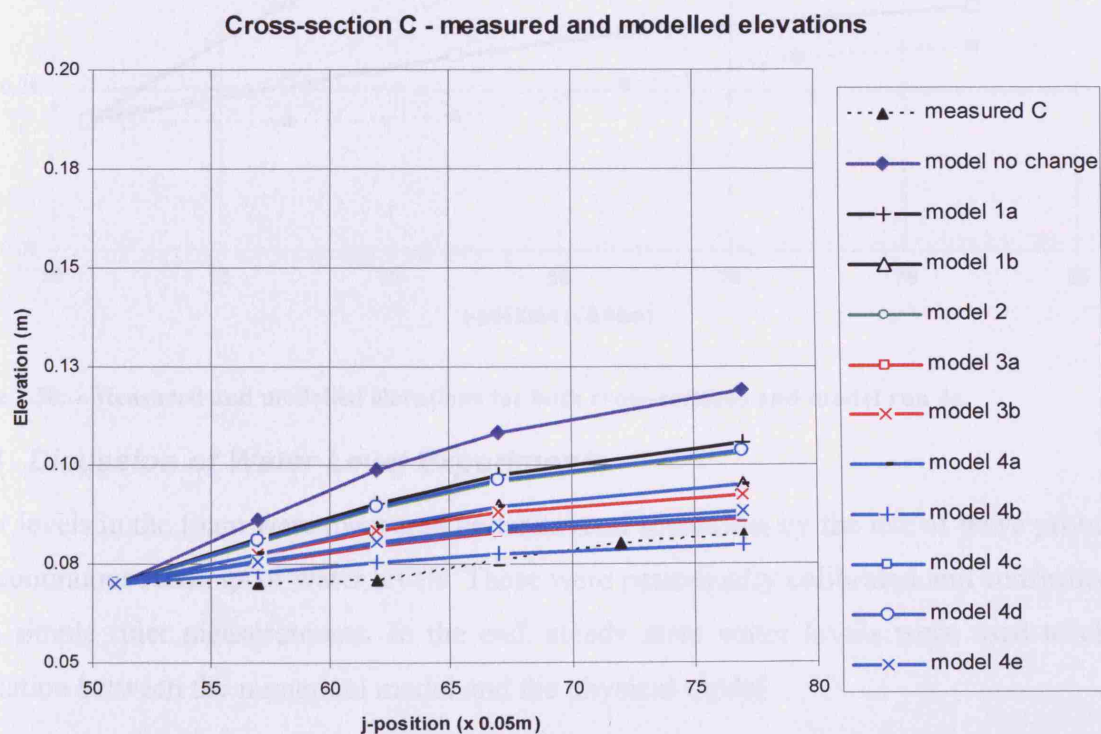


Figure 7.29: - Measured and modelled elevations for cross-section C. j-position is in grid cell reference or x 0.05m from the edge of the model

The input files used in this modelling study are included on the Appendix CD^a. Figure 7.28 and Figure 7.29 show plots of the elevation at two cross sections through the foam for each run in comparison with the measured data. It can be seen that using a combination of the approaches gives the best results, with model run 4e being closest to the measured data in gradient and elevation. Comparing the visualisation of 4e (Figure 7.27) with the measured data visualisation (Figure 7.23) confirms this. Figure 7.30 shows the measured and modelled data for the same two cross-sections just for model run 4e. This model set-up used open cells at the joints for half the width of the foam and an increased permeability (0.6m/s) for the other half (nearest the channel) of the joint.

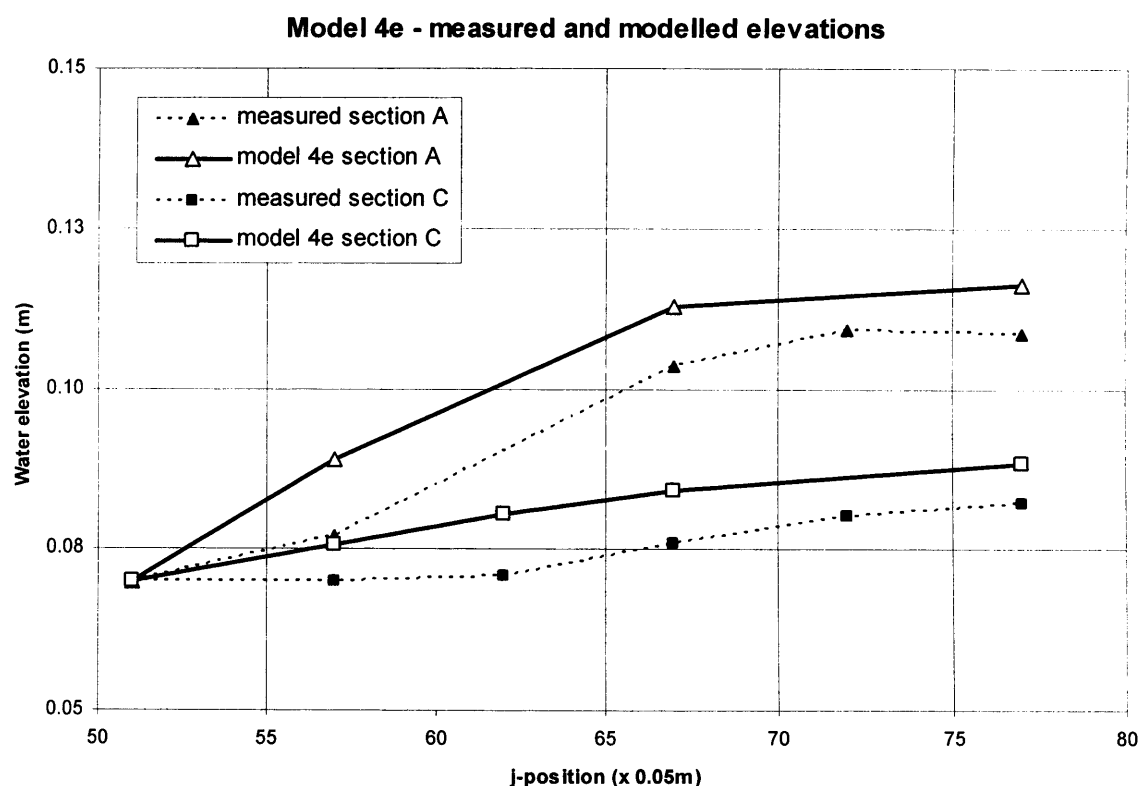


Figure 7.30: - Measured and modelled elevations for both cross-sections and model run 4e.

7.7.4 Discussion of Water Level Experiments

Water levels in the foam were measured under several scenarios, by the use of wave probes to give continuous readings of water levels. These were periodically calibrated and confirmed by using simple ruler measurements. In the end, steady state water levels were used to check correlation between the numerical model and the physical model.

^a Input files stored in D:\DIVAST-SG Laboratory Model\Water Level Experiments\waterlevels [run number].dsg

The first round of experiments (section 7.3) highlighted problems with the use of foam as a porous medium to simulate the flow of groundwater, mostly caused by the buoyancy of the foam. Most of these problems were addressed by the use of a much stronger adhesive to attach the foam to the flume floor. However, from the new measured data (section 7.7.1) it was clear that another factor was still affecting the water levels. The water level experiment described was designed to produce results independent of the permeability and porosity parameters. The water elevations were based on the steady-state boundary conditions, which are duplicated as precisely as possible in the numerical model. Yet, the measured values differed considerably from the numerical predictions e.g. at the wall side of section A the initial modelled value was 0.177m, but measured at 0.108m, a difference of 7cm or 65% of the measured value. This indicated that the initial numerical model did not duplicate the physical situation precisely.

The initial model run shows a smooth groundwater slope from the top edge of the foam to the channel. The measured data was only measured below the first joint in the foam, but showed a much lower elevation than the initial numerical model predicted. This indicated that somewhere between the top edge of the foam and cross-section A a significant head loss was occurring in the physical model. The obvious location of this head loss was at the edge of the foam (along row $i=10$ of the numerical model), and at the first joint between the foam blocks (along row $i=25$ of the numerical model). The measured data at cross-section A also shows a drop in elevation towards the wall of the flume, indicating that perhaps water was seeping along the wall boundary also.

Numerous approaches of introducing this head-loss into the numerical model were tried by varying the permeability and adding surface water (open) cells. The best results were obtained when the numerical model was adjusted by increasing the permeability of the foam along the joint locations (to approximately 0.6 m/s), and in addition a number of surface water cells were included at the joint between the foam blocks (as if the joint were not glued together) on the side of the foam furthest from the channel. The fact that this scenario gave numerical results that fit the measured data suggested that the joints were indeed responsible for the head-loss in the physical model. However, the way in which these parameters for the joints was determined was somewhat arbitrary, as the permeability of the joint was impossible to determine in practice, and the joint did not open up as wide as the open cells in the numerical model would suggest. By trialling several different approaches of modelling the joints in the

model set-up, a good agreement between the measured and modelled data was obtained. E.g. at hole A5 the elevation was modelled at 0.116 m, and measured at 0.108 m, only a 0.8 cm difference, 7% of the measured value, much improved from the 7cm (65% difference) initially.

The remaining differences could be due to the fact that unsaturated flow is not included in the model. The model assumes there is no water above the water table, but in actual fact this area is variably saturated. This problem was minimised by allowing the scenario to settle in it's steady state for some time, as most of the unsaturated behaviour occurs as the water level in the foam changes. However, even with the steady state set-up, the unsaturated portion of the foam could be affecting the flow behaviour. Seepage faces where the groundwater exits above the surface water level and trickles down the face were observed along the channel face of the foam, but mainly during transient scenarios where the water level in the channel drops rapidly – during the steady state scenarios they disappear once equilibrium is reached.

In this way the water level data collected from the laboratory was used to refine the numerical model of the physical laboratory model until relatively good agreement was reached. The numerical model was actually essential to understanding what processes were occurring in the physical model. By modelling increased flow rates along various joints in the foam it was concluded that preferential pathways existed in the physical model – while these were unintended in the original physical model plan, with hindsight, perhaps they were difficult to avoid – and they have served to show that the numerical model is flexible enough to include unforeseen elements such as these. The water levels in the physical model are now closely predicted by the numerical model (with a difference of the order of 5-10 mm), but the exact flow structure at the joints may not be correctly predicted because of the subjective nature of the adjustment to the numerical model. The adjusted numerical model can be used in the tracer experiments to assess the solute transport response.

7.8 Tracer Experiments

7.8.1 Experimental Set-up

Monitoring holes in cross-section A were used to inject tracer into the foam under the same steady-state conditions described in the previous section (7.7). The water level at the head of the flume behind the foam, and the water level in the channel were measured and recorded after steady state conditions were obtained. 100ml of Rhodamine WT at 1 ppt was then injected into the monitoring hole using a burette over a period of approximately 1min 30secs, although this varied slightly for each experiment depending on the burette used. The exact injection time was recorded in each case. Two fluorometers, the same as those used in the preliminary experimental work (section 7.4.3) were placed in other monitoring holes to record the concentration of dye passing through. Figure 7.31 shows an injection experiment in progress.

Numerous problems with the fluorometers, at one point necessitating complete repair, meant that results were slow in coming. However, once both fluorometers were running, each monitoring hole was measured in turn (using both fluorometers in the same hole) over approximately 2 hours to allow the dye to move through the foam fully. After a few attempts it was clear that flushing the foam out thoroughly before each experiment was important. Before each experiment the steady state pumped head was maintained for at least an hour to ensure the dye from the previous experiment had been flushed through the foam.

When injected into hole A5, the dye consistently exited the foam around the location of cross-section D (Figure 7.20), approximately one hour after injection (the dye emerging from the foam can be seen in Figure 7.32). Attempts to measure the dye in the monitoring holes along cross-section C were frequently frustrated by equipment failure in the peristaltic pump, the main pump and the fluorometers – but eventually clear readings were taken from all holes along cross-section C. However, only in hole C5 were any significant dye concentrations recorded. Table 7.12 summarises the experimental runs where useful data was obtained. Note was taken of where and what time the dye exited the foam into the channel.

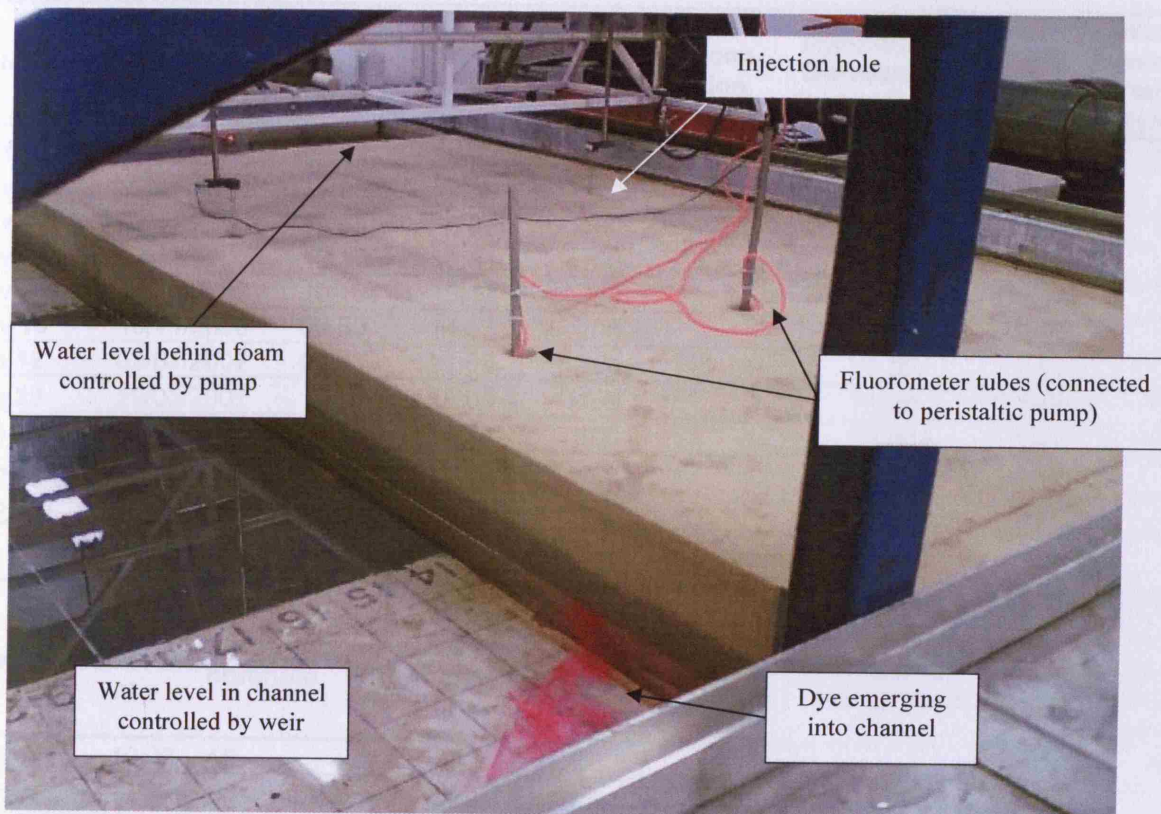


Figure 7.31: - Tracer experiment in progress, showing injection hole, two fluorometer measuring points, wave probes in upper holes, and dye emerging into the channel.



Figure 7.32: - Dye emerging from foam at approximate location of cross-section D.

Table 7.12: - Experimental Data for selected tracer experiments

Reference	Date	Pump started at	Time Injected	Tracer Volume (ml)	Tracer Concentration. (ppt)	Injection Duration (seconds)	Water Level Upstream (cm)	Water Level in Channel (cm)
Nov 2 A	02/11/2006	09:59	10:06	100	1	84.00	27.0	11.7
Nov 2 B	02/11/2006	11:50	11:56	100	1	103.00	27.0	11.0
Nov 2 C	02/11/2006	14:58	15:05	100	1	99.00	27.0	11.7
Nov 9 A	09/11/2006	10:10	10:31	100	1	80.00	27.5	11.2
Nov 9 B	09/11/2006	10:10	15:12	100	1	77.00	26.0	11.2
Nov 10	10/11/2006	09:50	14:59	100	1	75.00	26.0	11.9
Jan 12	02/01/2007	08:30	11:58	100	1	79.00	18.0	8.1
Jan 29	29/01/2007	10:30	18:05	100	1	79.00	24.0	8.0
Jan 31	31/01/2007	10:15	16:18	100	1	79.00	24.0	8.0
Feb 5	05/02/2007	12:00	20:36	100	1	78.00	26.0	8.0
Feb 7	07/02/2007	09:50	15:59	100	1	79.00	26.7	8.0

Ref	Logging started at	Injection borehole	Position of Fluorometer 1	Position of Fluorometer 2	Position tracer entered channel (m on flume ruler)	Time tracer entered channel (minutes after injection)
Nov 2 A	10:02	A5	C1	C5	2.28	32.00
Nov 2 B	11:55	A3	C3	C1	2.82	8.00
Nov 2 C	14:58	A3	C3	not used	3.85	7.00
Nov 9 A	10:29	A5	C4	C2	2.75	62.32
Nov 9 B	16:26	A5	C1	C1	2.78	56.00
Nov 10	14:58	A5	Not used	Not used	2.89	57.66
Jan 12	12:00	A5	not used	C5	not known	not known
Jan 29	18:01	A5	C3	C3	2.75	54.00
Jan 31	16:16	A5	C5	C5	2.75	54.00
Feb 5	20:34	A5	Channel at 2.5m	Channel at 2.5m	2.75	54.00
Feb 7	12:00	A5	Channel at 2.5m	Channel at 2.5m	2.75	52.50

Ref	Notes
Nov 2 A	
Nov 2 B	Small amount of dye observed in channel at 12:03 at 2.82m on side ruler Lots! of dye observed emerging at about 12:07, at the 3.8m mark. More dye emerging from 2.8m at approx 12:13, (12:15?) continues until 12:37ish.
Nov 2 C	Dye observed in channel approx 15:12, at 3.8-3.9m on side ruler. 15:18, fluorometer 1 moved to channel to measure plume concentration. 15:24 approx no more dye emerging
Nov 9 A	
Nov 9 B	After time 1:18:57 the point of entry had moved to 2.69m
Nov 10	At time 1:31 the point of entry into the channel had moved to 2.75m. At time 1:41 the point of entry into the channel had moved to 2.65m.
Jan 12	Peak detected in C5
Jan 29	No peak detected
Jan 31	Peak detected in C5
Feb 5	Peak detected on both fluorometers
Feb 7	No peak detected, but dye observed. Fluorometer malfunction?

7.8.2 Model set-up

The model that most accurately predicted the water levels in the previous section was taken and set-up to reflect the experimental set-up. A conservative tracer (referred to as ‘salt’ in the input files) was used to represent the Rhodamine WT. This tracer was added to the model at 0.35 hours to allow time for the water levels to stabilise to the desired levels. The water levels and injection location and duration were set in each input file to reflect each experimental run being modelled. The input files are stored on the Appendix CD^a.

7.8.3 Exit point of tracer from foam

The tracer results were collected in two methods – the detailed fluorometer data from the monitoring holes, and the exit point and time of the dye emerging from the foam into the channel. Figure 7.34 to Figure 7.48 show the modelled tracer plume at the time (minutes after injection) that tracer was first visible emerging from the foam in the laboratory. The point at which the tracer was observed is shown on each diagram. The axes are the model grid coordinates or $x \times 10$ cm from the edge of the flume. The tracer concentration is in ppt. All the runs have tracer injected into hole A5, except form runs Nov 2 B and Nov 2 C, where the tracer was injected into hole A3. All the runs listed in Table 7.12 are illustrated with the exception of Jan 12, when no exit point was recorded.

Figure 7.32 shows the tracer emerging from the foam after injection into A5. It can be seen that the tracer exits the foam and continues downstream, as would be expected. In the model, the tracer actually starts to move in the opposite direction once it reaches the channel – this is because of the velocities in the channel – the higher permeability of the joint upstream of cross-section A causes water to exit the foam at a higher velocity here than the rest of the foam, causing the velocities in the channel to circulate, as shown in Figure 7.49 and Figure 7.50. This explains the misleading shape of the plume in the models when it reaches the channel. It can be seen in the animations that the plume does actually move downstream after reaching the faster part of the channel.

Nov 2 A

The tracer was observed to exit the foam below the joint between the foam blocks surprisingly soon (32 mins) after injection. Figure 7.34 shows that the model for this scenario predicts that the plume would not have reached the edge of the foam by this time. When compared with other runs the discrepancy is big enough to be questioned. It was thought that

^a Input files stored in D:\DIVAST-SG Laboratory Model\Tracer Experiments\[run reference].dsg

perhaps this discrepancy was caused by tracer from a previous run remaining in the foam, that had not been flushed out before the run commenced. Table 7.12 shows that the pump was not switched on for long (only 7 minutes) before the injection occurred, which would tend to confirm this suspicion as old tracer would not have had time to be washed out of the foam before the experiment commenced. During runs on subsequent days the pump was switched on at least half an hour before experiments commenced. As a result of the lack of flushing of old tracer, the results from this run were disregarded.

Nov 2 B

Tracer was injected into hole A3 in this run. Three separate tracer exit points were observed. The first (Figure 7.35) occurred after only 8 minutes and was only a small amount of dye (see notes in Table 7.12); this was disregarded as the tracer finally emerging from the previous run (Nov 2 A). The second exit point occurred in a different location after 11 minutes (Figure 7.36). This was regarded as a genuine exit point for the injected tracer from this run. The model predicts the plume will emerge at the same time but slightly closer to the injection hole. An animation of the model run is stored on the Appendix CD^a and by watching this it can be seen that the main ‘slug’ of tracer is predicted to emerge almost exactly at the observed point, but at a slightly later time than observed - 15 mins after injection, or 0.6 hours after the model start, since the injection occurs at 0.35 hours.

The third exit point occurred 17 minutes after the injection in a similar position to the first exit point, and was regarded to be a continuation of this and disregarded accordingly.

Nov 2 C

The tracer was injected into hole A3 again. Tracer emerged after only 7 minutes at the point shown. The model suggests that this is quite soon for the tracer to be emerging so this could be tracer from the previous run – however there was no break in the tracer emerging – the tracer from this run could have mixed with some leftover tracer from the previous run.

Aside from the clearly separate result in Nov 2 B the first collection of runs served mainly to highlight that the foam needed to be flushed completely before each experiment.

Nov 9 A

Injecting tracer into hole A5, the tracer was observed to emerge after 62 mins at the point shown in Figure 7.39. The model predicts that the tracer will emerge at the same time at a

^a Animation for Nov 2 B stored as D:\DIVAST-SG Laboratory Model\Tracer Experiments\Nov 2 B.avi

position slightly upstream – however, the joint between the foam blocks influences the tracer distribution significantly. In section 7.7 it was described how the model was adjusted to simulate the joints between the foam blocks by increasing the permeability and using open cells. This causes the tracer to move much faster along the joints in the model, and so the model predicts that the exit of the tracer will occur at two places. The animation on the Appendix CD^a shows this clearly, although the plume becomes merged once it enters the channel. However, visible tracer was only observed at one exit point, and this was upstream of the joint between the foam blocks, in between the two exit points predicted in the model.

Nov 9 B

Two recordings of exit position and time were made on this run. Tracer was injected into A5 and observed to exit at 56 mins later at the point shown in Figure 7.40. After 79 minutes the position had moved to the point shown in Figure 7.41, 9 cm further downstream – giving an average velocity of approx. 0.000065 m/s in the downstream direction for the point where the tracer plume exits the foam.

The model predicts an initial exit of the tracer nearly 50cm upstream at the same time as the observed exit point, and by the second reading the main tracer plume exit point is still upstream of the observed point, although the joint causes tracer to leak into the channel closer to the observed point.

Nov 10

Three exit timings were taken on this run. Injected into hole A5, the tracer was observed to exit at 57 mins after the injection at a similar point to the previous runs (Figure 7.42). After 91 mins, the exit point had moved downstream by 14 cm (Figure 7.43), then after 101 mins it had moved a further 10 cm (Figure 7.44) giving velocities of 0.000069m/s, and 0.000167 m/s, or an average of 0.000118 m/s downstream.

The model again predicts an exit point upstream of the observed position but at the correct time, and the subsequent observations show the same pattern.

Comparing the observed apparent velocity of the edge of the tracer plume where it exits the foam with the modelled velocities shows a good correlation, as shown in Figure 7.33.

^a Animation for Nov 9 A stored as D:\DIVAST-SG Laboratory Model\Tracer Experiments\Nov 9 A.avi

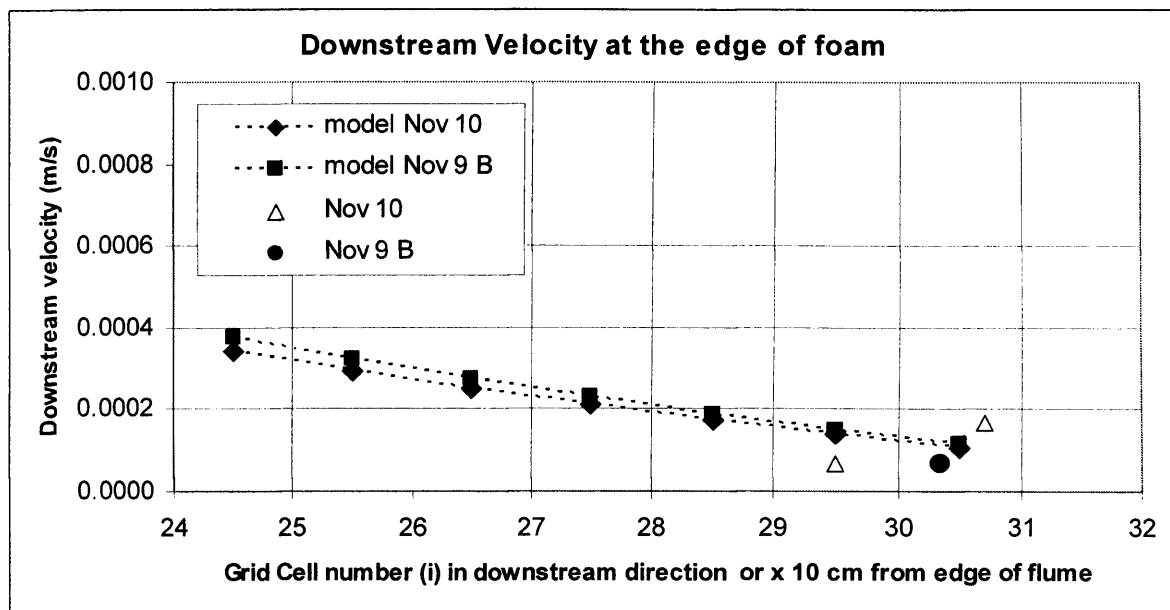


Figure 7.33: - Downstream velocity at edge of the foam, measured and modelled.

Jan 29 and Jan 31

These two runs have identical parameters (injection duration, upstream and channel water level). Tracer injected at A5 appeared after 54 minutes at the same point each time (2.75m on the flume ruler) as shown on Figure 7.45 and Figure 7.46. The model again predicts that the tracer emerges at this time but further upstream (40 cm upstream approx) – however, the main slug of tracer again reaches the channel at the observed point, but at a later time than observed. The animation stored on the Appendix CD^a shows this in action.

Feb 5

A similar scenario to Jan 29 and Jan 31, but with a slightly higher head elevation at the pumped end. Tracer injected into hole A5 emerged at 54 minutes at an identical location to the Jan 29 and Jan 31 runs, as shown in Table 7.12. This time the model predicts that the initial emergence of the tracer will be earlier than observed, due to the higher head difference between the upstream reservoir and the channel. By the time the tracer was observed to exit, the model predicts that a considerable amount of tracer will have already emerged into the channel. This can be seen in Figure 7.47. The animation^b shows that the bulk of the tracer does indeed exit near the observed point, but at a later time (approx 63 mins after injection or 9 minutes after it was observed).

^a Animation for Jan 31 stored as D:\DIVAST-SG Laboratory Model\Tracer Experiments\Jan 31.avi

^b Animation for Feb 5 stored as D:\DIVAST-SG Laboratory Model\Tracer Experiments\Feb 5.avi

Feb 7

Tracer injected into hole A5 emerged 52.5 minutes later at the same location as the previous three runs (Figure 7.48). The model again predicts an earlier initial exit time and an exit point higher upstream, but significant bulk of the tracer exits at the observed point at a later time, as in the previous run.

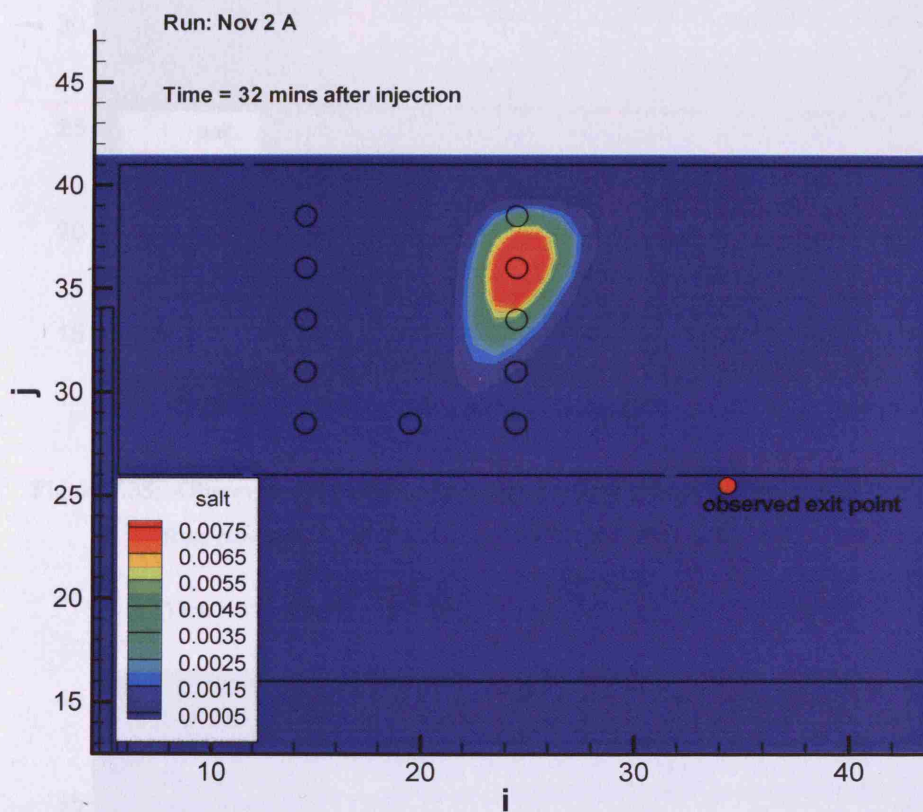


Figure 7.34: - Observed exit point and modelled tracer plume for Nov 2 A at 32 mins

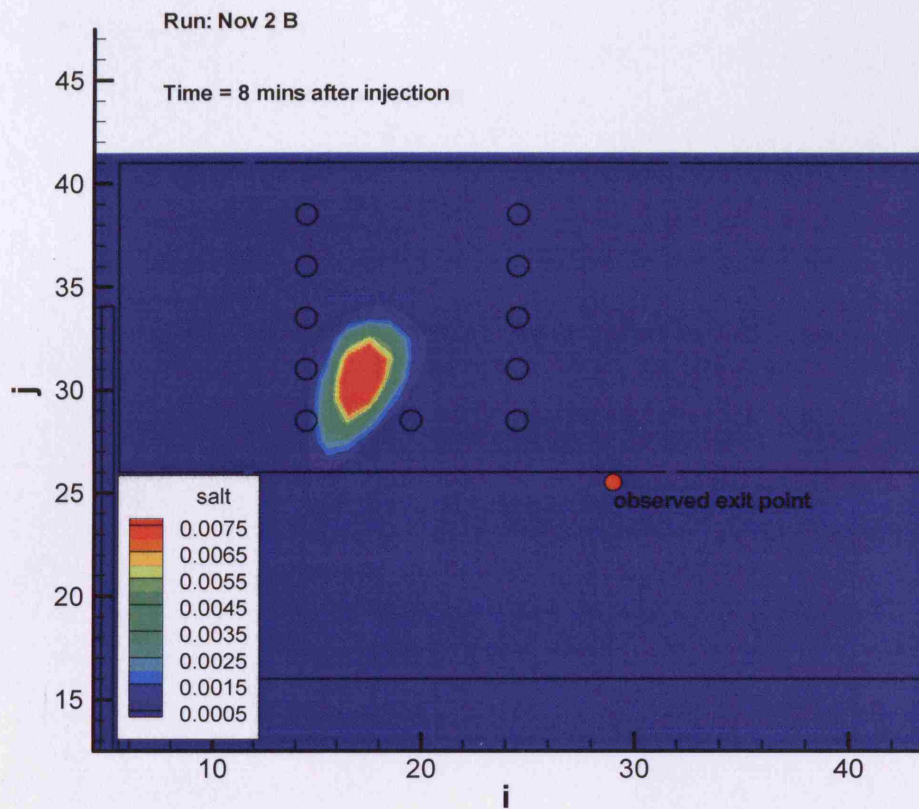


Figure 7.35: -Observed exit point and modelled tracer plume for Nov 2 B at 8 mins

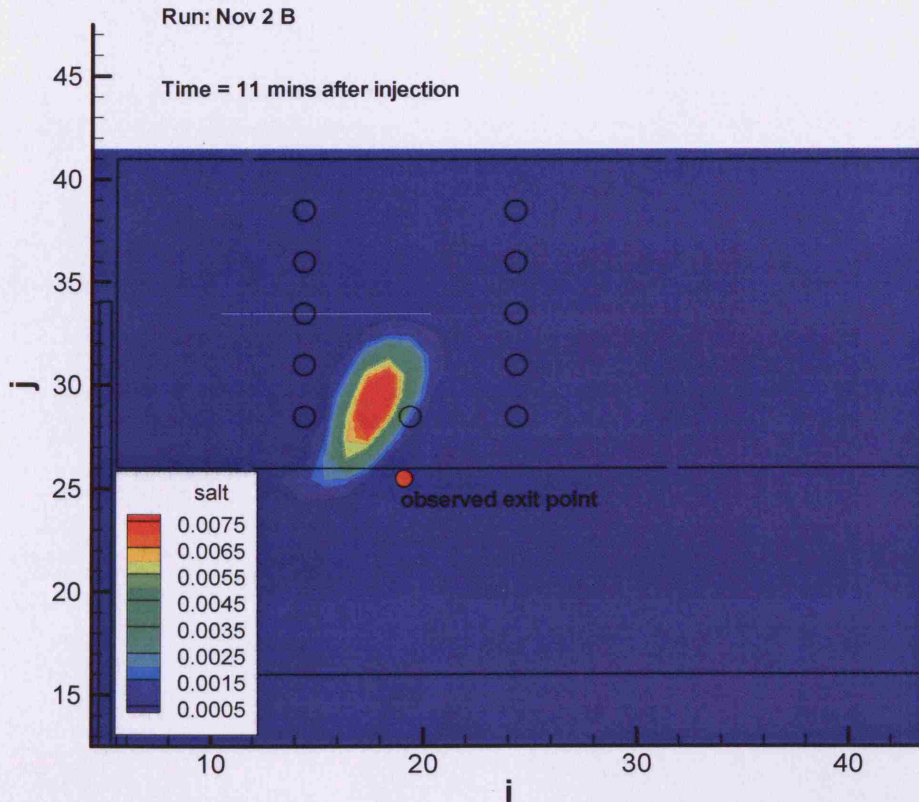


Figure 7.36: - Observed exit point and modelled tracer plume for Nov 2 B at 11 mins

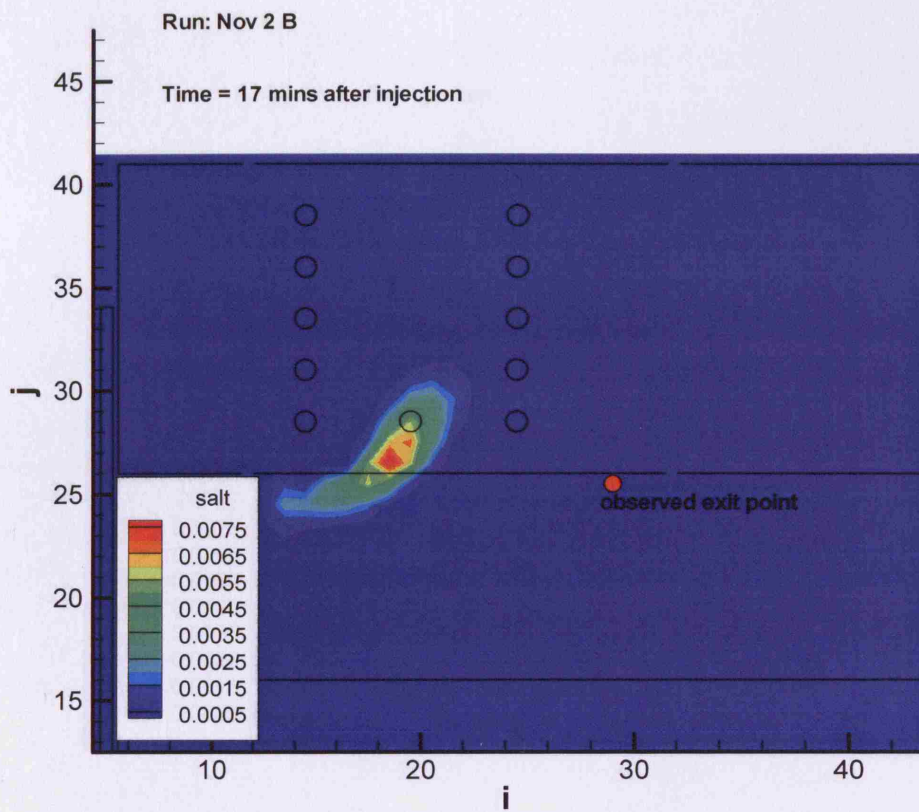


Figure 7.37: - Observed exit point and modelled tracer plume for Nov 2 B at 17 mins

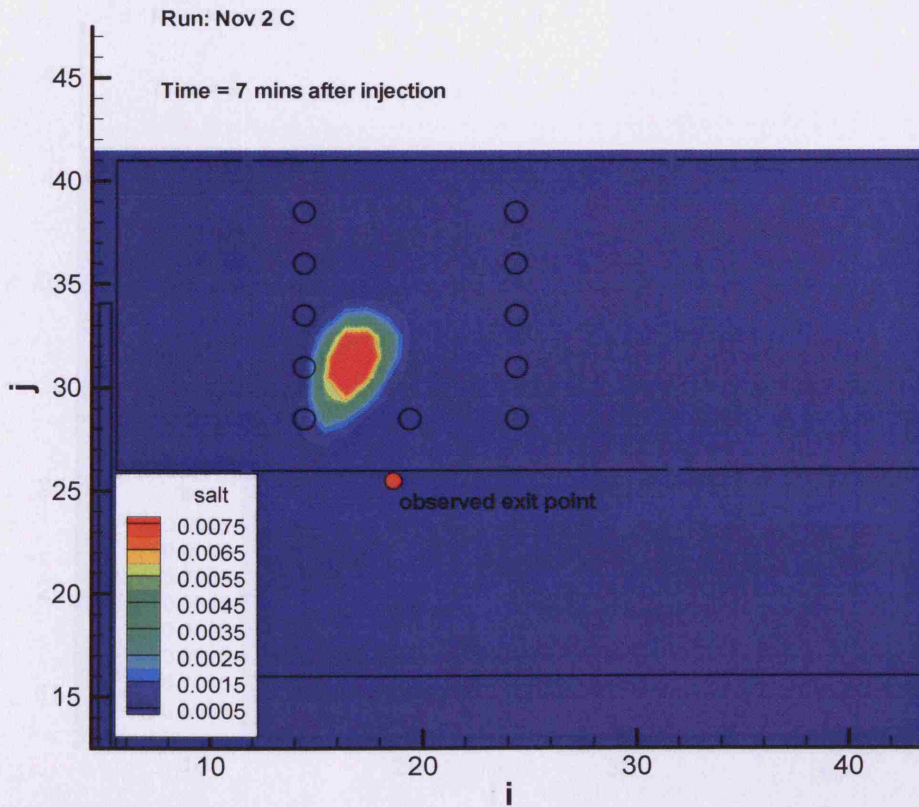


Figure 7.38: - Observed exit point and modelled tracer plume for Nov 2 C at 7 mins

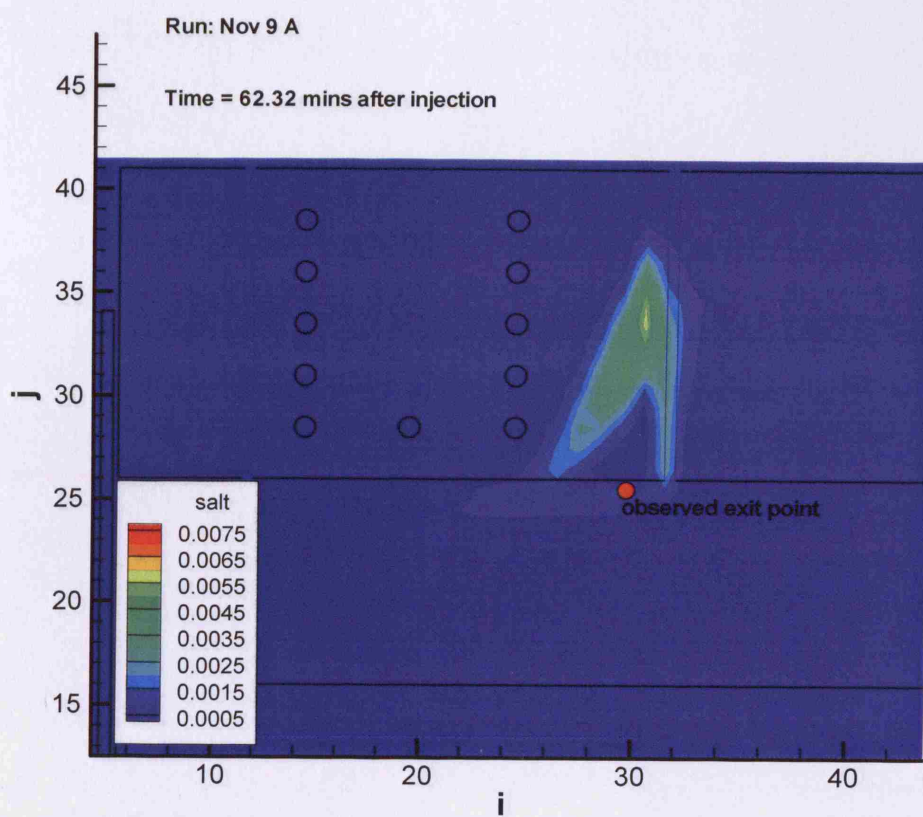


Figure 7.39: - Observed exit point and modelled tracer plume for Nov 9 A at 62.32 mins

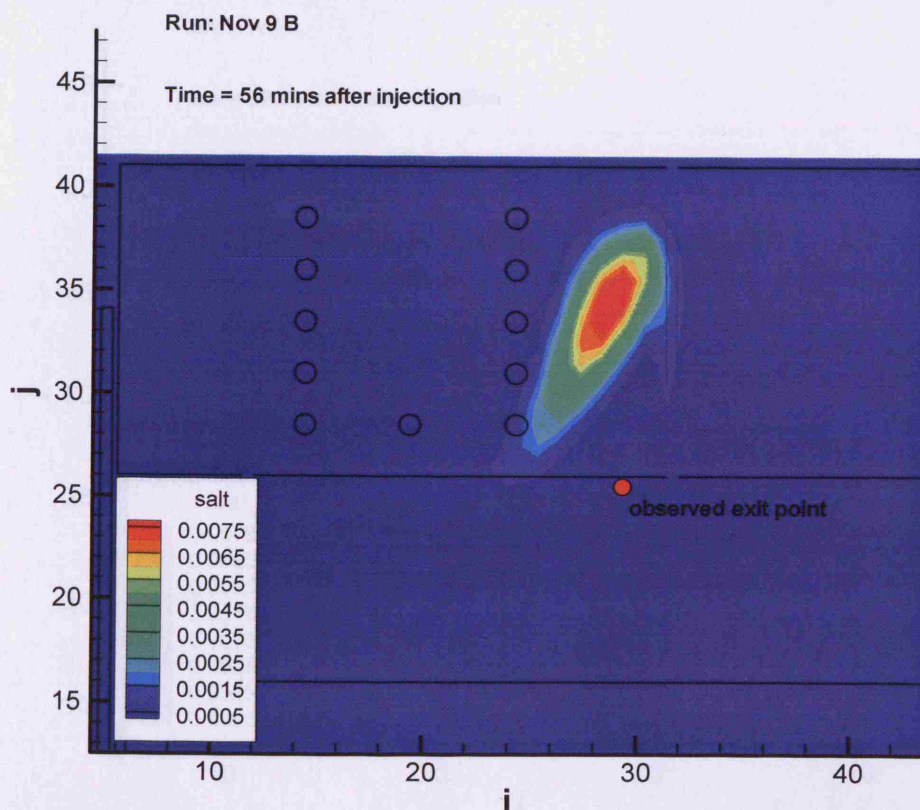


Figure 7.40: - Observed exit point and modelled tracer plume for Nov 9 B at 56 mins

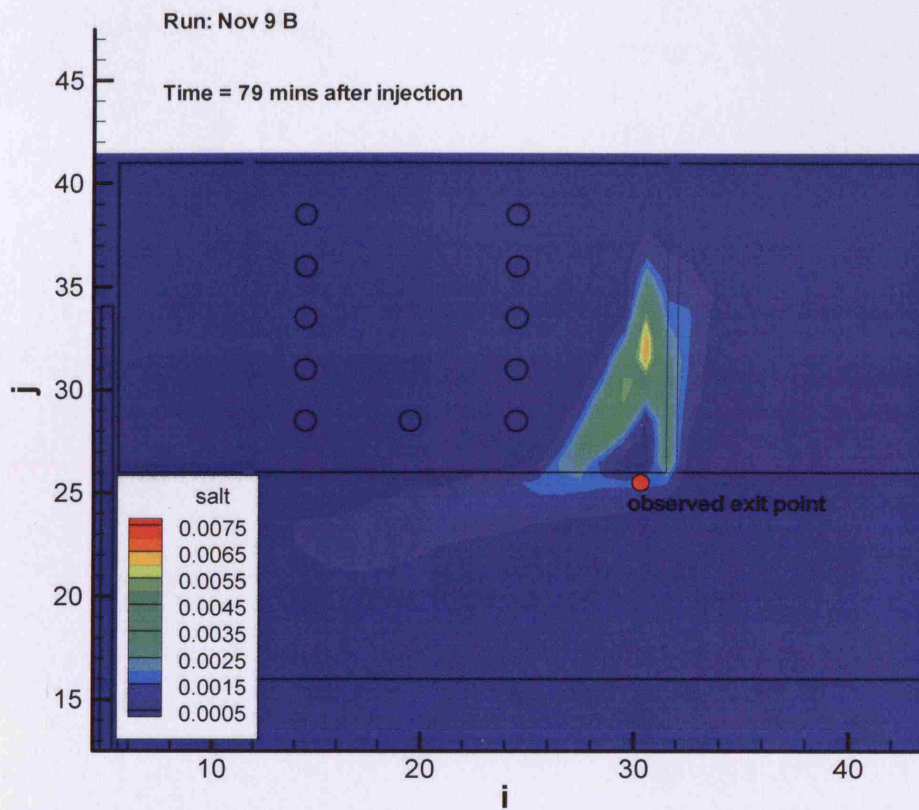


Figure 7.41: - Observed exit point and modelled tracer plume for Nov 9 B at 79 mins

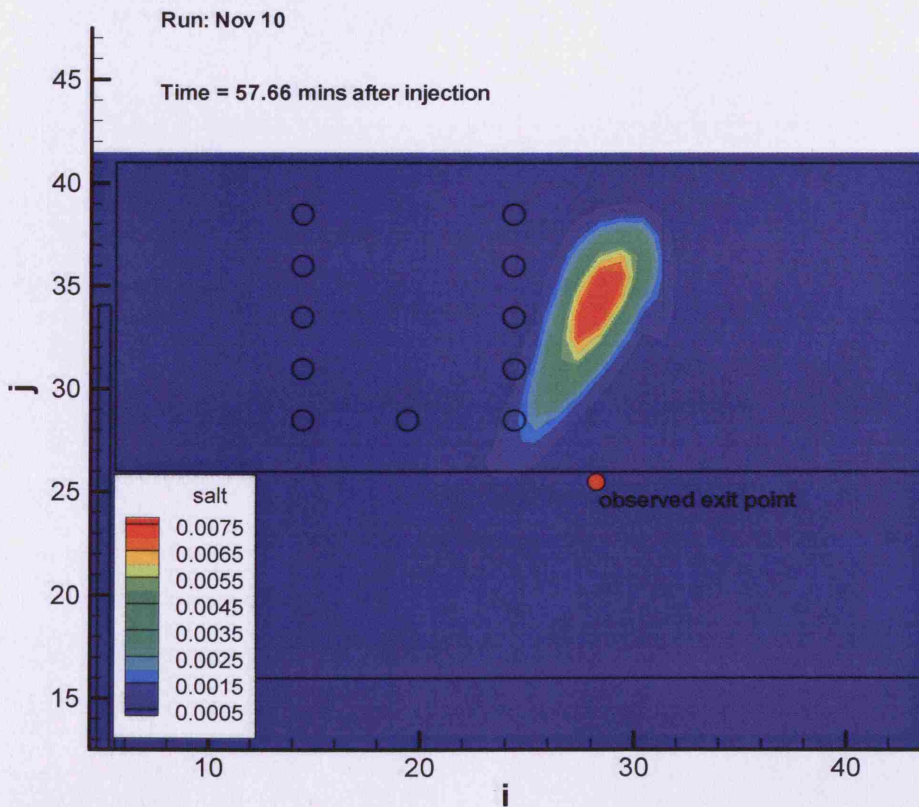


Figure 7.42: - Observed exit point and modelled tracer plume for Nov 10 at 57.66 mins

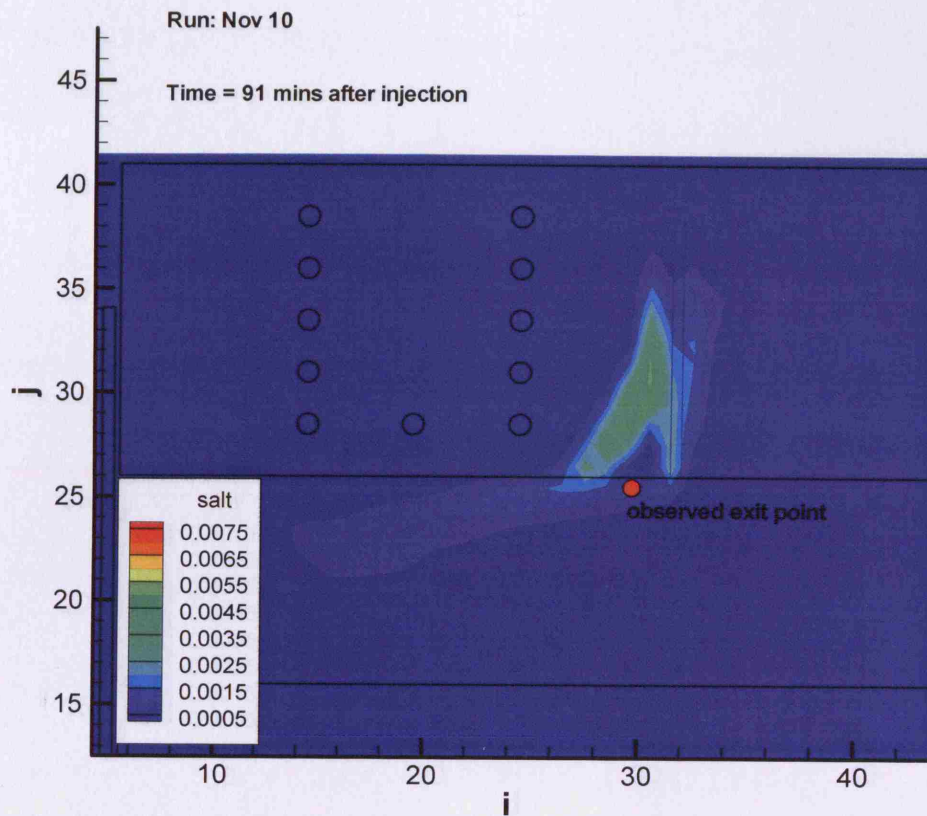


Figure 7.43: - Observed exit point and modelled tracer plume for Nov 10 at 91 mins

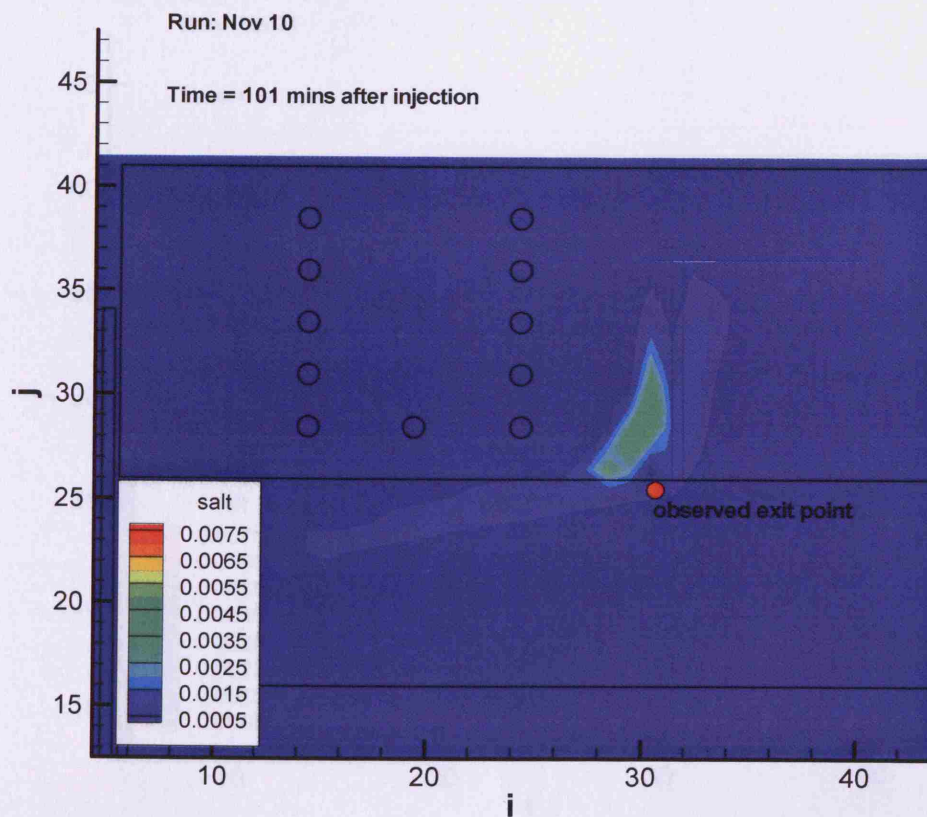


Figure 7.44: - Observed exit point and modelled tracer plume for Nov 10 at 101 mins

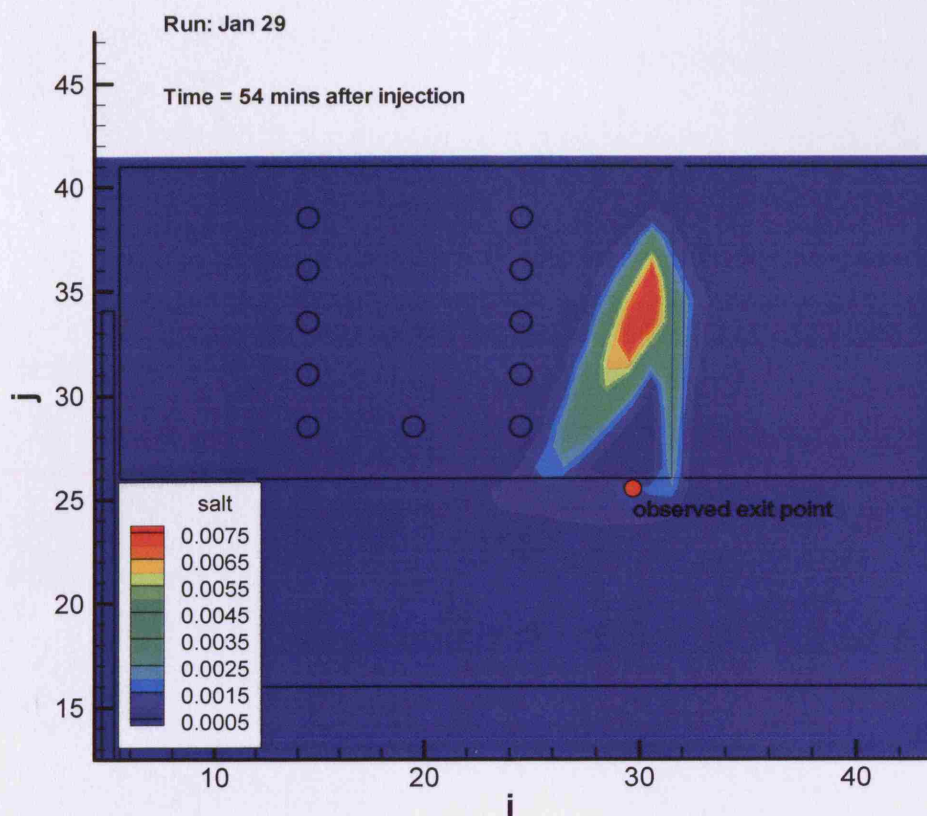


Figure 7.45: - Observed exit point and modelled tracer plume for Jan 29 at 54 mins

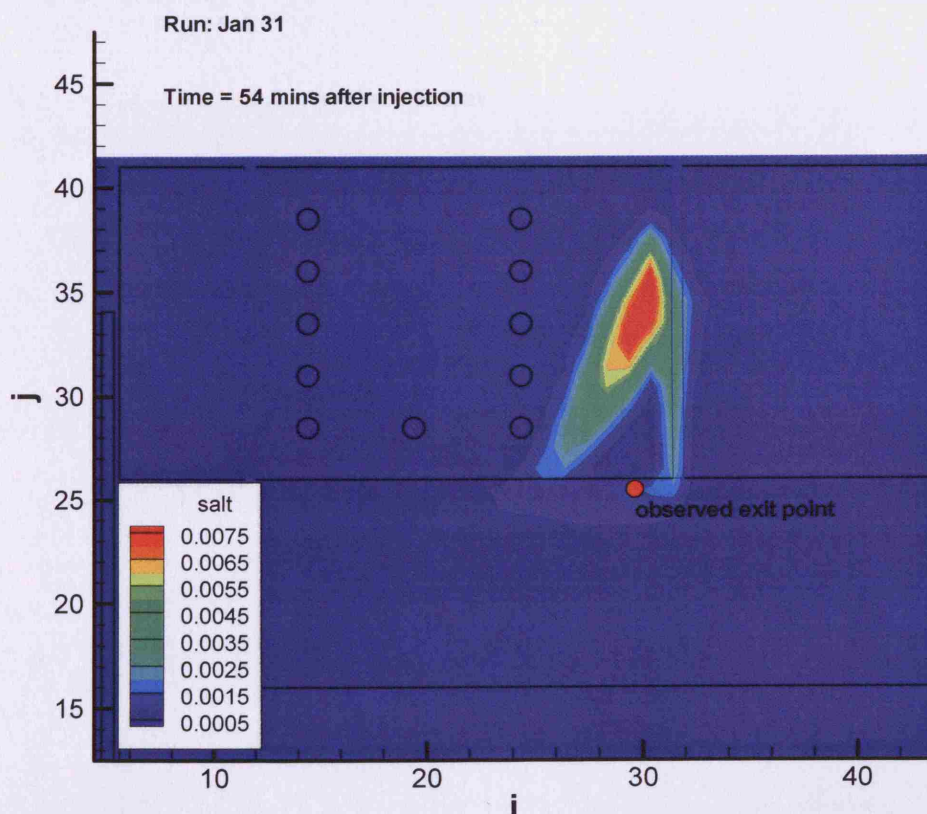


Figure 7.46: - Observed exit point and modelled tracer plume for Jan 31 at 54 mins

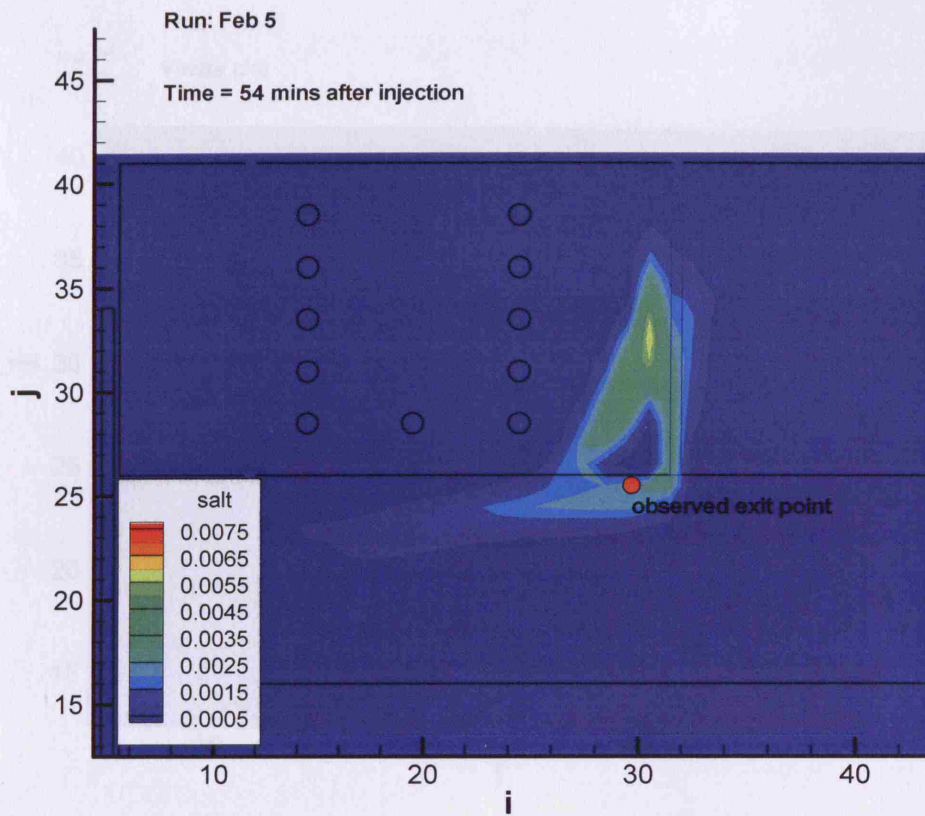


Figure 7.47: - Observed exit point and modelled tracer plume for Feb 5 at 54 mins

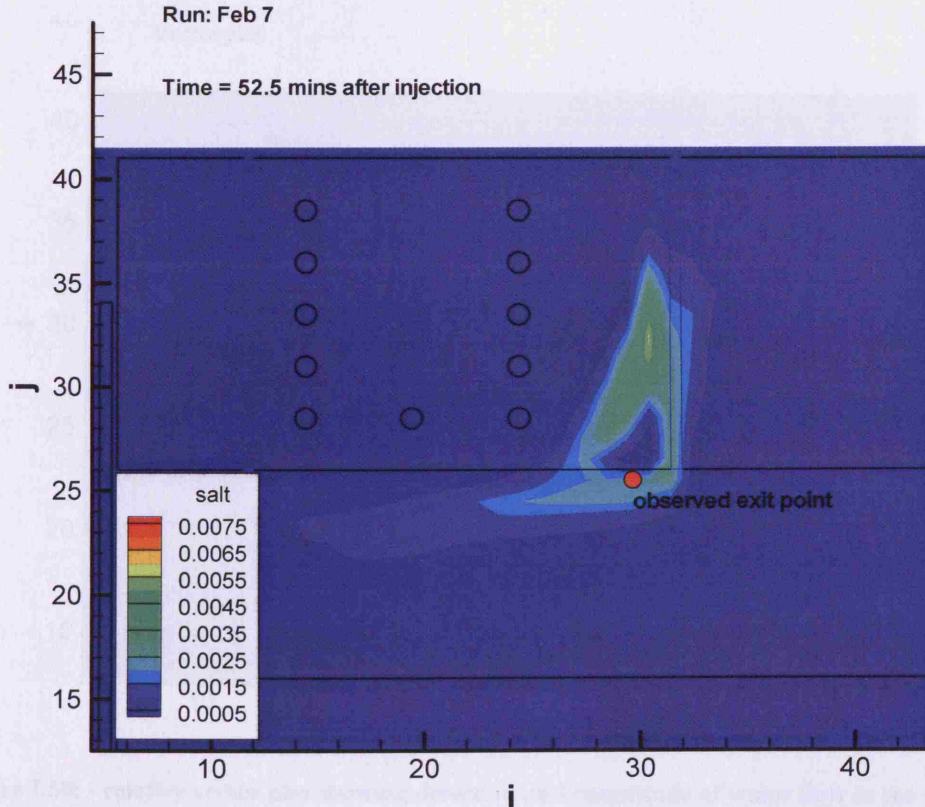


Figure 7.48: - Observed exit point and modelled tracer plume for Feb 7 at 52.5 mins

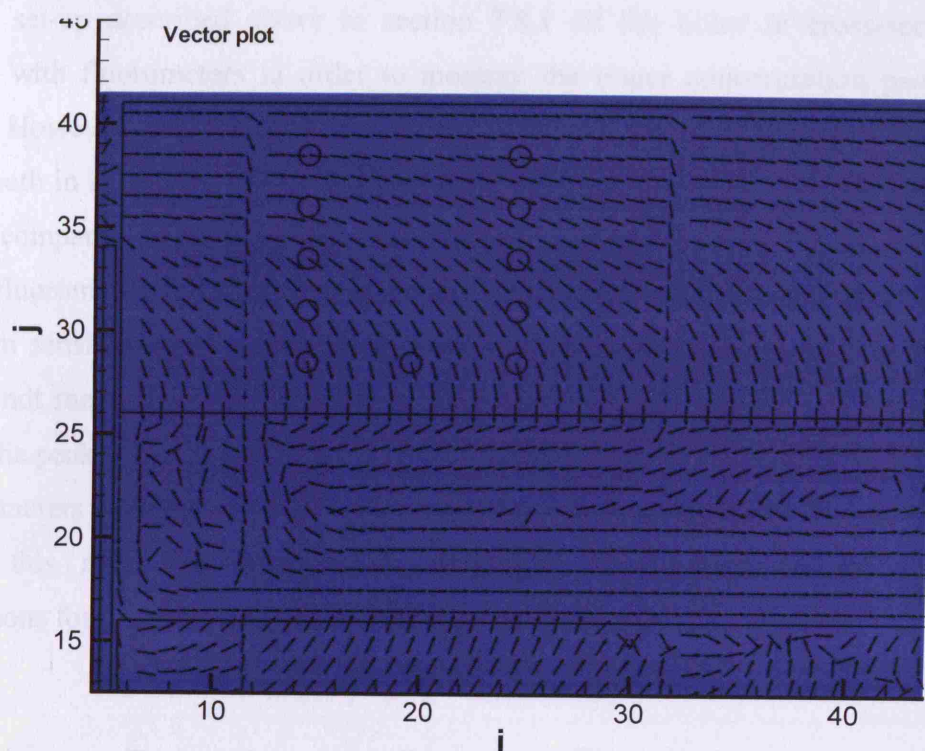


Figure 7.49: - Uniform Vector plot showing direction of water flow in the model.

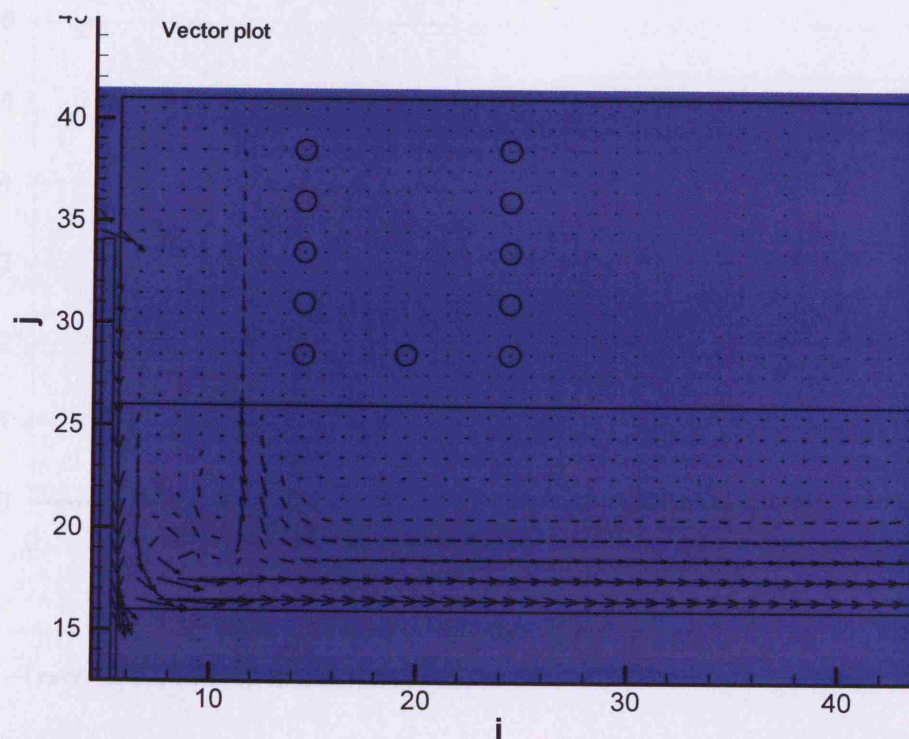


Figure 7.50: - relative vector plot showing direction and magnitude of water flow in the model

7.8.4 Fluorometer Data

Using the set-up described above in section 7.8.1 all the holes in cross-section C were monitored with fluorometers in order to measure the tracer concentration passing through each hole. However, out of all the experiments, only two peaks of tracer concentration were detected, both in hole C5 – one in the Jan 12 run, and one in the Jan 31 run. These measured peaks are compared to the modelled concentrations for each run in Figure 7.51 and Figure 7.52. The fluorometers did not detect any tracer on the low sensitivity setting, so in both cases the medium sensitivity setting was used, meaning that concentrations over 1000 ppb (0.001 ppt) were not measured. This meant that the peak concentration was not recorded, but the timing of the peak was still valid.

The fluorometers were placed in the channel for the Feb 5 run and both fluorometers detected peaks in this run. The measured concentrations are plotted against the modelled concentrations for the same point in the channel in Figure 7.53.

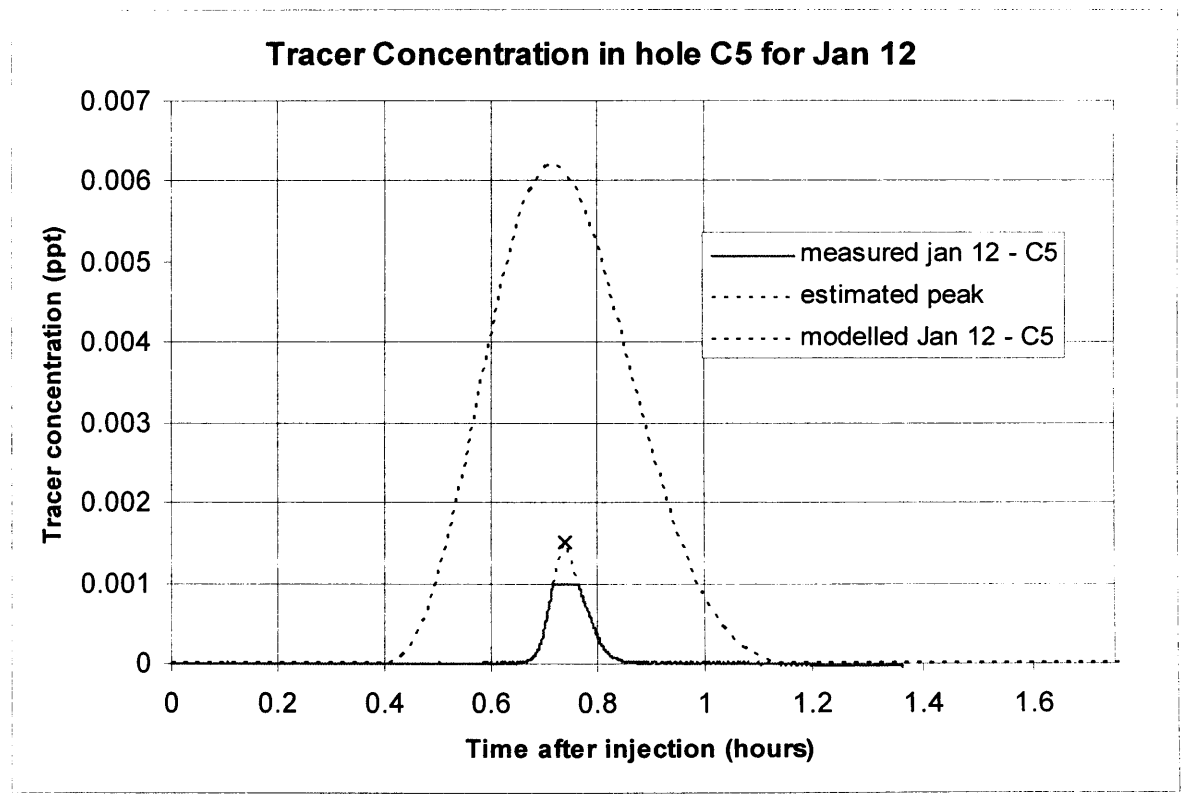


Figure 7.51: - Tracer concentration in hole C5 for Jan 12

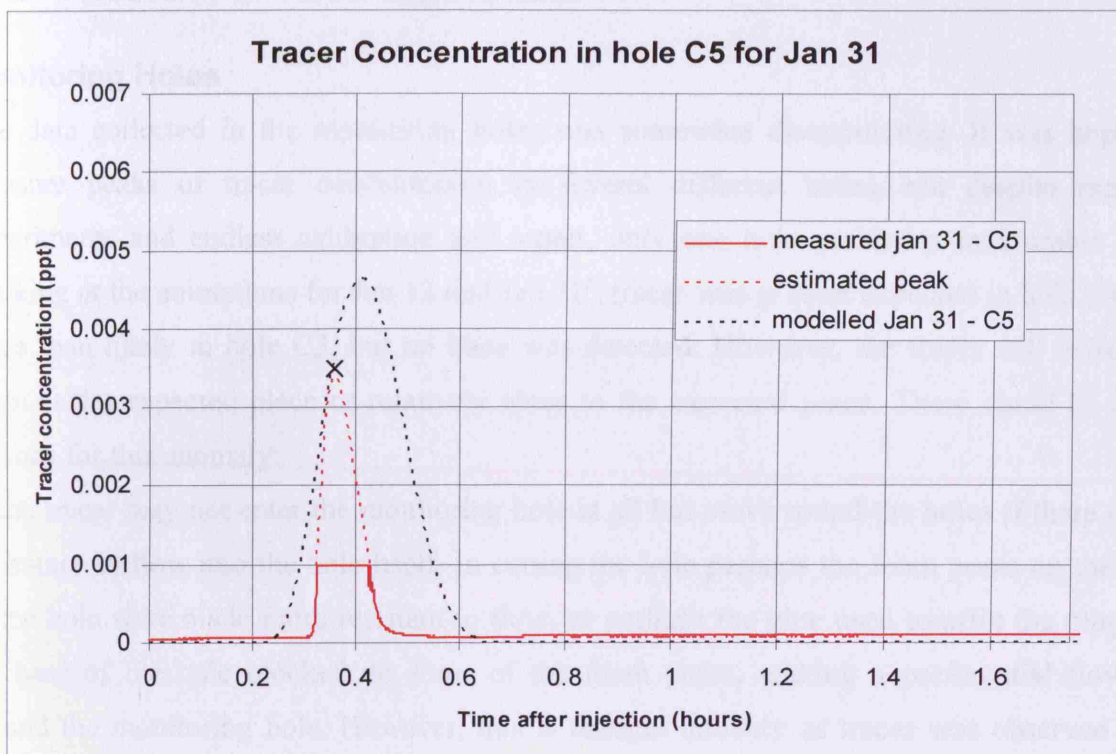


Figure 7.52: - Tracer concentration in hole C5 for Jan 31

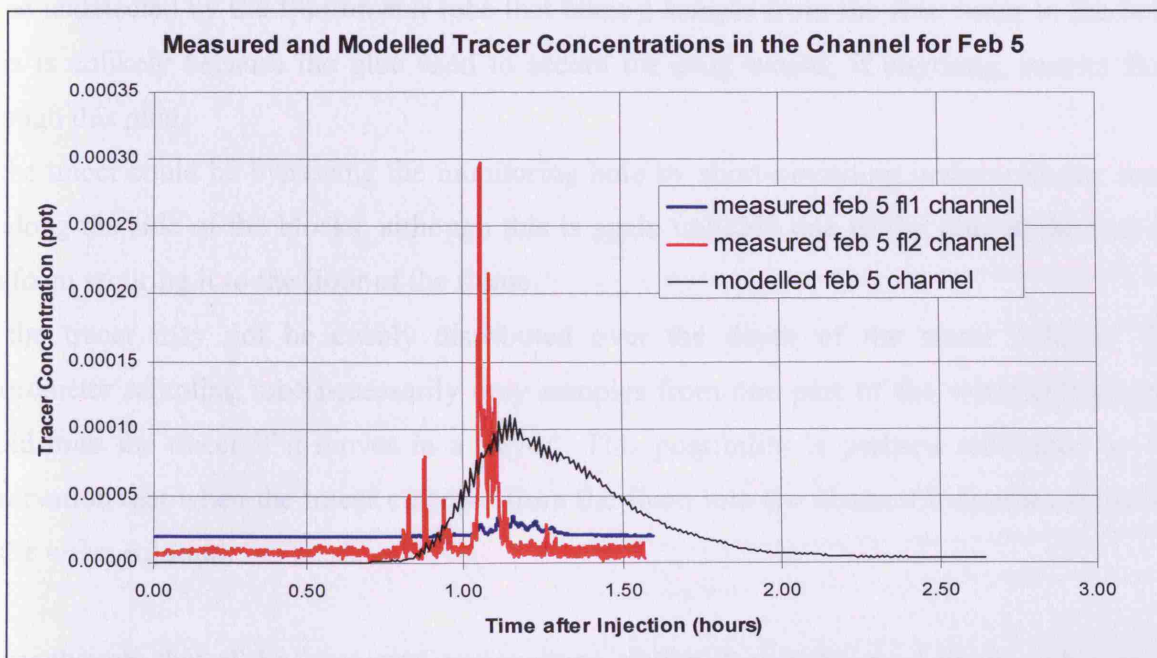


Figure 7.53: - Tracer concentration in the channel (2.5m on ruler) for Feb 5

7.8.5 Discussion of Tracer Experiments

Monitoring Holes

The data collected in the monitoring holes was somewhat disappointing. It was hoped to measure peaks of tracer concentration in several different holes, but despite repeated experiments and endless calibration and repair, only one hole yielded a measurable peak. Looking at the animations for Jan 12 and Jan 31^a, tracer was at least expected in hole C4, and more than likely in hole C3, but no trace was detected. However, the tracer still exited the foam at the expected place or relatively close to the expected place. There could be a few reasons for this anomaly:

- a) the tracer may not enter the monitoring hole at all but move round the holes if there is any resistance to flow into the hole itself. In cutting the hole perhaps the foam pores on the edge of the hole were made more resistant to flow, or perhaps the glue used to affix the plug into the base of the hole blocked up some of the foam pores, making a preferential flowpath around the monitoring hole. However, this is thought unlikely as tracer was observed in at least one of the monitoring holes,
- b) the tracer could be travelling through the foam plug at the base of the monitoring hole and so be undetected by the fluorometer tube that takes a sample from the free water in the hole. This is unlikely because the glue used to secure the plug would, if anything, restrict flow through this plug,
- c) the tracer could be bypassing the monitoring hole by short-circuiting underneath the foam or along the side of the blocks, although this is again unlikely due to the glue at the base of the foam securing it to the floor of the flume,
- d) the tracer may not be evenly distributed over the depth of the water column. The fluorometer sampling tube necessarily only samples from one part of the water column and could miss the tracer if it moves in a 'layer'. This possibility is perhaps reinforced by the observation that when the tracer emerges from the foam into the channel it appears at the top of the water column.

It was thought that of the suggested explanations, option d) was the most likely with perhaps option a) contributing slightly. Measurements were taken as near the surface of the water column as possible after this was decided, but the necessity of ensuring the fluorometer tube

^a Animations stored in D:\DIVAST-SG Laboratory Model\Tracer Experiments\Jan 12.avi etc

was always submerged limited the proximity to the water surface that could be achieved and no new tracer was detected in any of the holes.

The results that were obtained from hole C5 show good agreement with the modelled data. The timing of the modelled and observed peaks coincided almost exactly on the Jan 12 run, both occurring at approximately 43 mins after injection, although the modelled magnitude was considerably higher (at 0.0062 ppt) than the measured magnitude (estimated at 0.0015 ppt). The Jan 31 run appears to show a much larger measured peak, of the order of 0.0035 ppt at approximately 22 mins after injection, much closer to the modelled peak of 0.0046 ppt, which occurs 3 mins later.

The Jan 31 peak occurs sooner after injection than the Jan 12 peak, indicating that the tracer moved faster through the foam. This is borne out by the head difference recorded in Table 7.12. The run on Jan 12 had an upstream head of 18.0 cm, and a channel head of 8.1 cm, giving a 9.9 cm head difference. Jan 31 had a head of 24.0 cm upstream and 8.0 cm in the channel, giving a head difference of 16 cm, and hence faster velocities through the foam. The model predicts the same behaviour.

Channel monitoring point

When the fluorometers were placed in the channel to catch the exit plume of tracer the two fluorometers were placed side by side. Both recorded tracer peaks of different magnitudes, indicating the difficulty of exact measurement. Both were calibrated to the same scale and were responding accurately, yet fluorometer 1 records much lower concentrations than fluorometer 2. Figure 7.32 shows the exit plume, and it can be seen that the tracer is not evenly mixed, small eddies and disturbances cause the concentration to fluctuate at any given point, giving rise to the varied readings on the fluorometers in the channel, particularly as one fluorometer will be slightly closer to the centre of the plume than the other (Figure 7.53). The average of both the fluorometers gives a better match on the magnitude of the peak, however the peak is still sharper than the modelled. The timing of the peaks are more significant than the peak concentrations measured due to the difficulties of measuring the tracer. The modelled peak for the same location at the exit point of the plume shows good agreement for the timing of the exit point.

Exit Point Data

Data from the observed exit point of the tracer was much more easily obtained and allowed a more extensive comparison between the modelled and observed results. The results are encouraging, with the model predicting a similar flow pattern to the laboratory experiments, at least in terms of where the tracer exits the foam. An injection into hole A3 (Nov 2 B) quickly exits the foam after 10 minutes or so, at a point just upstream of cross-section B – and the model predicts very similar behaviour. An identical injection into A5 takes much longer to emerge (so much so that the first few experiments were abandoned in error before it had emerged) and eventually exits just upstream of cross-section D after nearly an hour. The model also predicts this behaviour, and the observed movement of the exit point of the plume is closely matched by that of the model; the modelled velocities at the edge of the foam agree well with these observations (Figure 7.33).

Solute Transport

The equations of solute transport in DIVAST have not been modified in this study – so the tracer movement in the model is according to the surface water solute transport equations defined in Falconer (2001a). While the velocities on which the tracer movement is based are calculated using the groundwater equations, the diffusion and dispersion of the tracer may be incorrectly calculated for groundwater movement, particularly as the foam is an unusual material with a high degree of tortuosity. Further work is suggested in this area (see section 10.5).

7.9 Summary of Laboratory Validation

This section of work was perhaps the most arduous – in timescale it stretched for nearly two years, mostly because of the large number of practical difficulties encountered on the way. To the author's knowledge no attempt has been made to simulate groundwater in the laboratory using permeable foam, so perhaps this accounts for the number of the difficulties encountered. Nevertheless, useful data has been obtained from the laboratory experiments, allowing the validity of the numerical model to be assessed.

The tidal basin in the Hyder Hydraulics Laboratory at Cardiff University was modified to allow simulated interactions between surface water and groundwater. Permeable foam blocks were used to represent permeable aquifers adjacent to a river. The properties of the foam were measured using several simple laboratory techniques, and values were determined for

hydraulic conductivity (permeability) and porosity, evaluated as 0.002 m/s and 75% respectively.

The initial experimental set-up used weights to prevent the foam blocks from floating, however this did not prevent short-circuiting of the tracer underneath the foam blocks and the results obtained from this initial set-up were more indicative of problems in the laboratory set-up. After analysing these results a series of improvements were suggested and carried out in the laboratory (section 7.5). The new laboratory set-up was used to collect water level information for a range of scenarios. The DIVAST-SG model was set-up to model these scenarios and predict the water levels in the foam. Modification to the input file to include representations of the joints between the foam blocks allowed a good fit between the observed and modelled water levels. The lack of an unsaturated flow model in the numerical model could account for some of the differences between the model and the observed behaviour. Tracer experiments were then carried out using Rhodamine-WT dye as in the initial experiments. Using the DIVAST-SG model that most accurately modelled the water levels, the tracer experiments were also modelled. Tracer proved difficult to measure in the foam boreholes for a variety of possible reasons (section 7.8.5) but the results that were obtained agreed well with the model. Encouraging correlation was observed between the observed exit point of the tracer from the foam, and the modelled exit point and time.

CHAPTER 8 VISUAL MODFLOW – MODELLING CARDIFF BAY

8.1 *Cardiff Bay Background and Geology*

Cardiff Bay (previously known as Tiger Bay) was, until November 1999, a tidal estuary through which the rivers Taff and Ely flowed into the Bristol Channel. When Cardiff Bay Development Corporation was given the task of making Cardiff ‘Europe’s most exciting waterfront city’, a vital part of their scheme was the impounding of the bay to form a permanent freshwater lake to replace the mudflats, and creating a desirable waterfront. The proposed scheme at the time naturally raised concerns among residents living around the bay. The proposed barrage was planned to artificially raise the water level in the Bay, more or less permanently, to 4.2m elevation above mean sea level. Previously most of the bay was mudflats for approximately 50% of the tidal cycle. With the barrage this situation would change and result in a permanently flooded freshwater lagoon.

When the barrage was proposed, local residents and several environmental groups were concerned about a number of issues, including the fact that by permanently raising the water level in the bay this could result in a permanent rise in the groundwater levels, thereby potentially flooding properties around the Bay, and creating what was termed an ‘urban swamp’ scenario. Cardiff Bay Development Corporation were statutorily required to investigate the groundwater conditions and show that they could be managed effectively if the barrage were to proceed. Thus, an extensive monitoring programme was set-up and groundwater levels were monitored both pre- and post-impoundment (since June 1995). Figure 8.1 shows the conceptual pre-impoundment hydrogeology of the area from the south-west to the north-east.

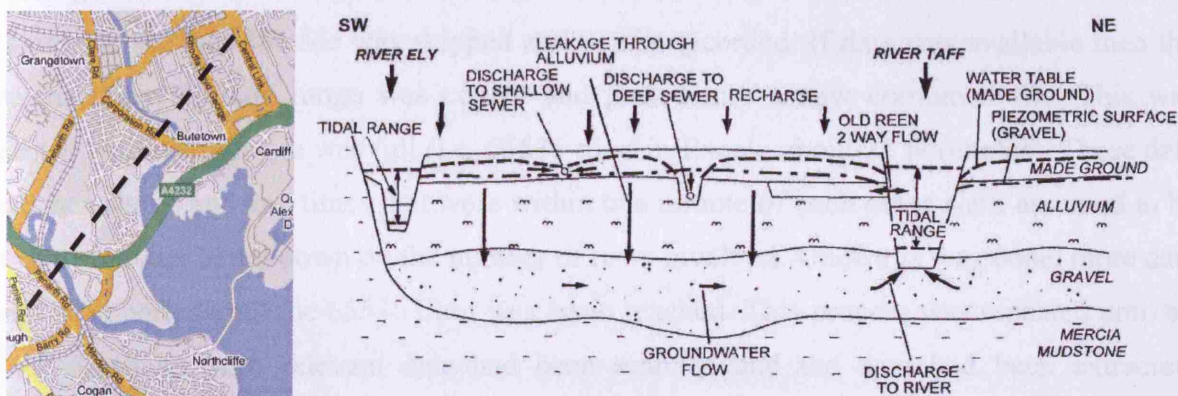


Figure 8.1: - Conceptual preimpoundment hydro-geology in Cardiff Bay area. Cross-section shown by dashed line on map. (Map from Google Maps, geology from Heathcote et al. 2003)

The monitoring programme was set-up primarily to monitor the groundwater levels in the made ground, as this is where flooding would potentially occur. However, many of the boreholes penetrate through to the gravels. This gravel aquifer is of most relevance to this study, as it exhibits a clear tidal response from connection to the surface waters in the Taff and Cardiff Bay. This data-set is almost unprecedented in its size and detail, and to-date has not been used for groundwater model calibration. The data covers both the pre-impoundment and post-impoundment period, however, after impoundment of the Bay in November 1999, the tidal fluctuations in the gravel ceased, since Cardiff Bay and the Taff were no longer subject to tidal fluctuations. For this reason it was decided to focus on only two months of the data, i.e. for a wet and a dry scenario. January and July 1999 were chosen as relatively complete data periods prior to impoundment. However, in the event, only the July 1999 was fully prepared as the amount of preparation time needed for each month was prohibitive.

8.2 Preparing the Data

The groundwater monitoring data were stored in a fairly rudimentary format in '.csv' files (comma separated variables) by Cardiff Harbour Authority. Each borehole was logged in its own directory, with records taken every 15 mins since 1995. Most of the records were not complete, with there being various gaps in the data due to equipment failure and scheduled maintenance. In total there was approximately 1.5GB of raw water level data stored in text files. The raw data can be found on the Appendix CD^a.

The first task was to convert all of the .csv files to simple text files so they could be developed further. All the borehole data was put into one folder and in separate text files for each borehole. A macro was then written in Excel to load each file in turn and look for data

^a Raw data stored in a zip file: D:\Cardiff Bay Borehole Data\original borehole data.zip

matching a certain time range (i.e. 1st July 1999 to 31st July 1999). If no data was found for this time period then the file was skipped and details recorded. If data was available then the data matching the date range was copied and pasted into a new combined file. This was repeated until the new file was full (i.e. 65536 rows in Excel– about 22 boreholes). These data were then sorted and any times that were within one minute of each other were assumed to be the same in order to cut down on the number of rows involved. Once this was done, more data could be imported until the 65536 limit was again reached. This process was repeated until all of the boreholes with relevant data had been scanned and the data had been extracted. Boreholes not penetrating through to the gravel were removed from the database.

This resulted in a spreadsheet, sorted according to time, with data for all of the available boreholes for July 1999. The data for each borehole were collected at 15 minute intervals, but the exact time of data collection varied widely (e.g. for one borehole data were taken at 21:12, 21:27, 21:42 and 21:57, while for another the data were taken at 21:07, 21:22, 21:37 and 21:52). This resulted in a non-continuous data series with gaps making it difficult to plot and use the data in models. To complete the data preparation these gaps were linearly interpolated for each borehole, at 2 min (0.00139 days) intervals, resulting in a spreadsheet that gives the estimated water level in *any* borehole at *any* time. This database can be found on the Appendix CD^a. The data was then used for visualisation and graphs, with times being extracted at regular intervals for use in boundary conditions for numerical modelling. The most tidally influenced borehole only moves by approximately 4 cm over 48 mins (0.0333 days), so this interval was considered appropriate as the 15min interval data set was unmanageably large.

The gravel database for July 1999 was used to create a Tecplot file to visualise the distribution of the groundwater. The groundwater heads could be animated to show the movement of the groundwater. This made it relatively easy to spot discrepancies in the data, e.g. boreholes out of synchronisation with the majority of the tidal responses, or boreholes close to each other with vastly differing water levels. There were 6-7 of these boreholes that needed to be removed from the dataset, and for one borehole the data initially appeared satisfactory, but then a 6 hour delay appeared in the data making the tidal response out of synchronisation with the other boreholes. The visualisation was invaluable in filtering out

^a Database filename D:\Cardiff Bay Borehole Data\Cardiff - Groundwater level in Gravels - July 1999.xls

these incorrect data points. After this process was completed the dataset containing data from the remaining boreholes was stored. The final animation is on the Appendix CD^a, and it is recommended to view this to get an idea of how the groundwater in Cardiff Bay behaves. Figure 8.2 and Figure 8.3 show the visualisation at high and low tide.

It can be seen from the visualisation that there was a significant change in the groundwater levels near the river Taff over the tidal cycle, but with the majority of the aquifer remaining undisturbed. The river Ely did not seem to affect the gravel aquifer very much – with this finding being consistent with the schematic illustration in Figure 8.1, where the Ely does not cut through to the gravel aquifer. However, the area close to the Taff (i.e. from the mouth of the Taff, through Grangetown and Riverside, and approximately up to Cardiff Castle and Bute Park) provided an excellent dataset for use in modelling the groundwater–surface water interactions.

^a Animation filename: D:\Cardiff Bay Borehole Data\Cardiff Bay groundwater elevations animation.avi

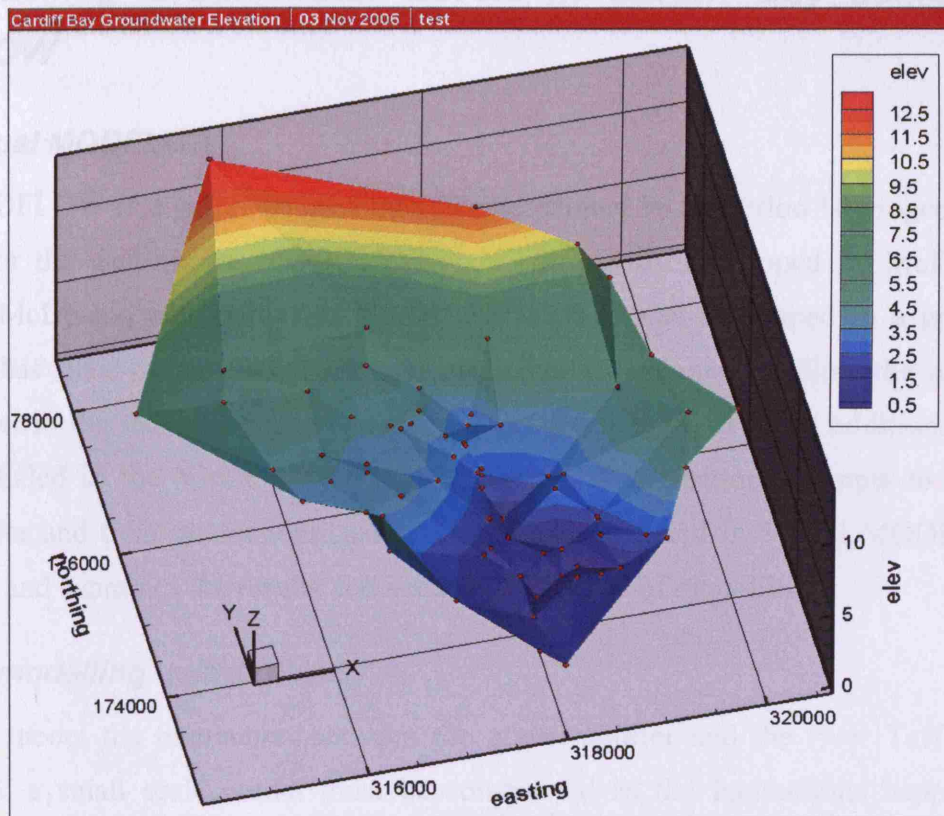


Figure 8.2: - Groundwater elevation in Gravel aquifer, Cardiff Bay area (low tide)

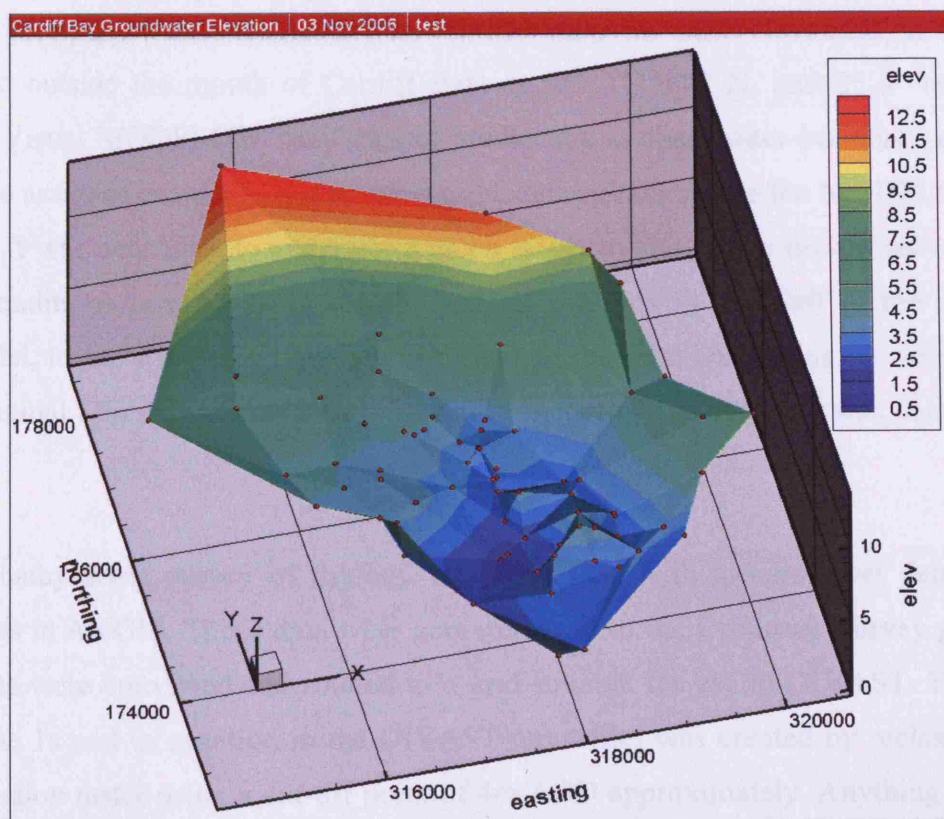


Figure 8.3: - Groundwater elevation in gravel aquifer, Cardiff Bay area, (high tide).

8.3 Modelling Groundwater Levels in Cardiff Bay using Visual MODFLOW

8.3.1 Visual MODFLOW

Visual MODFLOW is a graphical user interface developed by Waterloo Hydrogeologic, as a front end for the well-known MODFLOW code - originally developed by McDonald and Harbaugh (McDonald and Harbaugh 1988). MODFLOW was developed as a groundwater model, but has since been updated with several modules designed to allow the inclusion of surface water in the modelling (see Chapter 2). However, most of these additional modules are not included in the Visual MODFLOW software. This section attempts to model the gravel aquifer and tidal interactions, using the features included in Visual MODFLOW 2.8 (v2.8.2.50), and examines the results and accuracy, and ease of modelling.

8.3.2 Premodelling using DIVAST

In order to model the interaction between the gravel aquifer and the river Taff in Visual MODFLOW a small scale model must be constructed as the interactions happen over a relatively small area. Boundary conditions must be defined carefully for such a small scale model, but the only available boundary conditions were the tidal elevations in the Bristol Channel just outside the mouth of Cardiff Bay, at 51° 27' 44'' N, and 3° 8' 16'' W, see Figure 8.4. Visual MODFLOW itself cannot predict the surface water boundary conditions, they must be assigned manually and so need to be determined before the MODFLOW model can be run. It was necessary to construct a much larger model of the entire bay using these boundary conditions in order to obtain the water elevations in the Taff in the area of the smaller model, to see what effect the bay itself had on the tidal conditions. To undertake this task, the original DIVAST model was used and a model of Cardiff Bay was constructed as follows.

A detailed bathymetric survey of the bay was combined with ground level data from the borehole logs in ArcGIS. These data were georeferenced to the Ordnance Survey grid. Using GIS, the data were converted and rotated to a grid suitable for use in DIVAST. The domain input (i.e. the 1s and 0s notation in the DIVAST input file) was created by reclassifying the surface elevation raster using a cut-off point of 4m AOD approximately. Anything below this height was classified as potentially wet. The data were also rectified to a new horizontal resolution of 17m. This grid size was chosen to allow the river Taff to be more than one cell

wide, to prevent ‘bottlenecks’. The domain and depths were exported into text files, and used to construct the input file for DIVAST. Since the 2-D DIVAST-SG code does not allow flooding and drying (as the groundwater/surface water interface is assumed to be vertical), then the older version of DIVAST was used for this model study so that the tidal propagation could be modelled with the inclusion of flooding and drying.

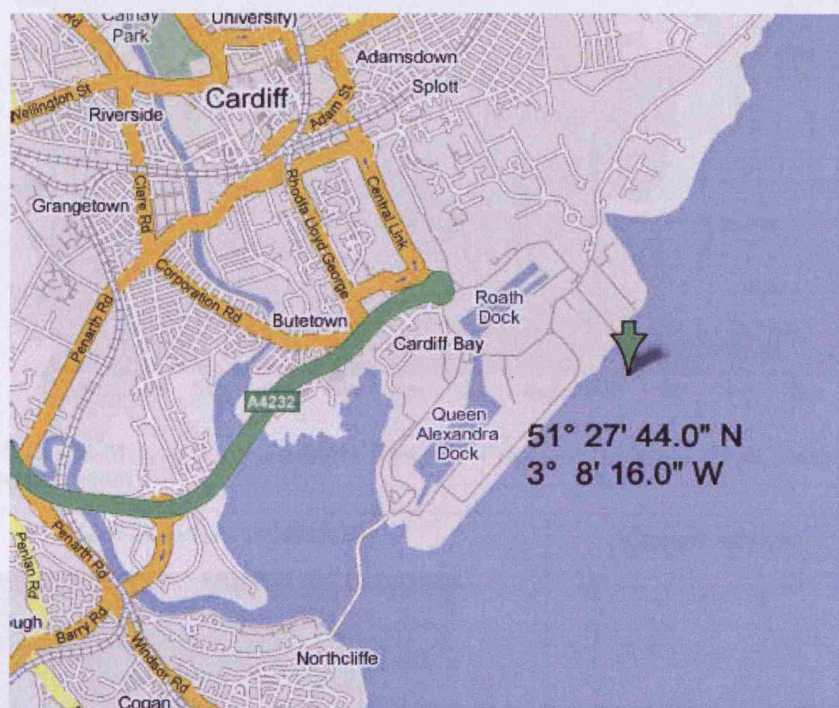


Figure 8.4: - Location of tidal data. (source: Google Maps)

A flow of $9 \text{ m}^3/\text{s}$ was used as the upstream boundary of the Taff, based on data from the National River Flow Archive (NRFA 2006). Figure 8.5 shows the maximum and minimum daily flows for the period 1965-1972 for the Taff at Tongwynlais, which is the closest gauging station to the bay, approximately 7 miles upstream. The flow in July was relatively low compared to that for the rest of the year, and from the figure $9 \text{ m}^3/\text{s}$ seemed an appropriate value to use for early July.

After running the model it was apparent that, even at this fine grid resolution, ‘bottlenecks’ occurred in the river Taff, effectively adding weirs to the river (in the model) and raising the upstream water elevation. The available bay bathymetry did not extend far up the river, and no cross-section or depth data were available for this stretch of the river, i.e. immediately preceding the mouth. Hence, model data were collected at the mouth of the Taff, just upstream of the road fly-over (A4323) (Figure 8.4).

An animation of the DIVAST model of Cardiff Bay can be found on the Appendix CD^a, and a screen shot is shown in Figure 8.6. The model itself can be found on the Appendix CD^{b,c} as well.

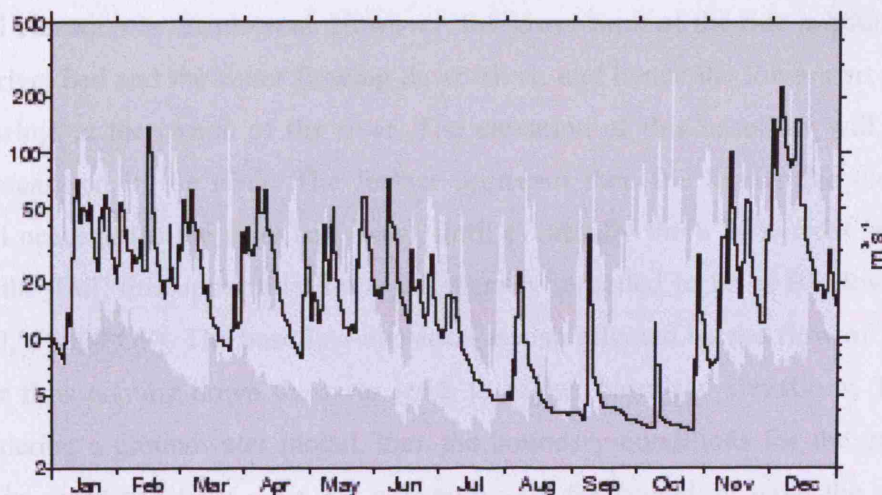


Figure 8.5: - Max. and Min. daily mean flows from 1965 to 1972 for the Taff at Tongwynlais (1972 in bold). (Source NRFA 2006)

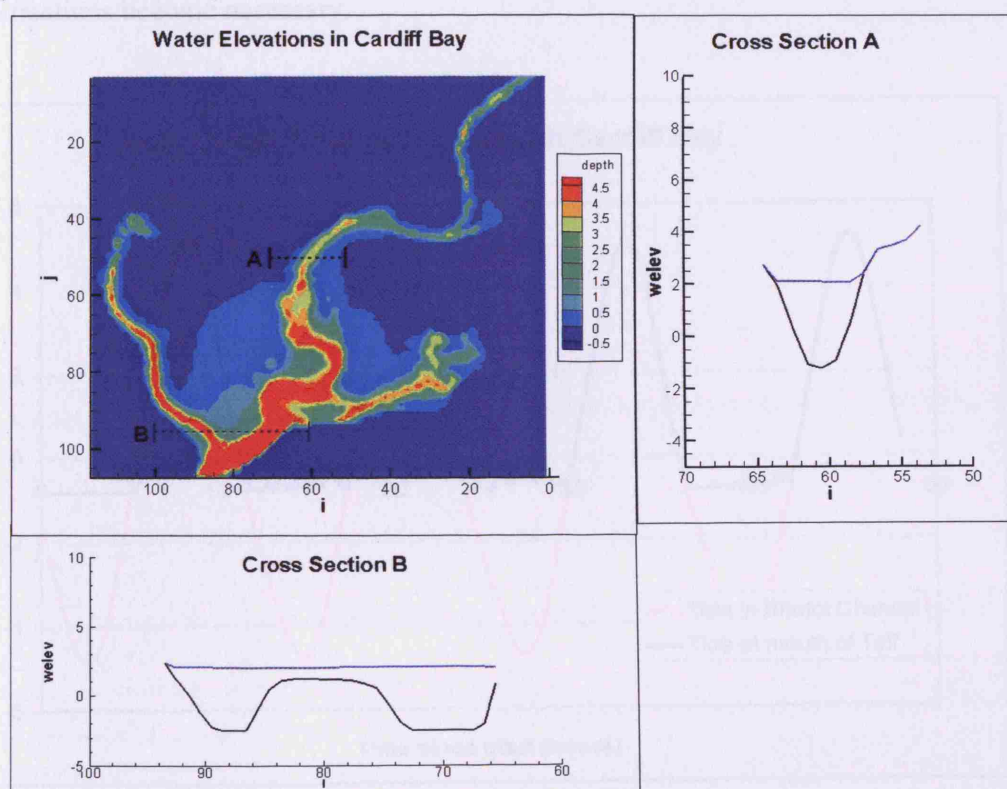


Figure 8.6: - DIVAST model of Cardiff Bay showing cross-sections and water levels at mid-tide

^a Animation: D:\ DIVAST Cardiff Bay Tidal Model\Cardiff Bay Tidal Animation.avi

^b Model exe file: D:\ DIVAST Cardiff Bay Tidal Model\Old Divast.exe

^c Model input file: D:\ DIVAST Cardiff Bay Tidal Model\cdfbay.dat

Figure 8.7 shows the tide in the Bristol Channel, compared with the mouth of the river Taff. As can be seen, no significant delay is present in the water elevation at the mouth of the Taff from the tidal elevation in the channel. However, the lower limit of the tide is bounded by the depth of the river bed and the water flowing down-river, and hence the lower part of the tidal cycle is 'missing' at the mouth of the river. The elevation of this baseflow will depend on where it is measured in the river. The further upstream then the higher the elevation the baseflow will occur at (as the river bed rises), until eventually there is no tidal influence on the river. In the Taff, this upper tidal limit is generally regarded to be at Blackweir in Bute Park (317000,178000 OS). The baseflow elevation is also affected by the flow of the river in that a greater flow coming down the river leads to higher baseflow elevations. This means that, if considering a groundwater model, then the boundary conditions for the groundwater are variable in space and time – i.e. no two points on the boundary have the exact same boundary conditions. This makes the Visual MODFLOW model hard to set up and simplifications become necessary.

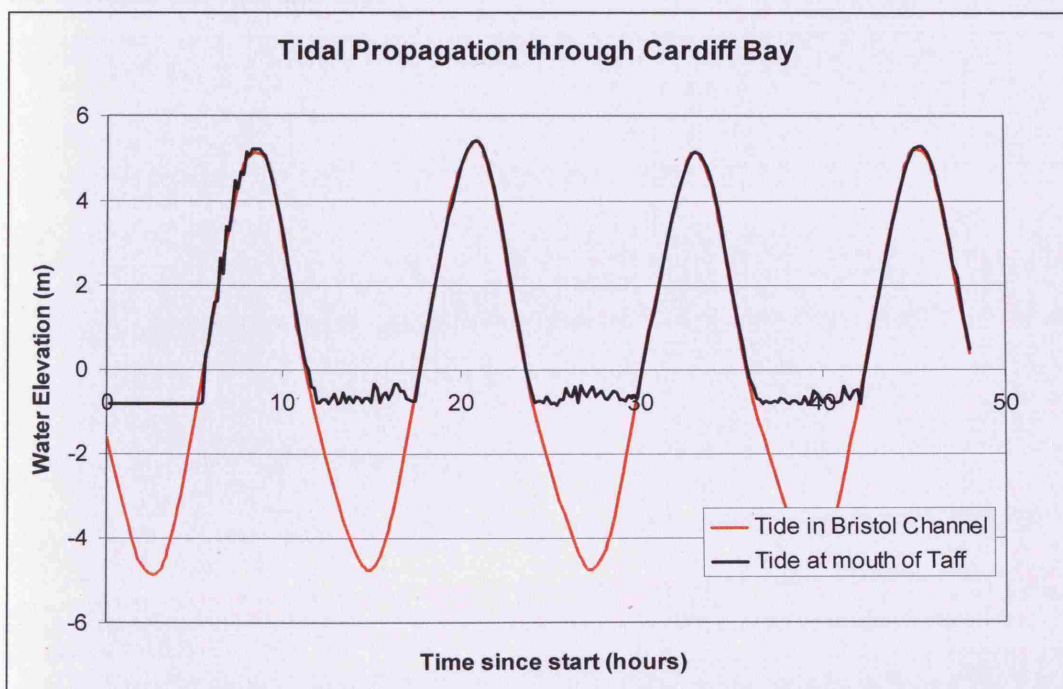


Figure 8.7: - Tidal propagation through Cardiff Bay

8.3.3 Setting up Visual MODFLOW

Once data from DIVAST had shown that the tidal times at the mouth of the Taff were identical to the known data for the Bristol channel, the model area was defined as in Figure 8.8. A 50m grid was used as compared with the 200m grid in Heathcote et al (2003), in order to give a good spatial resolution. The Heathcote grid was considered ‘relatively fine’, so a 50m grid should perhaps be a ‘very fine’ grid, although computing power permits much finer grids now.

Northern and Western Boundaries

The northern and western boundaries of the model area were considered to be constant head boundaries. Values were taken from the observed borehole heads (triangulated using Tecplot) and input into Visual MODFLOW. Where the heads along the boundary were not constant (e.g. the southern end of the western boundary, where the tides in the river and bay affect the groundwater heads), then the boundary was positioned midway between the Taff and Ely rivers, and perpendicular to the nearest tidal source. This portion of the boundary was treated as a no-flow boundary, i.e. it was assumed that this was the position of the groundwater divide between the Taff and Ely.

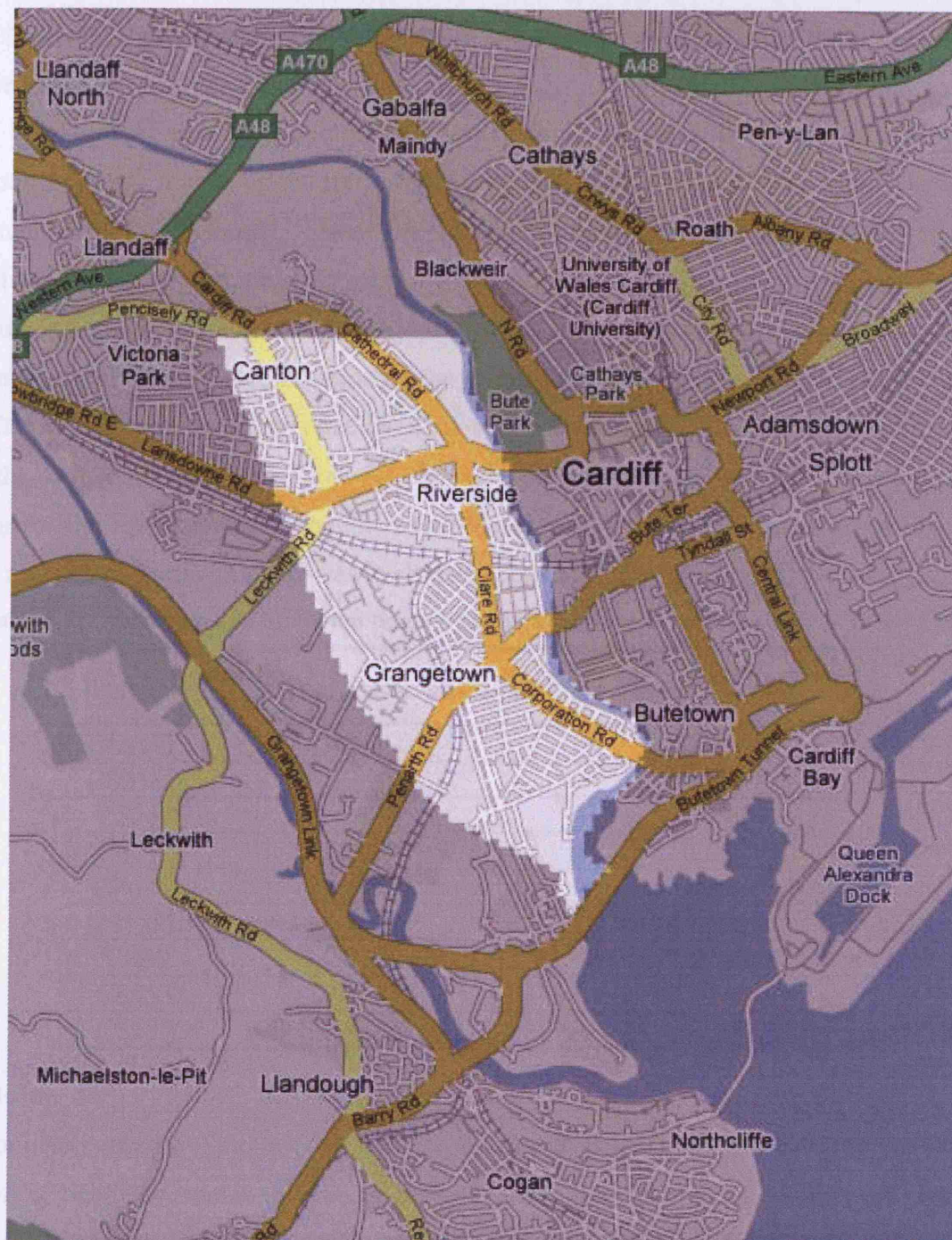


Figure 8.8: - Model Area

River Boundary

Because the tidal influence gradually decreases further away from the bay, the river boundary conditions were hard to define. Since Visual MODFLOW is primarily a groundwater modelling code it does not have the capability of modelling surface water elevations in a river. The model is concerned with groundwater flow only, and all the surface water elevations (boundary conditions) must be specified manually. The basic MODFLOW code

itself has several surface water modules written subsequently (see Chapter 2) but these are not included in Visual MODFLOW, which is the version used here. In the scenario being modelled the tide propagated up the river with a slight delay, and as the river bed rises, the lowest elevation of the tidal cycle rises accordingly, so these boundary variations vary continuously as one moves up the river. It is impossible to include this continuous variation in the Visual MODFLOW model; instead, the boundary conditions must be added in sections to allow them to vary up the river.

Extrapolating from the bay bathymetry and from the observed groundwater elevations adjacent to the river, an approximation of the minimum tidal elevation at various parts of the river Taff was arrived at, using ArcGIS. This was used to cut-off the tidal range in sections along the Taff. Figure 8.9 and Table 8.1 show the sections used. The approximate minimum tidal value was found for each section using the closest boreholes. This process involved a certain amount of guesswork and was fairly time-consuming.

Table 8.1: - Maximum and Minimum tidal elevations at various boreholes adjacent to the Taff.

Borehole	Max Water Elevation (m)	Min Water Elevation (m)
CS317L	3.060	0.021
CS238A	3.850	0.307
CS251	3.880	0.770
CS217	3.570	0.867
CP6AL	3.560	1.590
CS158L	2.540	2.295
5/PB2	2.520	2.380
CS093	4.500	3.140
CS107	4.380	4.300

Boreholes

Each borehole used in the model had its observed data imported into the model. The monitoring depth or screen elevation (absent from borehole data, aside from formation identity i.e. gravel, alluvium or made ground) was taken to be an elevation within the gravel aquifer, near the base for each borehole. This depth was found by visual inspection of the layers in Visual MODFLOW.

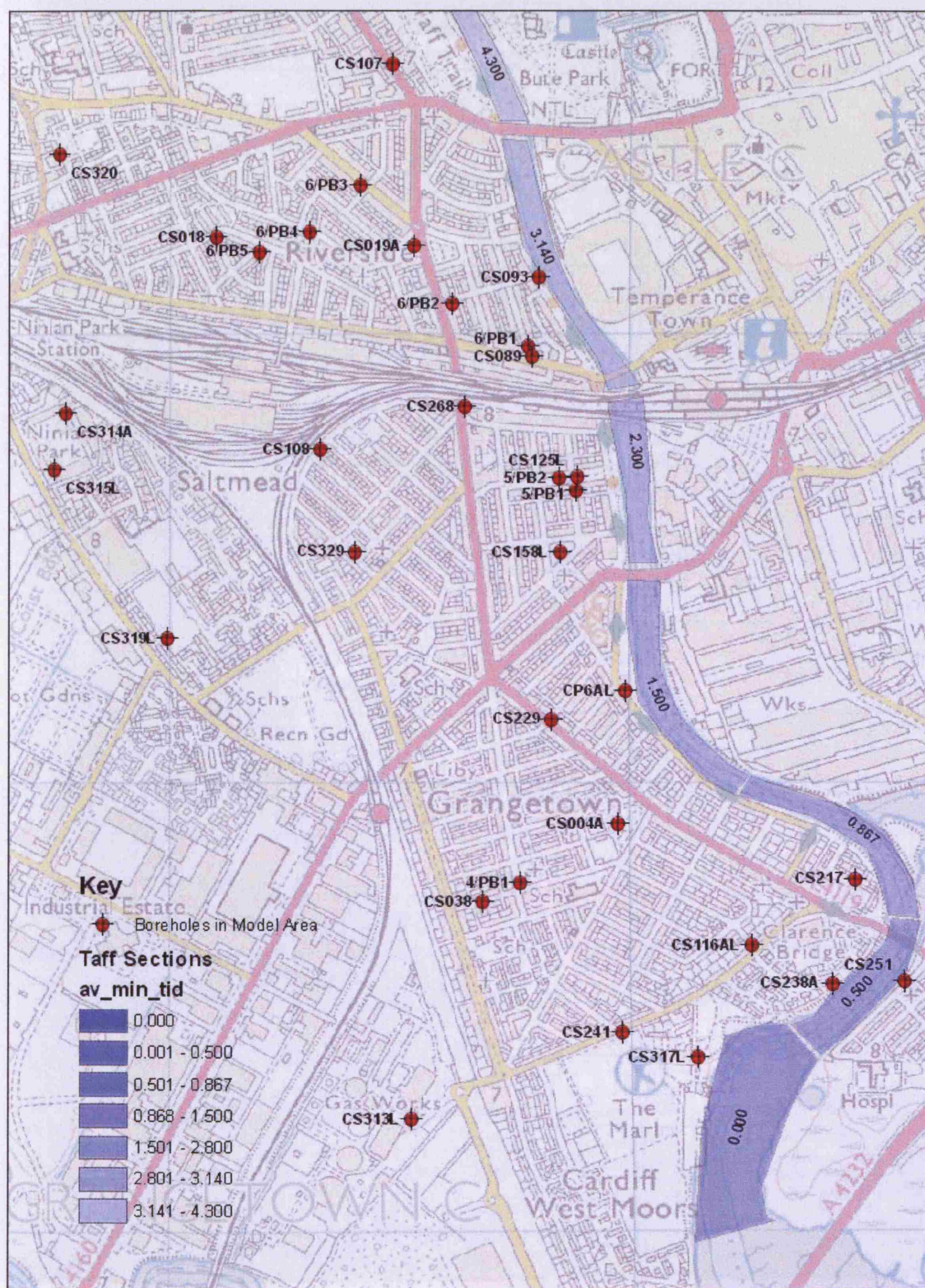


Figure 8.9: - Boreholes in model area, and sections of Taff with average minimum tidal elevation.



Figure 8.10: - Visual MODFLOW model showing head boundaries.

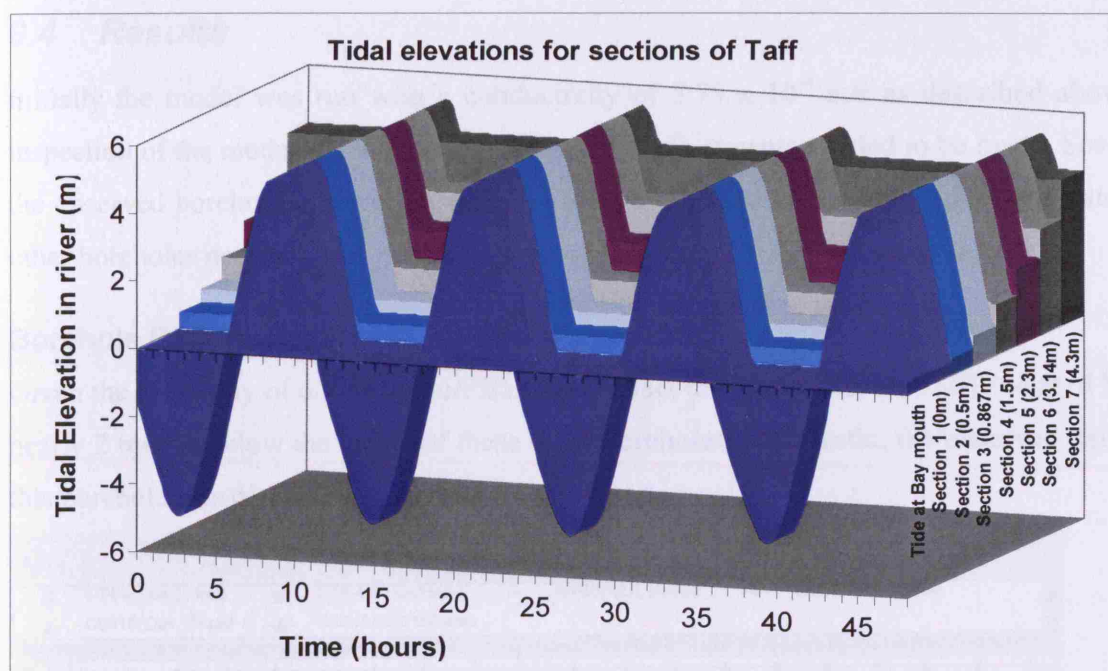


Figure 8.11: - Tidal elevations for sections of the Taff

Conductivity

Heathcote et al (2003) found the conductivity of the gravels in the Cardiff area to be approximately 50 m/d, which converts to 5.79×10^{-4} m/s. Textbook values of porosity for gravel aquifers range from 20-40% (Freeze and Cherry 1979); a value of 25% was used for the initial run.

Initial Conditions

A steady-state model was run with the river set to a constant head of 1.5m, and the northern and western boundaries were set-up as described above. This 1.5m level was determined to be approximately the time average level of the river for the area modelled, and would give an approximation of the initial heads. This steady-state run was used for the initial conditions for the transient model.

The transient model was then set-up to run for a two day period – longer than this required too large a database for the boundary conditions. However, after two days, some of the outlying wells, not directly linked to the tidal boundary, were still changing at a constant rate, indicating that the initial conditions had not been accurately estimated. The model was run several times using output from the previous run as the new initial conditions and these outlying wells were observed. Once they stayed more or less constant over the 2 day simulation it was decided that the water levels were appropriate for use as initial heads – and subsequent model runs used results from this run for the initial heads.

8.4 Results

Initially the model was run with a conductivity of 5.79×10^{-4} m/s as described above. On inspection of the model output, it was obvious that adjustments needed to be made. Several of the observed boreholes showed results that were thought to be incorrect given the data from other boreholes nearby.

Borehole CS018

Given the proximity of 6/PB4 and 6/PB5, and the fact that the observed CS018 logged level is nearly 2 metres below the levels of these other boreholes, and erratic, the observed data from this borehole was discarded.

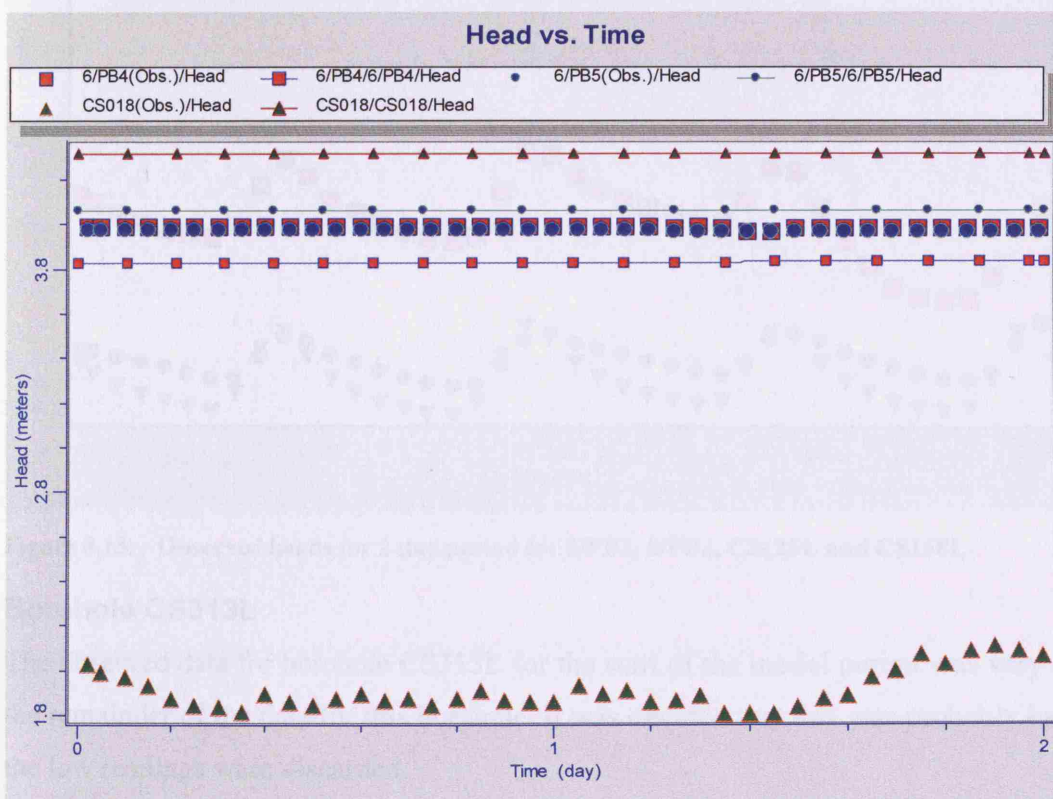


Figure 8.12: - CS018 compared to 6/PB4 and 6/PB5

Borehole cluster near 5/PB1

The three boreholes (5/PB1, 5/PB2, and CS125L) are very close to each other, and yet the observed data are at separate elevations. Borehole CS158L just a short distance away is very similar to borehole 5/PB2. Having such disparate data so close together confuses the calibration data. Hence, it was decided to use borehole 5/PB2 as the representative for the cluster of three, because it was closest in value to the next nearest borehole (CS158L). The

other boreholes (5/PB1, CS125L) were discarded. It is not clear why these boreholes should vary so much unless there was some sort of instrumental error.

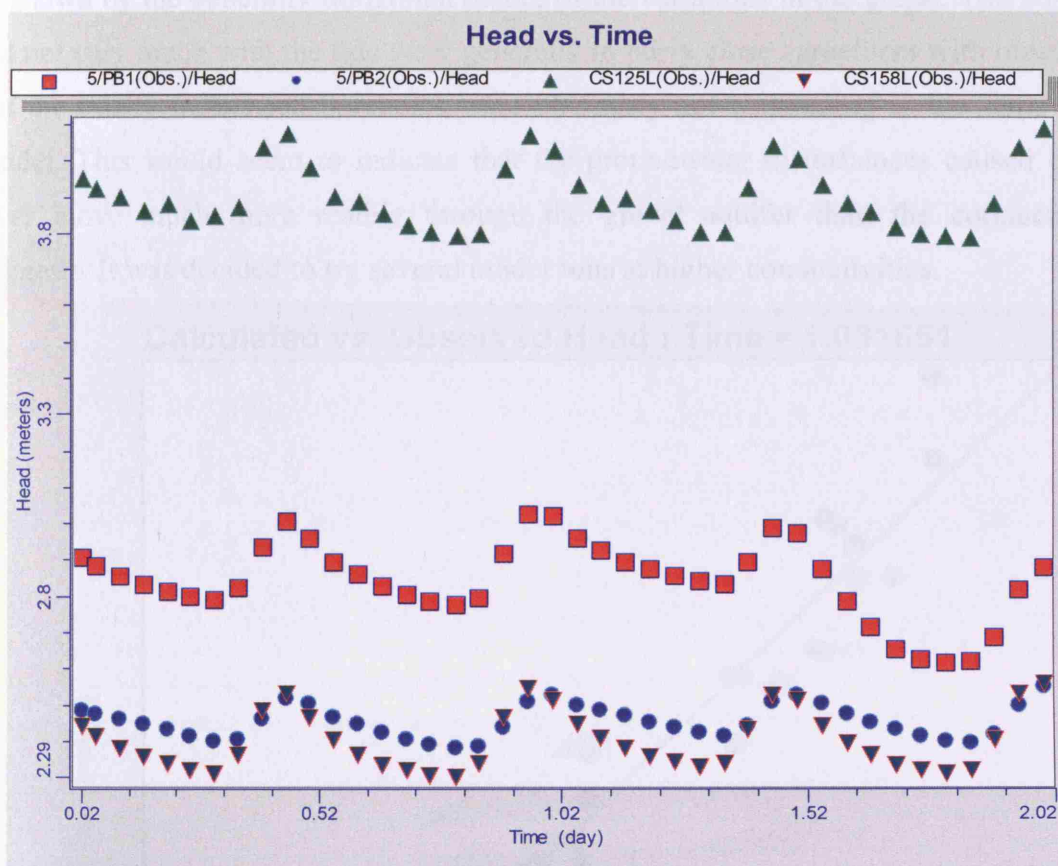


Figure 8.13: - Observed heads for 2 day period for 5/PB1, 5/PB2, CS125L and CS158L

Borehole CS313L

The observed data for borehole CS313L for the start of the model period was very different to the remainder of the data for this borehole. It was decided that this was probably bad data, and the low readings were discarded.

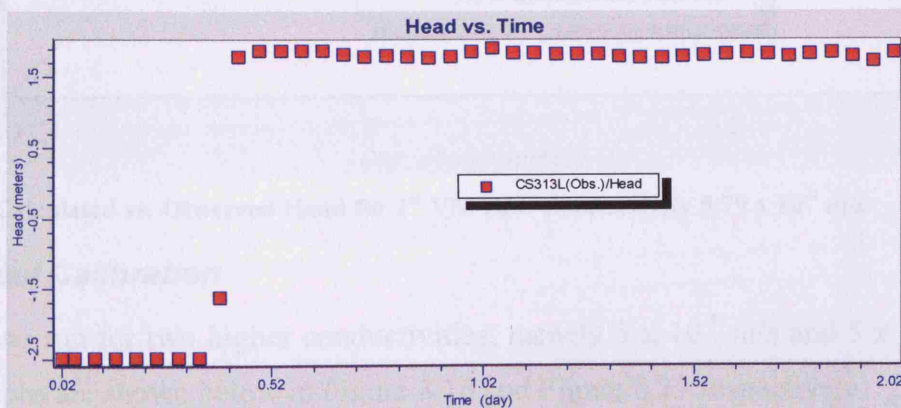


Figure 8.14: - Bad data at start of CS313L observed heads.

8.4.1 Model Run 1

Figure 8.15 shows a summary of the calculated vs. observed heads in the groundwater boreholes. It can be seen that the observed heads vary much more than the calculated heads, as shown by the generally horizontal nature of the variations in the graph. The boreholes that did not vary much with the tide were generally in fairly close agreement with observed heads, but the tidally influenced boreholes were obviously not responding in the same way in the model. This would seem to indicate that the groundwater disturbances caused by the tidal river move much more readily through the gravel aquifer than the conductivity value suggests. It was decided to try several model runs at higher conductivities.

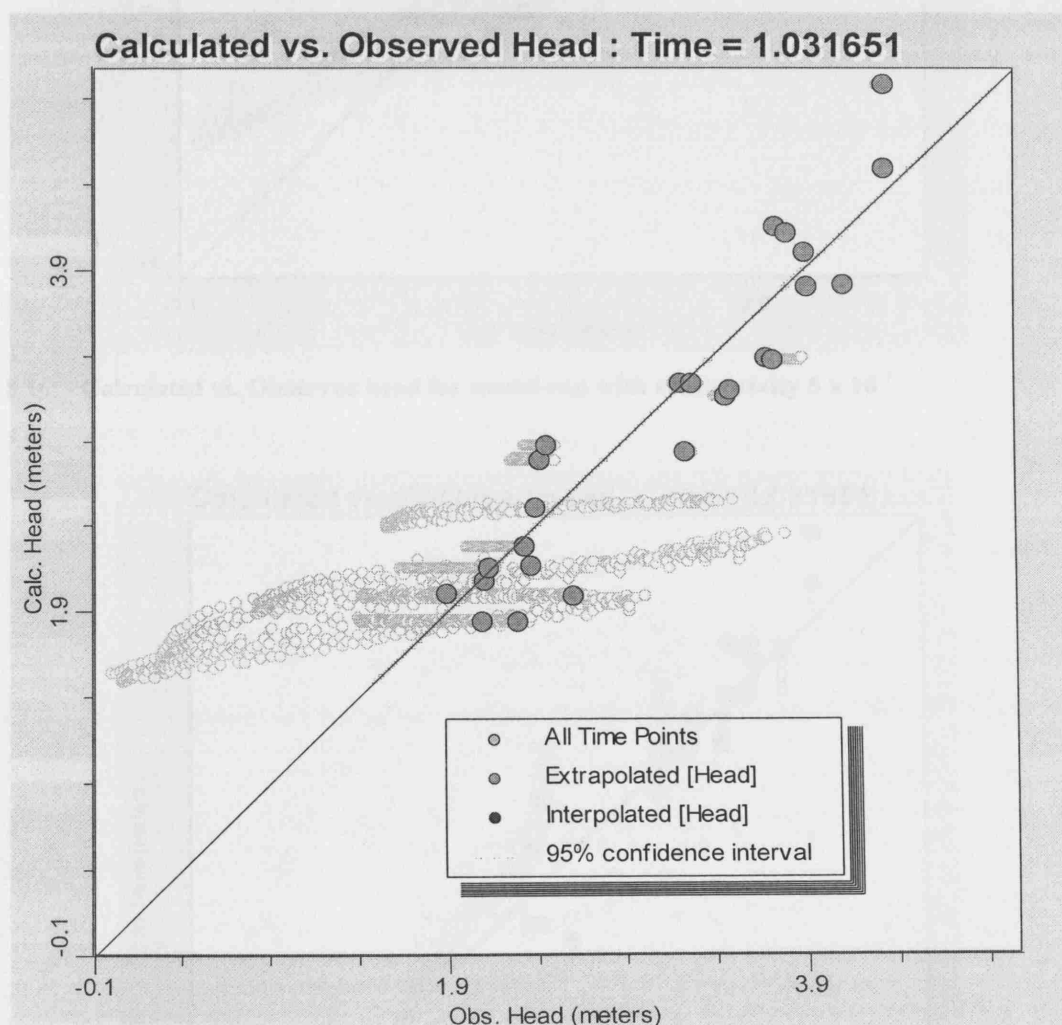


Figure 8.15: - Calculated vs. Observed Head for 1st VM run. Conductivity 5.79×10^{-4} m/s

8.4.2 Manual Calibration

The model was run for two higher conductivities, namely 5×10^{-3} m/s and 5×10^{-2} m/s. The summary graphs are shown below in Figure 8.16 and Figure 8.17 respectively.

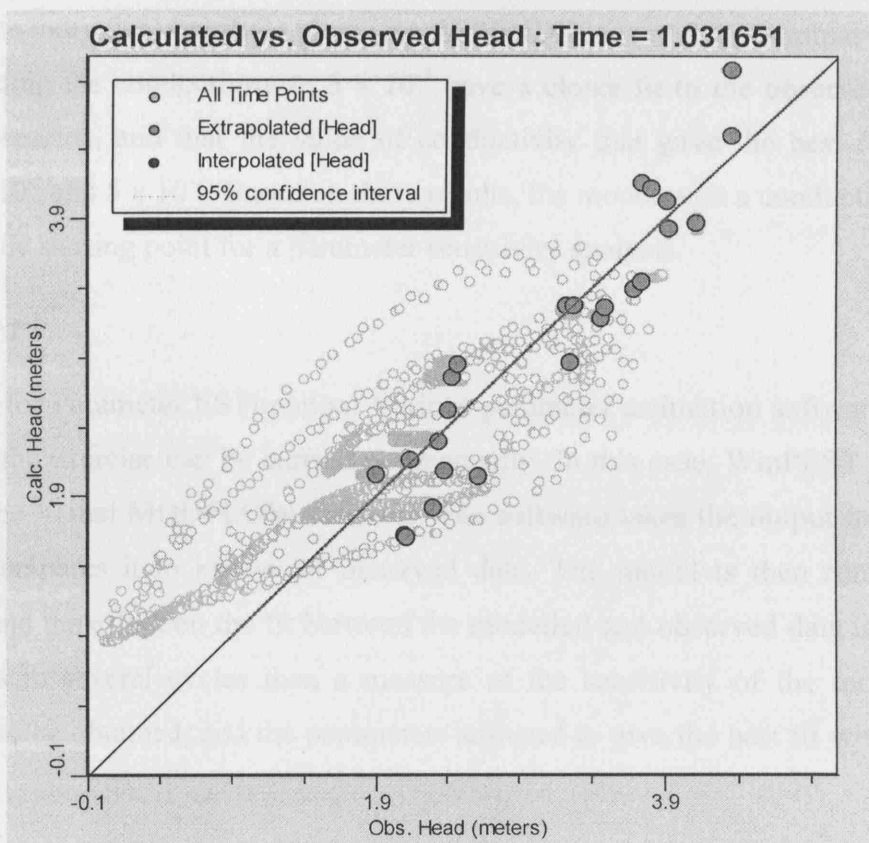


Figure 8.16: - Calculated vs. Observed head for model run with conductivity 5×10^{-3}

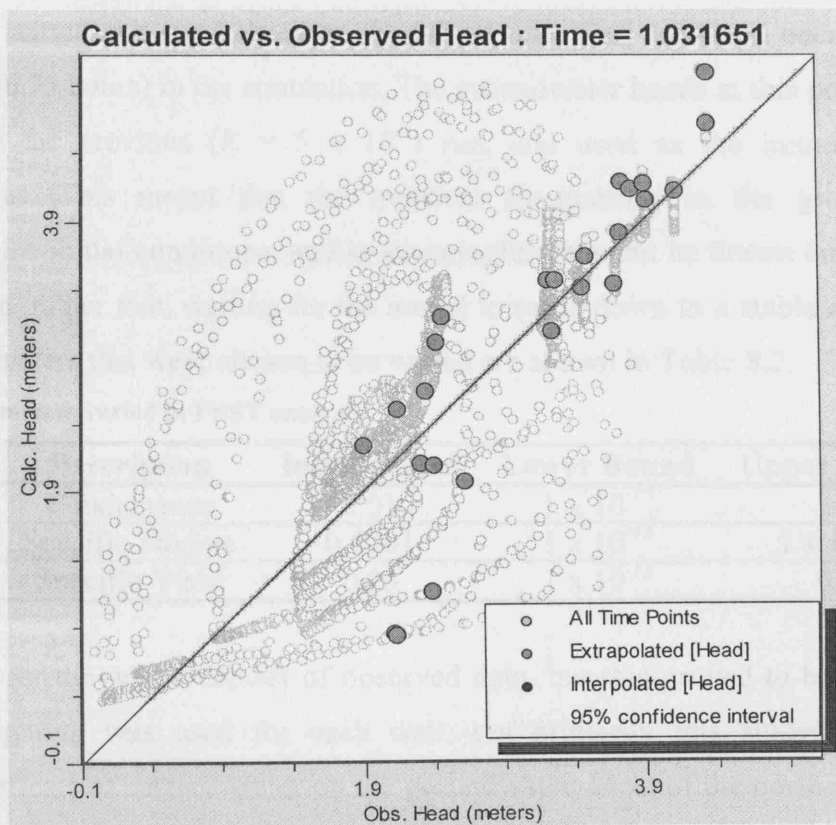


Figure 8.17: - Calculated vs. Observed head for model run with conductivity 5×10^{-2}

Looking at the individual borehole plots (see APPENDIX C) and the summary graphs, it was clear that setting the conductivity to 5×10^{-3} gave a closer fit to the observed data than the other two scenarios, and that the value of conductivity that gave the best fit probably lay between 5×10^{-3} and 5×10^{-2} . Based on these results, the model with a conductivity of 5×10^{-3} was used as the starting point for a parameter sensitivity analysis.

8.5 PEST

PEST stands for Parameter ESTimation. Various parameter estimation software packages are available, or the exercise can be carried out manually. In this case, WinPEST was used, as it is linked to the Visual MODFLOW software. The software takes the output from a computer model and compares it to known or observed data. The model is then run with changed parameters, and the effect on the fit between the modelled and observed data is measured. By repeating this in several cycles then a measure of the sensitivity of the model to various parameters can be obtained, and the parameters adjusted to give the best fit with the observed data.

8.5.1 PEST Run

The initial conditions were changed to match the start of the boundary tidal cycle. The boundary data started at a -1.61 level, on the falling tide. This condition occurred again after 1.53 days (or 36.75 hours) in the simulation. The groundwater heads at this point in time were collected from the previous ($K = 5 \times 10^{-3}$) run, and used as the initial conditions for subsequent runs. This meant that the transient fluctuations in the groundwater were represented in the initial conditions, and so meaningful data can be drawn out from all of the brief simulation, rather than waiting for the model to settle down to a stable equilibrium each time. The parameters that were chosen to be varied are shown in Table 8.2..

Table 8.2: - Parameters varied in PEST analysis

Parameter	Description	Initial Value	Lower Bound	Upper Bound
Kx (and Ky)	Conductance	0.01	1×10^{-15}	10
ss	Specific Storage	0.0001	1×10^{-15}	$1 \times 10^{+29}$
sy	Specific Yield	0.25	1×10^{-15}	0.5

PEST was run for the whole dataset of observed data, but this proved to be quite unwieldy. The same weighting was used for each well, but primarily this study was focused on predicting the effects of surface water on the groundwater. Most of the northern wells showed very little response to the tidal conditions. It was therefore decided to use just 6 wells that

show obvious tidal responses to calibrate the PEST run. The wells chosen were 4/PB1, CS116AL, CS158L, CS229, CS229, CS241, CS004A. It can be seen from Figure 8.9 that these boreholes are at a range of distances from the tidal river boundary, in the Grangetown area, but not too close to the river. This meant that the way the groundwater is propagated through the aquifer was tested, rather than simply how well the boundary conditions fitted with the close river boreholes. PEST estimated the parameters as follows, in Table 8.3. The PEST run graphs are shown in Figure 8.19.

Table 8.3: - Estimated Visual MODFLOW parameters.

Parameter	Estimated Value
Kx	0.01512
Ky	0.01512
Ss	0.0001
Sy	0.166639

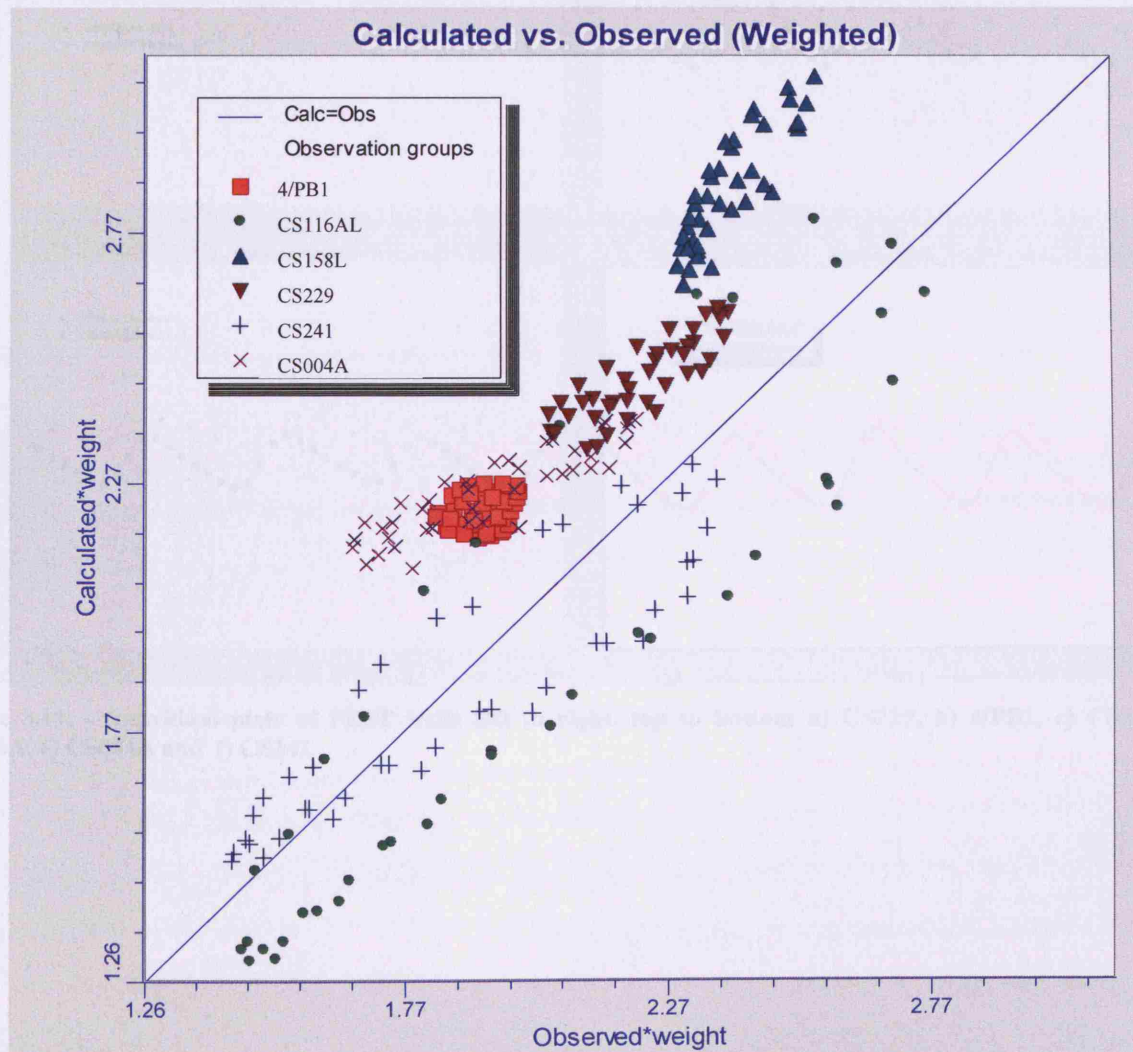


Figure 8.18: - Summary of PEST wells. Modelled heads against Observed heads.

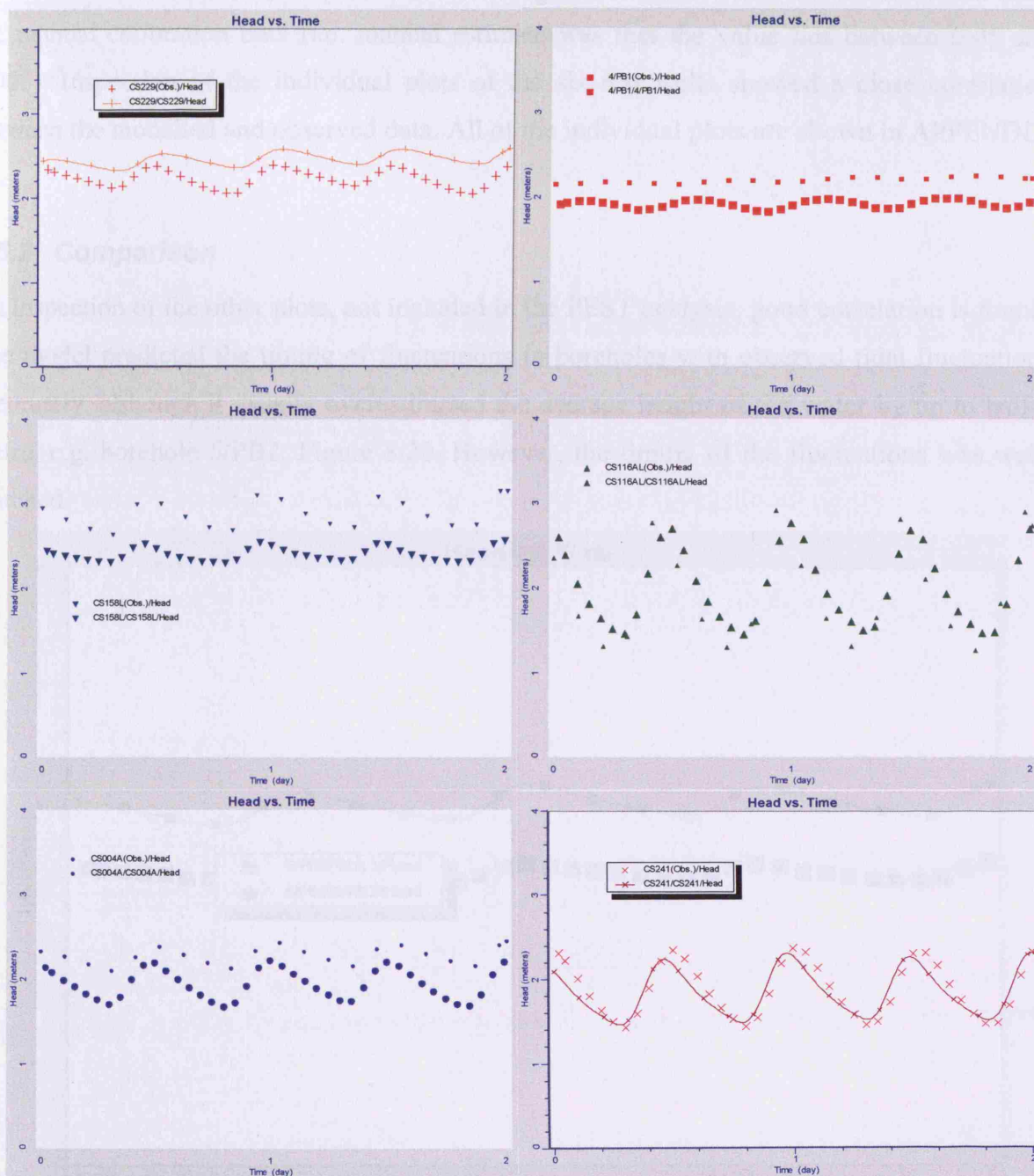


Figure 8.19: - Individual plots of PEST wells left to right, top to bottom a) CS229, b) 4/PB1, c) CS158L, d) CS116A, e) CS004A and f) CS241

The estimated conductivity value of 0.015 m/s agrees well with the conclusions drawn from the manual calibration data (i.e. manual estimate was that the value lies between 0.05 and 0.005). Inspection of the individual plots of the six test wells showed a close correlation between the modelled and observed data. All of the individual plots are shown in APPENDIX C.

8.5.2 Comparison

On inspection of the other plots, not included in the PEST analysis, good correlation is found. The model predicted the timing of fluctuations in boreholes with observed tidal fluctuations accurately, although it usually overestimated the average height of the water by up to half a metre, e.g. borehole 5/PB2, Figure 8.20. However, the timing of the fluctuations was well-matched.

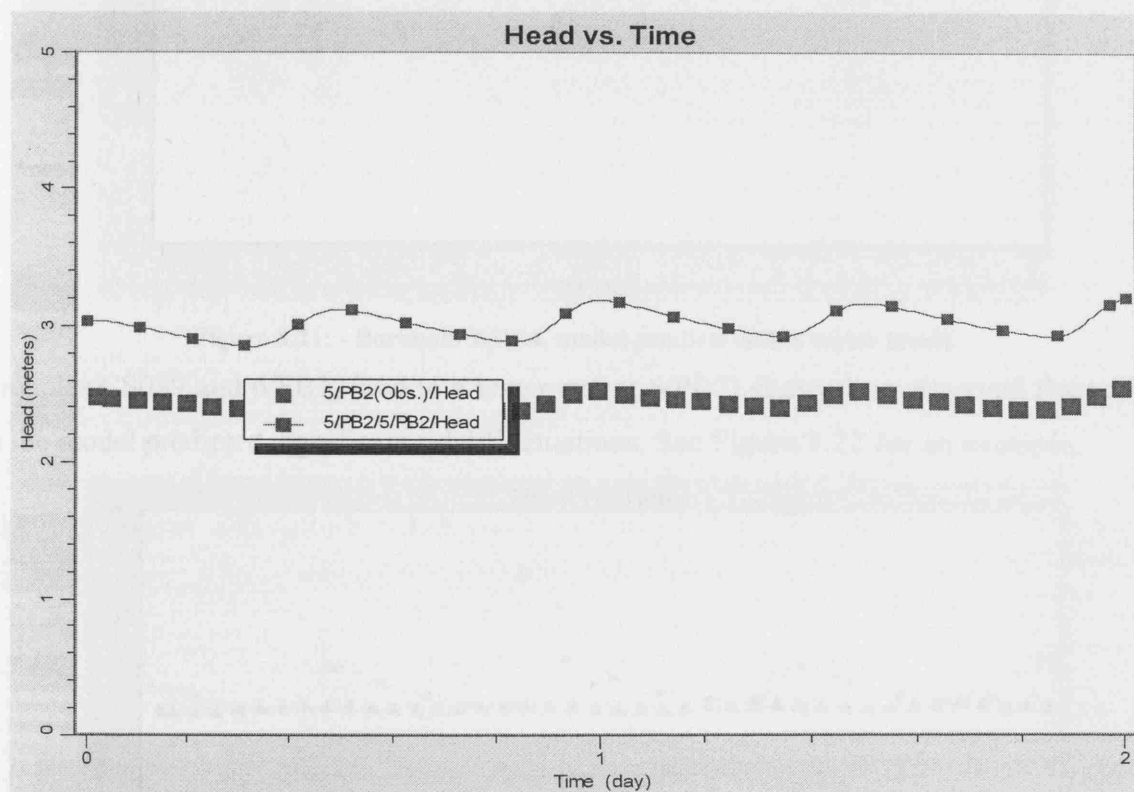


Figure 8.20: - Well 5/PB2, model predicts timing of tidal fluctuations.

In boreholes where no tidal fluctuation were observed, then the model predicts this too, e.g. boreholes CS019A, CS107, CS108, CS313L, CS314A, CS315L, CS319L, CS329, 6/PB2, 6/PB3, 6/PB4, 6/PB5. The head was overestimated slightly (approx 0.2-0.4 m) in CS107, CS314A and CS315L. Head predictions were very close to observed values in CS019A, CS108, CS313L, 6/PB2, 6/PB3, 6/PB4, 6/PB4 and 6/PB5 (illustrated in Figure 8.21). This figure shows a slight drift indicating that the model is still coming to equilibrium, however

this is small (less than 0.2m over 2 days). The equilibration period described in 8.3.3 (Initial Heads section) should perhaps have been extended for another few days of model time in order to eliminate this, but it is very slight. Heads were slightly underestimated in CS319L and CS329, by about 0.1-0.2m.

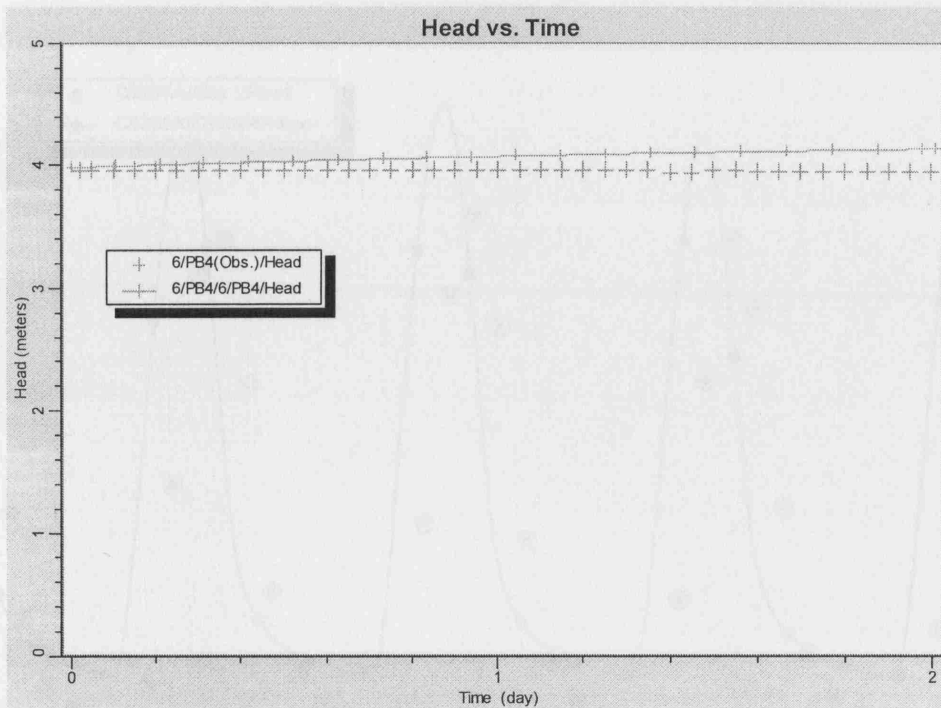


Figure 8.21: - Borehole 6/PB4, model predicts stable water levels.

Boreholes CS089 and 6/PB1, (and to a lesser extent 6/PB2) showed no observed fluctuations, but the model predicted significant tidal fluctuations. See Figure 8.22 for an example.

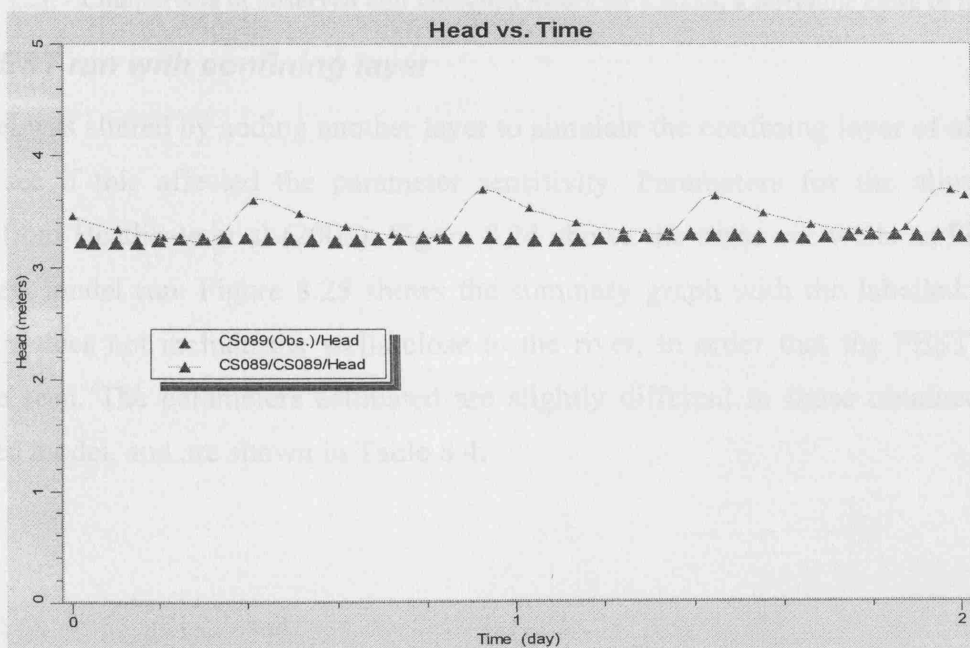


Figure 8.22: - Model predicts tidal fluctuations where none are observed.

Boreholes very close to the river showed large tidal fluctuations and the model predicted this, although it tended to slightly over-predict heads (0.1-0.3m) and anticipated the timings by 2 or 3 hours.

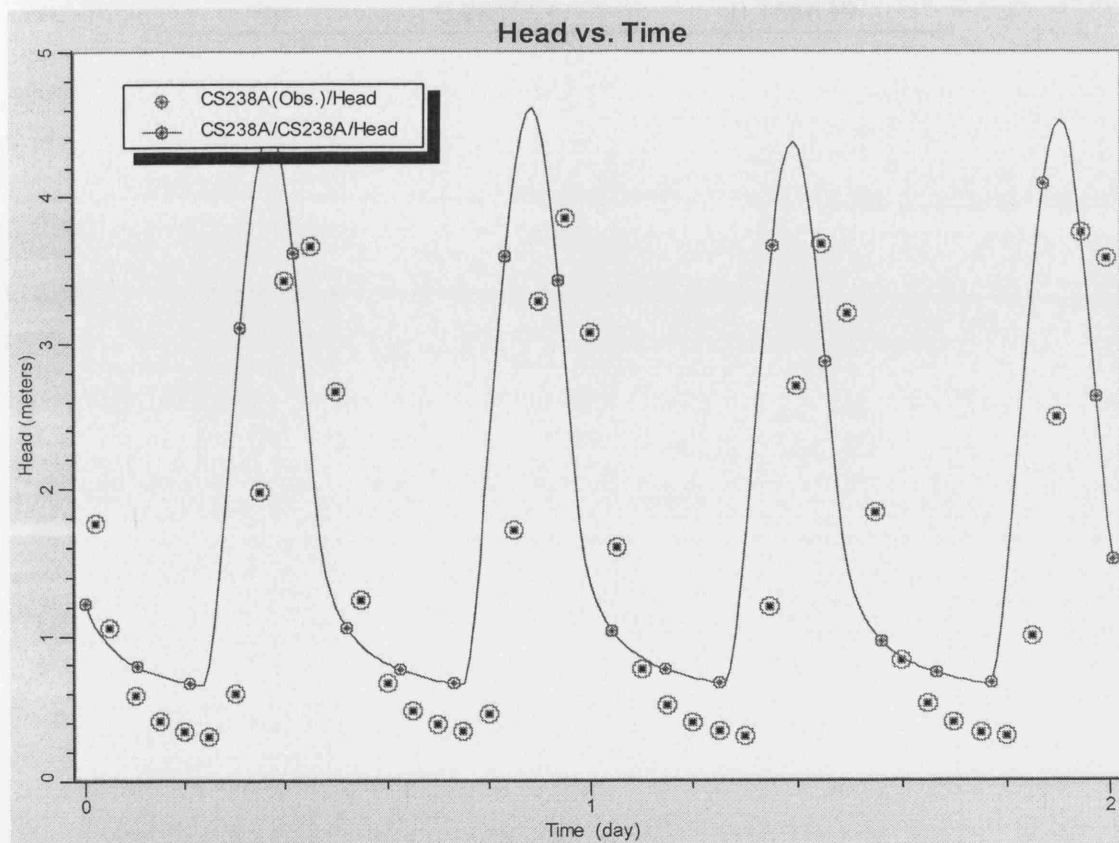


Figure 8.23: - Comparison of observed and modelled heads for CS238, a borehole close to the river.

8.5.3 PEST run with confining layer

The model was altered by adding another layer to simulate the confining layer of alluvium, in order to see if this affected the parameter sensitivity. Parameters for the alluvium were obtained from Heathcote et al (2003). Figure 8.24 shows the same six wells as Figure 8.19, for the new model run. Figure 8.25 shows the summary graph with the labelled boreholes. This figure does not include the wells close to the river, in order that the PEST wells can clearly be seen. The parameters estimated are slightly different to those obtained from the unconfined model, and are shown in Table 8.4.

Table 8.4: - Estimated Visual MODFLOW parameters using confined and unconfined model.

Parameter	Confined Aquifer	Unconfined Aquifer
Kx (m/s)	0.008319	0.01512
Ky (m/s)	0.008319	0.01512
Ss	0.009598	0.0001
Sy	0.085563	0.166639

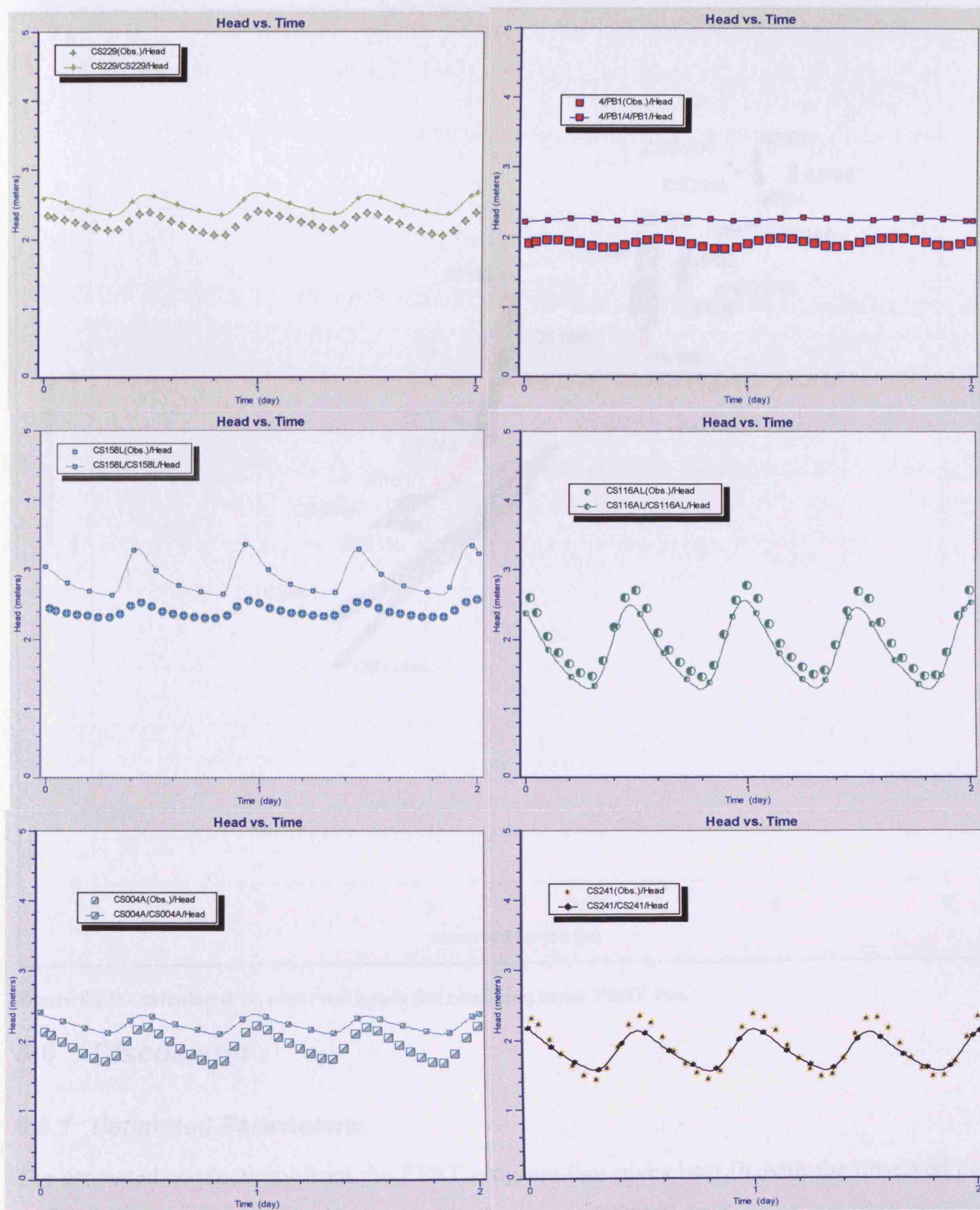


Figure 8.24: - 2-layer PEST run. Individual plots of PEST wells a) CS229, b) 4/PB1, c) CS158L, d) CS116A, e) CS004A and f) CS241

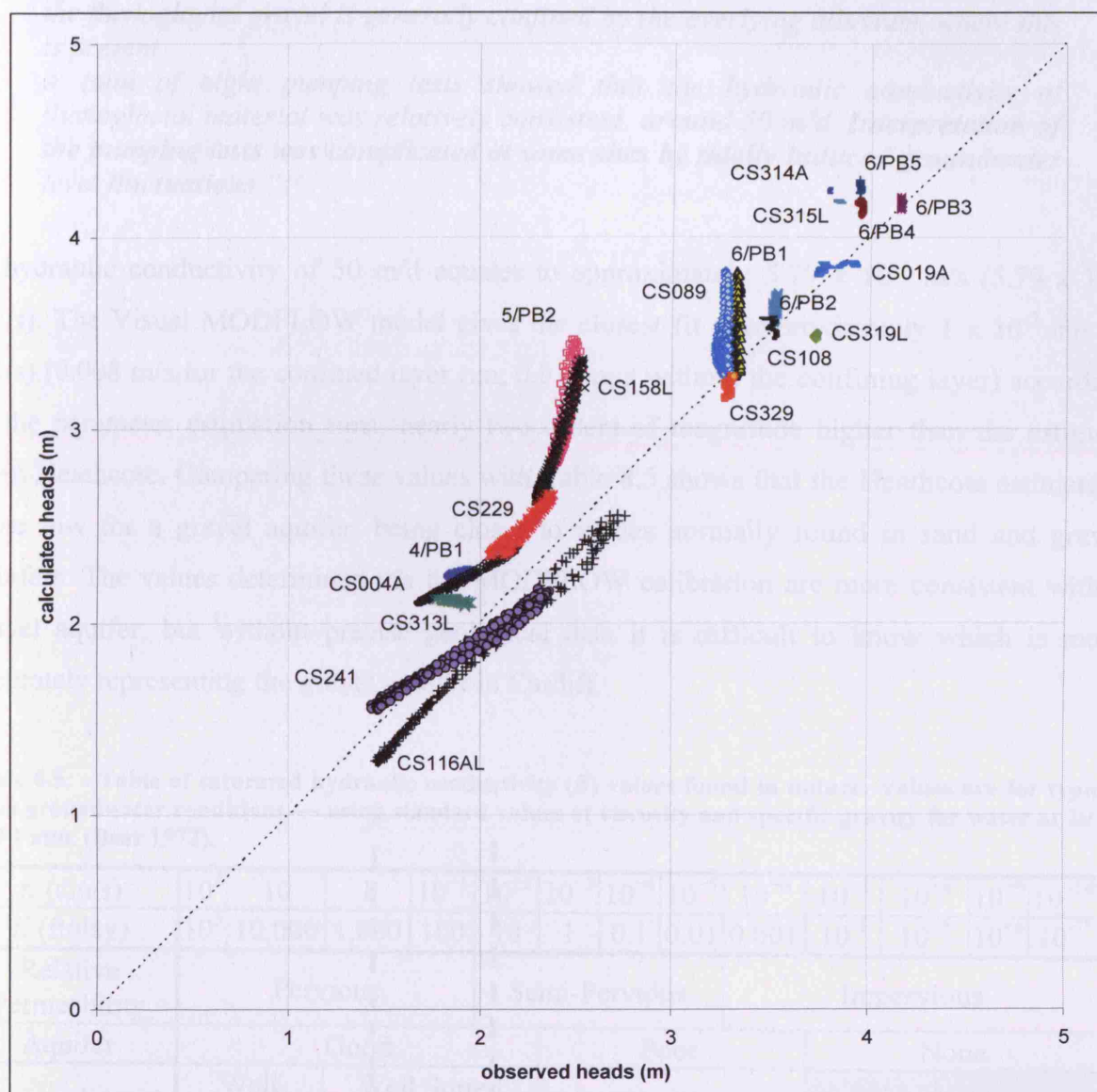


Figure 8.25: - calculated vs. observed heads for confining layer PEST run

8.6 Discussion

8.6.1 Estimated Parameters

The estimated conductivity from the PEST program that gives best fit with the observed data is different from the previous estimate. Heathcote et al (2003) performed pumping tests and stated the following (emphasis added):

“Early investigations (Edwards 1997) showed that the fluvioglacial gravels behave as an integrated aquifer with a well defined water table/piezometric surface, groundwater draining towards the River Taff and the bay. Groundwater levels in the gravel were clearly controlled by the mean elevation of water in these bodies, 0.3 m AOD in the bay, rising steadily along the River Taff. Before impoundment, water levels in the bay varied from +6.0 m AOD to -5.12 m AOD for mean spring tides. Groundwater levels in the fluvioglacial gravels showed

diurnal tidal fluctuations for up to 300m from the watercourses. Groundwater in the fluvioglacial gravel is generally confined by the overlying alluvium, where this is present.

A total of eight pumping tests showed that the hydraulic conductivity of fluvioglacial material was relatively consistent, around 50 m/d. Interpretation of the pumping tests was complicated at some sites by tidally induced groundwater level fluctuations."

A hydraulic conductivity of 50 m/d equates to approximately 5.79×10^{-4} m/s (5.79×10^{-2} cm/s). The Visual MODFLOW model gives the closest fit at approximately 1×10^{-2} m/s (1 cm/s) (0.008 m/s for the confined layer run, 0.015 m/s without the confining layer) according to the parameter estimation runs; nearly two orders of magnitude higher than the estimate from Heathcote. Comparing these values with Table 8.5 shows that the Heathcote estimate is quite low for a gravel aquifer, being closer to values normally found in sand and gravel aquifers. The values determined via the MODFLOW calibration are more consistent with a gravel aquifer, but without precise geological data it is difficult to know which is more accurately representing the gravel aquifer in Cardiff.

Table 8.5: - Table of saturated hydraulic conductivity (K) values found in nature. Values are for typical fresh groundwater conditions — using standard values of viscosity and specific gravity for water at 20°C and 1 atm. (Bear 1972).

and 1 atm. (Bear 1972).													
K (cm/s)	10^2	10	1	10^{-1}	10^{-2}	10^{-3}	10^{-4}	10^{-5}	10^{-6}	10^{-7}	10^{-8}	10^{-9}	10^{-10}
K (ft/day)	10^5	10,000	1,000	100	10	1	0.1	0.01	0.001	10^{-4}	10^{-5}	10^{-6}	10^{-7}
Relative Permeability	Pervious				Semi-Pervious				Impervious				
Aquifer	Good				Poor				None				
Unconsolidated Sand & Gravel	Well Sorted Gravel	Well Sorted Sand or Sand & Gravel		Very Fine Sand, Silt, Loess, Loam									
Unconsolidated Clay & Organic					Peat		Layered Clay		Fat / Unweathered Clay				
Consolidated Rocks	Highly Fractured Rocks				Oil Reservoir Rocks		Fresh Sandstone		Fresh Limestone, Dolomite		Fresh Granite		
MODFLOW estimate				Heathcote estimate									

However, Heathcote acknowledges that the interpretation of the pumping tests was complicated by the groundwater fluctuations. By using these same fluctuations to measure the conductivity a consistent estimate of the conductivity of the gravel aquifer has been arrived at; somewhat higher than the original estimate.

The porosity estimate using MODFLOW varies from 0.08 to 0.16. This range is quite low for a gravel aquifer, but not out of the question. Heathcote provides no estimate of the porosity of the gravel aquifer. Freeze and Cherry (1979) give a range of typical porosity values in Table 8.6. While the estimated value is below this range it is not inconceivable.

Table 8.6: - Approximate porosity values found in nature (Freeze and Cherry 1979).

	N (porosity)
Unconsolidated deposits	
Gravel	0.25 - 0.40
Sand	0.25 - 0.50
Silt	0.35 - 0.50
Clay	0.40 - 0.70
Rocks	
Fractured Basalt	0.05 - 0.50
Karst Limestone	0.05 - 0.50
Sandstone	0.05 - 0.30
Limestone, dolomite	0.00 - 0.20
Shale	0.00 - 0.10
Fractured Crystalline Rock	0.00 - 0.10
Dense Crystalline Rock	0.00 - 0.05

8.6.2 Comparing the model with field data

Generally, when the model was run using the estimated parameters the predictions showed good agreement with the observed data, although there were a few areas (highlighted in the results section) where discrepancies occur. These discrepancies are considered in turn.

Heads close to river anticipated.

The heads in the boreholes very close to the river were anticipated and slightly over-predicted. However, the shape of the fluctuation was accurately modelled, with a steep rising limb with the high tide and a rounded bottom at the low tide. Figure 8.26 and Figure 8.27 show comparisons between the observed and modelled heads with the relevant tidal boundary condition using the closest section of the river Taff. On inspection of these figures it shows that the modelled boreholes respond more quickly to the tidal boundary than the observed data. There are several possible causes for this: a) the conductivity and porosity parameters may cause the groundwater to be modelled as moving faster through the aquifer, b) the timing of the boundary condition may be earlier than in reality, or c) the grid discretisation is too coarse to allow accurate modelling over such a small gap between the borehole and the river (i.e. < 50m for some boreholes).

Possibility a) is unlikely, as if the parameters were inaccurate enough to cause a timing mismatch over such a short distance, then the effect in the boreholes further away from the

river would be even greater. Whereas in fact the boreholes further away from the river (at various distances) show a relatively good timing match, see Figure 8.19. Possibility c) was tested by refining the grid to 25m in the Grangetown area, and then down to 12.5m after this, but this made little difference to the results. Possibility b) was thought to be the most likely cause of the discrepancy. As the tidal elevations propagate up the river, there will obviously be a slight delay when compared to the elevations at the mouth of the river. The initial DIVAST model at the start of this chapter attempted to quantify this over the bay area and found the delay to be negligible. But that model could not be extended up the River Taff because of a lack of bed elevation data. Hence it is quite possible that the tidal levels in the river will be slightly delayed when compared to the boundaries used in the model.

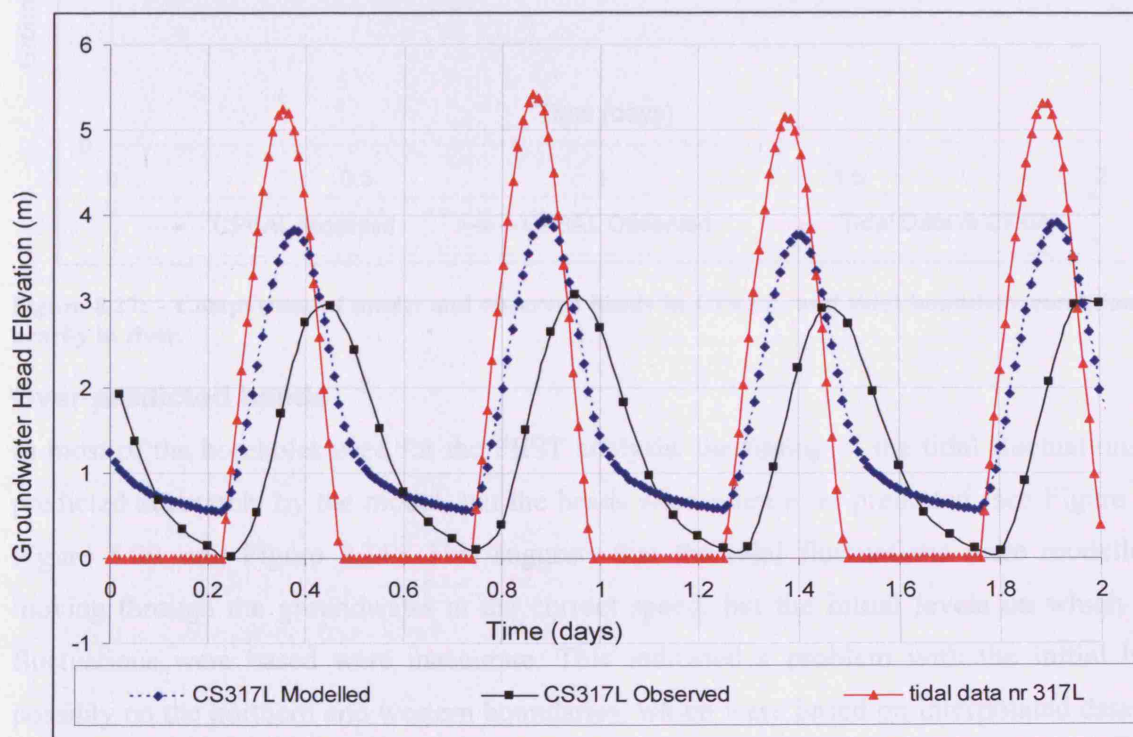


Figure 8.26: - Comparison of model and observed heads in CS317L, and tidal boundary condition used nearby in river.

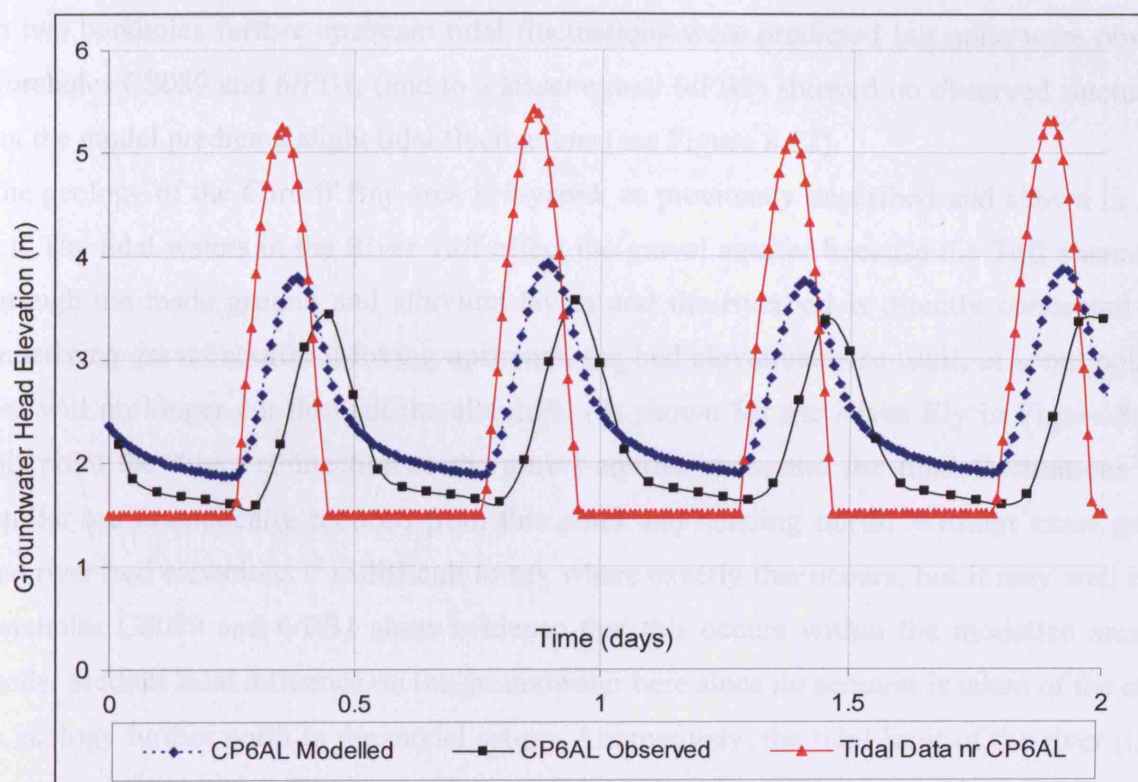


Figure 8.27: - Comparison of model and observed heads in CP6AL, and tidal boundary condition used nearby in river.

Over predicted heads

In most of the boreholes used for the PEST analysis, the timing of the tidal fluctuations was predicted accurately by the model, but the heads were often over-predicted (see Figure 8.19, Figure 8.20, and Figure 8.24). This suggests that the tidal fluctuations were modelled as moving through the groundwater at the correct speed, but the initial levels on which these fluctuations were based were inaccurate. This indicated a problem with the initial heads, possibly on the northern and western boundaries, which were based on interpolated data from the entire borehole data set. In essence, this seemed to suggest a problem with the boundary or initial conditions rather than the parameters. There was little that can be changed to correct any such inaccuracies, as these boundaries were based on interpolated data, and hence they may not be exact. The wells close to this boundary (CS314A and CS315L), are slightly overestimated by the model (by about 0.2 – 0.4m), reinforcing this suggestion. Due to a data loss incident, the model could not be re-run, but if set-up again, it is suggested that these boundaries are lowered slightly allowing boreholes CS314A and CS315L to be matched better, which in turn should give better correlation throughout.

Tidal Fluctuations

In two boreholes further upstream tidal fluctuations were predicted but none were observed. Boreholes CS089 and 6/PB1, (and to a lesser extent 6/PB2) showed no observed fluctuations, but the model predicted slight tidal fluctuations (see Figure 8.22).

The geology of the Cardiff Bay area is layered, as previously described and shown in Figure 8.1. The tidal waters in the River Taff affect the gravel aquifer because the Taff channel cuts through the made ground and alluvium layers and the riverbed is directly connected to the underlying gravel aquifer. Moving upstream, the bed elevations rise until, at some point, the bed will no longer cut through the alluvium, (as shown for the River Ely in Figure 8.1). At this point the direct connection to the gravel aquifer ends, and the tidal fluctuations in the aquifer are dramatically reduced from this point and heading north. Without exact geology and river-bed elevations it is difficult to say where exactly this occurs, but it may well be that boreholes CS089 and 6/PB1 show evidence that this occurs within the modelled area. The model predicts tidal influence on the groundwater here since no account is taken of the change in geology further north in the model set-up. Alternatively, the tidal limit of the river (i.e. the point at which the river level is unaffected by the tide) of the river may be further downstream than predicted for the time of the model simulations.

8.7 Summary

A large groundwater elevation database has been collected by Cardiff Harbour Authority since 1995. Hitherto, the data for the gravel aquifer beneath south Cardiff has not been analysed. Using this database an extensive interpolated dataset was created showing how the groundwater elevations varied over a two day period in July 1999, before the impoundment of Cardiff Bay. Extensive preparation and processing of this data resulted in a database for 83 boreholes with elevations given every 2 minutes. Visual animations of this dataset were used to filter out erroneous data points, and to understand the groundwater regime in the area. The groundwater elevations were seen to be tidally influenced in areas near the River Taff, which was consistent with previous studies of the geology of the area.

Using the original DIVAST model, Cardiff Bay itself was modelled to determine the water elevations in the river as compared to the tidal elevations in the Bristol Channel over the tidal cycle. Using data derived from this initial model, Visual MODFLOW was set-up for the area around the western bank of the River Taff, where the groundwater showed significant tidal fluctuations. The surface water boundary conditions had to be estimated from the initial

DIVAST model and from boreholes very close to the river. These boundary conditions were defined in sections along the river, as MODFLOW is not capable of calculating surface water elevations continuously along a river.

Initial heads were refined over several steady-state model runs, followed by a cycle of transient model runs. Having obtained the initial heads, the MODFLOW model was then run with the relevant boundary conditions for a cycle of two days, with conductivity estimated from a previous study ($K = 5.79 \times 10^{-4}$ m/s) and porosity determined from typical published values (0.25). These parameters were varied manually to obtain an improved fit with the observed data. Manual calibration indicated that the conductivity that gives the best fit with observed data lay between 5×10^{-2} and 5×10^{-3} m/s. These values were used as a starting point for two automatic parameter estimation (PEST) runs, one as an unconfined layer and one as a confined layer. The estimated conductivity for both runs was approximately 1×10^{-2} m/s and the estimated porosity was approximately 0.1. Running the model as a confined layer made little difference to the estimated parameters, even though the gravels are confined by a layer of alluvium in reality.

The modelled groundwater elevations showed good correlation to the observed data, with a few discrepancies. The elevations close to the river were anticipated somewhat, and some elevations were over-predicted slightly. It was concluded that the boundary conditions were probably causing most of the discrepancies due to interpolated data at the northern and western boundaries, and more significantly due to the fact that the surface water boundary was only able to be defined in sections, and had to be estimated in a fairly crude and time-consuming fashion.

CHAPTER 9 DIVAST-SG - MODELLING CARDIFF BAY

9.1 *Introduction*

The background to Cardiff Bay and its history and geology is given in section 8.1. Extensive field data was collected by Cardiff Harbour Authority on the groundwater in the area. The previous chapter described the use of an existing groundwater numerical code (MODFLOW) to model Cardiff Bay. This chapter describes the use of the new integrated surface water / groundwater code DIVAST-SG to model the same scenario.

9.2 *Creating the input file*

The structure of the input file for the DIVAST-SG model is given in Chapter 5. This section describes how the various parts of the input file were created, and describes the decisions that were involved in this process.

The area to be modelled was first defined. A similar area to the MODFLOW model (Figure 8.8) was chosen, i.e. the area east of the Taff, covering Grangetown and Riverside and extending up to the theoretical tidal limit of the Taff at Blackweir. The grid size was chosen to match the topographic data available, which was from the Digimap 25m Ordnance Survey data (EDINA 2006). Using ArcGIS to construct a georeferenced grid of elevations, the actual grid size was found to be 23.2m, which was then used in the input file. This was approximately half of the grid size of the MODFLOW model, and was kept at this fine resolution to allow the river Taff to be several cells wide in the model, thus ensuring 'bottlenecks' were kept to a minimum. The area chosen at a grid resolution of 23.2m gave 130 x 68 grid cells. The surface topography data was reclassified as follows. Cells with an elevation greater than 5m were classified as '0' and cells with an elevation less than 5m were

classified as '1'. From the reclassified dataset it was relatively easy to extract a grid of surface water and groundwater areas to be used in the model domain.

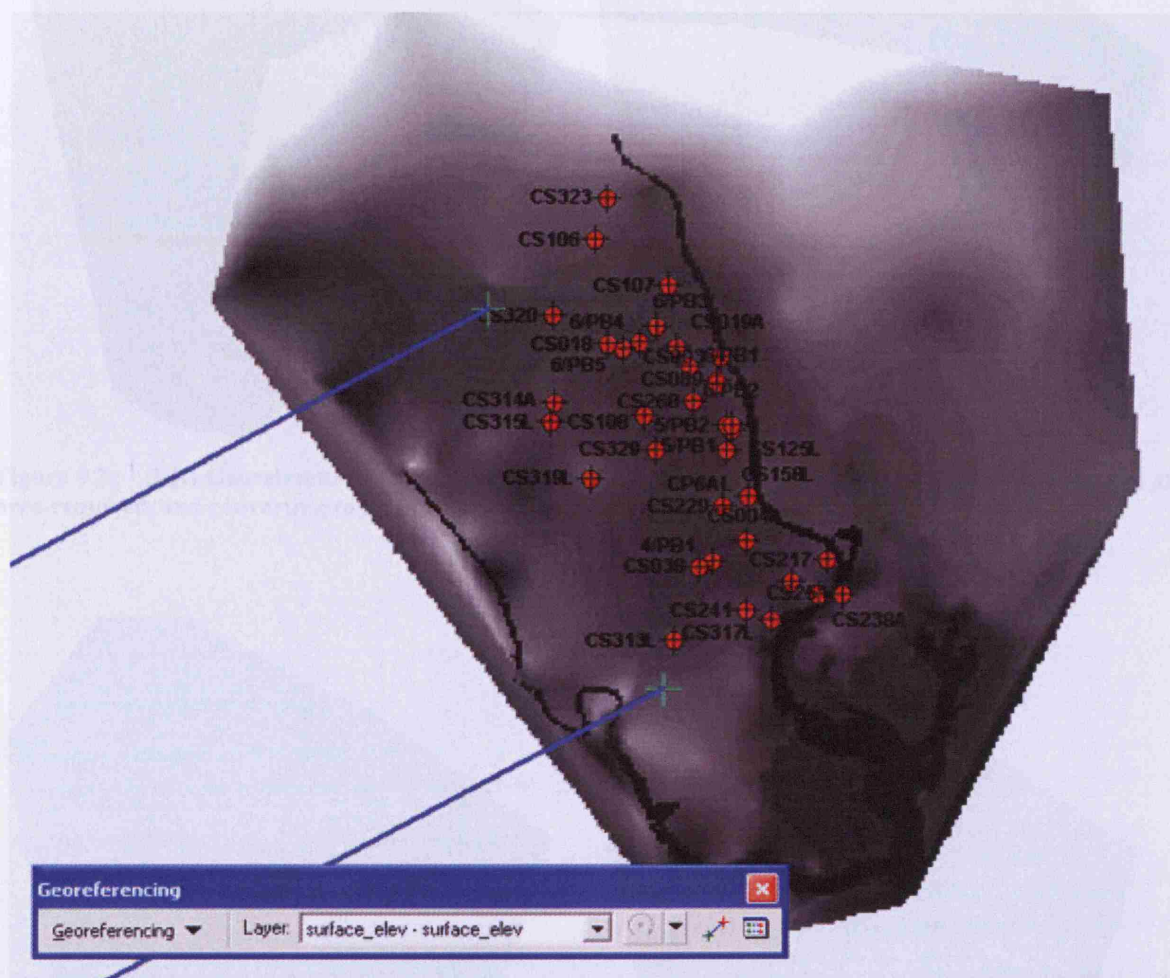


Figure 9.1: - Topography data in original orientation displayed in ArcGIS showing elevation (shading – light = high ground, dark = low ground), borehole locations (red), and georeference points (blue lines and cross).

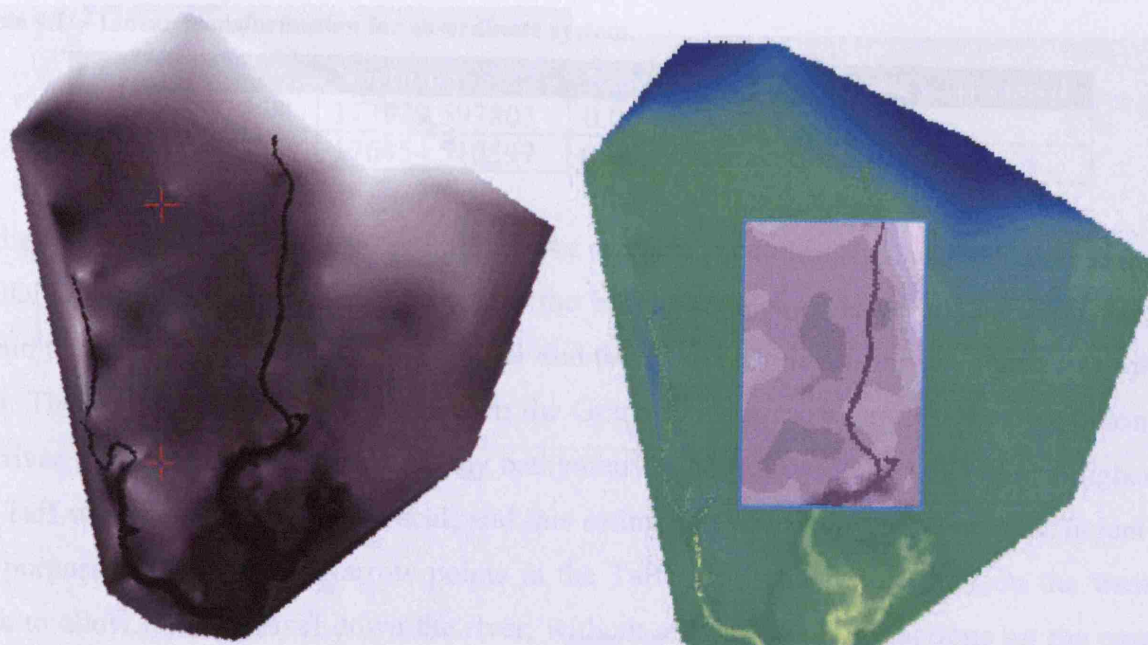


Figure 9.2: - (left) Georeferenced grid in new rotated coordinate system. (right) Clipping the data to the area required, and converting to an integer dataset.

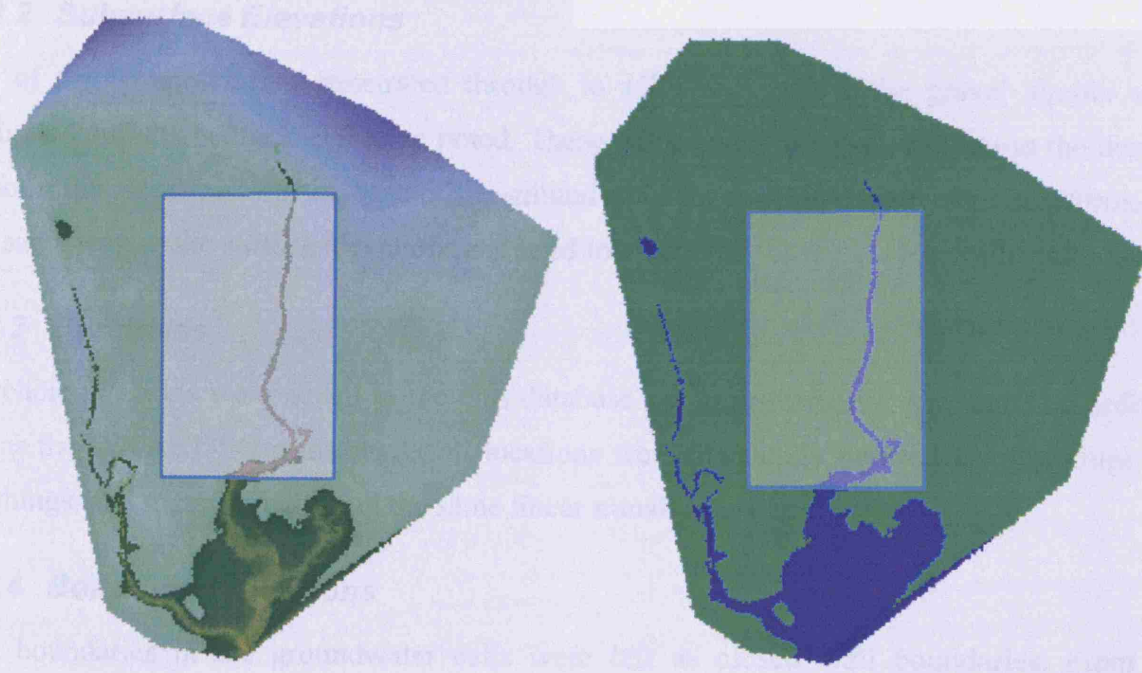


Figure 9.3: - Reclassifying the grid at a cut-off point of 5m as surface water (blue) or groundwater (green). Left = before reclassification, right = after reclassification.

9.2.1 Surface elevations

ArcGIS was used extensively to construct the initial grid. The surface topography data were rotated to allow all of the boreholes to be covered in the minimum rectangular area. The data were also converted to the new grid system i.e. 0 to 130 on the x-direction, and 0 to 68 in the y

direction, using the linear transformation shown in Table 9.1.

Table 9.1: - Linear transformation for co-ordinate system.

Easting	Northing	New x (i)-coord	New y (j)-coord
317449.102758	173929.597803	0.00	0.00
316340.223531	176454.510597	0.00	118.862

Bed elevations for the Taff higher up the river were estimated in the same fashion as in the MODFLOW model, (section 8.3.3) where the boreholes along the riverbank were used to obtain the minimum water level in the river and the river bed elevations estimated from these data. The boreholes of interest were all in the Grangetown area, where the bed elevations in the river were defined in the Cardiff Bay bathymetry. The estimated bed elevations higher up the Taff were therefore not as critical, and this estimation process was deemed sufficient for the purposes of this study. Narrow points in the Taff were widened slightly on the western bank to allow flow to travel down the river, without affecting the interactions on the eastern bank. Corner elevations were used for the depths instead of side-centred data, as the grid-resolution was considered high enough already.

9.2.2 Subsurface Elevations

All of the boreholes that penetrated through to solid rock below the gravel aquifer were compiled and the bedrock elevation noted. These values were interpolated across the domain to form the elevations for the base of the groundwater layer. This dataset was transformed in the same way as the surface elevations and used to create the 'base of layer 1' elevation grid.

9.2.3 Boreholes

Borehole positions were added to the GIS database and transformed to the same co-ordinate set as the DIVAST-SG grid, hence, all locations were physically derived from eastings and northings, and transformed using the same linear transformation.

9.2.4 Boundary Conditions

The boundaries in the groundwater cells were left as closed wall boundaries. From the borehole logs and the MODFLOW model it was clear that groundwater levels at these boundaries did not vary with the tide, except at south-western corner of the model – where the boundary was chosen to lie along a potential groundwater divide (see section 8.3.3 for further details), and hence a wall boundary was deemed to be appropriate. Constant head boundaries could have been set up for each cell, but this would have been a lengthy process in the DIVAST-SG model and would have had little effect on the groundwater head near the river,

which are almost exclusively tidally driven. Checks were undertaken to ensure that the levels at these boundaries were in equilibrium (i.e. not changing other than with tidal variations) before the model was used for predictions. See section 9.3 for how these checks were undertaken using an initial lengthy model run and subsequent hot-start models.

The same tidal boundary used in the MODFLOW model (i.e. tide in the Severn cut-off at -1.5m AOD) was used in the DIVAST-SG model, and specified at hourly intervals for 48 hours. This boundary was located at the southern end of the model across the mouth of the Taff as it enters Cardiff Bay. See section 8.3.2 for further discussion of this boundary representation. The upper model limit of the Taff was set as a flow boundary with a discharge of $9 \text{ m}^3/\text{s}$, based on the NRA monitoring data (NRFA 2006). See section 8.3.2 and Figure 8.5 for further details.

In this context the setting up of the DIVAST-SG model is easier than MODFLOW. MODFLOW cannot predict the surface elevations continuously up the river without separate models or additional programs being bolted on to the model, as outlined in Chapter 2. For MODFLOW the river elevation had to be defined in sections, which was a laborious and inaccurate process. The advantage of using a code which was in origin a surface-water code (DIVAST) meant that DIVAST-SG simply required the tidal elevation at one end of the river, and a flow or another elevation at the other boundary with the surface water elevations being then calculated continuously at all points.

9.2.5 Inactive cells at north of domain.

Because the geology data was derived from the boreholes, the data was subject to interpolation artefacts outside the zone of the boreholes. Towards the north of the domain, the boreholes ceased to provide information about what happened beneath the surface and as a result the geology data became increasingly suspect towards this end of the model area. From inspection of the borehole logs it was clear that the northerly boreholes were not tidally influenced and so this area was less significant to the accuracy of the model predictions. In addition, in this area the bed elevations of the Taff were increasingly derived from an assessment of a range of data. As a result the area north of the boreholes was set to be inactive, and the upper boundary of the Taff was moved southward to where the data was more reliable. The DIVAST-SG grid is shown overlaying the MODFLOW area map in Figure 9.4, and the domain showing the borehole locations is shown in Figure 9.5.

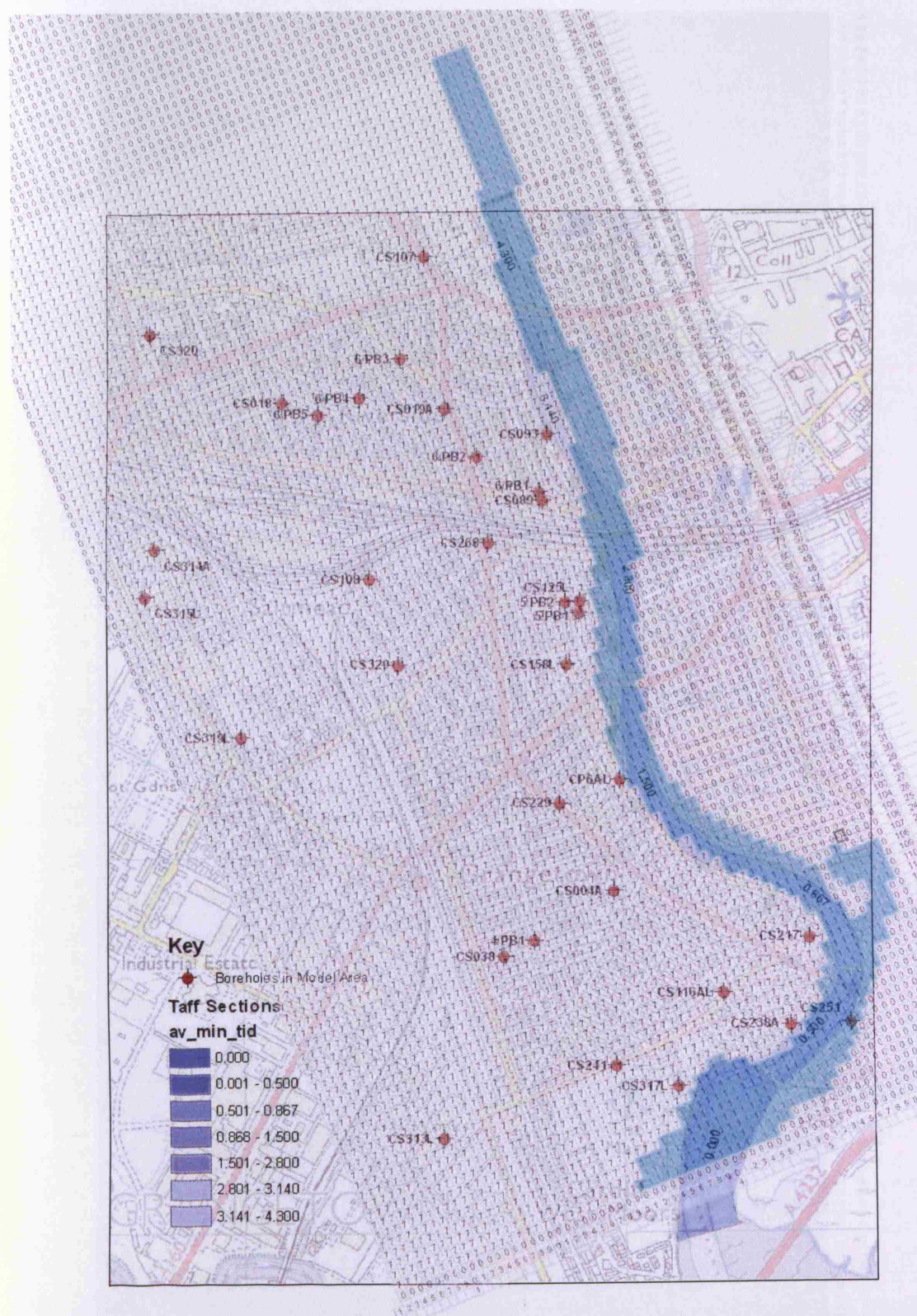


Figure 9.4: - DIVAST-SG grid overlaying Cardiff map used for MODFLOW area.

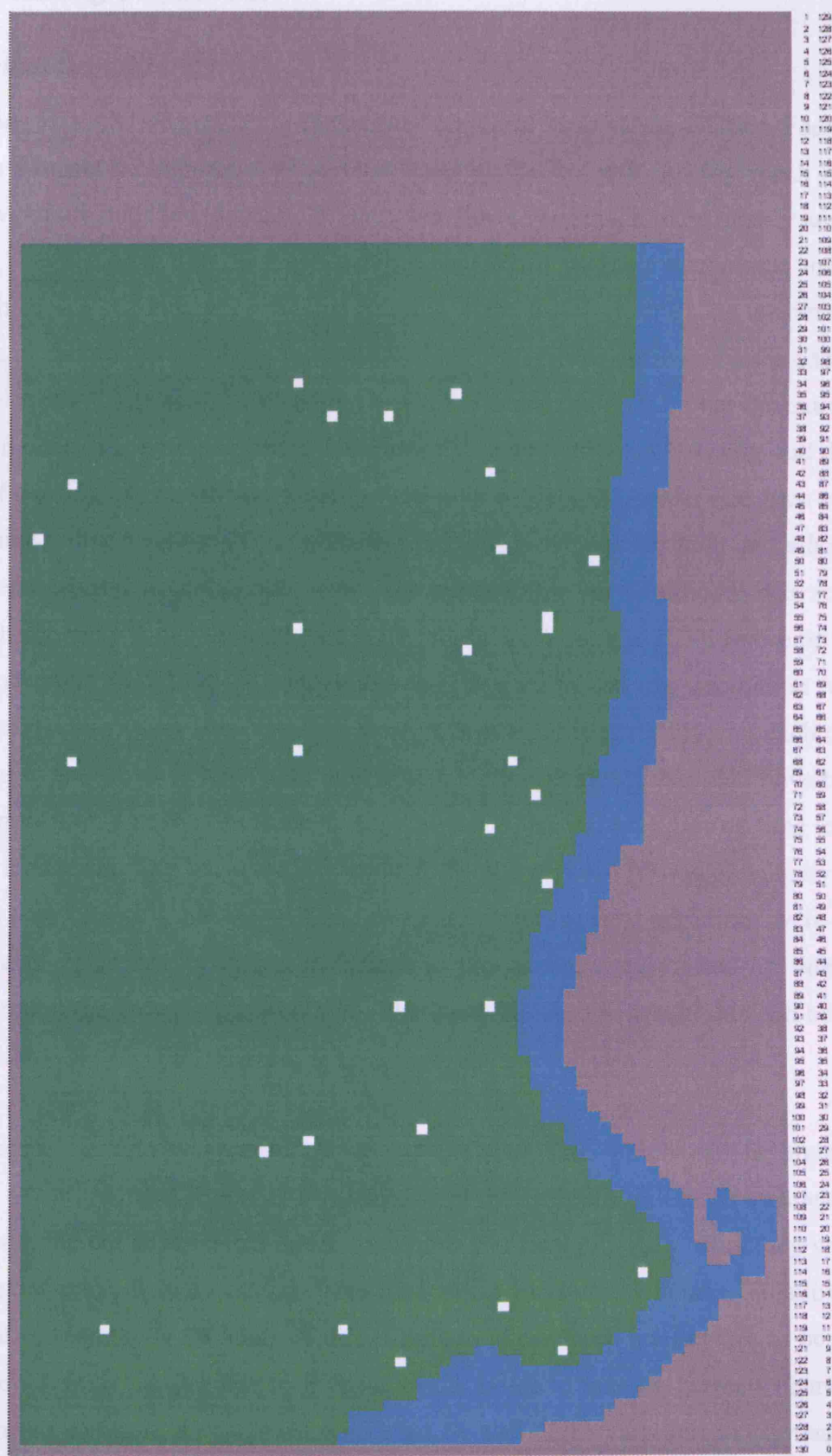


Figure 9.5: - DIVAST-SG domain for Cardiff Bay model. Blue indicates a surface water cell (1), green indicates a groundwater cell (7), and grey indicates inactive cells (0 - wall boundary). White indicates the location of a borehole. Varying boundary conditions were specified at either end of the river.

9.3 *Running the model*

9.3.1 *Initial Conditions*

The existing DIVAST-SG model does not have an initial head set-up facility. For the surface water this was not so important, as surface water elevations will quickly reach equilibrium irrespective of the initial conditions. Groundwater flows vary much more slowly and therefore generally take a longer time to reach equilibrium. When running a transient model (i.e. a model which has boundary conditions varying with time) it must be ensured that the conditions in the groundwater are consistent with the initial time period of the model.

The model was initially set-up with a high head of water (4.5m AOD) over the entire domain. This ensured all cells were flooded at the start of the simulation, as flooding and drying was not part of the single layer surface water-groundwater model. The model was then run for 500 hours of model time to allow the groundwater levels to reach equilibrium, and a hot-start file was created from this model at 500 hours. The permeability for this model was set to 0.005 m/s, and the porosity to 0.25. These values are largely irrelevant, as the purpose of this phase of the study was to allow the model to reach a state of steady oscillation where the groundwater heads distant from the river were no longer falling steadily and each tidal cycle was similar to the previous tide. With hindsight, a higher permeability could have been used, as equilibrium would have been reached more quickly – the 500 hour run-up time required an overnight model run. The hot-start file output at the end of this run was essentially an initial conditions data file, with the model frozen at a state where the tidal variations were occurring smoothly and repeatably. Transient variations in the groundwater caused by tidal ‘waves’ moving through the gravel were preserved. The input file used to create this can be found on the Appendix CD^a.

Each different scenario was started from this hot-start file, which can be found on the Appendix CD^b. The new scenarios each used slightly different values of permeability and porosity from the hot-start file, so initial conditions were not precisely what they would have been if the hot-start file had been run from time zero with the new values. To allow for this, each scenario was run for 36 hours of model time to allow three tidal cycles to be simulated with the new values and so allow their groundwater heads to take on the new characteristics. Only the heads close to the river were affected by the slight variation in permeability and

^a Input file: D:\DIVAST-SG Cardiff Bay Model\gtown500.dsg

^b Hot-start file: D:\DIVAST-SG Cardiff Bay Model\gtown500.hst

porosity, the distant heads achieved the same values no matter what the permeability and porosity values. After this 36 hour period, the model readings were collected and compared to measured readings. The appendix CD contains all of the input files used, and a number of images and animations from the modelling. Specific model runs referred to in the text are also referred to by a filename so the data can be readily examined. Figure 9.6 shows a visualisation of a model run from the hot-start file at low tide.

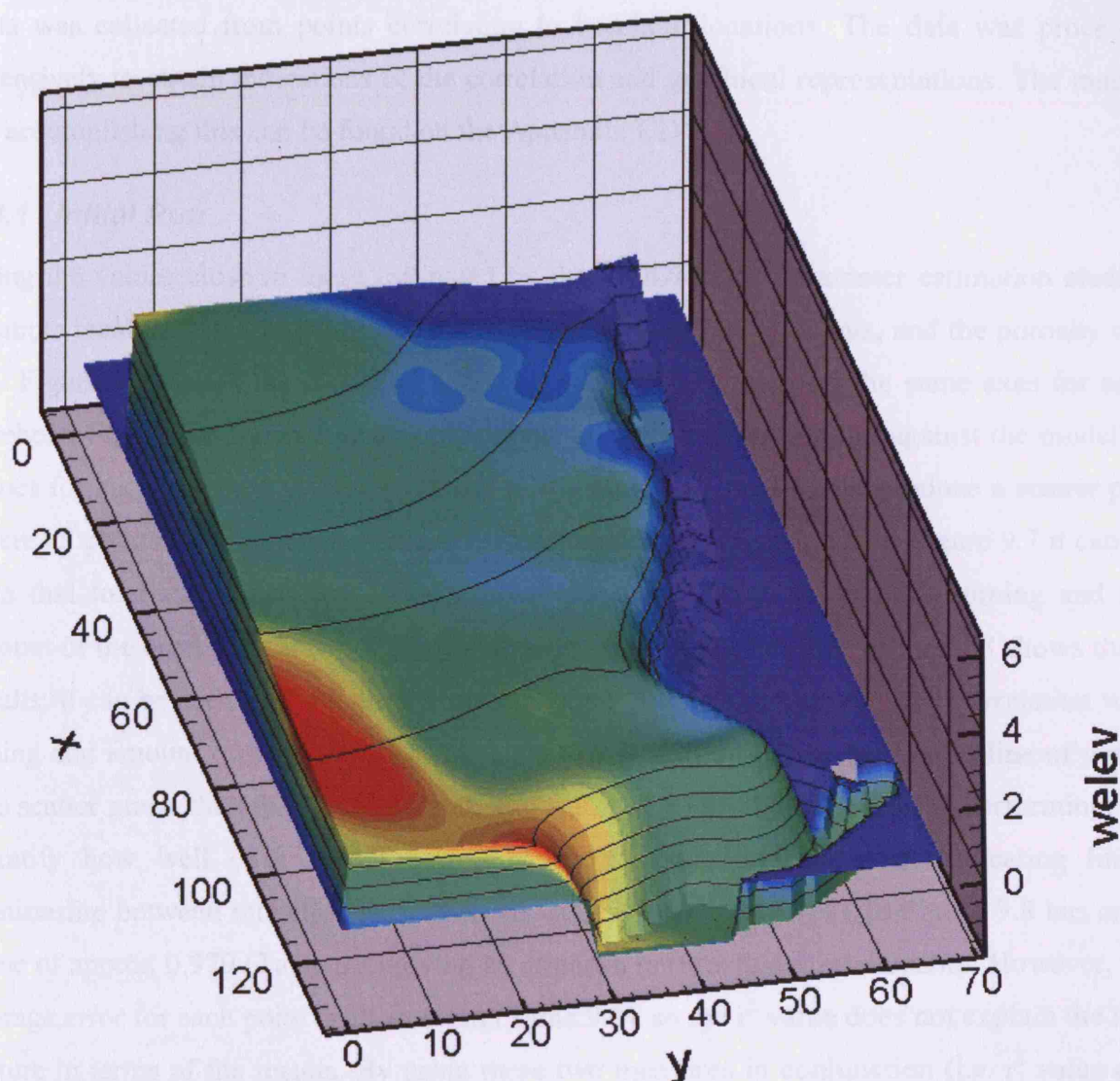


Figure 9.6: - Tecplot image of the DIVAST-SG model at low tide. Black contour lines indicate groundwater head, colours indicate depth of aquifer (red - deep, blue - shallow).

9.4 Parameter estimation

The model was run with several different permeability and porosity values. The values determined by MODFLOW were used initially and then a manual parameter estimation was undertaken. To check the correlation between the model and measured values, five boreholes

that show significant variations over the tidal cycle were used (CS116AL, CS217, CS238A, CS241, CS317L). An additional borehole with a stable elevation was used to check the general average head agreement (CS313L). The locations of these boreholes can be seen in Figure 8.9 or Figure 9.4.

A total of 24 model runs were carried out at the following permeabilities: 0.0025, 0.0040, 0.0050, 0.0075, and 0.0100 m/s, and each was run with porosities of 0.1, 0.2, 0.3, and 0.4.

Data was collected from points correlating to borehole locations. The data was processed extensively to obtain indications of the correlation and graphical representations. The macros for accomplishing this can be found on the Appendix CD^a.

9.4.1 Initial Run

Using the values close to those estimated by the MODFLOW parameter estimation studies, example results are presented here. The permeability used was 0.01 m/s, and the porosity was 0.2. Figure 9.7 shows the modelled and observed heads, plotted on the same axes for each borehole. Figure 9.8 shows a scatter plot of the observed values plotted against the modelled values for each timestep. A perfect model of the measured data would produce a scatter plot where all points fall on the $y = x$ line, shown as the dotted diagonal. From Figure 9.7 it can be seen that for these parameters CS241 shows good correlation in terms of timing and the amount of the head variation, but all of the values are slightly too low. Figure 9.8 shows these results; it can be seen that the plots form a diagonal line of gradient 1 (good correlation with timing and amount of head variation), but the line is slightly below the dotted line of $y = x$. The scatter graph therefore gives a quick indication of how well the model is performing. To quantify how well each model performs, the r^2 value can be used, indicating linear relationship between modelled and observed values. Borehole CS241 in Figure 9.8 has an r^2 value of approx 0.979 (Table 9.2) giving an almost a perfect linear relationship. However, the average error for each point is about 0.5m (Table 9.3), so the r^2 value does not explain the true picture in terms of the results. By using these two measures in conjunction (i.e. r^2 value and the average error) the optimum permeability and porosity to fit the measured data can be found.

^a Macro file: D:\DIVAST-SG Cardiff Bay Model\macros.xls

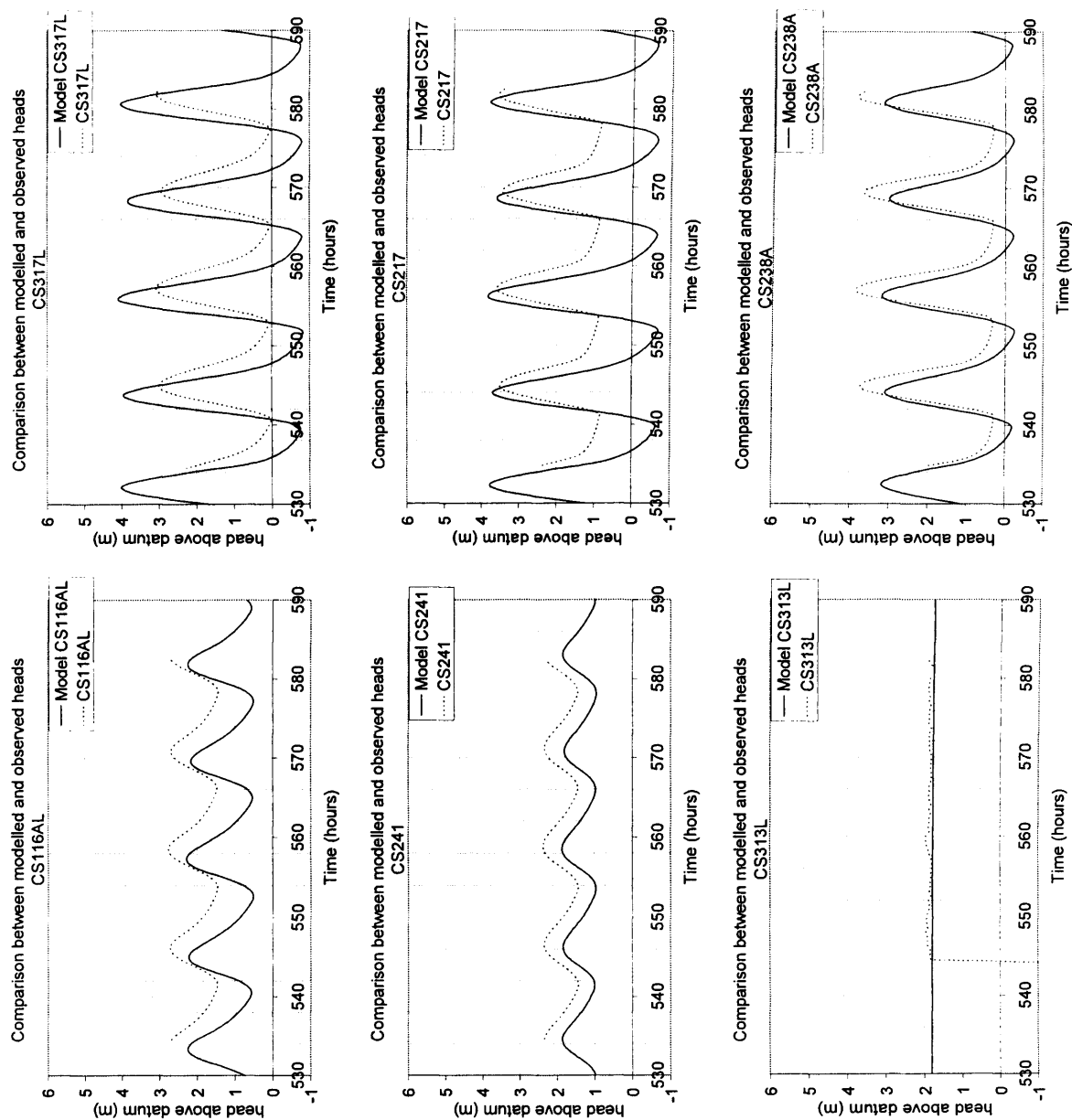


Figure 9.7: - Model and observed head time series for $k = 0.01$ $n = 0.2$

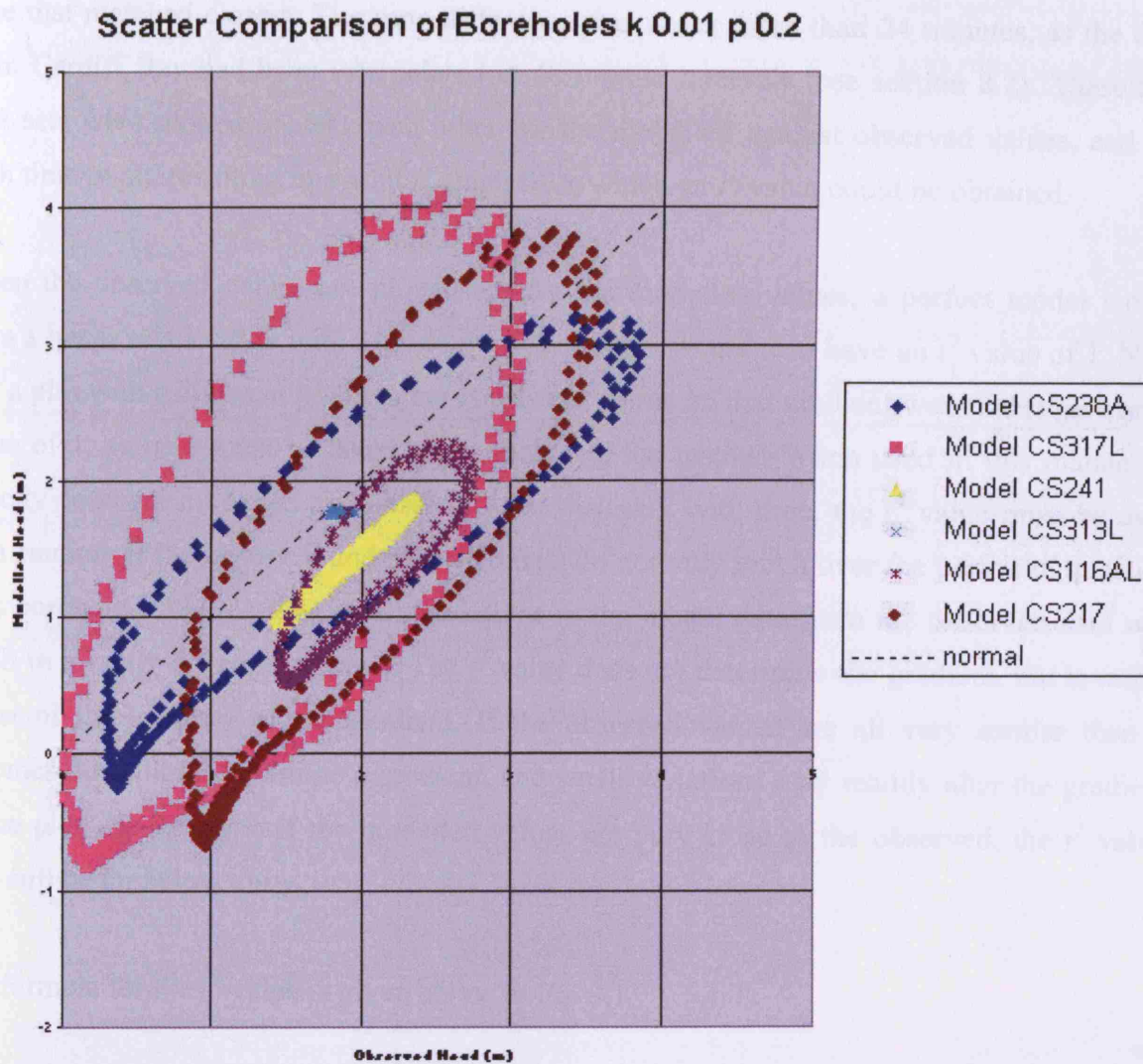


Figure 9.8: - Scatter plot of test boreholes, observed head against modelled head - Permeability 0.01 Porosity 0.2

9.4.2 R^2 value.

The r-squared value is the square of the Pearson coefficient, i.e. a measure of how well two variables relate linearly to each other. In brief, r^2 is the relative predictive power of a model and is a descriptive measure between 0 and 1. The closer the value to unity, the closer the linear relationship between the model and the observed data is. An r^2 value of 1 indicates a perfect linear relationship, i.e. knowing one variable means that the other variable can be accurately predicted. An r^2 value of zero means that knowing one variable does not enable the other to be predicted. Values in between indicate the ability of one variable to predict the other, e.g. a value of 0.9 means that approximately 90% of the observed variable can be predicted by the model variable using a linear relationship.

Each modelled data point was matched with the observed data point at the same time or the time that matched closest. The time difference was never more than 24 minutes, as the data from Cardiff Bay had been interpolated at 48 minute intervals (see section 8.2). These two data sets were plotted against each other for the modelled against observed values, and for each time point, resulting in a scatter graph from which an r^2 value could be obtained.

When the observed values are plotted against the modelled values, a perfect model would form a linear relationship with a gradient of 1, and this would also have an r^2 value of 1. Note that a plot with a different gradient but consistent points on that gradient would also give an r^2 value of 1, so care must be taken when analysing the results. When used in this manner to directly compare modelled and observed data that vary with time, the r^2 value must be used with caution. If the observed and modelled data do not vary much over the period in question (e.g. borehole CS313L) then small deviations in the model data from the observed data will result in a vastly different r^2 value. The r^2 value does not determine the gradient, but is rather a test of the linearity of the gradient. If the observed values are all very similar then it becomes difficult to determine a gradient, and small variations may readily alter the gradient of the plot. Hence, even if the modelled values are very close to the observed, the r^2 value may still be far below unity.

The formula for the r^2 value is given below in Eq. 9.1.

9.1

$$r^2 = \left(\frac{\sum (x - \bar{x})(y - \bar{y})}{\sqrt{\sum (x - \bar{x})^2 \sum (y - \bar{y})^2}} \right)^2$$

Table 9.2 shows the r^2 values obtained for each borehole and for each set of conditions. Inspection of these results allowed the optimum conditions (i.e. those that give the closest linear fit with the observed data) to be determined. The 2-D contour plots of the r^2 value against porosity and permeability are shown in Figure 9.9 to highlight how the fit varies as the variables change.

Table 9.2: - R^2 values for individual boreholes and porosity and permeability settings.

Permeability (m/s)	Porosity	R^2 Values							Average (exc. CS241 and CS313L)
		CS116AL	CS217	CS238A	CS241	CS317L	CS313L	Average (exc. CS313L)	
0.02	0.4	0.7052	0.7469	0.8262	0.9791	0.5663	0.0002	0.7648	0.7112
0.02	0.3	0.5566	0.6578	0.7430	0.8510	0.4869	0.0012	0.6591	0.6111
0.02	0.2	0.3740	0.5447	0.6292	0.5653	0.3950	0.0476	0.5017	0.4857
0.02	0.1	0.1546	0.3929	0.4733	0.1835	0.2827	0.1423	0.2974	0.3259
0.01	0.4	0.9796	0.9431	0.9606	0.5369	0.7955	0.0037	0.8431	0.9197
0.01	0.3	0.9011	0.8724	0.9257	0.8669	0.6964	0.0010	0.8525	0.8489
0.01	0.2	0.7054	0.7469	0.8262	0.9791	0.5663	0.0002	0.7648	0.7112
0.01	0.1	0.3741	0.5448	0.6292	0.5654	0.3951	0.0474	0.5017	0.4858
0.0075	0.4	0.9560	0.9735	0.9397	0.1480	0.8892	0.0040	0.7813	0.9396
0.0075	0.3	0.9796	0.9431	0.9606	0.5369	0.7955	0.0037	0.8431	0.9197
0.0075	0.2	0.8504	0.8374	0.9009	0.9442	0.6569	0.0002	0.8379	0.8114
0.0075	0.1	0.4996	0.6232	0.7090	0.7729	0.4579	0.0066	0.6125	0.5724
0.005	0.4	0.6983	0.8936	0.7720	0.0947	0.9800	0.0035	0.6877	0.8360
0.005	0.3	0.9085	0.9678	0.9093	0.0409	0.9225	0.0040	0.7498	0.9270
0.005	0.2	0.9796	0.9431	0.9606	0.5369	0.7955	0.0037	0.8431	0.9197
0.005	0.1	0.7054	0.7470	0.8262	0.9791	0.5664	0.0002	0.7648	0.7113
0.004	0.4	0.4676	0.7698	0.6063	0.4595	0.9890	0.4618	0.6584	0.7082
0.004	0.3	0.7560	0.9185	0.8108	0.0359	0.9709	0.5012	0.6984	0.8641
0.004	0.2	0.9721	0.9716	0.9503	0.2254	0.8700	0.5000	0.7979	0.9410
0.004	0.1	0.8211	0.8188	0.8865	0.9706	0.6378	0.4770	0.8270	0.7911
0.0025	0.4	0.0351	0.3595	0.1845	0.2692	0.8580	0.2790	0.3413	0.3593
0.0025	0.3	0.2685	0.6264	0.4421	0.6839	0.9647	0.4258	0.5971	0.5754
0.0025	0.2	0.6982	0.8936	0.7720	0.0947	0.9800	0.5082	0.6877	0.8360
0.0025	0.1	0.9796	0.9431	0.9606	0.5368	0.7955	0.0037	0.8431	0.9197

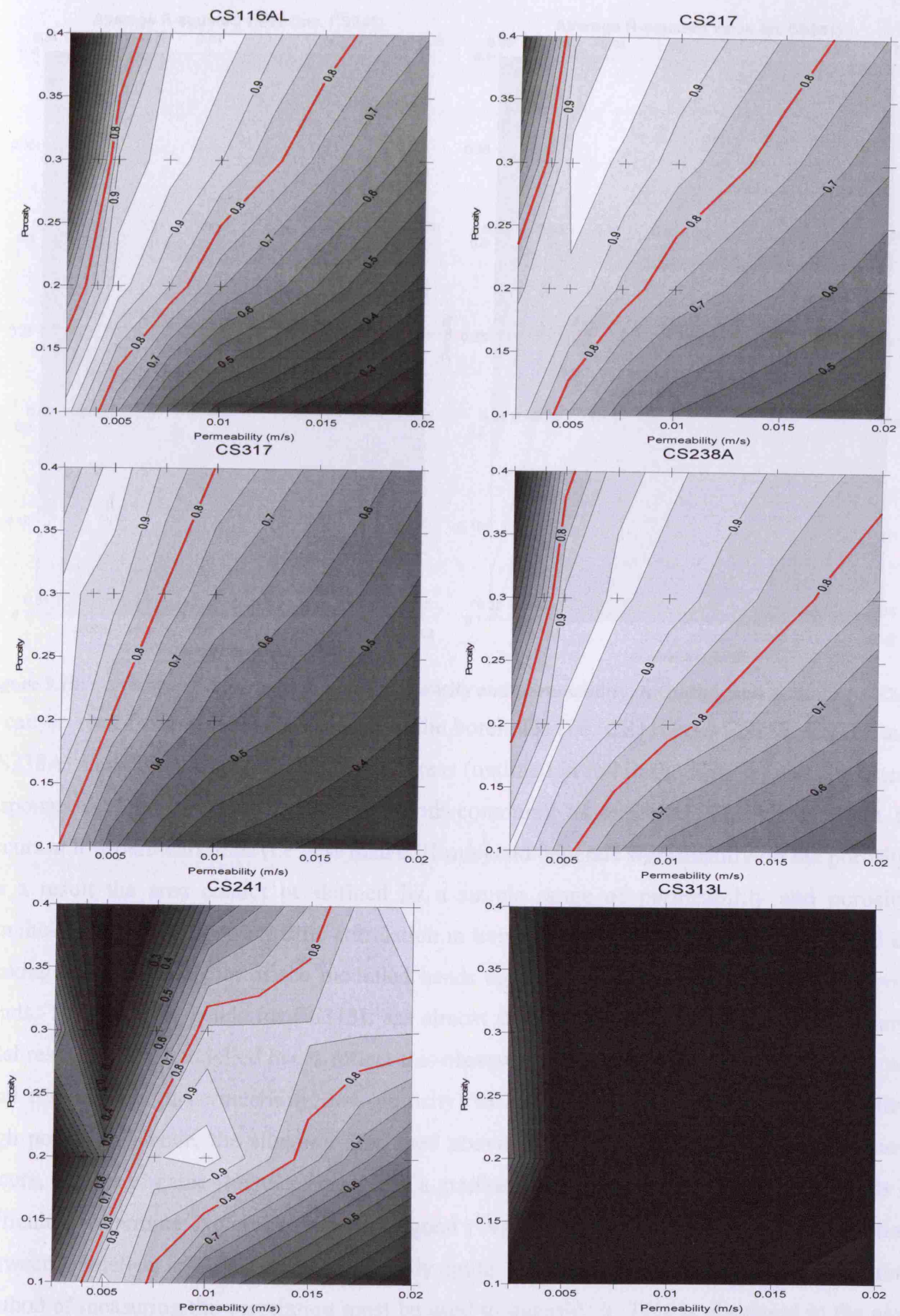


Figure 9.9: - r^2 value as a function of porosity and permeability. Light areas indicate high values, and the 80% contour line is in red.

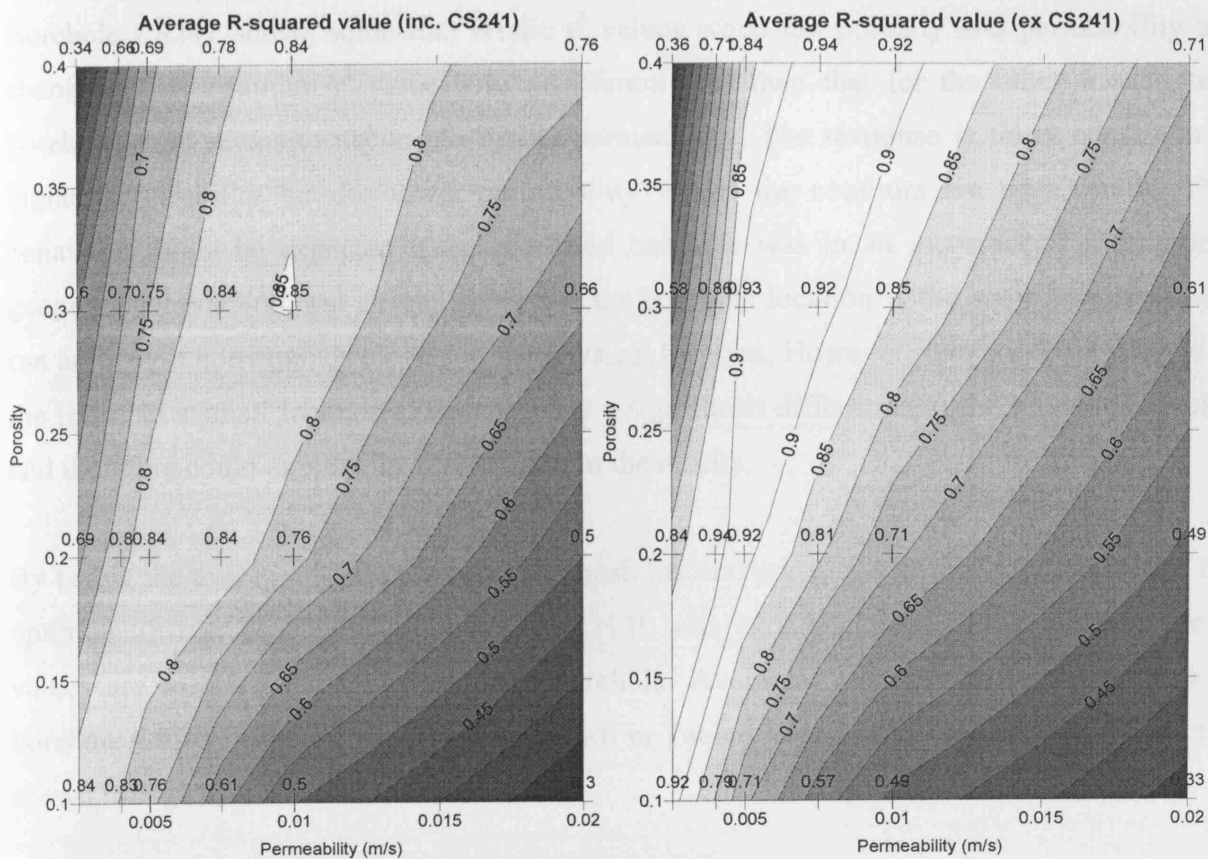


Figure 9.10: - Average r^2 values as a function of porosity and permeability, including and excluding CS241

It can be seen from the results that four of the boreholes (i.e. CS116AL, CS217, CS317 and CS238A) show good correlation in similar areas (outlined in red in the figures) and consistent response to changes in the variables (smooth contours), as expected. The area of best fit occurs at low permeabilities (i.e. less than 0.01 m/s) and depends significantly on the porosity. As a result the area cannot be defined by a simple range of permeability and porosity. Borehole CS313L shows very little correlation in terms of linear fit. This can be explained by looking at the simple plot of the modelled heads against time compared with the observed heads. The observed heads for CS313L are almost stationary, and exhibit very little, if any, tidal response. The modelled heads reflect this observed response, and vary from a very small tidal response (high permeability, low porosity) to a flat tidal response (low permeability, high porosity). Hence, the situation discussed above (all data points having similar values) occurs, and the r^2 value fluctuates easily, as a gradient of modelled against observed heads is difficult to determine. No conditions give a good r^2 value for this borehole, but the correlation between modelled and observed is generally quite good in all the conditions. A different method of measuring the correlation must be used to quantify it. This is discussed in the next section.

Borehole CS241 shows somewhat erratic r^2 values when the porosity and permeability are changed. This optimum r^2 value is in a different area than that for the other 4 consistent boreholes, and seems to occur at a higher permeability. The response is fairly consistent at higher permeability but for lower permeability values the contours are very erratic. This behaviour might be expected if the modelled borehole was in an incorrect or inconsistent geographical position, but checks show that the borehole location is the same in each model run and that it corresponds closely to the physical location. However, this borehole is close to the river, so a small location shift will make a significant difference to the modelled results, and therefore could explain the discrepancy in the results.

By taking the average r^2 value for each permeability and porosity setting, values that give the optimum fit can be obtained. Borehole CS313L was excluded from the average as the r^2 values are meaningless for a non-tidal borehole. Averages were taken with and without borehole CS241, with the results being shown in Table 9.2 and with the contour plots being shown in Figure 9.10.

The average plots show that including the CS241 r^2 values in the average does not shift the location of the maximum significantly, but it does reduce the maximum r^2 value from approximately 0.94 to approx 0.84. In both cases the maximum values occur in a band, showing that the values of permeability and porosity that give the highest r^2 value lie within a range rather than being limited to one value. Another method of assessing fit is used in the next section to address the limitations of the r^2 value.

9.4.3 Average Error

While the r^2 value measures the linearity of the relationship between the modelled and observed values, this value gives no information about the accuracy of the results. For instance, if the change in the modelled heads follows the observed heads exactly, but is 3 metres lower than the observed heads, then the r^2 value would be nearly 1 but clearly the model would not be predicting the heads accurately. Hence an additional method is used to measure the absolute error between the modelled and observed heads. Each observed data point is subtracted from the modelled point at the corresponding time, using the same data set described for the r^2 method in section 9.4.2, to give the difference between the data sets. The absolute of this value is used to avoid negative and positive errors cancelling each other out.

This method has its own limitations. If the modelled heads are predicted accurately but slightly out of synchronisation with the observed heads, then the error may be significantly large when the heads change rapidly, even though the graphs may be very similar. However, it can be used on borehole CS313L, where the r^2 method fails to give meaningful results. This method is also a simpler measure of the accuracy of the modelled results. When used in conjunction with the r^2 method, this method enables an optimum permeability and porosity to be determined. Table 9.3 shows the average error for each borehole and each set of conditions. Figure 9.11 shows the 2-D contour plots of this data for each borehole. Figure 9.12 shows the average error for all the boreholes together.

Table 9.3: - Average error from observed values for each borehole.

Permeability (m/s)	Porosity	Average Error (m)						Average
		CS116AL	CS217	CS238A	CS241	CS317L	CS313L	
0.0200	0.4	0.7255	1.0442	0.5659	0.4917	1.0601	0.0912	0.6631
0.0200	0.3	0.7603	1.2126	0.7038	0.5018	1.2231	0.1113	0.7522
0.0200	0.2	0.9155	1.4340	0.8987	0.5433	1.4239	0.1462	0.8936
0.0200	0.1	1.2742	1.7550	1.1896	0.8087	1.6989	0.2220	1.1581
0.0100	0.4	0.7291	0.7390	0.3778	0.4745	0.5985	0.0592	0.4964
0.0100	0.3	0.7267	0.8134	0.4089	0.4805	0.8012	0.0700	0.5501
0.0100	0.2	0.7262	1.0443	0.5660	0.4920	1.0601	0.0913	0.6633
0.0100	0.1	0.9158	1.4340	0.8988	0.5436	1.4239	0.1465	0.8938
0.0075	0.4	0.7321	0.7348	0.4562	0.4706	0.3891	0.0515	0.4724
0.0075	0.3	0.7293	0.7391	0.3778	0.4745	0.5985	0.0591	0.4964
0.0075	0.2	0.7262	0.8758	0.4464	0.4836	0.8800	0.0755	0.5813
0.0075	0.1	0.7985	1.2791	0.7618	0.5070	1.2849	0.1209	0.7920
0.0050	0.4	0.7359	0.7417	0.6736	0.4698	0.1435	0.0433	0.4680
0.0050	0.3	0.7333	0.7353	0.5129	0.4698	0.3049	0.0485	0.4675
0.0050	0.2	0.7294	0.7392	0.3778	0.4745	0.5985	0.0592	0.4964
0.0050	0.1	0.7266	1.0443	0.5661	0.4922	1.0600	0.0914	0.6634
0.0040	0.4	0.7066	0.7152	0.7876	0.4726	0.2187	0.0409	0.4903
0.0040	0.3	0.7048	0.7084	0.6382	0.4695	0.1664	0.0443	0.4553
0.0040	0.2	0.7064	0.7124	0.4308	0.4704	0.4347	0.0531	0.4680
0.0040	0.1	0.7161	0.8963	0.4678	0.4832	0.9187	0.0780	0.5934
0.0025	0.4	0.7159	0.7491	0.9719	0.4826	0.5107	0.0377	0.5780
0.0025	0.3	0.7080	0.7218	0.8704	0.4751	0.3326	0.0394	0.5246
0.0025	0.2	0.7048	0.7085	0.6736	0.4698	0.1436	0.0434	0.4573
0.0025	0.1	0.7296	0.7393	0.3778	0.4746	0.5985	0.0592	0.4965
Maximum		1.2742	1.7550	1.1896	0.8087	1.6989	0.2220	
Minimum		0.7048	0.7084	0.3778	0.4695	0.1435	0.0377	

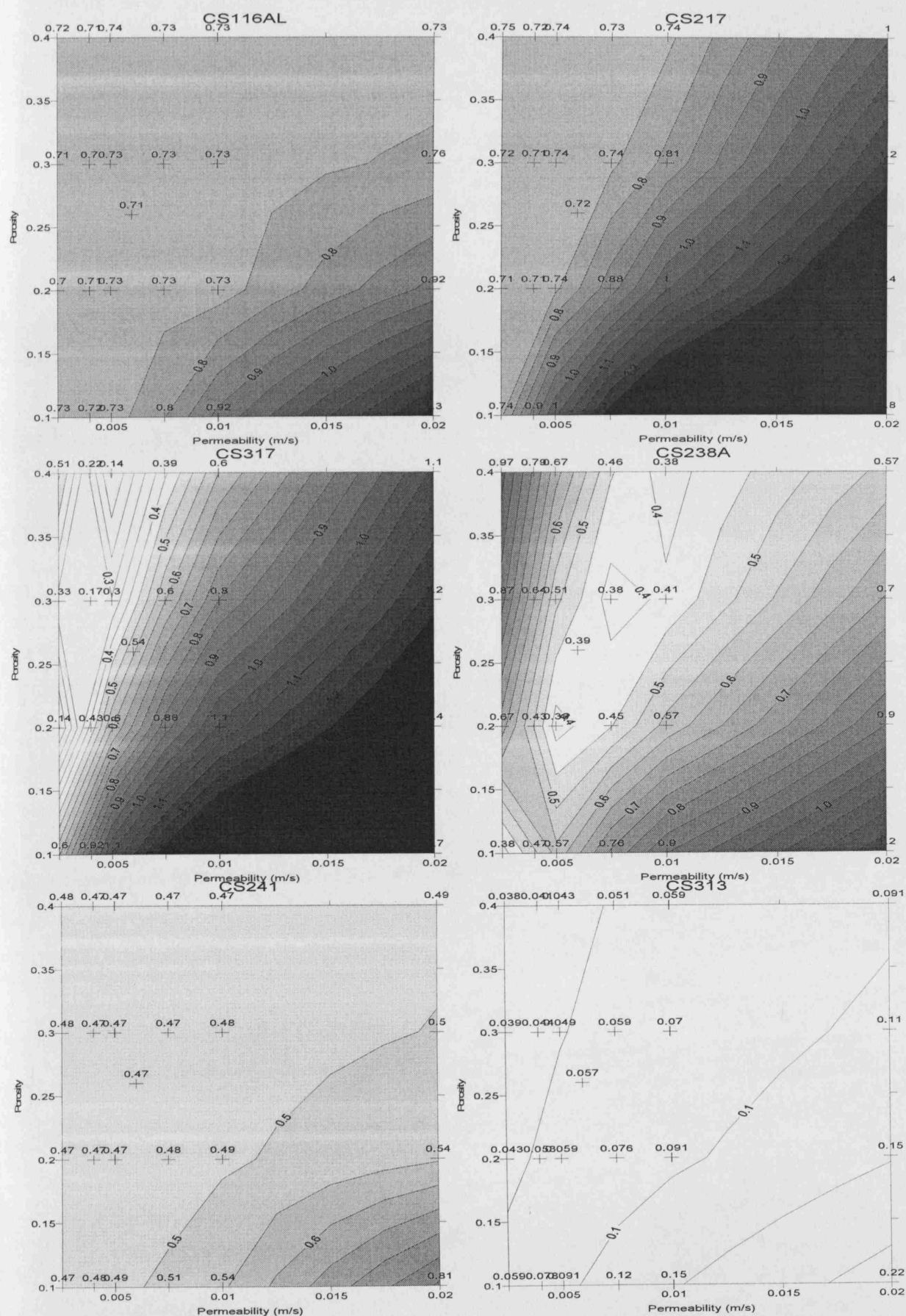


Figure 9.11: - Average error from observed values with respect to porosity and permeability. Light areas indicate low average error.

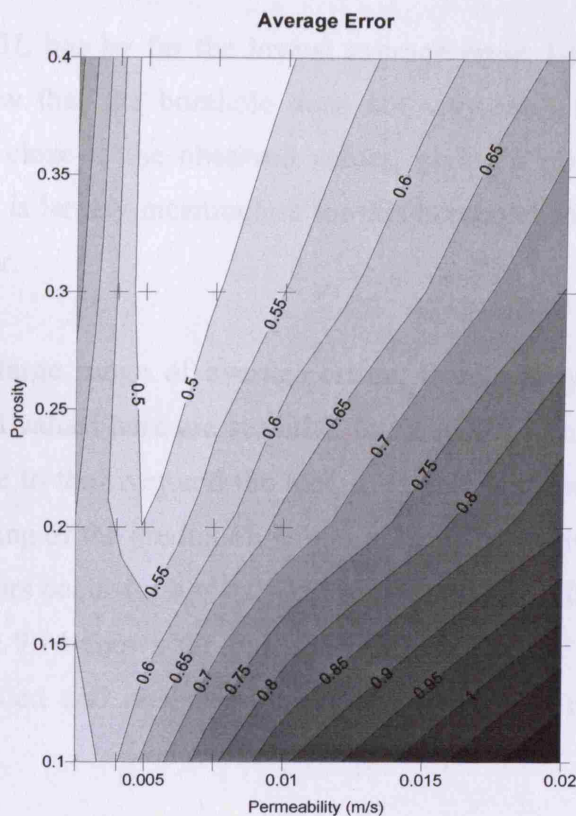


Figure 9.12: - Average error for all boreholes as a function of porosity and permeability.

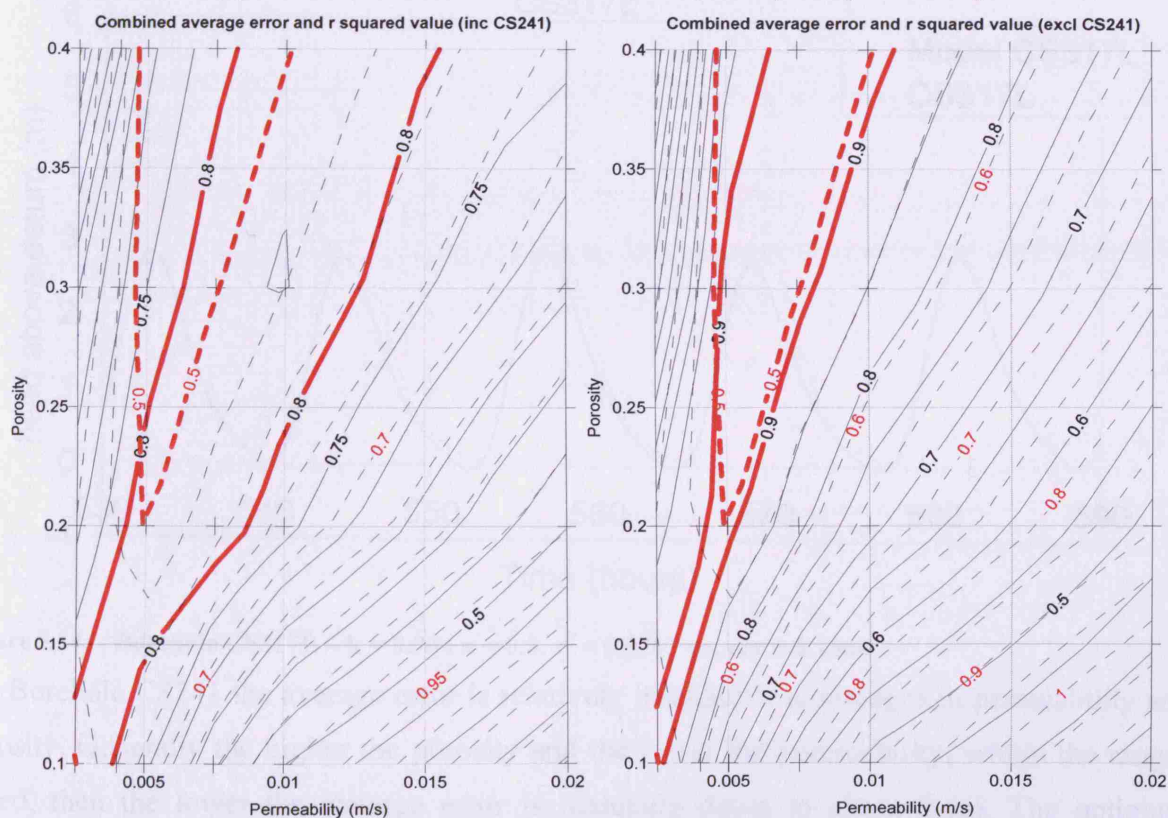


Figure 9.13: - Average error and average r^2 value as a function of porosity and permeability. Solid contours for r^2 value, dotted contours for average error. Red contours indicate 0.5m error, and 0.8 r^2 for graph including CS241 (left), and 0.9 r^2 value for graph excluding CS241 (right).

9.4.4 Optimum parameters

It can be seen that CS313L has by far the lowest average error. Looking at the time series graphs, these results show that the borehole does not vary with the tide, and the model prediction is consistently close to the observed values, giving a minimum average error of about 0.03m. The r^2 value is largely meaningless for this borehole. Most of the scenarios give an acceptable level of error.

Borehole CS317L has a large range of average errors, from nearly 1.7m down to 0.14m, showing that the modelled values here are sensitive to changes in permeability and porosity. This borehole is very close to the river and the measured values show a large tidal influence. Hence a small error in timing of the prediction will be magnified to give a large average error. The minimum average errors occur for $k = 0.0025$ and $n = 0.2$, $k = 0.004$ and $n = 0.3$, and $k = 0.005$ and $n = 0.4$. Figure 9.14 shows the plot for $k = 0.004$ and $n = 0.3$, illustrating good agreement between modelled and observed results. The optimum r^2 values are found for similar conditions.

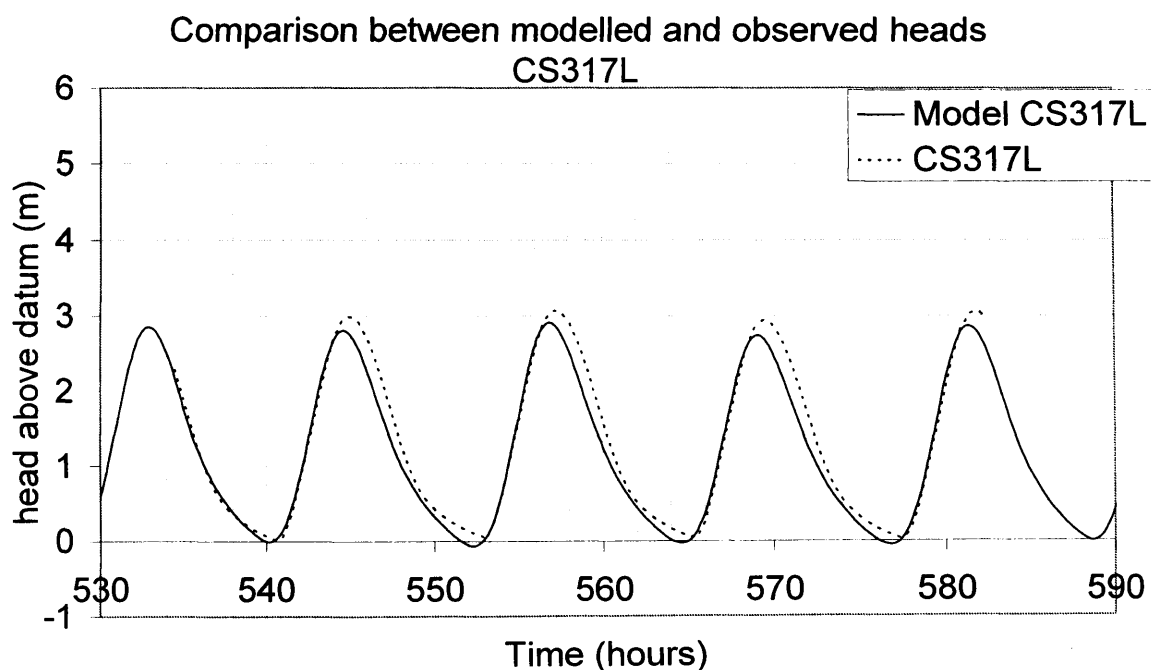


Figure 9.14: - Borehole CS317L – $k = 0.004$ $n = 0.3$. $r^2 = 0.9709$ av. err = 0.1664

For Borehole CS241 the average error is relatively insensitive to changes in permeability and porosity. Generally the higher the porosity and the lower the permeability, within the ranges tested, then the lower the average error is; reducing down to about 0.4m. The optimum permeability and porosity for the r^2 values occurred around $k = 0.01$ and $n = 0.2$, as shown in Figure 9.15.

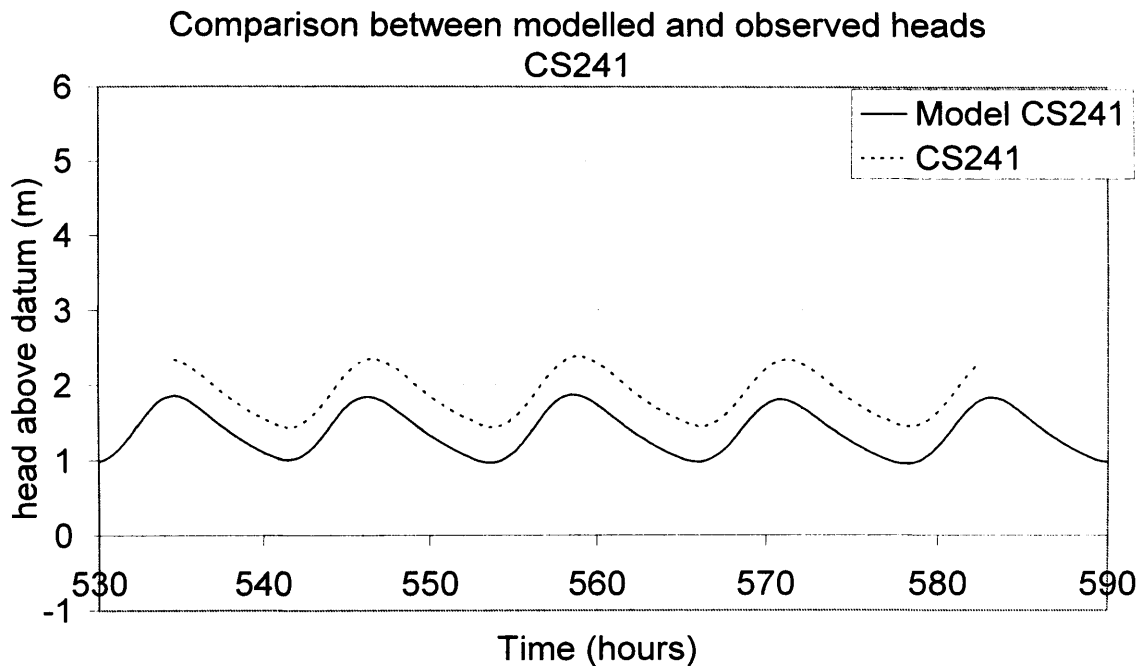


Figure 9.15: - Borehole CS241 at $k = 0.01$ $n = 0.2$. $r^2 = 0.9791$ av. err = 0.4290

Borehole CS238A shows a greater sensitivity than CS241, although for this borehole the average error may be misleading. With a permeability of 0.005 m/s and a porosity of 0.2, the average error is low at 0.3778m. At $k=0.01$ and $n=0.2$, the average error is higher at 0.5660m but visually the fit is somewhat better (see Figure 9.16 and Figure 9.17). The measured values show flattened troughs, probably indicating the borehole is more connected to the tidal waters than its position alone indicates even though it is already very close to the river. The tidal elevation in the river will also have a similar flattened trough. Generally the head elevations are under-predicted using the model, again indicating an additional connection to the river in the actual borehole.

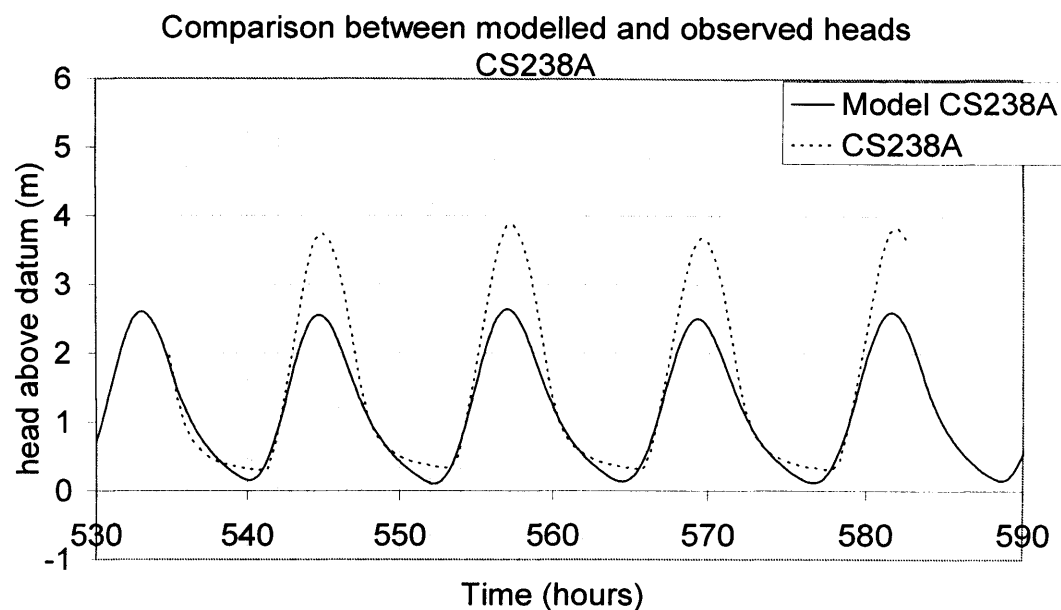


Figure 9.16: - Borehole CS238A at $k = 0.005$ and $n = 0.2$. Average error = 0.3778

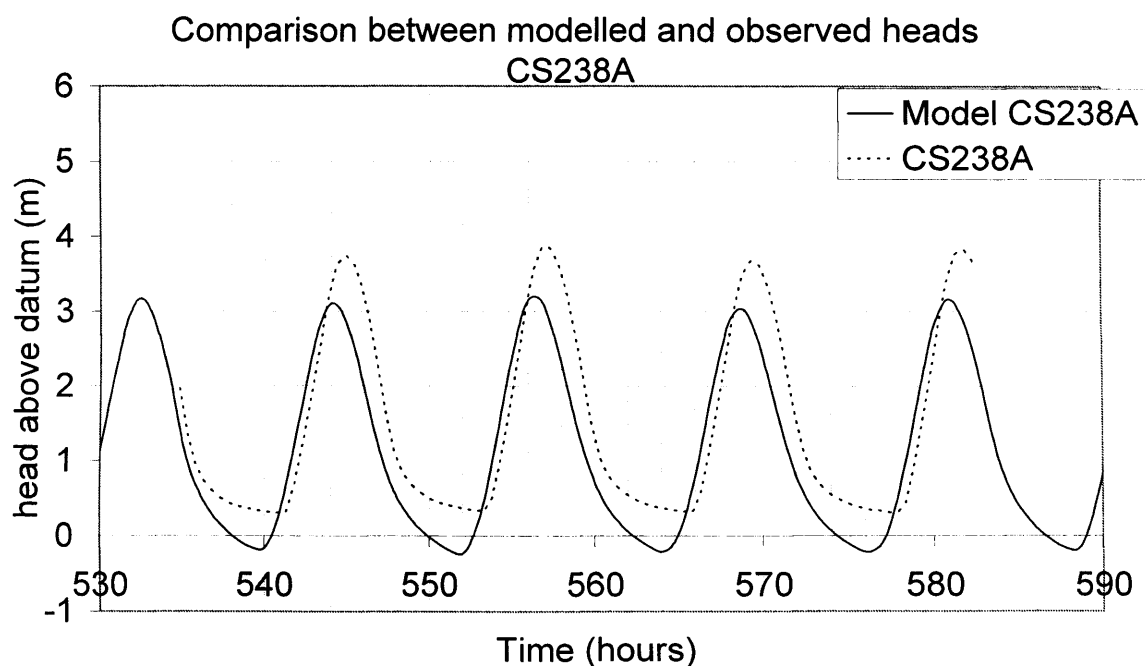


Figure 9.17: - Borehole CS238A at $k = 0.01$ and $n = 0.2$. Average error = 0.5660

Borehole CS217 has a minimum average error of approximately. 0.7m. The observed values flatten off at the bottom of the troughs as for the borehole CS238A, probably because, as for CS238A, the borehole CS217 is adjacent to the river bank.

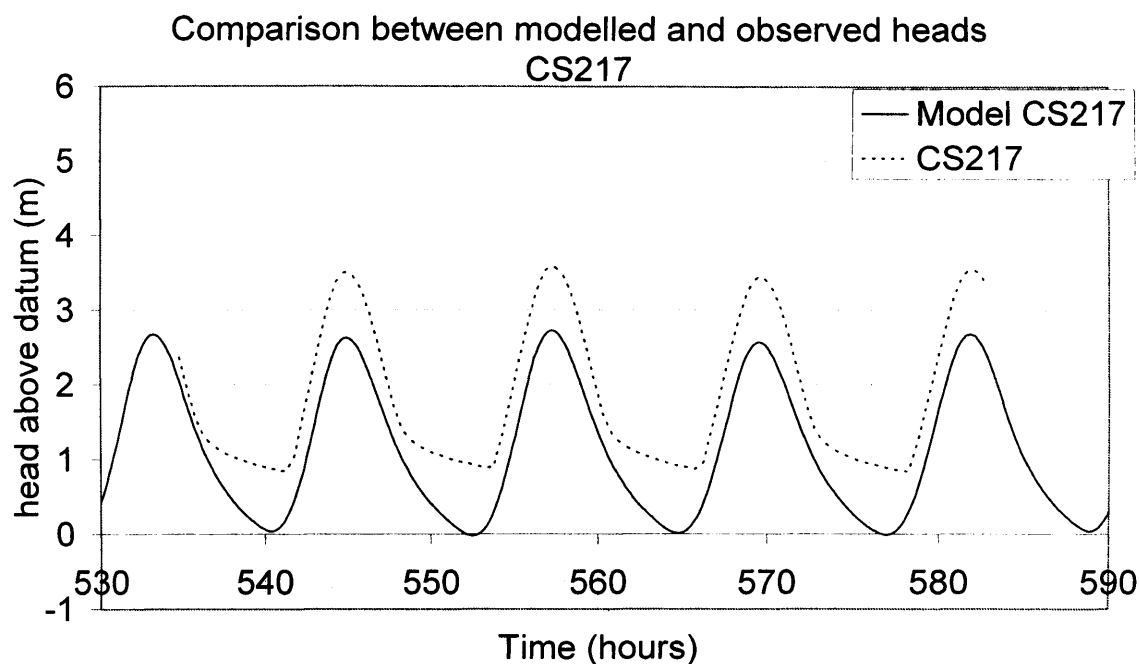


Figure 9.18: - Borehole CS217 - $k = 0.005$ and $n = 0.3$

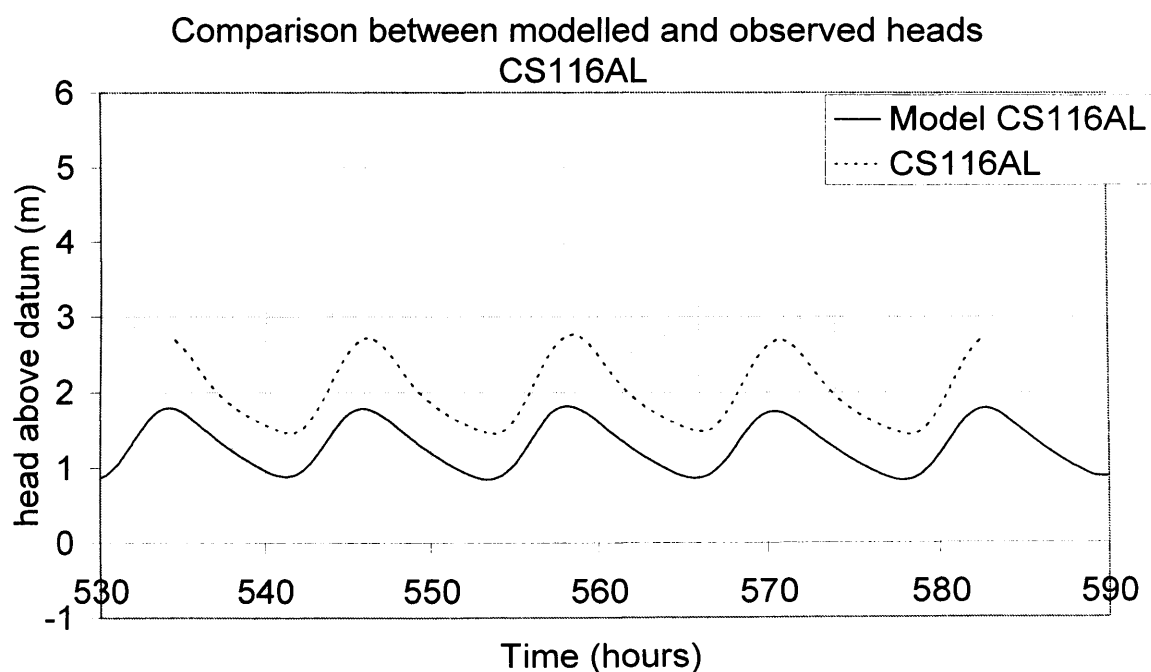


Figure 9.19: - Borehole CS116 at $k = 0.005$ and $n = 0.2$

Figure 9.13, which shows the average error and average r^2 values on the same axes, can be used to find an optimum permeability and porosity for all the boreholes. The red contour lines on the figure indicate the 0.5 m average error, and 0.8 r^2 values. Where the areas surrounded by the red contours overlap, it was considered that the model was performing fairly accurately (i.e. with less than a 0.5m average error, and an r^2 value greater than 0.8). It is clear that based

on this analysis, the estimated permeability and porosity lie within a specific range. The performance is much better if the r^2 values for CS241 are not included, but there does not seem to be a physical reason to disregard these values, since the borehole is in the correct location and the data is correctly aligned. So, including the CS241 data, an optimum point within the likely range of porosities (0.15-0.35) was chosen as $k = 0.006$ m/s and $n = 0.26$. The model was run once more with these settings. The results are shown in Figure 9.20.

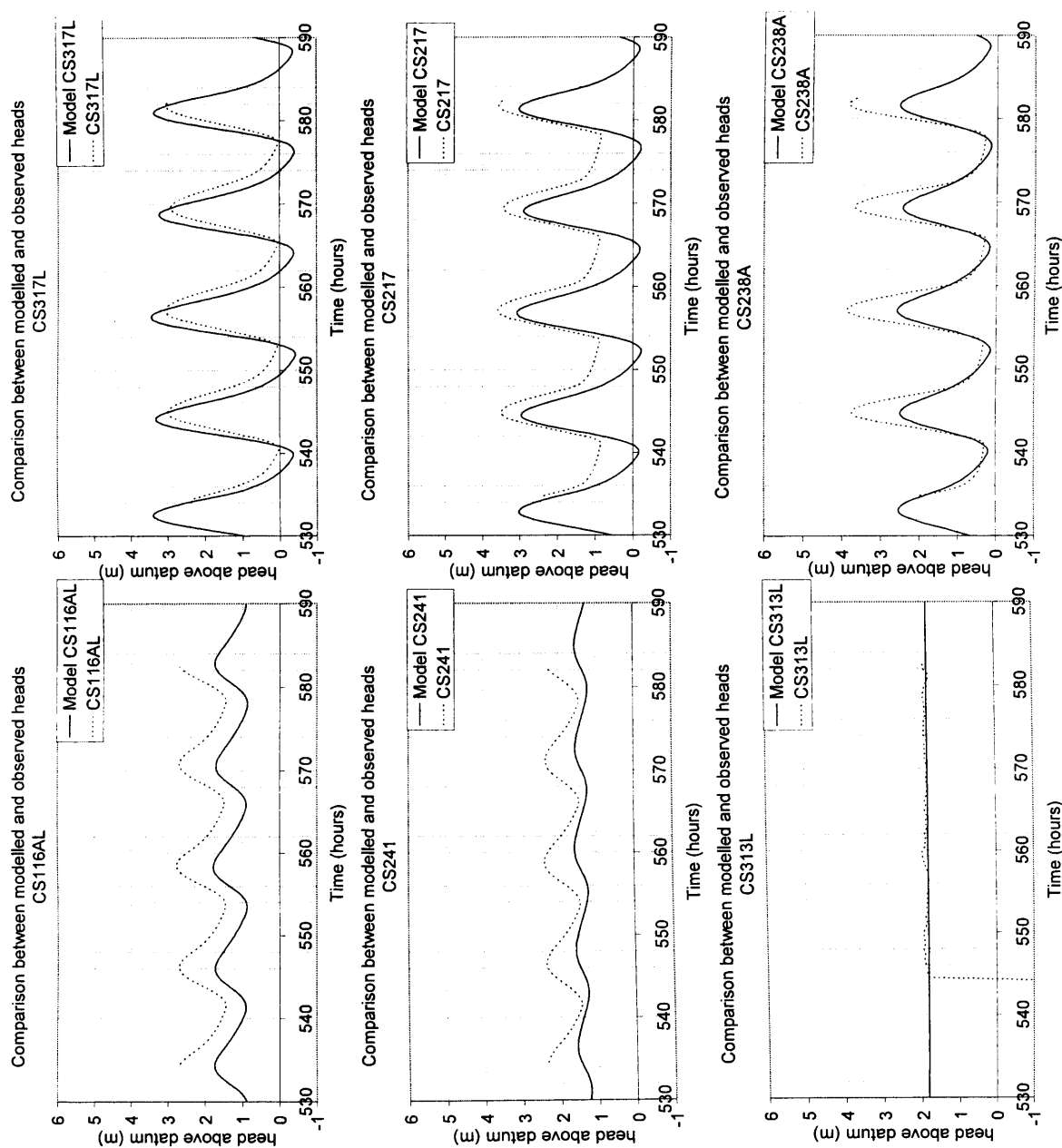


Figure 9.20: - Modelled and Observed head time series for $k = 0.006$ and $n = 0.26$

Scatter Comparison of Boreholes k 0.006 p 0.26

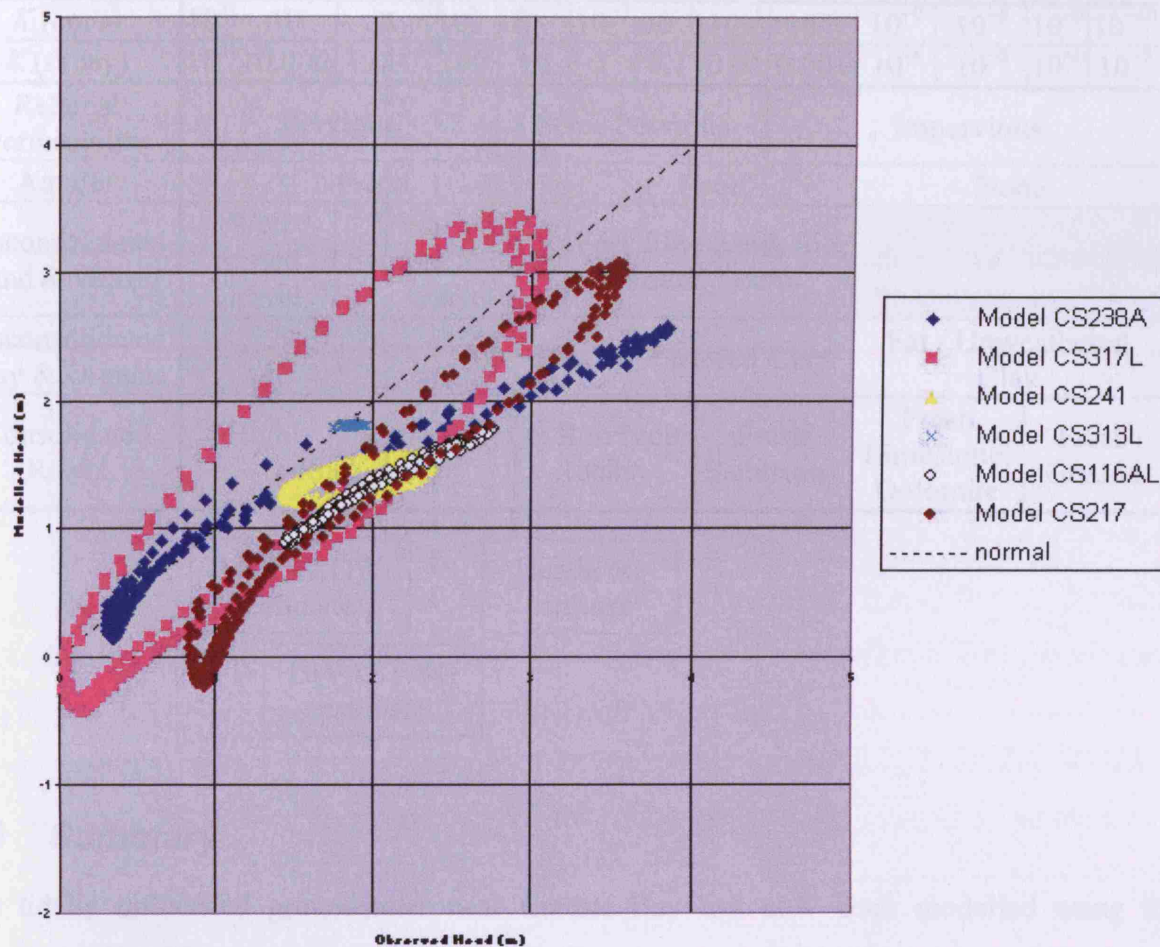


Figure 9.21: - Scatter graph of modelled against observed values for test boreholes. Permeability 0.006 Porosity 0.26

Using DIVAST-SG to estimate the parameters, an estimated conductivity of between 0.005 and 0.01 m/s was found. The fit between modelled and observed data deteriorates rapidly below a conductivity of 0.005 m/s. Above 0.005 m/s and below 0.01 m/s the fit between the data is good, and is improved by increasing the porosity. Above 0.01 m/s, the fit can only be made acceptable by increasing the porosity above 0.4, which was considered too high for a gravel aquifer.

Table 9.4: - Table of saturated hydraulic conductivity (K) values found in nature. Values are for typical fresh groundwater conditions — using standard values of viscosity and specific gravity for water at 20°C and 1 atm. (Bear 1972).

and 1 atm. (Bear 1972).													
K (cm/s)	10^2	10	1	10^{-1}	10^{-2}	10^{-3}	10^{-4}	10^{-5}	10^{-6}	10^{-7}	10^{-8}	10^{-9}	10^{-10}
K (ft/day)	10^5	10,000	1,000	100	10	1	0.1	0.01	0.001	10^{-4}	10^{-5}	10^{-6}	10^{-7}
Relative Permeability	Pervious				Semi-Pervious				Impervious				
Aquifer	Good					Poor				None			
Unconsolidated Sand & Gravel	Well Sorted Gravel	Well Sorted Sand or Sand & Gravel				Very Fine Sand, Silt, Loess, Loam							
Unconsolidated Clay & Organic					Peat		Layered Clay		Fat / Unweathered Clay				
Consolidated Rocks	Highly Fractured Rocks				Oil Reservoir Rocks		Fresh Sandstone		Fresh Limestone, Dolomite		Fresh Granite		
</													

9.5 Summary

The tidally influenced groundwater near Cardiff Bay has now been modelled using the extended DIVAST-SG code. Surface topography data was obtained and transformed to a model grid and geological data was interpolated to the same model grid. The boundary conditions were set at the edges of the model domain, and the model was run for a variety of parameter scenarios. An extensive parameter optimisation study was carried out and the optimum permeability and porosity were found to lie within the ranges shown in Figure 9.13. Representative values were chosen as a permeability of 0.006 m/s and a porosity of 0.26, with model runs being undertaken for these values to show the extent of the fit between modelled and measured values.

CHAPTER 10 DISCUSSION AND CONCLUSIONS

10.1 Introduction

Chapters 2, 3, 4 and 5 describe the development of an extended version of the hydrodynamic model DIVAST, named DIVAST-SG (standing for Depth Integrated Velocities And Solute Transport with Surface water and Groundwater). The remaining chapters in this study (6, 7, 8 and 9) test this extended model – using analytical solutions, extensive laboratory scale experiments, and finally a large database of field observations and comparison to an existing groundwater model. This final chapter ties these experiments and validations together to discuss how successful they have been. Detailed discussions of the experiments can be found in the individual chapters, a brief summary for each section is included here for clarity.

10.2 Analytical Validation

The first hurdle any new numerical code must overcome is that of comparison with an independent solution to an identical problem. Analytical solutions provide a definitive answer to simplified scenarios. Although complex mathematics may have to be used to obtain the solution, the process can be peer-reviewed and assessed by completely different methods than a numerical code, providing a truly independent solution. An analytical solution to the groundwater / surface water interaction was found in Cooper and Rorabaugh (1963). Chapter 6 outlines the derivation of the solution and the set-up of the numerical model in order to compare it to the analytical solution.

Comparing two different scenarios and varying the numerical solution by changing the grid size and timestep shows very good agreement between the analytical solution and the numerical model. It was therefore concluded that the numerical model was capable of

accurately solving the groundwater flow equations and simulating a simple vertical groundwater – surface water interface such as that in the analytical solution.

10.3 Laboratory Verification

The next step was to show that the numerical model can accurately predict actual scenarios in addition to analytical solutions. Laboratory scale experiments allow customised scenarios to be constructed with relative ease, as opposed to field data which usually contains unwanted complications in scenarios not ideal for model validation.

Foam blocks were used in a tidal flume in the Hyder Hydraulics Laboratory at Cardiff University to simulate permeable river banks. Several scenarios were tested and the laboratory set-up was modified extensively to work around practical difficulties. Diagrams showing the layout of the flume can be found in Figure 7.19 and Figure 7.20, on pages 128 and 129 respectively.

10.3.1 Water Level Experiments

Water levels in the foam were measured under several scenarios, by the use of wave probes to give continuous readings of water levels. These were periodically calibrated and confirmed by using simple ruler measurements. In the end, steady state water levels were used to check correlation between the numerical model and the physical model. The results to which this section refers can be found in section 7.7 starting on page 128. Detailed discussion of the individual experiments can be found in section 7.7.4.

These experiments were the first test of the extended numerical model against real-life data. The first observations from the experimental work made it clear that laboratory experiments are rarely as simple as originally planned. The smooth groundwater slope envisaged was impossible to obtain in practice and the numerical model itself was invaluable in assessing how the physical model was behaving. After the idea that the groundwater head in the foam followed a smooth slope was abandoned, much better progress was made. Leaving the main model parameters unchanged (permeability and porosity of the foam itself), the numerical model was modified to include joints in the foam of higher permeability than the surrounding foam. Adjusting these joints in the model allowed a much closer match between the numerical predictions and the measured elevations: from an initial 70 mm error (65% of measured value), the adjusted model

reduced the error to 8 mm (7% of the measured value). Figure 10.1 shows the adjusted model water levels in comparison with the measured water levels.

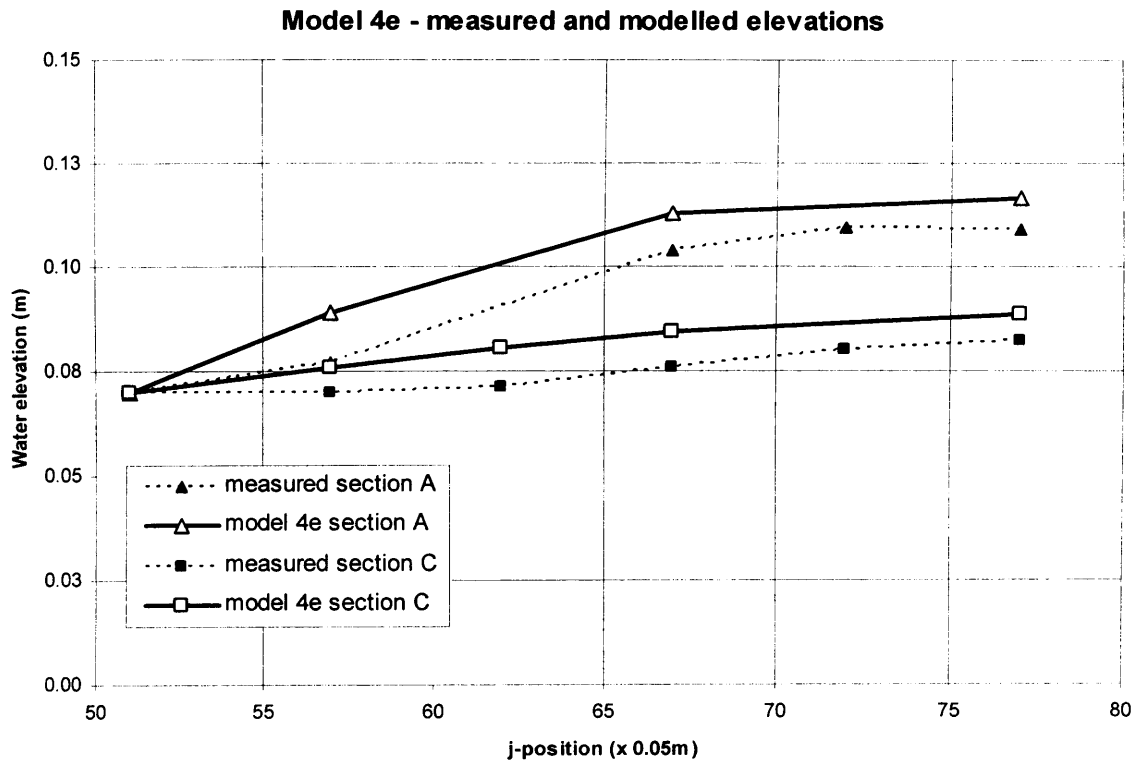


Figure 10.1: - Measured and Modelled Water Elevations after adjustment to the numerical model, to include foam joints.

10.3.2 Tracer Experiments

Rhodamine WT dye was injected into several of the monitoring holes under the same (or similar) flow conditions as the water level experiments. Fluorometers were used in downstream monitoring holes to detect peaks of the dye concentration as it moved through the foam. The point and time where and when the dye first visibly exited the foam into the channel was also recorded. The results to which this section refers to can be found in section 7.8, starting on page 140, and a more detailed discussion of the experiments can be found in section 7.8.5.

Detection of the tracer in the monitoring holes in the foam proved harder than expected, various possible reasons for this are discussed in the relevant chapter. However, the tracer still exited the foam close to the expected locations (e.g. Figure 7.36 or Figure 7.44), and tracer was detected in one of the monitoring holes at the expected time on repeated occasions (Figure 7.51 and Figure 7.52). Tracking the exit plume as it moves downstream,

as an estimate of the water velocity at the edge of the foam also yielded good correlation with the numerical model (Figure 7.33). Despite the baffling non-detection of tracer in the other holes, in the light of these other correctly predicted results it was concluded that the numerical model was predicting the general tracer movement correctly. However, the accuracy is not very high. The numerical model consistently predicts that the dye will exit further upstream than the point observed, although the timing of the exit is generally closely predicted (usually to within 5 minutes, after approximately an hour of flow). This discrepancy is possibly caused by the fact that the water elevations in the numerical model are very slightly higher than those measured (by approximately 5-10 mm), causing the groundwater gradient to be marginally steeper and hence the tracer to take a slightly more direct route towards the channel; causing the modelled exit point to be slightly further upstream than measured. At the time of the water level modelling this difference in elevation was thought not to be significant, but it seems that it has more of an effect than first thought. However the water level model was adjusted using the methods mentioned in Chapter 7, the modelled levels were always slightly higher and it was thought that these last few millimetres difference was probably due to no unsaturated flow being modelled, which is an addition to the model beyond the scope of this study (see section 10.5 on further work). In addition, the flow pattern (in the numerical model) at the joints causes the modelled tracer to exit the foam much sooner than observed and in a fashion that is not observed at all.

Discrepancies like this tend to suggest that the flow pattern in the foam is more complex than the numerical model predicts. Certainly, the flow pattern at the joints between the foam blocks is very difficult to model with a broad surface water / groundwater model such as the one in this study. Situations such as glued joints between foam blocks are not what the model has been designed for and hence these are unlikely to be represented accurately in the model. To avoid this obvious shortcoming, the tracer experiments were mostly carried out within the compass of one foam block, but of course the joints between the blocks do have an effect on the surrounding foam. Adjusting the numerical model to model the joints allows the water levels to be predicted relatively well, which in turn allows the general movement of the tracer to be predicted, but predictions in close proximity to the joints are hampered by the method of modelling these joints.

This highlights a shortcoming in the laboratory set-up, rather than the numerical model. In attempting to create a simple laboratory experiment in order to test the numerical model, a far more complex scenario was inadvertently created, with unsaturated flow and seepage along joints – factors which are not included in this numerical model. While it has been possible to adapt the model to represent the physical set-up, this actually shows the flexibility of the model rather than the efficacy of the laboratory set-up. Nevertheless, it was regarded that the numerical model performed well once calibrated with the water levels.

10.4 Modelling of Cardiff Bay

The field data available for the groundwater under Cardiff, collected before and after the construction of Cardiff Bay Barrage, should be considered as an excellent resource for research. Much of it is unused, perhaps because of the amount of processing needed to make it ready for use in model calibration. Section 8.2 describes how one month's worth of this data was prepared for use as field observations in model calibration, in itself a significant amount of work. The result was a dataset of 83 boreholes for the gravel aquifer under Cardiff, with water elevations given every 2 minutes for the entire month of July 1999. This can be found on the Appendix CD^a. The field data was used as a benchmark to test an existing groundwater numerical model (MODFLOW) and the new extended numerical model DIVAST-SG.

Before the MODFLOW model was created, the boundary conditions had to be determined. Because the only tidal data available was from a geographical location outside Cardiff Bay, a 'premodelling model' had to be used in order to determine the tidal conditions inside the Bay. The existing DIVAST model was used for this, and the process is described in section 8.3.2. The premodelling showed that there was no significant time delay between the tidal water levels outside Cardiff Bay and those at the mouth of the river Taff, where the boundary to the smaller local model was to be. However, the river flow and the bed elevation of the river affected the tidal low water elevation at this point.

^a Database filename D:\Cardiff Bay Borehole Data\Cardiff - Groundwater level in Gravels - July 1999.xls

10.4.1 MODFLOW modelling

The boundary condition was determined in this way for the edge of the model, but since MODFLOW has no surface water modelling capabilities, there was no way of varying this boundary condition along the line of the river – as the bed elevation increases, the lower limit of the tidal boundary condition increases. This boundary condition was defined in sections via a laborious process of extrapolation and inspection of nearby groundwater observations, as section 8.3.3 describes. The other boundary conditions were defined in more conventional fashions.

The estimate of the conductivity of the gravel aquifer from Heathcote et al (2003) was used as a starting point for the model parameters, and the first model runs were used to define the initial heads for this transient simulation. Subsequent runs were undertaken with modified parameters to obtain a better fit with the observed data, both manually and using parameter estimation software. A good fit with the observed data was arrived at with the parameters of 0.01 m/s for hydraulic conductivity and between 0.08 and 0.16 for porosity. Running the model with an additional confining layer of alluvium made little difference to the parameter estimates. Heathcote's estimate was a hydraulic conductivity of 0.000579 m/s, two orders of magnitude lower than the MODFLOW estimate – although Heathcote acknowledges that the hydraulic conductivity pumping tests in the gravels were complicated by the tidal fluctuations themselves.

The fit between the modelled and observed data was good, considering the lengthy and laborious set-up of the model. Modelling a river boundary in the version of MODFLOW used required a lot of effort and a considerable amount of educated guesswork to define the boundary conditions. It would be far simpler if the surface water conditions could be modelled within the model itself rather than defining arbitrary sections as was done here. It was this that was attempted with the DIVAST-SG model.

10.4.2 DIVAST-SG modelling

The same field data was used, but this time the extended DIVAST-SG model was used to model both the river and the groundwater adjacent to the surface water. Whereas Visual MODFLOW has a commercial graphical user interface (GUI) to allow the domain to be set-up, DIVAST-SG has a simple text-file set-up. ArcGIS was used to facilitate the domain set-up as described in Chapter 9. The boundary conditions were much simpler to define –

the same conditions as in the MODFLOW model were used for the northern and western boundaries. The river Taff was simply assigned a flow at the northern boundary ($9 \text{ m}^3/\text{s}$) and the pre-modelled tidal boundary at the southern end. The elevations in the river were then calculated continuously in the model itself, rather than assigned as discrete boundary conditions.

While the boundary conditions were far simpler to define in the integrated model than the MODFLOW model, other areas of the model set-up took longer. The lack of a customised GUI for DIVAST-SG meant that ArcGIS was used instead, which was efficient, but without it the domain set-up would be time consuming. In addition, the initial heads were harder to obtain as a long run time was required for the model to reach equilibrium. The addition of a hotstart facility allowing DIVAST-SG to be started from a previous run was a vital addition to the code, without which the initial heads could not be incorporated into the model.

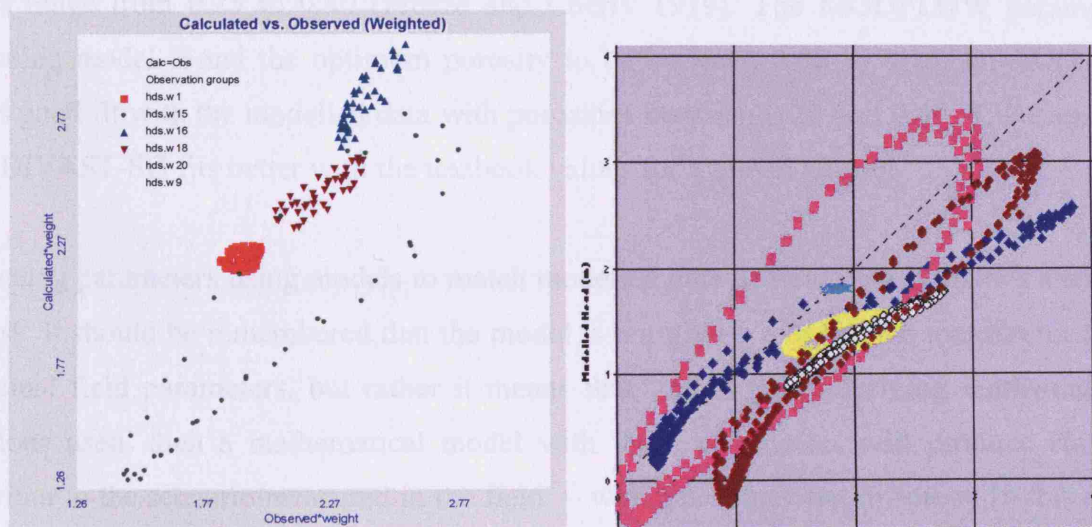


Figure 10.2: - comparison of modelled and observed heads for MODFLOW and DIVAST-SG models.

The DIVAST-SG model of Cardiff Bay was adjusted manually to perform a similar parameter estimation. A suite of 24 different parameters settings was run and visual plots made to assess the fit of the modelled data with the observed data. The fit between the modelled and observed data was measured by the r^2 value and the average error. Optimum parameters were determined as 0.006 m/s for hydraulic conductivity and 0.26 for porosity – the average error was less than 0.5m and the r^2 value was greater than 0.9 when using these parameters. Figure 9.21 shows the scatter graph of measured against modelled water

elevations for these parameters. In comparison with Figure 8.18 showing the same plot for the optimum parameters for the MODFLOW model the fit is of a similar level of accuracy. Reduced images of these figures are included in Figure 10.2.

10.4.3 Comparison

Table 9.4 shows the estimated hydraulic conductivity for MODFLOW, DIVAST-SG and the Heathcote study. These estimates initially appear widely disparate, but when it is considered that hydraulic conductivity in rocks and soils varies from 1 m/s (highly fractured rocks) to 10^{-12} m/s (fresh granite or fat clay) (Bear 1972), then these three estimates of 1×10^{-3} m/s (MODFLOW), 6×10^{-4} m/s (DIVAST-SG), and 6×10^{-5} m/s (Heathcote), seem relatively close. All three estimates fall within the range expected for a gravel aquifer so it is difficult to say which is closer to reality. Heathcote acknowledges that the field estimate was complicated by the tidal fluctuations in the aquifer, and by using those tidal fluctuations in comparison to the modelling studies, slightly higher estimated conductivities were obtained. Heathcote provides no estimate of porosity, but published values range from 0.25 to 0.40 (Freeze and Cherry 1979). The MODFLOW parameter estimation model found the optimum porosity to be between 0.08 to 0.16. DIVAST-SG shows good fit with the modelled data with porosities between 0.20 and 0.40. The estimate from DIVAST-SG fits better with the textbook values for a gravel aquifer.

Estimating parameters using models to match modelled data to field data is always a tricky process. It should be remembered that the model is not giving a definitive measurement of the actual field parameters, but rather it means that ‘given the underlying mathematical equations used, then a mathematical model with these parameters will produce similar behaviour to the scenario measured in the field’ – which is somewhat different. In this case the parameters that allow the DIVAST-SG to fit the measured data best are closer to the published (porosity) and measured (conductivity) parameters than those that allow the MODFLOW model to fit the measured data.

While the boundary conditions were far easier to define in the DIVAST-SG model (as was the intention), this ease of modelling was counteracted by the lack of a good GUI for DIVAST-SG so in actual fact the time saved on the boundary condition set-up was probably spent on the defining the domain. However, what the results do show is that the new extended model can simulate field data involving surface-water and groundwater

interactions, just as easily as an established groundwater code. For any situations where the surface water boundary conditions are more complex e.g. a flood wave in the river, or where the water bodies under investigation are surface water bodies, e.g. groundwater contributions to lakes or rivers, then the new model would be far easier to use than the MODFLOW. Even with the scenario modelled here, (when it was shown that it was possible to model it with an established groundwater code), the main advantage MODFLOW had was the visual interface and parameter estimation software – both commercial additions to the numerical model. The focus during this project has been on the post-processing visualisation for the new model, rather than the pre-processing set-up. DIVAST-SG can output data in the traditional text-based manner, but mostly during this project the data was output to Tecplot format, which was used for the visualisations and animations. This was an important means of understanding the model output and speeded up the interpretation process. Without MODFLOW's commercial GUI and PEST software it would have been impractical to use MODFLOW to model this scenario. If DIVAST-SG had a GUI and was linked to parameter estimation software, then this advantage would be negated, and for this scenario DIVAST-SG would be a better choice for modelling surface-water / groundwater interactions in a 2-D plane, and certainly the better choice for concurrent modelling of an estuary or complex water body in the same model as groundwater.

10.5 Further Work

10.5.1 3-D layered model

Figure 10.3 shows a schematic of the model development. The original DIVAST model modelled just surface water in 2-D, allowing complex water bodies to be modelled (e.g. estuaries, coastal areas and large rivers), but no groundwater. Then the model was extended sideways (while maintaining a single layer approach) to include groundwater horizontally adjacent to the surface water. The combined surface-water – groundwater model was then extended downwards by allowing layers to be defined and defining seepage relationships between the layers (see Chapters 3, 4 and 5). The model used in the Cardiff Bay model is the 3-D layered DIVAST-SG, but only one layer is actually used, so the model remains a 2-D model. At this point, although the equations and code are all in place, the 3-D layered model has not been rigorously tested. The multi-layer capability was not required for the studies carried out in this thesis. The analytical verification used was only for the 2-D

situation where the aquifer is horizontally adjacent to a surface water body. The laboratory set-up was far more suited to the single layer approach, and the Cardiff Bay scenario was easily represented in this fashion too, especially as additional confining layers in MODFLOW made little difference to the parameter estimation. During the model development it was envisaged that the 3-D capability would be required to model field sites such as the Cardiff Bay but in the end it was more than enough work to test the 2-D extension of the code into adjacent groundwater, and the 3-D capability was unnecessary for the Cardiff Bay scenario.

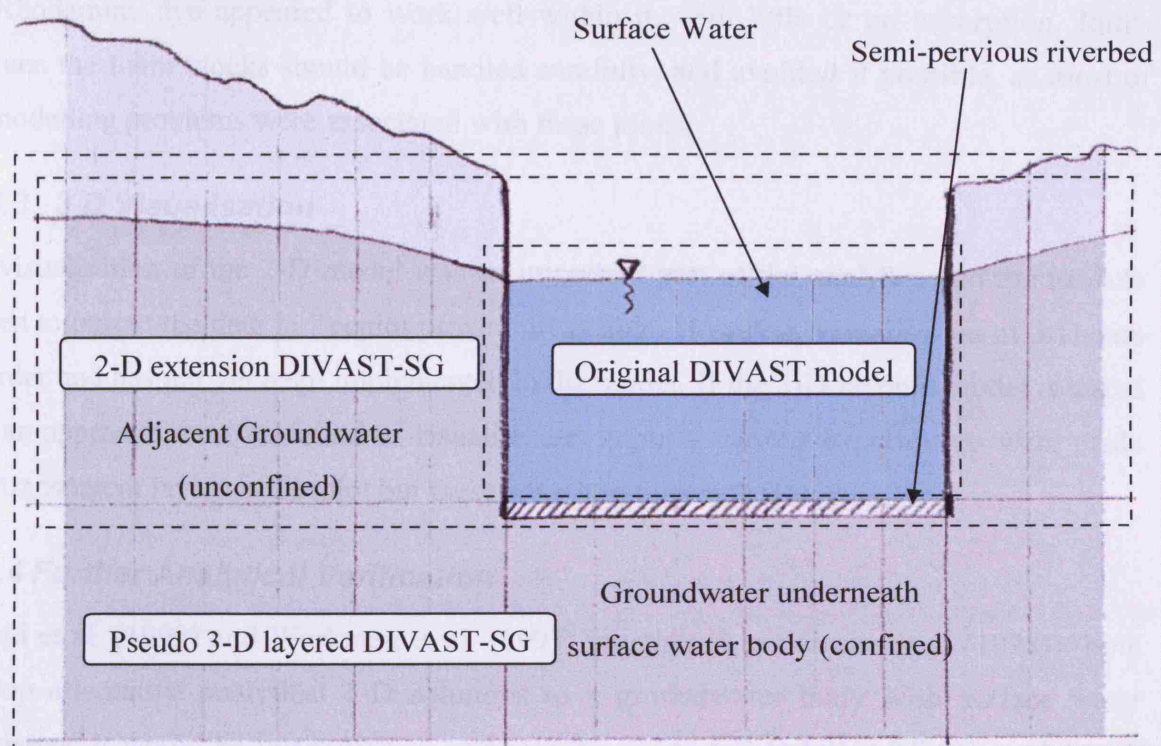


Figure 10.3: - Current state of model development

Therefore, the main area of further work that is suggested is to fully test the layered 3-D model. As noted in Squillace (1996), flow through the river bottom can be a significant portion of the total bank storage when the river is wide and shallow. This could account for the difference between the DIVAST-SG and MODFLOW estimates of the Cardiff gravel aquifer conductivity, even though the Taff is relatively narrow as rivers go – MODFLOW is essentially modelling flow into the aquifer through the bed of the river (in this case without any low conductivity riverbed), whereas DIVAST-SG is essentially modelling flow into the aquifer through the banks of the river, because of the single-layer approach. Using

the multi-layered code would allow a low-conductivity riverbed to be included (as outlined in Chapter 3), and flow through the bed into the aquifer would be included. Since the Taff is not particularly wide, it perhaps would not make a large difference, but the possibility would be worth testing.

10.5.2 Laboratory Foam

Further laboratory work could valuably be carried out using the foam, if a similar flume is available. Now that the pitfalls of using the foam are known, experimental progress would be much quicker. The foam has the advantage of high permeability and light weight, and the Rhodamine dye appeared to work well within it, with little or no adsorption. Joints between the foam blocks should be handled carefully, and avoided if possible, as most of the modelling problems were associated with these joints.

10.5.3 3-D Visualisation

The visualisation of the 2-D model was an important part of the analysis, and the module written to output the data in Tecplot proved invaluable. However, visualisation of 3-D data is harder and has not yet been implemented in the model. If the 3-D layered model is tested then an approach must be found to visualise the output – various experiments were made with transparent layers in Tecplot but these were less than satisfactory.

10.5.4 Further Analytical Verification

Ostfeld et al. (1999) and Workman et al. (1997) (continued in Serrano et al (1998)) both develop alternative analytical 1-D solutions to a groundwater body with surface water boundaries. It would be instructive to compare the existing 2-D DIVAST-SG model with these solutions, particularly Ostfeld, which has already been compared to MODFLOW. In addition, if the 3-D layered version of DIVAST-SG is furthered, then a new analytical solution would be required to verify the equations are performing as expected. Boufadel, and Peridier (2002) could be used in this way for a confined aquifer situation. The 3-D model could be set up and compared to conditions A,B,C and D in Rushton (2007).

10.5.5 Unsaturated Flow, Seepage Faces and Recharge

If the model is to be used on a smaller scale than the Cardiff Bay study, then unsaturated flow in the groundwater will become important. The water table in groundwater is often thought of as being a definite level, as when a well is dug, water will rise to a certain height. But in reality, water is stored in the pores of the aquifer even above this saturated

level, affecting seepage and wetting and drying as water levels go up and down. Not many coupled models include unsaturated flow (see Table 2.1), but it is becoming increasingly recognised as significant to storage and run-off processes and should be considered as a valuable addition to the code if DIVAST-SG is developed further.

Similarly seepage faces, where groundwater exits a vertical face and trickles down, are impossible to model with a 2-D code, and hence are unable to be included in the current model – although with the 3-D layered code it should not be too hard to implement them.

A simple rainfall recharge addition is missing in DIVAST because of the negligible effect of rainfall on surface waters, but it will become more important as more groundwater is modelled – this can be added very simply in another section of the input file, and by including the recharge \times cell area in the continuity equation. An infiltration / runoff routine could also profitably be added if large areas of land are modelled.

10.5.6 Solute Transport in Groundwater

The equations for solute transport were not modified in this study – if modelling of solute movement in groundwater is undertaken then the transport equations will need to be examined and modified if necessary, particularly the approach to diffusion and dispersion in the groundwater cells.

10.5.7 Grid size and timestep

As larger areas of groundwater are modelled, the fine grid resolution used in surface water problems becomes less and less necessary. A significant efficiency improvement to the groundwater facility would be to allow the coarsening of grid cells when groundwater heads do not vary particularly fast – this could be done manually or on an adaptive grid approach, amalgamating groups of cells when the model detects little change in head with time. If the grid size is changed, then the timestep may be changed as well – it would be advantageous to allow multiple surface water and highly connected groundwater timesteps for each distant groundwater timestep, as is done in several of the models reviewed in Chapter 2 .

10.5.8 Visual Interface

As mentioned in the comparison between MODFLOW and DIVAST-SG, the lack of a visual interface to set up the model in DIVAST-SG is severe disadvantage. Attempts have been made before to add a visual set-up interface, but as the numerical model evolves

constantly it is almost always out-of-date by the time work is completed. Using ArcGIS to create the domain grids and georeferenced data speeded up the process – but if the model is developed further it will quickly lag behind competitors without a customisable interface that can evolve with the numerical model itself. In order for this to happen the coding needs to be centralised and a definitive version of the DIVAST or DIVAST-SG code created, to which modules can be added without disrupting the main central code, much as MODFLOW is designed. This is perhaps why so many extra modules have been written for MODFLOW, it is inherently adaptable. Development of DIVAST should follow a similar line.

10.6 Conclusion

The numerical model DIVAST-SG has had three trials performed upon it in this thesis: analytical verification, laboratory validation, and comparison with an established code and field data. In all of them it has performed well, and achieves a similar level of accuracy to MODFLOW when applied to field data. It can therefore be concluded that the existing surface water model DIVAST has been successfully extended to model horizontally adjacent groundwater in addition to the surface water. This thesis also describes and implements a method for extending this further to model groundwater in several layers beneath surface water bodies, although this aspect has yet to be tested.

Several novel approaches have been used in this work. The method by which DIVAST was extended means that the model solves both the groundwater and surface water equations in the same solver, rather than coupling two models together as is traditional. In addition, porous foam was utilised in the laboratory study, a novel approach which yielded good results after overcoming the practical difficulties of an untried process. The data for the field study was also extensively processed to produce a highly detailed groundwater dataset for future studies.

The outcome of this work is the production of a new version of the well-regarded DIVAST hydrodynamic numerical model. The new version is known as DIVAST-SG (Depth Integrated Velocities And Solute Transport with Surface water and Groundwater) and can simulate interactions between surface water and groundwater in the 2-D plane, in addition to the facilities of the original code. It has successfully been tested against analytical solutions, laboratory studies and field data, and also compared to an existing groundwater code, when it successfully modelled a gravel aquifer adjacent to a tidal water body. An extensive framework has been laid for continuing this work in order to produce a pseudo 3-D surface-water / groundwater code. In addition, novel techniques have been pioneered in the laboratory study, where valuable lessons were learnt about using open cell foam to simulate porous media. A highly detailed dataset of groundwater data was also produced in the course of the work, for the gravel aquifer underneath the city of Cardiff.

REFERENCES

- Bear, J. (1972). **"Dynamics of Fluids in Porous Media"**, American Elsevier Publishing Company, Inc.
- Boufadel, Michel C., and Vallorie Peridier (2002) **Exact analytical expressions for the piezometric profile and water exchange between stream and groundwater during and after a uniform rise of the stream level.** Water Resources Research, Vol. 38, No. 7
- Bras, R. L. (1990). **"Hydrology - An Introduction to Hydrologic Science"**, Addison-Wesley Publishing Company.
- BS1377 (1990). **"BS 1377 : Part 5 : 1990 Determination of permeability by the constant-head method"**, British Standards.
- Butler, David and John W. Davies (2000) **Urban Drainage** Taylor & Francis 2000 ISBN 0419223401
- Calver, A. (2001). **"Riverbed permeabilities: Information from Pooled Data."** Ground Water **39**(4): 546-553.
- Cartwright, N., O. Z. Jessen and P. Nielsen (2006). **"Application of a coupled ground-surface water flow model to simulate periodic groundwater flow influenced by a sloping boundary, capillarity and vertical flows."** Environmental Modelling & Software **21**: 770-778.
- Chen, X. and X. Chen (2003). **"Stream water infiltration, banks storage, and storage zone changes due to stream stage fluctuations."** Journal of Hydrology **280**: 246-264.
- Conant Jr, B., J. Cherry and R. Gillham (2004). **"A PCE groundwater plume discharging to a river: Influence of the streambed and near-river zone on contaminant distributions."** Journal of Contaminant Hydrology **73**: 249-279.
- Cooper, H. H. J. and M. I. Rorabaugh (1963). **"Ground-water Movements and Bank Storage due to Flood stages in Surface Streams"**, U.S. Geological Survey.
- Darcy, H. (1856). **"Les Fontaines Publiques de la Ville de Dijon"**. Dalmont, Paris.
- DHI (2008), Website of DHI Group, Software, Water Resources, MIKE-SHE, <http://www.dhigroup.com/Software/WaterResources/MIKESHE.aspx> accessed 18th Jan 2008.
- Dupuit, J. (1863). **"Études théoriques et pratiques sur le mouvement des eaux"**. Paris, Dunod.
- Ebrahimi, K. (2004) **"Development of an Integrated Free Surface and Groundwater Flow Model"**, Kumars Ebrahimi, Feb. 2004, PhD thesis, Cardiff University.
- EC (2000) **"DIRECTIVE 2000/60/EC OF THE EUROPEAN PARLIAMENT AND OF THE COUNCIL of 23 October 2000 establishing a framework for Community action in the field of water policy"** European Parliament and Council 2000/60/EC
- EDINA (2006). **"Digimap - Ordnance Survey Data Download"**, EDINA.
- EMS. (2002). **"Stream/Aquifer Interaction Package"** Retrieved 03/02/04, 2004, from http://www.ems-i.com/gmshelp/gmsv40help.htm#Numerical_Models/MODFLOW/Packages/Stream-Aquifer_Interaction_Package.htm.
- Ernst, L. F. (1978). Drainage of undulating sandy soils with high groundwater tables. Journal of Hydrology. **39**: 1-50.
- Fairbanks, J., S. Panday and P. Huyakorn (2001). **"Comparisons of Linked and fully coupled Approaches to Simulating Conjunctive Surface/Subsurface Flow and their Interactions"**. MODFLOW 2001 and other Modeling Odysseys.
- Falconer, R. A. (1993). **"An Introduction to Nearly Horizontal Flows"**. Coastal, Estuarial and Harbour Engineers' Reference Book. M. B. Abbott and W. A. Price, E. & F. N. Spon Ltd: 27-36.

- Falconer, R. A., B. Lin, Y. Wu and E. Harris (2001a). **"DIVAST Reference Manual"**. Cardiff, Hydroenvironmental Research Centre, Cardiff School of Engineering, Cardiff University.
- Falconer, R. A., B. Lin, Y. Wu and E. Harris (2001b). **"DIVAST User Manual"**. Cardiff, Hydroenvironmental Research Centre, Cardiff School of Engineering, Cardiff University.
- Fenske, J. P., S. A. Leake and D. E. Prudic (1996). **"Documentation of a Computer Program (RES1) to Simulate Leakage from Reservoirs Using the Modular Finite-Difference Ground-Water Flow Model (MODFLOW)"**, U.S. Geological Survey: 51.
- Fox, G. A. and D. S. Durnford (2003). **"Unsaturated hyporheic zone flow in stream/aquifer conjunctive systems."** *Advances in Water Resources* 26(9 SU -): 989-1000.
- Freeze, R. and J. A. Cherry (1979). **"Groundwater"**, Prentice-Hall, Inc.
- Freeze, R. A. (1972). **"Role of Subsurface Flow in Generating Surface Runoff 1. Base flow Contributions to Channel Flow."** *Water Resources Research* 8(3): 609-623.
- Gunduz, O. and M. M. Aral (2005). **"River networks and groundwater flow: a simultaneous solution of a coupled system."** *Journal of Hydrology* 301: 216-234.
- Heathcote, J. A., R. T. Lewis and J. S. Sutton (2003). **"Groundwater Modelling for the Cardiff Bay Barrage, UK - prediction, implementation of engineering works and validation of modelling."** *Quarterly Journal of Engineering Geology and Hydrogeology* 36: 159-172.
- Hunt, R. (2003). **"Ground Water-Lake Interaction Modelling Using the LAK3 Package for Modflow 2000."** *Ground Water* 41(2): 114 -118.
- Hussein, M. and F. W. Schwartz (2003). **"Modeling of Flow and Contaminant Transport in coupled stream-aquifer systems."** *Journal of Contaminant Hydrology* 65: 41-64.
- Jobson, H. E. and A. W. Harbaugh (1999). **"Modifications to the Diffusion Analogy Surface-Water Flow model (DAFLOW) for coupling to the Modular Finite-Difference Ground-Water Flow model (MODFLOW)"**. Reston, Virginia, U.S. Geological Survey: 59.
- Kadlec, R. H. (1990). **"Overland flow in Wetlands: Vegetation Resistance."** *Journal of Hydraulic Engineering* 116(No. 5): 691-706.
- Kasnavia, T., D. Vu and D. A. Sabatini (1999). **"Fluorescent Dye and Media Properties Affecting Sorption and Tracer Selection."** *Ground Water* 37(3): 376-381.
- Konikow, L. F., D. J. Goode and G. Z. Hornberger (1996). **"A Three-Dimensional Method-of-Characteristics Solute-Transport Model (MOC3D)"**.
- Lin, Y.-C. and M. A. Medina Jr (2003). **"Incorporating transient storage in conjunctive stream-aquifer modeling."** *Advances in Water Resources* 26(9): 1001-1020.
- McDonald, M. G. and A. W. Harbaugh (1988). **"A Modular Three-dimensional Finite Difference Ground-water Flow Model"**, U. S. Geological Survey. *Techniques of Water-Resources Investigations of the United States Geological Survey*, Book 6, Chapter A1
- Merrit, M. L. and L. F. Konikow (2000). **"Documentation of a Computer Program to Simulate Lake-Aquifer Interaction using the MODFLOW Ground-Water flow model and the MOC3D Solute-Transport Model"**. Tallahassee, Florida, U.S. Geological Survey: 146p.
- MP Associates. (2004). Retrieved 16 December 2004, from <http://www.mpassociates.gr/software/environment/modflow.html>.
- NRFA. (2006). **"The National River Flow Archive, Centre for Ecology and Hydrology"** Retrieved 18/9/2006, from <http://www.ceh.ac.uk/data/nrfa/index.html>.
- Ostfeld, A., E. Mazaffar and K. E. Lansey (1999). **"Analytical Ground-Water Flow Solutions For Channel-Aquifer Interaction."** *Journal of Irrigation and Drainage Engineering* 125(4): 196-202.

- Panday, S. and P. S. Huyakorn (2004). **"A fully coupled physically-based spatially-distributed model for evaluating surface/subsurface flow."** *Advances in Water Resources* **27**: 361-382.
- Peaceman, D. W. and H. H. Rachford-Jr. (1955). **"The numerical solution of parabolic and elliptic differential equations."** *Journal of the Society for Industrial and Applied Mathematics* **3**: pp. 28–41.
- Pinder, G. F. and S. P. Sauer (1971). **"Numerical Simulation of Flood Wave Modification Due to Bank Storage Effects."** *Water Resources Research* **7**(1): 63-70.
- Pollock, D. W. (1994). **"User's Guide for MODPATH/MODPATH-PLOT, Version 3: A particle tracking post-processing package for MODFLOW, the U. S. Geological Survey finite-difference ground-water flow model"**, USGS.
- Prudic, D. E. (1989). **"Documentation of a computer program to simulate stream-aquifer relations using a modular, finite difference, ground-water flow model."** 113.
- Prudic, D. E., L. F. Konikow and E. R. Banta (2004). **"A new Streamflow-Routing (SFR1) Package to simulate stream-aquifer interaction with MODFLOW-2000"**. Carson City, Nevada, USGS: 95.
- Querner, E. P. (1997). **"Description and application of the combined surface and groundwater flow model MOGROW."** *Journal of Hydrology* **192**: 158-188.
- Refsgaard, J.C. and Storm, B., (1995). In: Singh, V.P., Editor, , 1995. *Computer Models of Watershed Hydrology*, Water Resources Publications, Englewood, USA, pp. 809–846.
- Restrepo, J. I., A. M. Montoya and J. Obeysekera (1998). **"A Wetland Simulation Module for the MODFLOW Ground Water Model."** *Ground Water* **36**(No. 5): 764-770.
- Rouse, H., Ed. (1950). **"Engineering Hydraulics"**. Iowa, John Wiley & Sons, Inc.
- Rushton, K. R. and S. C. Redshaw (1979). **"Seepage and Groundwater Flow"**, Wiley.
- Rushton, K. R. (2007) **Representation in regional models of saturated river-aquifer interaction for gaining/losing rivers.** *Journal of Hydrology*, Volume 334, Issues 1-2, 20 February 2007, Pages 262-281
- Schlichting, H. (1979). **"Boundary Layer Theory"**. New York, McGraw-Hill Book Co.
- Smith, R. E. and D. A. Woolhiser (1971). **"Overland flow on an Infiltrating Surface."** *Water Resources Research* **7**(4): 899-913.
- Sokrut, N. (2001). **"A distributed coupled model of surface and subsurface dynamics as a tool for catchment management"**, Royal Institute of Technology, Stockholm, Sweden.
- Sokrut, N., J. Motovilov and R. Thunvik (2001). **"ECOMAG-MODFLOW: An example of the integration of surface and groundwater hydrological models."** *MODFLOW 2001 and Other Modeling Odysseys*, IGWMC, Colorado School of Mines and the U.S. Geological Survey. **Vol. 1**: 404.
- Sophocleous, M., A. Koussis, J. L. Martin and S. P. Perkins (1995). **"Evaluation of simplified Stream-Aquifer Depletion Models for Water Rights Administration."** *Ground Water* **33**(4): 579-588.
- Sophocleous, Marios (2002) **Interactions between groundwater and surface water: the state of the science.** *Hydrogeology Journal* Volume 10, Number 1, February, 2002
- Sparks, Tim, Diana Kountcheva, Bettina Bockelmann, Roger Falconer, (2006) **"Physical and Numerical Modelling of Groundwater and Surface-Water Interactions with a Conservative Tracer."** *Proceedings of ISSMGE: 5th International Congress on Environmental Geotechnics* Cardiff, Wales, UK, June 2006
- Squillace, P. J. (1996). **"Observed and Simulated Movement of Bank-Storage Water."** *Ground Water* **34**(1): 121-134.
- Stelling, G. S., A. K. Wiersma and J. B. T. M. Willemse (1986). **"Practical Aspects of Accurate Tidal Computations."** *Journal of Hydraulic Engineering* **112**: 802-817.

- Swain, E. D. and E. J. Wexler (1996). **"A Coupled Surface-water and Ground-water flow model (Modbranch) for simulation of stream-aquifer interaction."** Techniques of Water-Resources Investigations of the United States Geological Survey **Book 6, Chapter A6**.
- Turner_Designs. (2006a). **"Application Support Bulletin 103: Fluorescein and a Fluorometer"**, from http://www.turnerdesigns.com/t2/doc/appnotes/998_5103.html.
- Turner_Designs. (2006b). **"Application Support Bulletin 104: Fluorescent Tracer Dyes"** Retrieved 5/1/2007, 2006, from http://www.turnerdesigns.com/t2/doc/appnotes/998_5104.html.
- Turner_Designs. (2006c). **"Fluorescent Tracer Studies"** Retrieved 5/1/2007, from http://www.turnerdesigns.com/t2/doc/appnotes/998_5121.html.
- Winter, Thomas C., Judson W. Harvey, O. Lehn Franke, William M. Alley, (1998) Ground Water and Surface Water - A Single Resource. U.S. Geological Survey Circular 1139 ISBN 0-607-89339-7
- Workman, S. R., S. E. Serrano and K. Liberty (1997). **"Development and application of an analytical model of stream/aquifer interaction."** Journal of Hydrology **200**(1997): 149-163.

Topography data used in models:

© Crown Copyright/database right 2006. An Ordnance Survey/EDINA supplied service.

INDEX OF FIGURES

Figure 1.1: - Gaining and Losing streams, and illustration of bank storage. (from Winter et al 1998)	10
Figure 2.1 – Pinder and Sauer (1971) model of aquifer-stream interaction.	15
Figure 2.2 – Freeze model. “A 3-D, saturated-unsaturated subsurface flow system with rainfall input, which delivers base flow to a one-dimensional stream channel.” (Freeze 1972)	15
Figure 2.3: - a) Cross-section of an aquifer containing a stream, and b) conceptual representation. (McDonald and Harbaugh 1988).....	16
Figure 2.4: -Schematization in SIMGRO of the hydrological system within a sub-region (modified from Querner 1997).....	19
Figure 2.5: - Interaction between surface and groundwater in four categories. (Querner 1997)	19
Figure 2.6: - Unsaturated zone per land use. Pn, net precipitation; Ps, sprinkling (watering); E, evapotranspiration; V, moisture storage; Qc, upward flux.....	20
Figure 2.7: Vertical Schematic of surface water pathways in wetlands (Restrepo et al. 1998).	22
Figure 2.8: - Schematic of problem solved by Ostfeld (1999).	23
Figure 2.9: - Schematic of DAFLOW-MODFLOW stream layout, showing numbered nodes and branches (Jobson and Harbaugh 1999).....	24
Figure 2.10: - Seepage when aquifer head drops below lake bed, assuming full saturation. (Modified from McDonald and Harbaugh 1988).....	26
Figure 2.11: - ECOFLOW layers schematisation.	28
Figure 2.12: - Adapted from Chen and Chen (2003) - illustrating the concept of maximum storage zone with varying flood durations ($T = \text{flood duration}$).....	29
Figure 2.13: - Seepage from the river is linked directly to the 2-D vertically averaged aquifer below. (Gunduz and Aral 2005)	32
Figure 3.1: - Elemental control volume, surrounded by fluid on all sides.....	37
Figure 3.2: - Elemental volume over complete depth of water.....	38
Figure 3.3: - Elemental volume in a semi-confined aquifer	43
Figure 3.4: - Simple underlying aquifer schematic. A surface water cell is shown above a groundwater cell with no lower conductivity layer between them. L_{be1} is layer base elevation 1, and $surf$ is the ground surface elevation.....	44
Figure 3.5: - Low permeability riverbed schematic. Surface water cell overlying aquifer with low conductivity layer in between.	45
Figure 3.6: - Schematic for seepage between layers.....	46
Figure 3.7: - Elemental volume showing forces acting at faces	48
Figure 3.8: - Schematic for Darcy’s Law.....	52
Figure 3.9: - Darcy’s law in a Confined Aquifer	53
Figure 4.1: - ADI method. The grey variable is known (from previous timestep)	57
Figure 4.2: - Finite difference staggered grid. Adapted from Falconer et. al (2001a).....	58
Figure 4.3: - Flowchart for iteration of seepage and head values.....	71
Figure 5.1: - example boundary condition.	76
Figure 5.2: - Example outfall flows	78
Figure 5.3: - layout of grid cells. i refers to cell and positive side of cell.	81
Figure 5.4: - Visualisation of 'bar.dsg' model from Appendix A (green for land surface, blue for water surface).	81

Figure 5.5: - Defining a constant permeability over the domain. The commands used are in the top left corner, the grid and surface plot show what the code interpolates these commands as.....	83
Figure 5.6: - Defining a permeability that changes in a slope. Definition in top left and surface plot shows the result.....	83
Figure 5.7: - Defining a permeability grid with a peak or similar. Definition at top left; grid and surface plot show result.....	83
Figure 5.8: - Schematic Structure of DIVAST-SG code	84
Figure 5.9: - Possible values for <i>subsurface(i,j,k)</i> array	85
Figure 6.1: - Schematic illustration of aquifer (from Cooper and Rorabaugh 1963)	92
Figure 6.2: - original and adjusted value of theta function	97
Figure 6.3: - Groundwater head using original and adjusted value of phi.....	98
Figure 6.4: - Comparison of analytical result and numerical model - scenario 1	100
Figure 6.5: - Comparison of semi-infinite aquifer equations and finite aquifer equations with a β value of 0.0028.....	101
Figure 6.6: - Effect of changing the grid size on the model.	102
Figure 6.7: - Comparison of analytical solution and numerical model – scenario 2	103
Figure 7.1: - Construction of Tidal Basin at Hyder Hydraulics Laboratory, Cardiff University.....	106
Figure 7.2: - Movable weir on left, perforated inflow pipe, and baffle screen.....	106
Figure 7.3: - Layout of foam blocks in flume and initial set-up of channel.	107
Figure 7.4: - Foam block after cutting (top), and monitoring/injection holes being drilled (bottom).....	108
Figure 7.5: Discs cut from foam.	110
Figure 7.6: - Saturated discs stacked in variable thicknesses in measuring tube (hole drilled in base).....	110
Figure 7.7: Constant head maintained above foam, and flow rate recorded in measuring cylinder below.....	110
Figure 7.8: Hydraulic Gradient x area, against flow, enabling the permeability to be calculated from the gradient of the line.	112
Figure 7.9: - Schematic for permeability test. The depths in two wells in the foam aquifer are measured, while pumping water at a constant rate from one well.	113
Figure 7.10 - Example of iterative predictions of conductivity (Test number 3). Head distribution is varied until the variation in K (dotted line) is a minimum.	115
Figure 7.11: - Flume Design	119
Figure 7.12: - Flume with no water, showing location of injection and monitoring points (A+B).	120
Figure 7.13: - weighted boards to prevent foam rising with the tide.....	120
Figure 7.14: - Plot I – Graph of the numerical prediction of change of concentration of Rhodamine WT with time at point A for 75ml of 1g/l dye injected over two minutes. Plot II – the concentration of Rhodamine WT recorded at point A during physical experiment 4. Plot III – the respective tidal phase.....	123
Figure 7.15: - Injecting the dye.....	124
Figure 7.16: - Inserting and glueing small discs of foam in base of holes	125
Figure 7.17: - Glueing a foam block in place.	126
Figure 7.18: - Diagram showing how foam blocks were glued at joints.	127
Figure 7.19: - New flume setup with water pumped to upper reservoir.	128
Figure 7.20: - schematic diagram of the tidal flume showing labelling of monitoring holes and reference ruler.	129

Figure 7.21: - Interpolated contour plot of measured elevation data in the foam. (i and j units are x 5 cm: the grid size used in the model).....	130
Figure 7.22: - Model results of water elevations for initial run of physical scenario. i and j axes are x5 cm from edge of the model, or grid cell reference.....	131
Figure 7.23: - Measured water elevations (solid) compared to initial modelled elevations (transparent). i and j axes are in x5 cm from edge of the model, or in grid cell reference coordinates.	132
Figure 7.24: - Modelling joints by increased permeability along joints (run 1b).....	134
Figure 7.25: - Modelling joints as combination of open cells and foam (run 2)	134
Figure 7.26: - Model results with open cells at joints (run 3b).....	135
Figure 7.27: - Model results for increased permeability and half open cells (run 4e).....	135
Figure 7.28: - Measured and modelled elevations for cross-section A. j-position is in grid cell reference or x 0.05m from the edge of the model	136
Figure 7.29: - Measured and modelled elevations for cross-section C. j-position is in grid cell reference or x 0.05m from the edge of the model	136
Figure 7.30: - Measured and modelled elevations for both cross-sections and model run 4e.	137
Figure 7.31: - Tracer experiment in progress, showing injection hole, two fluorometer measuring points, wave probes in upper holes, and dye emerging into the channel.	141
Figure 7.32: - Dye emerging from foam at approximate location of cross-section D.	141
Figure 7.33: - Downstream velocity at edge of the foam, measured and modelled.	146
Figure 7.34: - Observed exit point and modelled tracer plume for Nov 2 A at 32 mins ...	147
Figure 7.35: -Observed exit point and modelled tracer plume for Nov 2 B at 8 mins	148
Figure 7.36: - Observed exit point and modelled tracer plume for Nov 2 B at 11 mins ...	148
Figure 7.37: - Observed exit point and modelled tracer plume for Nov 2 B at 17 mins ...	149
Figure 7.38: - Observed exit point and modelled tracer plume for Nov 2 C at 7 mins	149
Figure 7.39: - Observed exit point and modelled tracer plume for Nov 9 A at 62.32 mins	150
Figure 7.40: - Observed exit point and modelled tracer plume for Nov 9 B at 56 mins ...	150
Figure 7.41: - Observed exit point and modelled tracer plume for Nov 9 B at 79 mins ...	151
Figure 7.42: - Observed exit point and modelled tracer plume for Nov 10 at 57.66 mins ...	151
Figure 7.43: - Observed exit point and modelled tracer plume for Nov 10 at 91 mins	152
Figure 7.44: - Observed exit point and modelled tracer plume for Nov 10 at 101 mins ...	152
Figure 7.45: - Observed exit point and modelled tracer plume for Jan 29 at 54 mins.....	153
Figure 7.46: - Observed exit point and modelled tracer plume for Jan 31 at 54 mins.....	153
Figure 7.47: - Observed exit point and modelled tracer plume for Feb 5 at 54 mins.....	154
Figure 7.48: - Observed exit point and modelled tracer plume for Feb 7 at 52.5 mins.....	154
Figure 7.49: - Uniform Vector plot showing direction of water flow in the model.	155
Figure 7.50: - relative vector plot showing direction and magnitude of water flow in the model.....	155
Figure 7.51: - Tracer concentration in hole C5 for Jan 12.....	156
Figure 7.52: - Tracer concentration in hole C5 for Jan 31	157
Figure 7.53: - Tracer concentration in the channel (2.5m on ruler) for Feb 5.....	157
Figure 8.1: - Conceptual preimpoundment hydro-geology in Cardiff Bay area. Cross-section shown by dashed line on map. (Map from Google Maps, geology from Heathcote et al. 2003)	163
Figure 8.2: - Groundwater elevation in Gravel aquifer, Cardiff Bay area (low tide)	166
Figure 8.3: - Groundwater elevation in gravel aquifer, Cardiff Bay area, (high tide).	166
Figure 8.4: - Location of tidal data. (source: Google Maps)	168

Figure 8.5: - Max. and Min. daily mean flows from 1965 to 1972 for the Taff at Tongwynlais (1972 in bold). (Source NRFA 2006)	169
Figure 8.6: - DIVAST model of Cardiff Bay showing cross-sections and water levels at mid-tide	169
Figure 8.7: - Tidal propagation through Cardiff Bay	170
Figure 8.8: - Model Area	172
Figure 8.9: - Boreholes in model area, and sections of Taff with average minimum tidal elevation	174
Figure 8.10: - Visual MODFLOW model showing head boundaries	175
Figure 8.11: - Tidal elevations for sections of the Taff	176
Figure 8.12: - CS018 compared to 6/PB4 and 6/PB5	177
Figure 8.13: - Observed heads for 2 day period for 5/PB1, 5/PB2, CS125L and CS158L	178
Figure 8.14: - Bad data at start of CS313L observed heads	178
Figure 8.15: - Calculated vs. Observed Head for 1 st VM run. Conductivity 5.79×10^{-4} m/s	179
Figure 8.16: - Calculated vs. Observed head for model run with conductivity 5×10^{-3}	180
Figure 8.17: - Calculated vs. Observed head for model run with conductivity 5×10^{-2}	180
Figure 8.18: - Summary of PEST wells. Modelled heads against Observed heads	182
Figure 8.19: - Individual plots of PEST wells left to right, top to bottom a) CS229, b) 4/PB1, c) CS158L, d) CS116A, e) CS004A and f) CS241	183
Figure 8.20: - Well 5/PB2, model predicts timing of tidal fluctuations.	184
Figure 8.21: - Borehole 6/PB4, model predicts stable water levels	185
Figure 8.22: - Model predicts tidal fluctuations where none are observed	185
Figure 8.23: - Comparison of observed and modelled heads for CS238, a borehole close to the river	186
Figure 8.24: - 2-layer PEST run. Individual plots of PEST wells a) CS229, b) 4/PB1, c) CS158L, d) CS116A, e) CS004A and f) CS241	188
Figure 8.25: - calculated vs. observed heads for confining layer PEST run	189
Figure 8.26: - Comparison of model and observed heads in CS317L, and tidal boundary condition used nearby in river	192
Figure 8.27: - Comparison of model and observed heads in CP6AL, and tidal boundary condition used nearby in river	193
Figure 9.1: - Topography data in original orientation displayed in ArcGIS showing elevation (shading – light = high ground, dark = low ground), borehole locations (red), and georeference points (blue lines and cross)	197
Figure 9.2: - (left) Georeferenced grid in new rotated coordinate system. (right) Clipping the data to the area required, and converting to an integer dataset	198
Figure 9.3: - Reclassifying the grid at a cut-off point of 5m as surface water (blue) or groundwater (green). Left = before reclassification, right = after reclassification.	198
Figure 9.4: - DIVAST-SG grid overlaying Cardiff map used for MODFLOW area	201
Figure 9.5: - DIVAST-SG domain for Cardiff Bay model. Blue indicates a surface water cell (1), green indicates a groundwater cell (7), and grey indicates inactive cells (0 - wall boundary). White indicates the location of a borehole. Varying boundary conditions were specified at either end of the river	202
Figure 9.6: - Tecplot image of the DIVAST-SG model at low tide. Black contour lines indicate groundwater head, colours indicate depth of aquifer (red - deep, blue - shallow)	204
Figure 9.7: - Model and observed head time series for $k = 0.01$ $n = 0.2$	206
Figure 9.8: - Scatter plot of test boreholes, observed head against modelled head - Permeability 0.01 Porosity 0.2	207

Figure 9.9: - r^2 value as a function of porosity and permeability. Light areas indicate high values, and the 80% contour line is in red.	210
Figure 9.10: - Average r^2 values as a function of porosity and permeability, including and excluding CS241	211
Figure 9.11: - Average error from observed values with respect to porosity and permeability. Light areas indicate low average error.....	214
Figure 9.12: - Average error for all boreholes as a function of porosity and permeability.	215
Figure 9.13: - Average error and average r^2 value as a function of porosity and permeability. Solid contours for r^2 value, dotted contours for average error. Red contours indicate 0.5m error, and 0.8 r^2 for graph including CS241 (left), and 0.9 r^2 value for graph excluding CS241 (right).	215
Figure 9.14: - Borehole CS317L – $k = 0.004$ $n = 0.3$. $r^2 = 0.9709$ av. err = 0.1664.....	216
Figure 9.15: - Borehole CS241 at $k = 0.01$ $n = 0.2$. $r^2 = 0.9791$ av. err = 0.4290	217
Figure 9.16: - Borehole CS238A at $k = 0.005$ and $n = 0.2$. Average error = 0.3778	218
Figure 9.17: - Borehole CS238A at $k = 0.01$ and $n = 0.2$. Average error = 0.5660	218
Figure 9.18: - Borehole CS217 - $k = 0.005$ and $n = 0.3$	219
Figure 9.19: - Borehole CS116 at $k = 0.005$ and $n = 0.2$	219
Figure 9.20: - Modelled and Observed head time series for $k = 0.006$ and $n = 0.26$	220
Figure 9.21: - Scatter graph of modelled against observed values for test boreholes. Permeability 0.006 Porosity 0.26.....	221
Figure 10.1: - Measured and Modelled Water Elevations after adjustment to the numerical model, to include foam joints.....	225
Figure 10.2: - comparison of modelled and observed heads for MODFLOW and DIVAST-SG models.....	229
Figure 10.3: - Current state of model development.....	232

INDEX OF TABLES

Table 2.1: - Numerical Studies	33
Table 2.2 – Analytical Studies	33
Table 2.3: - Field Studies	34
Table 3.1: - Range of values of Porosity (Freeze and Cherry 1979)	41
Table 4.1: - Summary of Coefficients for x -sweep.....	67
Table 4.2: - Summary of Coefficients for y -sweep.....	68
Table 4.3: - Summary of Seepage Equations.....	68
Table 5.1: - i , j and k data required for Hotstart file	89
Table 5.2: - i , and j data (surface water layer only) required for Hotstart file.....	89
Table 6.1: - variables used in Figures 6.2 and 6.3.	97
Table 6.2: - Scenario 1	99
Table 6.3: - Scenario 2	102
Table 7.1: Details of the equipment - Constant Head Test	111
Table 7.2: Results from Constant Head Test	111
Table 7.3: Summary of results and calculations	111
Table 7.4 - Pumping Test to determine Conductivity.....	114
Table 7.5 - Iterative K values compared to theoretical K values from theoretical equation.	115
Table 7.6 – Conductivity Values for the laboratory foam.	116
Table 7.7: - Example Permeability Values (adapted from values in Bear 1972)	116
Table 7.8: - Calculating the porosity of the foam	117
Table 7.9: - Approximate porosity values found in nature (Freeze and Cherry 1979).....	117
Table 7.10: - Measured Water elevations at steady state.....	130
Table 7.11: - Methods of joint modelling	133
Table 7.12: - Experimental Data for selected tracer experiments.....	142
Table 8.1: - Maximum and Minimum tidal elevations at various boreholes adjacent to the Taff.....	173
Table 8.2: - Parameters varied in PEST analysis.....	181
Table 8.3: - Estimated Visual MODFLOW parameters.	182
Table 8.4: - Estimated Visual MODFLOW parameters using confined and unconfined model.....	187
Table 8.5: - Table of saturated hydraulic conductivity (K) values found in nature. Values are for typical fresh groundwater conditions — using standard values of viscosity and specific gravity for water at 20°C and 1 atm. (Bear 1972).	190
Table 8.6: - Approximate porosity values found in nature (Freeze and Cherry 1979).....	191
Table 9.1: - Linear transformation for co-ordinate system.	199
Table 9.2: - R^2 values for individual boreholes and porosity and permeability settings. ..	209
Table 9.3: - Average error from observed values for each borehole.	213
Table 9.4: - Table of saturated hydraulic conductivity (K) values found in nature. Values are for typical fresh groundwater conditions — using standard values of viscosity and specific gravity for water at 20°C and 1 atm. (Bear 1972).	222

APPENDIX A SAMPLE INPUT FILES

Bar.dsg

Located in D:\DIVAST-SG General Model and Input Files\bar.dsg

3-D code, restricted to one layer.

Simple demonstration model of permeable sandbar separating two small water bodies.

Open elevation boundary (sinusoidal tide) at one side causes groundwater fluctuations in sandbar, which then affect the isolated water body.

```

Layered DIVAST SG Model
-----General Data-----
IMAX      =      30      MAXIMUM NO. OF GRID POINTS IN I (OR X) DIRECTION
JMAX      =      10      MAXIMUM NO. OF GRID POINTS IN J (OR Y) DIRECTION
KMAX      =      1       MAXIMUM NO. OF LAYERS
JSPACE    =      4       INTEGER SPACE BETWEEN PRINTOUT VALUES
NADVIT    =      2       NO. OF ITERATIONS FOR ADVECTIVE ACCELERATIONS
NDFORM    =      0       FORM OF DEPTH DATA: SIDE CENTRES = 0 & CORNERS = 1
NFLRUF    =      0       ROUGH TURBULENT FLOW ASSUMED: NO=0 & YES=1
TECTIM    =      30      interval (secs) to output tecplot data
TECOUT    =      1       Output to tecplot data file? (LARGE FILES!) no=0 & yes=1
NUMPRT    =      4       NUMBER OF PRINTOUT TIMES SPECIFIED AS DATA
NWEPRN    =      1       FLAG FOR WATER ELEVATION PRINTOUT: NO=0 & YES=1
NVEPRN    =      1       FLAG FOR VELOCITY COMPONENT PRINTOUT: NO=0 & YES=1
NDEPRN    =      1       FLAG FOR DEPTHS AT CENTRE PRINTOUT: NO=0 & YES=1
NRFPRN    =      0       FLAG FOR ROUGHNESS NO=0, CHEZY=1, MAN.=2 & DARCY=3
NEDPRN    =      0       FLAG FOR EDDY VISCOSITY PRINTOUT: NO=0 & YES=1
NRNPRN    =      0       FLAG FOR REYNOLDS NUMBER PRINTOUT: NO=0 & YES=1
NDIPRN    =      0       FLAG FOR DISPERSION-DIFF. PRINTOUT: NO=0 & YES=1
NSOPRN    =      1       FLAG FOR SOLUTE LEVEL PRINTOUT: NO=0 & YES=1
NTAPRN    =      0       FLAG FOR BED SHEAR STRESS PRINTOUT: NO=0 & YES=1
NERPRN    =      0       FLAG FOR CALCULATING & PRINTING EROSION: NO=0 & YES=1
NRDPRN    =      0       FLAG FOR RESIDUAL COMPONENTS PRINTOUT: NO=0 & YES=1
NFLWIN    =      0       FLAG FOR INCLUDING A SURFACE WIND STRESS: NO=0 & YES=1
NFLDRY    =      0       FLAG FOR INCLUDING FLOODING & DRYING: NO=0 & YES=1
NFLSOL    =      0       FLAG FOR INCLUDING SOLUTE PREDICTIONS: NO=0 & YES=1
NFLSGI    =      1       FLAG FOR INCLUDING SURFACE-GROUNDWATER INTERACTIONS: NO=0 & YES=1
-----Hot-Start Info-----
.false.    HOTSTART      Start Model from Hot-start file (true or false)
nothing.hst HSTFNAM      Filename for Hot-start Data
.false.    HSTOUT       Output Hot-start data (create hot-start file
filename.hst)
0.0        HSTTIME      Time to Output hot-start data (hours)
-----Point Data Collection-----
NUMPNT     =      0      NUMBER OF POINTS TO RECORD DATA FROM
-----Boundary Conditions-----
----IOBD and JOBD arrays - (boundary type, row or column num, start, end, layer number)----
IENDOB     =      1      NO. OF OPEN BOUNDARY REACHES IN I DIRECTION
JENDOB     =      0      NO. OF OPEN BOUNDARY REACHES IN J DIRECTION
IOBD 1     =      3 30 2 9 1
-----Model Data-----
TIMESM     =      1.00    TIME OF SIMULATION (HOURS)
HFDT       =      0.5000  HALF TIME STEP (S)
DELX       =      1.00    GRID SPACING (M)
ANGLAT     =      0.00    ANGLE OF LATITUDE OF DOMAIN IN DEGREES
RUFFMM     =      1.00    ROUGHNESS LENGTH K (MM)
VISCM      =      1.31    KINEMATIC VISCOSITY OF FLUID (MM^2/S)
REMIN      =      100.0    MINIMUM REYNOLDS NUMBER
TCHEZY     =      0.01    TIME AT WHICH ROUGHNESS COEFF. IS CHANGED (HRS)
TEDDY      =      0.01    TIME AT WHICH EDDY VISCOSITY IS CHANGED (HRS)
TDISP      =      0.01    TIME AT WHICH DISPERSION COEFF. IS CHANGED (HRS)
ALPHA      =      0.7143  SLIP BOUND COEFF NO =-1.0 FREE =1.0 PARTIAL =0.7143
BETA       =      1.016   MOMENTUM CORRECTION FACTOR
COED       =      0.15    EDDY VISCOSITY COEFFICIENT
GAMMA      =      0.000   LONGITUDINAL DISPERSION COEFFICIENT
DELTA      =      0.000   LATERAL TURBULENT DIFFUSION COEFFICIENT
ADDIS      =      0.000   ADDITIONAL DISPERSION-DIFFUSION (M^2/S)
WINDIS     =      0.000   WIND INDUCED DISPERSION (M^2/S)
PRESET     =      0.005   MINIMUM DEPTH FOR FLOODING & DRYING (M)
ANGNOR     =      0.00    CLOCKWISE ANGLE FROM NORTH TO X-DIRECTION IN DEG.
WINSPEED   =      0.00    WIND SPEED (M/S)
WINANG     =      0.00    WIND ANGLE - CLOCKWISE FROM NORTH IN DEGREES

```

```

DENAIR = 1.25 DENSITY OF AIR (KG/M^3)
DENWAT = 1000.00 DENSITY OF WATER (KG/M^3)
WATEMP = 10.00 WATER TEMPERATURE IN DEG. CENTIGRADE
-----Outfall and Solute Data-----
NUMOUT = 0 NUMBER OF OUTFALLS
NFLSAL = 0 FLAG FOR SALINITY INPUT NO=0 & YES=1
NFLTMP = 0 FLAG FOR TEMPERATURE INPUT NO=0 & YES=1
NFLTCL = 0 FLAG FOR T. COLI INPUT NO=0 & YES=1
NFLFCL = 0 FLAG FOR F. COLI INPUT NO=0 & YES=1
NFLBOD = 0 FLAG FOR B.O.D. INPUT NO=0 & YES=1
NBOD5D = 0 CONVERT ULTIMATE BOD TO 5-DAY BOD NO=0 & YES=1
NFLORG = 0 FLAG FOR ORGANIC NIT. NO=0 & YES=1
NFLAMN = 0 FLAG FOR AMMONIA NIT. NO=0 & YES=1
NFLNTA = 0 FLAG FOR NITRATE NIT. NO=0 & YES=1
NFLDOX = 0 FLAG FOR DISSOLVED OXYG. NO=0 & YES=1
NFLALG = 0 FLAG FOR ALGAL BIOMASS NO=0 & YES=1
NFLPHS = 0 FLAG FOR PHOSPHORUS NO=0 & YES=1
NFLSED = 0 FLAG FOR SEDIMENT TRANSPORT NO=0 & YES=1
NSFORM = 0 SEDIMENT FORMULA TYPE: ENG-HAN = 0 & VAN RIJN = 1
NFLCHS = 0 FLAG FOR COHESIVE SEDIMENT TRANSPORT NO=0 & YES=1
FACWAT = 1.0E+2 FACTOR FOR SCALING LEVELS PRINTOUT (<0-VARIABLE SCALING)
FACVEL = -1.E+0 FACTOR FOR SCALING VELOCITY PRINTOUT
FACDEP = 1.0E+2 FACTOR FOR SCALING WATER DEPTH PRINTOUT
FACRUF = -1.E+0 FACTOR FOR SCALING CHEZY, MANNING OR DARCY PRINTOUT
FACEDD = -1.E+0 FACTOR FOR SCALING EDDY VISCOSITY PRINTOUT
FACRNO = -1.E+0 FACTOR FOR SCALING REYNOLDS NO. PRINTOUT
FACDIS = -1.E+0 FACTOR FOR SCALING DISPERSION PRINTOUT
FACFAL = 1.0E+1 FACTOR FOR SCALING SALINITY PRINTOUT
FACTEM = -1.E+0 FACTOR FOR SCALING TEMPERATURE PRINTOUT
FACTCL = -1.E+0 FACTOR FOR SCALING TOTAL COLIFORM PRINTOUT
FACFCL = -1.E+0 FACTOR FOR SCALING FAECAL COLIFORM PRINTOUT
FACBOD = -1.E+0 FACTOR FOR SCALING BIOCHEM OXYG DEM PRINTOUT
FACORG = -1.E+0 FACTOR FOR SCALING ORGANIC NITROGEN PRINTOUT
FACAMN = -1.E+0 FACTOR FOR SCALING AMMONIA NITROGEN PRINTOUT
FACNTA = -1.E+0 FACTOR FOR SCALING NITRATE NITROGEN PRINTOUT
FACDOX = -1.E+0 FACTOR FOR SCALING DISSOLVED OXYGEN PRINTOUT
FACALG = -1.E+0 FACTOR FOR SCALING ALGAL BIOMASS PRINTOUT
FACPHS = -1.E+0 FACTOR FOR SCALING PHOSPHORUS PRINTOUT
FACSED = -1.E+0 FACTOR FOR SCALING NON-COHESIVE SEDIMENT PRINTOUT
FACCHS = -1.E+0 FACTOR FOR SCALING SUSP. COHESIVE SEDIMENT PRINTOUT
FACCHB = -1.E+0 FACTOR FOR SCALING DEPO. COHESIVE SEDIMENT PRINTOUT
FACNSD = -1.E+0 FACTOR FOR SCALING NET SEDIMENT FLUX PRINTOUT
FACSTR = -1.E+0 FACTOR FOR SCALING BED SHEAR STRESS PRINTOUT
FACRVL = -1.E+0 FACTOR FOR SCALING RESIDUAL VELOCITY PRINTOUT
FACRST = -1.E+0 FACTOR FOR SCALING RESIDUAL BED SHEAR PRINTOUT
FACRER = -1.E+0 FACTOR FOR SCALING RESIDUAL EROSION PRINTOUT
SALINT = 0.00 INITIAL SALINITY LEVELS ACROSS DOMAIN (PPT)
SAL OUTS:- 0.00 1.00 OUTFALL SALINITY LEVELS (PPT)
TMPINT = 0.00 INITIAL TEMPERATURE LEVELS ACROSS DOMAIN (DEG C)
TMP OUTS:- 0.00 OUTFALL TEMPERATURE LEVELS (DEG C)
TCLINT = 0.00 INITIAL TOTAL COL. LEVELS ACROSS DOMAIN (CTS/100ML)
TCL OUTS:- 0.00 OUTFALL TOTAL COLIFORM LEVELS (CTS/100ML)
FCLINT = 0.00 INITIAL FAECAL COL LEVELS ACROSS DOMAIN (CTS/100ML)
FCL OUTS:- 0.00 OUTFALL FAECAL COLIFORM LEVELS (CTS/100ML)
BODINT = 0.00 INITIAL BOD LEVELS ACROSS DOMAIN (MG/L)
BOD OUTS:- 0.00 OUTFALL BOD LEVELS (MG/L)
ORGINT = 0.00 INITIAL ORGANIC NIT. LEVELS ACROSS DOMAIN (MG/L)
ORG OUTS:- 0.00 OUTFALL ORGANIC NITROGEN LEVELS (MG/L)
AMNINT = 0.00 INITIAL AMMONIA NIT. LEVELS ACROSS DOMAIN (MG/L)
AMN OUTS:- 0.00 OUTFALL AMMONIA NITROGEN LEVELS (MG/L)
TRAINT = 0.00 INITIAL NITRATE NIT. LEVELS ACROSS DOMAIN (MG/L)
TRA OUTS:- 0.00 OUTFALL NITRATE NITROGEN LEVELS (MG/L)
SALFDO = 0.00 SALINITY LEVEL FOR SATURATION DO CALCULATION (PPT)
DOX OUTS:- 0.00 OUTFALL DISSOLVED OXYGEN LEVELS (MG/L)
ALGINT = 0.00 INITIAL ALGAL BIOMASS LEVELS ACROSS DOMAIN (MG/L)
ALG OUTS:- 0.00 OUTFALL ALGAL BIOMASS LEVELS (MG/L)
PS1INT = 0.00 INITIAL ORGANIC PHOS. LEVELS ACROSS DOMAIN (MG/L)
PS1 OUTS:- 0.00 OUTFALL ORGANIC PHOSPHORUS LEVELS (MG/L)
PS2INT = 0.00 INITIAL DISSOLVED PHOS. LEVELS ACROSS DOMAIN (MG/L)
PS2 OUTS:- 0.00 OUTFALL DISSOLVED PHOSPHORUS LEVELS (MG/L)
SEDINT = 0.00 INITIAL SUSPENDED SED. LEVELS ACROSS DOMAIN (MG/L)
GAMSUS = 5.00 GAMMA FOR SUSPENDED SEDIMENTS
SPGRAV = 2.65 SPECIFIC GRAVITY OF SUSPENDED SEDIMENTS
D16MMS = 0.00 SEDIMENT DIAMETER WITH 16% FINER (MM)
D50MMS = 0.00 SEDIMENT DIAMETER WITH 50% FINER (MM)
D84MMS = 0.00 SEDIMENT DIAMETER WITH 84% FINER (MM)
D90MMS = 0.00 SEDIMENT DIAMETER WITH 90% FINER (MM)
CHSINT = 0.00 INITIAL COHESIVE SUSP. SED. CONCENTRATION (KG/M^3)
CSGRAV = 2.65 SPECIFIC GRAVITY OF SUSPENDED COHESIVE SEDIMENTS
C50MMS = 0.063 AVERAGE SIZE OF COHESIVE FLOCS (MM)
COFERO = 0.0015 EMPIRICAL EROSION COEFFICIENT (KG/N/S)
CRTDEP = 0.100 CRITICAL STRESS FOR DEPOSITION (N/M^2)
CRTERO = 0.300 CRITICAL STRESS FOR RE-SUSPENSION (N/M^2)
WSFIDX = 4.0 EXPONENT INDEX FOR HINDERED SETTLING VELOCITY
WSFGAM = 1.0 COEFFICIENT FOR HINDERED SETTLING VELOCITY
CHS OUTS:- 100.1 OUTFALL COHESIVE SEDIMENT CONCENTRATIONS
SPHTEC = 0.000 SURFACE HEAT EXCHANGE COEFFICIENT (WATTS/M^2/DEG C)

```

```

SPTMCF = 4.200 SPECIFIC THERMAL CAP. OF FLUID (JOULES/M^3/DEG C)
TCLK5D = 2.400 DECAY RATE FOR T. COLI (1/DAY)
TH5TCL = 1.047 TEMPERATURE CORRECTION FOR T. COLI
FCLK5D = 2.400 DECAY RATE FOR F. COLI (1/DAY)
TH5FCL = 1.047 TEMPERATURE CORRECTION FOR F. COLI
BODK1D = 5.000 DECAY RATE FOR BOD VIA DEOXYGENATION (1/DAY)
TH1BOD = 1.000 TEMPERATURE CORRECTION FOR BOD VIA DEOXYGENATION
BODK3D = 0.000 DECAY RATE FOR BOD VIA SETTLING LOSS (1/DAY)
TH3BOD = 1.000 TEMPERATURE CORRECTION FOR BOD VIA SETTLING LOSS
ORGB3D = 0.400 DECAY RATE FOR ORG NIT TO CONVERT TO NH3 (1/DAY)
TH3ORG = 1.047 TEMPERATURE CORRECTION FOR ORG NIT VIA CONVERSION
ORGS4D = 0.100 DECAY RATE FOR ORG NIT VIA SETTLING (1/DAY)
TH4ORG = 1.024 TEMPERATURE CORRECTION FOR ORG. NIT. VIA SETTLING
AMNB1D = 1.000 DECAY RATE FOR BIOL. OXIDATION OF NH3 (1/DAY)
TH1AMN = 1.083 TEMPERATURE CORRECTION FOR BIOL. OXIDATION OF NH3
TH2DOX = 1.024 TEMPERATURE CORRECTION FOR REAERATION RATE
DOXK4D = 5.000 SEDIMENT OXYGEN DEMAND RATE (MG/M^2 PER DAY)
TH4DOX = 1.060 TEMPERATURE CORRECTION FOR SEDIMENT OXYGEN DEMAND
DOXA5C = 3.500 RATE OF OXYGEN UPTAKE PER UNIT OF AMMONIA NITROGEN
DOFMMH = 5.000 DO EXCHANGE COEFF. FOR STAGNANT WATER (MM/HOUR)
DOLMT2 = 2.000 HALF-SATURATION DO LIMITING CONSTANT (MG/L)
DOXA3C = 0.133 DO PRODUCTION / UNIT OF CHLOROPHYLL (MG-DO/MG-CHLA)
DOXA4C = 0.100 DO UPTAKE / UNIT OF CHLOROPHYLL (MG-DO/MG-CHLA)
ALGMAX = 2.000 MAX. ALGAE GROWTH RATE AT REFERENCE TEMP. (1/DAY)
THMALG = 1.047 TEMPERATURE CORRECTION FOR MAX. ALGAE GROWTH RATE
ALGRSP = 0.060 RATE OF RESPIRATION PLUS EXCRETION (1/DAY)
THARSP = 1.047 TEMPERATURE CORRECTION FOR RESPIRATION & EXCRETION
VELALG = 0.050 ALGAE (CHLOROPHYLL) SETTLING VELOCITY (M/DAY)
ALGNPM = 0.010 NON-PREDATORY MORTALITY RATE FOR ALGAE (1/DAY)
ALGLGZ = 0.020 RATE OF ALGAL LOSSES DUE TO GRAZING (1/DAY)
FPHOTP = 0.500 PHOTOPERIOD (EXPRESSED AS FRACTION OF THE DAY)
EXTLT0 = 0.090 LIGHT EXT COEF FOR ALL ABSORPT COMPS BUT PHYT (1/M)
EXTLT1 = 0.0088 LIGHT EXT COEF FOR PHYTOPLANKTON (1/M)
EXTLT2 = 0.054 LIGHT EXT COEF FOR PHYTOPLANKTON (1/M)
EXTLT3 = 0.667 LIGHT EXT COEF FOR PHYTOPLANKTON (1/M)
SURFLT = 250.1 LIGHT INTENSITY AT WATER SURFACE
HFSATL = 6.0 LIGHT LEVEL AT WHICH GROWTH IS HALF OF MAX. RATE
HFSATN = 0.060 HALF-SATURATION CONSTANT FOR NITROGEN (MG/L)
HFSATP = 0.010 HALF-SATURATION CONSTANT FOR PHOSPHORUS (MG/L)
ALGA1C = 7.000 NIT. FRACTION OF ALGAL CHLOROPHYLL (MG-N/MG-CHLA)
FRCORG = 0.100 FRACTION OF DEAD & RESPIRED PHYTOPLANKTON RECYCLED
FRCPHS = 0.100 FRACTION OF DEAD & RESPIRED PHYTOPLANKTON RECYCLED
PHSA2C = 1.000 PHOS FRACTION OF ALGAL CHLOROPHYLL (MG-P/MG-CHLA)
PHSB4D = 0.085 HYDROLYSIS RATE FOR ORG. PH TO INORG. PH (1/DAY)
THPSB4 = 1.047 TEMPERATURE CORRECTION FOR ORG. P TO INORG. P
PHSS5D = 0.010 SETTLING RATE CONST OF ORGANIC PHOSPHORUS (1/DAY)
THPSS5 = 1.047 TEMPERATURE CORRECTION FOR ORG. P SETTLING RATE
PHSF2D = 0.010 SETTLING RATE CONST OF INORG. PHOSPHORUS (1/DAY)
THPSF2 = 1.047 TEMPERATURE CORRECTION FOR INORG. P SETTLING RATE
NFLDOF = 1 0 (FT UNIT); 1 (OWENS RELATION); 2 (BANKS FOR LAKE)
0.00000 0.05000 0.25000 0.50000 (PRINTOUT TIMES)
-----Tidal boundary (water elevation) Data-----
SINTIDE = 1 I6 Sinusoidal tide, 1= yes, 0= no
TIDEAMP = 1.0000 F10.4 Tidal Amplitude (only used if SINTIDE=1)
TIDEMWL = 0.0000 F10.4 Tidal Mean Water Level (only used if SINTIDE=1)
TIDEHR = 0.5000 F10.4 Tidal period (wavelength for sinusoidal tide, length of cycle
to repeat for non-sinusoidal tide) (hours)
TIDESTART=HIGH A4 Start sinusoidal tidal cycle at: high tide (HIGH), Rising
Mean Water Level (MWL+), Falling Mean Water Level (MWL-) or low tide (LOW)
PRETIDE = 0.0000 F10.4 Time before tidal boundary cycle is started. (hours)
NOPTS = 0 I6 Number of points specified for non-sinusoidal tide
NUMTDS = 10.0000 F10.4 Number of tidal cycles time elevation
(non-sinusoidal tide points on NOPTS lines below here F6.3 F8.3)
-----Flow or velocity boundary data:-----
FLOWTYPE = 0 I6 Type of Boundaries (0=Flow 1=velocity)
FPHASE = 0.0500 F10.4 Time over which flow at boundary is introduced
CDWEIR = 0.6100 F10.4 Weir coefficient
-----Layer Domain Specification-----
Layer1
0000000000 1
0111111110 2
0111111110 3
0111111110 4
0111111110 5
0111111110 6
0111111110 7
0111111110 8
0111111110 9
0111111110 10
0777777770 11
0777777770 12
0777777770 13
0777777770 14
0777777770 15
0777777770 16
0777777770 17
0777777770 18

```

[illegible]

251

Cooper100.dsg

Located in D:\Analytical Validation\cooper100.dsg together with several other input files used in the Analytical Validation.

Layered Divast SG Model

```

-----General Data-----
IMAX      =      106      MAXIMUM NO. OF GRID POINTS IN I (OR X) DIRECTION
JMAX      =      18      MAXIMUM NO. OF GRID POINTS IN J (OR Y) DIRECTION
JSPACE    =      4      INTEGER SPACE BETWEEN PRINTOUT VALUES
NADVIT    =      2      NO. OF ITERATIONS FOR ADVECTIVE ACCELERATIONS
NDFORM     =      0      FORM OF DEPTH DATA: SIDE CENTRES = 0 & CORNERS = 1
NFLRUF    =      0      ROUGH TURBULENT FLOW ASSUMED: NO=0 & YES=1
TECTIM    =      450     interval (secs) to output tecplot data
TECOUT     =      1      Output to tecplot data file? (LARGE FILES!) no=0 & yes=1
NUMPRT    =      4      NUMBER OF PRINTOUT TIMES SPECIFIED AS DATA
NWEPRN    =      1      FLAG FOR WATER ELEVATION PRINTOUT: NO=0 & YES=1
NVEPRN    =      1      FLAG FOR VELOCITY COMPONENT PRINTOUT: NO=0 & YES=1
NDEPRN    =      1      FLAG FOR DEPTHS AT CENTRE PRINTOUT: NO=0 & YES=1
NRFPRN    =      0      FLAG FOR ROUGHNESS NO=0, CHEZY=1, MAN.=2 & DARCY=3
NEDPRN    =      0      FLAG FOR EDDY VISCOSITY PRINTOUT: NO=0 & YES=1
NRNPRN    =      0      FLAG FOR REYNOLDS NUMBER PRINTOUT: NO=0 & YES=1
NDIPRN    =      0      FLAG FOR DISPERSION-DIFF. PRINTOUT: NO=0 & YES=1
NSOPRN    =      1      FLAG FOR SOLUTE LEVEL PRINTOUT: NO=0 & YES=1
NTAPRN    =      0      FLAG FOR BED SHEAR STRESS PRINTOUT: NO=0 & YES=1
NERPRN    =      0      FLAG FOR CALCULATING & PRINTING EROSION: NO=0 & YES=1
NRDPRN    =      0      FLAG FOR RESIDUAL COMPONENTS PRINTOUT: NO=0 & YES=1
NFLWIN    =      0      FLAG FOR INCLUDING A SURFACE WIND STRESS: NO=0 & YES=1
NFLDRY    =      0      FLAG FOR INCLUDING FLOODING & DRYING: NO=0 & YES=1
NFLSOL    =      0      FLAG FOR INCLUDING SOLUTE PREDICTIONS: NO=0 & YES=1
NFLSGI    =      1      FLAG FOR INCLUDING SURFACE-GROUNDWATER INTERACTIONS: NO=0 &
YES=1

-----Point Data Collection-----
NUMPNT    =      50      NUMBER OF POINTS TO RECORD DATA FROM
point1    =      2      9
point2    =      4      9
point3    =      6      9
point4    =      8      9
point5    =     10      9
point6    =     12      9
point7    =     14      9
point8    =     16      9
point9    =     18      9
point10   =     20      9
point11   =     22      9
point12   =     24      9
point13   =     26      9
point14   =     28      9
point15   =     30      9
point16   =     32      9
point17   =     34      9
point18   =     36      9
point19   =     38      9
point20   =     40      9
point21   =     42      9
point22   =     44      9
point23   =     46      9
point24   =     48      9
point25   =     50      9
point26   =     52      9
point27   =     54      9
point28   =     56      9
point29   =     58      9
point30   =     60      9
point31   =     62      9
point32   =     64      9
point33   =     66      9
point34   =     68      9
point35   =     70      9
point36   =     72      9
point37   =     74      9
point38   =     76      9
point39   =     78      9
point40   =     80      9
point41   =     82      9
point42   =     84      9
point43   =     86      9
point44   =     88      9
point45   =     90      9
point46   =     92      9
point47   =     94      9

```

```

point48 = 96 9
point49 = 98 9
point50 = 100 9
-----Boundary Conditions-----
IENDOB = 1 NO. OF OPEN BOUNDARY REACHES IN I DIRECTION
JENDOB = 0 NO. OF OPEN BOUNDARY REACHES IN J DIRECTION
IOBD 1 = 2 2 2 17
-----Model Data-----
TIMESM = 20.00 TIME OF SIMULATION (HOURS)
HFDT = 0.2000 HALF TIME STEP (S)
DELX = 1.00 GRID SPACING (M)
ANGLAT = 0.00 ANGLE OF LATITUDE OF DOMAIN IN DEGREES
RUFFMM = 1.00 ROUGHNESS LENGTH K (MM)
VISCMM = 1.31 KINEMATIC VISCOSITY OF FLUID (MM^2/S)
REMIN = 100.0 MINIMUM REYNOLDS NUMBER
TCHEZY = 0.01 TIME AT WHICH ROUGHNESS COEFF. IS CHANGED (HRS)
TEDDY = 0.01 TIME AT WHICH EDDY VISCOSITY IS CHANGED (HRS)
TDISP = 0.01 TIME AT WHICH DISPERSION COEFF. IS CHANGED (HRS)
ALPHA = 0.7143 SLIP BOUND COEFF NO =-1.0 FREE =1.0 PARTIAL =0.7143
BETA = 1.016 MOMENTUM CORRECTION FACTOR
COED = 0.15 EDDY VISCOSITY COEFFICIENT
GAMMA = 0.000 LONGITUDINAL DISPERSION COEFFICIENT
DELTA = 0.000 LATERAL TURBULENT DIFFUSION COEFFICIENT
ADDIS = 0.000 ADDITIONAL DISPERSION-DIFFUSION (M^2/S)
WINDIS = 0.000 WIND INDUCED DISPERSION (M^2/S)
PRESET = 0.005 MINIMUM DEPTH FOR FLOODING & DRYING (M)
ANGNOR = 0.00 CLOCKWISE ANGLE FROM NORTH TO X-DIRECTION IN DEG.
WINSPP = 0.00 WIND SPEED (M/S)
WINANG = 0.00 WIND ANGLE - CLOCKWISE FROM NORTH IN DEGREES
DENAIR = 1.25 DENSITY OF AIR (KG/M^3)
DENWAT = 1000.00 DENSITY OF WATER (KG/M^3)
WATEMP = 10.00 WATER TEMPERATURE IN DEG. CENTIGRADE
-----Outfall and Solute Data-----
NUMOUT = 0 NUMBER OF OUTFALLS
NFLSAL = 0 FLAG FOR SALINITY INPUT NO=0 & YES=1
NFLTMP = 0 FLAG FOR TEMPERATURE INPUT NO=0 & YES=1
NFLTCL = 0 FLAG FOR T. COLI INPUT NO=0 & YES=1
NFLFCL = 0 FLAG FOR F. COLI INPUT NO=0 & YES=1
NFLBOD = 0 FLAG FOR B.O.D. INPUT NO=0 & YES=1
NBOD5D = 0 CONVERT ULTIMATE BOD TO 5-DAY BOD NO=0 & YES=1
NFLORG = 0 FLAG FOR ORGANIC NIT. NO=0 & YES=1
NFLAMN = 0 FLAG FOR AMMONIA NIT. NO=0 & YES=1
NFLNTA = 0 FLAG FOR NITRATE NIT. NO=0 & YES=1
NFLDOX = 0 FLAG FOR DISSOLVED OXYG. NO=0 & YES=1
NFLALG = 0 FLAG FOR ALGAL BIOMASS NO=0 & YES=1
NFLPHS = 0 FLAG FOR PHOSPHORUS NO=0 & YES=1
NFLSED = 0 FLAG FOR SEDIMENT TRANSPORT NO=0 & YES=1
NSFORM = 0 SEDIMENT FORMULA TYPE: ENG-HAN = 0 & VAN RIJN = 1
NFLCHS = 0 FLAG FOR COHESIVE SEDIMENT TRANSPORT NO=0 & YES=1
FACWAT = 1.0E+2 FACTOR FOR SCALING LEVELS PRINTOUT (<0-VARIABLE SCALING)
FACVEL = -1.E+0 FACTOR FOR SCALING VELOCITY PRINTOUT
FACDEP = 1.0E+2 FACTOR FOR SCALING WATER DEPTH PRINTOUT
FACRUF = -1.E+0 FACTOR FOR SCALING CHEZY, MANNING OR DARCY PRINTOUT
FACEDD = -1.E+0 FACTOR FOR SCALING EDDY VISCOSITY PRINTOUT
FACRNO = -1.E+0 FACTOR FOR SCALING REYNOLDS NO. PRINTOUT
FACDIS = -1.E+0 FACTOR FOR SCALING DISPERSION PRINTOUT
FACCSAL = 1.0E+1 FACTOR FOR SCALING SALINITY PRINTOUT
FACTEM = -1.E+0 FACTOR FOR SCALING TEMPERATURE PRINTOUT
FACTCL = -1.E+0 FACTOR FOR SCALING TOTAL COLIFORM PRINTOUT
FACFCL = -1.E+0 FACTOR FOR SCALING FAECAL COLIFORM PRINTOUT
FACBOD = -1.E+0 FACTOR FOR SCALING BIOCHEM OXYG DEM PRINTOUT
FACORG = -1.E+0 FACTOR FOR SCALING ORGANIC NITROGEN PRINTOUT
FACAMN = -1.E+0 FACTOR FOR SCALING AMMONIA NITROGEN PRINTOUT
FACNTA = -1.E+0 FACTOR FOR SCALING NITRATE NITROGEN PRINTOUT
FACDOX = -1.E+0 FACTOR FOR SCALING DISSOLVED OXYGEN PRINTOUT
FACALG = -1.E+0 FACTOR FOR SCALING ALGAL BIOMASS PRINTOUT
FACPHS = -1.E+0 FACTOR FOR SCALING PHOSPHORUS PRINTOUT
FACSED = -1.E+0 FACTOR FOR SCALING NON-COHESIVE SEDIMENT PRINTOUT
FACCHS = -1.E+0 FACTOR FOR SCALING SUSP. COHESIVE SEDIMENT PRINTOUT
FACCHB = -1.E+0 FACTOR FOR SCALING DEPO. COHESIVE SEDIMENT PRINTOUT
FACNSD = -1.E+0 FACTOR FOR SCALING NET SEDIMENT FLUX PRINTOUT
FACSTR = -1.E+0 FACTOR FOR SCALING BED SHEAR STRESS PRINTOUT
FACRVL = -1.E+0 FACTOR FOR SCALING RESIDUAL VELOCITY PRINTOUT
FACRST = -1.E+0 FACTOR FOR SCALING RESIDUAL BED SHEAR PRINTOUT
FACRER = -1.E+0 FACTOR FOR SCALING RESIDUAL EROSION PRINTOUT
SALINT = 0.00 INITIAL SALINITY LEVELS ACROSS DOMAIN (PPT)
SAL OUTS:- 100.00 100.00 0.00 0.00 100.00 100.00 OUTFALL SALINITY LEVELS (PPT)
TMPINT = 0.00 INITIAL TEMPERATURE LEVELS ACROSS DOMAIN (DEG C)
TMP OUTS:- 0.00 OUTFALL TEMPERATURE LEVELS (DEG C)
TCLINT = 0.00 INITIAL TOTAL COL. LEVELS ACROSS DOMAIN (CTS/100ML)
TCL OUTS:- 0.00 OUTFALL TOTAL COLIFORM LEVELS (CTS/100ML)
FCLINT = 0.00 INITIAL FAECAL COL LEVELS ACROSS DOMAIN (CTS/100ML)
FCL OUTS:- 0.00 OUTFALL FAECAL COLIFORM LEVELS (CTS/100ML)
BODINT = 0.00 INITIAL BOD LEVELS ACROSS DOMAIN (MG/L)
BOD OUTS:- 0.00 OUTFALL BOD LEVELS (MG/L)
ORGINT = 0.00 INITIAL ORGANIC NIT. LEVELS ACROSS DOMAIN (MG/L)

```

```

ORG OUTS:- 0.00      OUTFALL ORGANIC NITROGEN LEVELS (MG/L)
AMNINT = 0.00      INITIAL AMMONIA NIT. LEVELS ACROSS DOMAIN (MG/L)
AMN OUTS:- 0.00      OUTFALL AMMONIA NITROGEN LEVELS (MG/L)
TRAINT = 0.00      INITIAL NITRATE NIT. LEVELS ACROSS DOMAIN (MG/L)
TRA OUTS:- 0.00      OUTFALL NITRATE NITROGEN LEVELS (MG/L)
SALFDO = 0.00      SALINITY LEVEL FOR SATURATION DO CALCULATION (PPT)
DOX OUTS:- 0.00      OUTFALL DISSOLVED OXYGEN LEVELS (MG/L)
ALGINT = 0.00      INITIAL ALGAL BIOMASS LEVELS ACROSS DOMAIN (MG/L)
ALG OUTS:- 0.00      OUTFALL ALGAL BIOMASS LEVELS (MG/L)
PS1INT = 0.00      INITIAL ORGANIC PHOS. LEVELS ACROSS DOMAIN (MG/L)
PS1 OUTS:- 0.00      OUTFALL ORGANIC PHOSPHORUS LEVELS (MG/L)
PS2INT = 0.00      INITIAL DISSOLVED PHOS. LEVELS ACROSS DOMAIN (MG/L)
PS2 OUTS:- 0.00      OUTFALL DISSOLVED PHOSPHORUS LEVELS (MG/L)
SEDINT = 0.00      INITIAL SUSPENDED SED. LEVELS ACROSS DOMAIN (MG/L)
GAMSUS = 5.00      GAMMA FOR SUSPENDED SEDIMENTS
SPGRAV = 2.65      SPECIFIC GRAVITY OF SUSPENDED SEDIMENTS
D16MMS = 0.00      SEDIMENT DIAMETER WITH 16% FINER (MM)
D50MMS = 0.00      SEDIMENT DIAMETER WITH 50% FINER (MM)
D84MMS = 0.00      SEDIMENT DIAMETER WITH 84% FINER (MM)
D90MMS = 0.00      SEDIMENT DIAMETER WITH 90% FINER (MM)
CHSINT = 0.00      INITIAL COHESIVE SUSP. SED. CONCENTRATION (KG/M^3)
CSGRAV = 2.65      SPECIFIC GRAVITY OF SUSPENDED COHESIVE SEDIMENTS
C50MMS = 0.063     AVERAGE SIZE OF COHESIVE FLOCS (MM)
COFERO = 0.0015     EMPIRICAL EROSION COEFFICIENT (KG/N/S)
CRTDEP = 0.100      CRITICAL STRESS FOR DEPOSITION (N/M^2)
CRTERO = 0.300      CRITICAL STRESS FOR RE-SUSPENSION (N/M^2)
WSFIDX = 4.0        EXPONENT INDEX FOR HINDERED SETTLING VELOCITY
WSFGAM = 1.0        COEFFICIENT FOR HINDERED SETTLING VELOCITY
CHS OUTS:- 100.1     OUTFALL COHESIVE SEDIMENT CONCENTRATIONS
SPHTEC = 0.000      SURFACE HEAT EXCHANGE COEFFICIENT (WATTS/M^2/DEG C)
SPTMCF = 4.200      SPECIFIC THERMAL CAP. OF FLUID (JOULES/M^3/DEG C)
TCLK5D = 2.400      DECAY RATE FOR T. COLI (1/DAY)
TH5TCL = 1.047      TEMPERATURE CORRECTION FOR T. COLI
FCLK5D = 2.400      DECAY RATE FOR F. COLI (1/DAY)
TH5FCL = 1.047      TEMPERATURE CORRECTION FOR F. COLI
BODK1D = 5.000      DECAY RATE FOR BOD VIA DEOXYGENATION (1/DAY)
TH1BOD = 1.000      TEMPERATURE CORRECTION FOR BOD VIA DEOXYGENATION
BODK3D = 0.000      DECAY RATE FOR BOD VIA SETTLING LOSS (1/DAY)
TH3BOD = 1.000      TEMPERATURE CORRECTION FOR BOD VIA SETTLING LOSS
ORGB3D = 0.400      DECAY RATE FOR ORG NIT TO CONVERT TO NH3 (1/DAY)
TH3ORG = 1.047      TEMPERATURE CORRECTION FOR ORG NIT VIA CONVERSION
ORGS4D = 0.100      DECAY RATE FOR ORG NIT VIA SETTLING (1/DAY)
TH4ORG = 1.024      TEMPERATURE CORRECTION FOR ORG. NIT. VIA SETTLING
AMNB1D = 1.000      DECAY RATE FOR BIOL. OXIDATION OF NH3 (1/DAY)
TH1AMN = 1.083      TEMPERATURE CORRECTION FOR BIOL. OXIDATION OF NH3
TH2DOX = 1.024      TEMPERATURE CORRECTION FOR REAERATION RATE
DOXK4D = 5.000      SEDIMENT OXYGEN DEMAND RATE (MG/M^2 PER DAY)
TH4DOX = 1.060      TEMPERATURE CORRECTION FOR SEDIMENT OXYGEN DEMAND
DOXA5C = 3.500      RATE OF OXYGEN UPTAKE PER UNIT OF AMMONIA NITROGEN
DOFMMH = 5.000      DO EXCHANGE COEFF. FOR STAGNANT WATER (MM/HOUR)
DOLMT2 = 2.000      HALF-SATURATION DO LIMITING CONSTANT (MG/L)
DOXA3C = 0.133      DO PRODUCTION / UNIT OF CHLOROPHYLL (MG-DO/MG-CHLA)
DOXA4C = 0.100      DO UPTAKE / UNIT OF CHLOROPHYLL (MG-DO/MG-CHLA)
ALGMAX = 2.000      MAX. ALGAE GROWTH RATE AT REFERENCE TEMP. (1/DAY)
THMALG = 1.047      TEMPERATURE CORRECTION FOR MAX. ALGAE GROWTH RATE
ALGRSP = 0.060      RATE OF RESPIRATION PLUS EXCRETION (1/DAY)
THARSP = 1.047      TEMPERATURE CORRECTION FOR RESPIRATION & EXCRETION
VELALG = 0.050      ALGAE (CHLOROPHYLL) SETTLING VELOCITY (M/DAY)
ALGNPM = 0.010      NON-PREDATORY MORTALITY RATE FOR ALGAE (1/DAY)
ALGLGZ = 0.020      RATE OF ALGAL LOSSES DUE TO GRAZING (1/DAY)
FPHOTP = 0.500      PHOTOPERIOD (EXPRESSED AS FRACTION OF THE DAY)
EXTLT0 = 0.090      LIGHT EXT COEF FOR ALL ABSORPT COMPS BUT PHYT (1/M)
EXTLT1 = 0.0088     LIGHT EXT COEF FOR PHYTOPLANKTON (1/M)
EXTLT2 = 0.054      LIGHT EXT COEF FOR PHYTOPLANKTON (1/M)
EXTLT3 = 0.667      LIGHT EXT COEF FOR PHYTOPLANKTON (1/M)
SURFLT = 250.1      LIGHT INTENSITY AT WATER SURFACE
HFSATL = 6.0        LIGHT LEVEL AT WHICH GROWTH IS HALF OF MAX. RATE
HFSATN = 0.060      HALF-SATURATION CONSTANT FOR NITROGEN (MG/L)
HFSATP = 0.010      HALF-SATURATION CONSTANT FOR PHOSPHORUS (MG/L)
ALGA1C = 7.000      NIT. FRACTION OF ALGAL CHLOROPHYLL (MG-N/MG-CHLA)
FRCORG = 0.100      FRACTION OF DEAD & RESPIRED PHYTOPLANKTON RECYCLED
FRCPHS = 0.100      FRACTION OF DEAD & RESPIRED PHYTOPLANKTON RECYCLED
PHSA2C = 1.000      PHOS FRACTION OF ALGAL CHLOROPHYLL (MG-P/MG-CHLA)
PHSB4D = 0.085      HYDROLYSIS RATE FOR ORG. PH TO INORG. PH (1/DAY)
THPSB4 = 1.047      TEMPERATURE CORRECTION FOR ORG. P TO INORG. P
PHSS5D = 0.010      SETTLING RATE CONST OF ORGANIC PHOSPHORUS (1/DAY)
THPS55 = 1.047      TEMPERATURE CORRECTION FOR ORG. P SETTLING RATE
PHSF2D = 0.010      SETTLING RATE CONST OF INORG. PHOSPHORUS (1/DAY)
THPSF2 = 1.047      TEMPERATURE CORRECTION FOR INORG. P SETTLING RATE
NFLDOF = 1          0 (FT UNIT); 1 (OWENS RELATION); 2 (BANKS FOR LAKE)
0.00000 0.05000 0.25000 0.50000 (PRINTOUT TIMES)
-----Tidal boundary (water elevation) Data-----
SINTIDE = 0          I6      Sinusoidal tide, 1= yes, 0= no
TIDEAMP = 0.4000     F10.4    Tidal Amplitude (only used if SINTIDE=1)
TIDEMWL = 0.5000     F10.4    Tidal Mean water Level (only used if SINTIDE=1)
TIDEHR = 20.0000     F10.4    Tidal period (wavelength for sinusoidal tide, length of cycle
to repeat for non-sinusoidal tide) (hours)

```

```

TIDESTART=HIGH      A4      Start sinusoidal tidal cycle at: high tide (HIGH), Rising
Mean water Level (MWL+), Falling Mean water Level (MWL-) or low tide (LOW )
PRETIDE = 0.0000 F10.4 Time before tidal boundary cycle is started. (hours)
NOPTS = 52 I6 Number of points specified for non-sinusoidal tide
NUMTDS = 2.0000 F10.4 Number of tidal cycles
time elevation (non-sinusoidal tide points on NOPTS lines below here F6.3 F8.3)
0.000 10.000
0.160 10.004
0.320 10.016
0.480 10.035
0.640 10.062
0.800 10.095
0.960 10.136
1.120 10.181
1.280 10.232
1.440 10.287
1.600 10.345
1.760 10.406
1.920 10.469
2.080 10.531
2.240 10.594
2.400 10.655
2.560 10.713
2.720 10.768
2.880 10.819
3.040 10.864
3.200 10.905
3.360 10.938
3.520 10.965
3.680 10.984
3.840 10.996
4.000 11.000
4.160 10.996
4.320 10.984
4.480 10.965
4.640 10.938
4.800 10.905
4.960 10.864
5.120 10.819
5.280 10.768
5.440 10.713
5.600 10.655
5.760 10.594
5.920 10.531
6.080 10.469
6.240 10.406
6.400 10.345
6.560 10.287
6.720 10.232
6.880 10.181
7.040 10.136
7.200 10.095
7.360 10.062
7.520 10.035
7.680 10.016
7.840 10.004
8.000 10.000
20.000 10.000
-----Flow or velocity boundary data:-----
FLOWTYPE = 0 I6 Type of Boundaries (0=Flow 1=Velocity )
FPHASE = 0.0500 F10.4 Time over which flow at boundary is introduced
CDWEIR = 0.6100 F10.4 weir coefficient
-----Layer Domain Specification-----
Layer1
00000000000000000000 1
00000000000000000000 2
01111111111111111110 3
01111111111111111110 4
01111111111111111110 5
07777777777777777770 6
07777777777777777770 7
07777777777777777770 8
07777777777777777770 9
07777777777777777770 10
07777777777777777770 11
07777777777777777770 12
07777777777777777770 13
07777777777777777770 14
07777777777777777770 15
07777777777777777770 16
07777777777777777770 17
07777777777777777770 18
07777777777777777770 19
07777777777777777770 20
07777777777777777770 21
07777777777777777770 22
07777777777777777770 23

```


[illegible]

257

258

2,2
1,18
1,5E-5,5E-5
106,5E-5,5E-5

Water Levels Run 4e

Used in the water level experiments

Located in D:\DIVAST-SG Laboratory Model\Water level experiments\

```

Layered Divast SG Model
-----General Data-----
IMAX      =      120      MAXIMUM NO. OF GRID POINTS IN I (OR X) DIRECTION
JMAX      =      82      MAXIMUM NO. OF GRID POINTS IN J (OR Y) DIRECTION
JSPACE    =      4      INTEGER SPACE BETWEEN PRINTOUT VALUES
NADVIT    =      2      NO. OF ITERATIONS FOR ADVECTIVE ACCELERATIONS
NDFORM    =      0      FORM OF DEPTH DATA: SIDE CENTRES = 0 & CORNERS = 1
NFLRUF    =      0      ROUGH TURBULENT FLOW ASSUMED: NO=0 & YES=1
TECTIM    =      30      interval (secs) to output tecplot data
TECOUT    =      1      Output to tecplot data file? (LARGE FILES!) no=0 & yes=1
NUMPRT    =      4      NUMBER OF PRINTOUT TIMES SPECIFIED AS DATA
NWEPRN    =      1      FLAG FOR WATER ELEVATION PRINTOUT: NO=0 & YES=1
NVEPRN    =      1      FLAG FOR VELOCITY COMPONENT PRINTOUT: NO=0 & YES=1
NDEPRN    =      1      FLAG FOR DEPTHS AT CENTRE PRINTOUT: NO=0 & YES=1
NRFPRN    =      0      FLAG FOR ROUGHNESS NO=0, CHEZY=1, MAN.=2 & DARCY=3
NEDPRN    =      0      FLAG FOR EDDY VISCOSITY PRINTOUT: NO=0 & YES=1
NRNPRN    =      0      FLAG FOR REYNOLDS NUMBER PRINTOUT: NO=0 & YES=1
NDIPRN    =      0      FLAG FOR DISPERSION-DIFF. PRINTOUT: NO=0 & YES=1
NSOPRN    =      1      FLAG FOR SOLUTE LEVEL PRINTOUT: NO=0 & YES=1
NTAPRN    =      0      FLAG FOR BED SHEAR STRESS PRINTOUT: NO=0 & YES=1
NERPRN    =      0      FLAG FOR CALCULATING & PRINTING EROSION: NO=0 & YES=1
NRDPRN    =      0      FLAG FOR RESIDUAL COMPONENTS PRINTOUT: NO=0 & YES=1
NFLWIN    =      0      FLAG FOR INCLUDING A SURFACE WIND STRESS: NO=0 & YES=1
NFLDRY    =      0      FLAG FOR INCLUDING FLOODING & DRYING: NO=0 & YES=1
NFLSOL    =      0      FLAG FOR INCLUDING SOLUTE PREDICTIONS: NO=0 & YES=1
NFLSGI    =      1      FLAG FOR INCLUDING SURFACE-GROUNDWATER INTERACTIONS: NO=0 & YES=1
-----Point Data Collection-----
NUMPNT    =      30      NUMBER OF POINTS TO RECORD DATA FROM
hole 1a   =      89      7
hole 1    =      89      17      i-coord, j-coord
hole 2    =      89      27
channel1  =      89      41
hole 3a   =      69      7
hole 3    =      69      17
hole 4    =      69      27
hole 5a   =      49      7
hole 5    =      49      17
hole 6    =      49      27
channel3  =      49      41
hole 7a   =      29      7
hole 7    =      29      17
hole 8    =      29      27
channel4  =      29      41
weir      =      119     41
hole 9    =      89      57      i-coord, j-coord
hole 10   =      89      67
hole 10a  =      89      77
hole 11   =      69      57
hole 12   =      69      67
hole 12a  =      69      77
hole 13   =      49      57
hole 13b  =      49      62
hole 14   =      49      67
hole 14a  =      49      77
hole 13n  =      39      57
hole 15   =      29      57
hole 16   =      29      67
hole 16a  =      29      77
-----Boundary Conditions-----
IENDOB    =      2      NO. OF OPEN BOUNDARY REACHES IN I DIRECTION
JENDOB    =      0      NO. OF OPEN BOUNDARY REACHES IN J DIRECTION
IOBD 1    =      2      1      2      81
IOBD 2    =      3      120     2      81
-----Model Data-----
TIMESM    =      0.40      TIME OF SIMULATION (HOURS)
HFDT      =      0.0500     HALF TIME STEP (S)
DELX      =      0.05      GRID SPACING (M)
ANGLAT    =      0.00      ANGLE OF LATITUDE OF DOMAIN IN DEGREES
RUFFMM    =      1.00      ROUGHNESS LENGTH K (MM)
VISCM      =      1.31      KINEMATIC VISCOSITY OF FLUID (MM^2/S)
REMIN     =      100.0     MINIMUM REYNOLDS NUMBER

```

```

TCHEZY = 0.01 TIME AT WHICH ROUGHNESS COEFF. IS CHANGED (HRS)
TEDDY = 0.01 TIME AT WHICH EDDY VISCOSITY IS CHANGED (HRS)
TDISP = 0.01 TIME AT WHICH DISPERSION COEFF. IS CHANGED (HRS)
ALPHA = 0.7143 SLIP BOUND COEFF NO =-1.0 FREE =1.0 PARTIAL =0.7143
BETA = 1.016 MOMENTUM CORRECTION FACTOR
COED = 0.15 EDDY VISCOSITY COEFFICIENT
GAMMA = 0.000 LONGITUDINAL DISPERSION COEFFICIENT
DELTA = 0.000 LATERAL TURBULENT DIFFUSION COEFFICIENT
ADDIS = 0.000 ADDITIONAL DISPERSION-DIFFUSION (M^2/S)
WINDIS = 0.000 WIND INDUCED DISPERSION (M^2/S)
PRESET = 0.005 MINIMUM DEPTH FOR FLOODING & DRYING (M)
ANGNOR = 0.00 CLOCKWISE ANGLE FROM NORTH TO X-DIRECTION IN DEG.
WINSPE = 0.00 WIND SPEED (M/S)
WINANG = 0.00 WIND ANGLE - CLOCKWISE FROM NORTH IN DEGREES
DENAIR = 1.25 DENSITY OF AIR (KG/M^3)
DENWAT = 1000.00 DENSITY OF WATER (KG/M^3)
WATEMP = 10.00 WATER TEMPERATURE IN DEG. CENTIGRADE
-----Outfall and solute Data-----
NUMOUT = 0 NUMBER OF OUTFALLS
NFLSAL = 0 FLAG FOR SALINITY INPUT NO=0 & YES=1
NFLTMP = 0 FLAG FOR TEMPERATURE INPUT NO=0 & YES=1
NFLTCL = 0 FLAG FOR T. COLI INPUT NO=0 & YES=1
NFLFCL = 0 FLAG FOR F. COLI INPUT NO=0 & YES=1
NFLBOD = 0 FLAG FOR B.O.D. INPUT NO=0 & YES=1
NBOD5D = 0 CONVERT ULTIMATE BOD TO 5-DAY BOD NO=0 & YES=1
NFLORG = 0 FLAG FOR ORGANIC NIT. NO=0 & YES=1
NFLAMN = 0 FLAG FOR AMMONIA NIT. NO=0 & YES=1
NFLNTA = 0 FLAG FOR NITRATE NIT. NO=0 & YES=1
NFLDOX = 0 FLAG FOR DISSOLVED OXYG. NO=0 & YES=1
NFLALG = 0 FLAG FOR ALGAL BIOMASS NO=0 & YES=1
NFLPHS = 0 FLAG FOR PHOSPHORUS NO=0 & YES=1
NFLSED = 0 FLAG FOR SEDIMENT TRANSPORT NO=0 & YES=1
NSFORM = 0 SEDIMENT FORMULA TYPE: ENG-HAN = 0 & VAN RIJN = 1
NFLCHS = 0 FLAG FOR COHESIVE SEDIMENT TRANSPORT NO=0 & YES=1
FACWAT = 1.0E+2 FACTOR FOR SCALING LEVELS PRINTOUT (<0-VARIABLE SCALING)
FACVEL = -1.E+0 FACTOR FOR SCALING VELOCITY PRINTOUT
FACDEP = 1.0E+2 FACTOR FOR SCALING WATER DEPTH PRINTOUT
FACRUF = -1.E+0 FACTOR FOR SCALING CHEZY, MANNING OR DARCY PRINTOUT
FACEDD = -1.E+0 FACTOR FOR SCALING EDDY VISCOSITY PRINTOUT
FACRNO = -1.E+0 FACTOR FOR SCALING REYNOLDS NO. PRINTOUT
FACDIS = -1.E+0 FACTOR FOR SCALING DISPERSION PRINTOUT
FACSAL = 1.0E+1 FACTOR FOR SCALING SALINITY PRINTOUT
FACTEM = -1.E+0 FACTOR FOR SCALING TEMPERATURE PRINTOUT
FACTCL = -1.E+0 FACTOR FOR SCALING TOTAL COLIFORM PRINTOUT
FACFCL = -1.E+0 FACTOR FOR SCALING FAECAL COLIFORM PRINTOUT
FACBOD = -1.E+0 FACTOR FOR SCALING BIOCHEM OXYG DEM PRINTOUT
FACORG = -1.E+0 FACTOR FOR SCALING ORGANIC NITROGEN PRINTOUT
FACAMN = -1.E+0 FACTOR FOR SCALING AMMONIA NITROGEN PRINTOUT
FACNTA = -1.E+0 FACTOR FOR SCALING NITRATE NITROGEN PRINTOUT
FACDOX = -1.E+0 FACTOR FOR SCALING DISSOLVED OXYGEN PRINTOUT
FACALG = -1.E+0 FACTOR FOR SCALING ALGAL BIOMASS PRINTOUT
FACPHS = -1.E+0 FACTOR FOR SCALING PHOSPHORUS PRINTOUT
FACSED = -1.E+0 FACTOR FOR SCALING NON-COHESIVE SEDIMENT PRINTOUT
FACCHS = -1.E+0 FACTOR FOR SCALING SUSP. COHESIVE SEDIMENT PRINTOUT
FACCHB = -1.E+0 FACTOR FOR SCALING DEPO. COHESIVE SEDIMENT PRINTOUT
FACNSD = -1.E+0 FACTOR FOR SCALING NET SEDIMENT FLUX PRINTOUT
FACSTR = -1.E+0 FACTOR FOR SCALING BED SHEAR STRESS PRINTOUT
FACRVL = -1.E+0 FACTOR FOR SCALING RESIDUAL VELOCITY PRINTOUT
FACRST = -1.E+0 FACTOR FOR SCALING RESIDUAL BED SHEAR PRINTOUT
FACRER = -1.E+0 FACTOR FOR SCALING RESIDUAL EROSION PRINTOUT
SALINT = 0.00 INITIAL SALINITY LEVELS ACROSS DOMAIN (PPT)
SAL OUTS:- 0.00 1.00 OUTFALL SALINITY LEVELS (PPT)
TMPINT = 0.00 INITIAL TEMPERATURE LEVELS ACROSS DOMAIN (DEG C)
TMP OUTS:- 0.00 OUTFALL TEMPERATURE LEVELS (DEG C)
TCLINT = 0.00 INITIAL TOTAL COL. LEVELS ACROSS DOMAIN (CTS/100ML)
TCL OUTS:- 0.00 OUTFALL TOTAL COLIFORM LEVELS (CTS/100ML)
FCLINT = 0.00 INITIAL FAECAL COL LEVELS ACROSS DOMAIN (CTS/100ML)
FCL OUTS:- 0.00 OUTFALL FAECAL COLIFORM LEVELS (CTS/100ML)
BODINT = 0.00 INITIAL BOD LEVELS ACROSS DOMAIN (MG/L)
BOD OUTS:- 0.00 OUTFALL BOD LEVELS (MG/L)
ORGINT = 0.00 INITIAL ORGANIC NIT. LEVELS ACROSS DOMAIN (MG/L)
ORG OUTS:- 0.00 OUTFALL ORGANIC NITROGEN LEVELS (MG/L)
AMNINT = 0.00 INITIAL AMMONIA NIT. LEVELS ACROSS DOMAIN (MG/L)
AMN OUTS:- 0.00 OUTFALL AMMONIA NITROGEN LEVELS (MG/L)
TRAINT = 0.00 INITIAL NITRATE NIT. LEVELS ACROSS DOMAIN (MG/L)
TRA OUTS:- 0.00 OUTFALL NITRATE NITROGEN LEVELS (MG/L)
SALFDO = 0.00 SALINITY LEVEL FOR SATURATION DO CALCULATION (PPT)
DOX OUTS:- 0.00 OUTFALL DISSOLVED OXYGEN LEVELS (MG/L)
ALGINT = 0.00 INITIAL ALGAL BIOMASS LEVELS ACROSS DOMAIN (MG/L)
ALG OUTS:- 0.00 OUTFALL ALGAL BIOMASS LEVELS (MG/L)
PS1INT = 0.00 INITIAL ORGANIC PHOS. LEVELS ACROSS DOMAIN (MG/L)
PS1 OUTS:- 0.00 OUTFALL ORGANIC PHOSPHORUS LEVELS (MG/L)
PS2INT = 0.00 INITIAL DISSOLVED PHOS. LEVELS ACROSS DOMAIN (MG/L)
PS2 OUTS:- 0.00 OUTFALL DISSOLVED PHOSPHORUS LEVELS (MG/L)
SEDINT = 0.00 INITIAL SUSPENDED SED. LEVELS ACROSS DOMAIN (MG/L)
GAMSUS = 5.00 GAMMA FOR SUSPENDED SEDIMENTS
SPGRAV = 2.65 SPECIFIC GRAVITY OF SUSPENDED SEDIMENTS

```



```

D16MMS = 0.00 SEDIMENT DIAMETER WITH 16% FINER (MM)
D50MMS = 0.00 SEDIMENT DIAMETER WITH 50% FINER (MM)
D84MMS = 0.00 SEDIMENT DIAMETER WITH 84% FINER (MM)
D90MMS = 0.00 SEDIMENT DIAMETER WITH 90% FINER (MM)
CHSINT = 0.00 INITIAL COHESIVE SUSP. SED. CONCENTRATION (KG/M^3)
CSGRAV = 2.65 SPECIFIC GRAVITY OF SUSPENDED COHESIVE SEDIMENTS
C50MMS = 0.063 AVERAGE SIZE OF COHESIVE FLOCS (MM)
COFERO = 0.0015 EMPIRICAL EROSION COEFFICIENT (KG/N/S)
CRTDEP = 0.100 CRITICAL STRESS FOR DEPOSITION (N/M^2)
CRTERO = 0.300 CRITICAL STRESS FOR RE-SUSPENSION (N/M^2)
WSFIDX = 4.0 EXPONENT INDEX FOR HINDERED SETTLING VELOCITY
WSFGAM = 1.0 COEFFICIENT FOR HINDERED SETTLING VELOCITY
CHS OUTS:- 100.1 OUTFALL COHESIVE SEDIMENT CONCENTRATIONS
SPHTEC = 0.000 SURFACE HEAT EXCHANGE COEFFICIENT (WATTS/M^2/DEG C)
SPTMCF = 4.200 SPECIFIC THERMAL CAP. OF FLUID (JOULES/M^3/DEG C)
TCLK5D = 2.400 DECAY RATE FOR T. COLI (1/DAY)
TH5TCL = 1.047 TEMPERATURE CORRECTION FOR T. COLI
FCLK5D = 2.400 DECAY RATE FOR F. COLI (1/DAY)
TH5FCL = 1.047 TEMPERATURE CORRECTION FOR F. COLI
BODK1D = 5.000 DECAY RATE FOR BOD VIA DEOXYGENATION (1/DAY)
TH1BOD = 1.000 TEMPERATURE CORRECTION FOR BOD VIA DEOXYGENATION
BODK3D = 0.000 DECAY RATE FOR BOD VIA SETTLING LOSS (1/DAY)
TH3BOD = 1.000 TEMPERATURE CORRECTION FOR BOD VIA SETTLING LOSS
ORGB3D = 0.400 DECAY RATE FOR ORG NIT TO CONVERT TO NH3 (1/DAY)
TH3ORG = 1.047 TEMPERATURE CORRECTION FOR ORG NIT VIA CONVERSION
ORGS4D = 0.100 DECAY RATE FOR ORG NIT VIA SETTLING (1/DAY)
TH4ORG = 1.024 TEMPERATURE CORRECTION FOR ORG. NIT. VIA SETTLING
AMNB1D = 1.000 DECAY RATE FOR BIOL. OXIDATION OF NH3 (1/DAY)
TH1AMN = 1.083 TEMPERATURE CORRECTION FOR BIOL. OXIDATION OF NH3
TH2DOX = 1.024 TEMPERATURE CORRECTION FOR REAERATION RATE
DOXK4D = 5.000 SEDIMENT OXYGEN DEMAND RATE (MG/M^2 PER DAY)
TH4DOX = 1.060 TEMPERATURE CORRECTION FOR SEDIMENT OXYGEN DEMAND
DOXA5C = 3.500 RATE OF OXYGEN UPTAKE PER UNIT OF AMMONIA NITROGEN
DOFMMH = 5.000 DO EXCHANGE COEFF. FOR STAGNANT WATER (MM/HOUR)
DOLMT2 = 2.000 HALF-SATURATION DO LIMITING CONSTANT (MG/L)
DOXA3C = 0.133 DO PRODUCTION / UNIT OF CHLOROPHYLL (MG-DO/MG-CHLA)
DOXA4C = 0.100 DO UPTAKE / UNIT OF CHLOROPHYLL (MG-DO/MG-CHLA)
ALGMAX = 2.000 MAX. ALGAE GROWTH RATE AT REFERENCE TEMP. (1/DAY)
THMALG = 1.047 TEMPERATURE CORRECTION FOR MAX. ALGAE GROWTH RATE
ALGRSP = 0.060 RATE OF RESPIRATION PLUS EXCRETION (1/DAY)
THARSP = 1.047 TEMPERATURE CORRECTION FOR RESPIRATION & EXCRETION
VELALG = 0.050 ALGAE (CHLOROPHYLL) SETTLING VELOCITY (M/DAY)
ALGNPM = 0.010 NON-PREDATORY MORTALITY RATE FOR ALGAE (1/DAY)
ALGLGZ = 0.020 RATE OF ALGAL LOSSES DUE TO GRAZING (1/DAY)
FPHOTP = 0.500 PHOTOPERIOD (EXPRESSED AS FRACTION OF THE DAY)
EXTLT0 = 0.090 LIGHT EXT COEF FOR ALL ABSORPT COMPS BUT PHYT (1/M)
EXTLT1 = 0.0088 LIGHT EXT COEF FOR PHYTOPLANKTON (1/M)
EXTLT2 = 0.054 LIGHT EXT COEF FOR PHYTOPLANKTON (1/M)
EXTLT3 = 0.667 LIGHT EXT COEF FOR PHYTOPLANKTON (1/M)
SURFLT = 250.1 LIGHT INTENSITY AT WATER SURFACE
HFSATL = 6.0 LIGHT LEVEL AT WHICH GROWTH IS HALF OF MAX. RATE
HFSATN = 0.060 HALF-SATURATION CONSTANT FOR NITROGEN (MG/L)
HFSATP = 0.010 HALF-SATURATION CONSTANT FOR PHOSPHORUS (MG/L)
ALGA1C = 7.000 NIT. FRACTION OF ALGAL CHLOROPHYLL (MG-N/MG-CHLA)
FRCORG = 0.100 FRACTION OF DEAD & RESPIRED PHYTOPLANKTON RECYCLED
FRCPHS = 0.100 FRACTION OF DEAD & RESPIRED PHYTOPLANKTON RECYCLED
PHSA2C = 1.000 PHOS FRACTION OF ALGAL CHLOROPHYLL (MG-P/MG-CHLA)
PHSB4D = 0.085 HYDROLYSIS RATE FOR ORG. PH TO INORG. PH (1/DAY)
THPSB4 = 1.047 TEMPERATURE CORRECTION FOR ORG. P TO INORG. P
PHSS5D = 0.010 SETTLING RATE CONST OF ORGANIC PHOSPHORUS (1/DAY)
THPSS5 = 1.047 TEMPERATURE CORRECTION FOR ORG. P SETTLING RATE
PHSF2D = 0.010 SETTLING RATE CONST OF INORG. PHOSPHORUS (1/DAY)
THPSF2 = 1.047 TEMPERATURE CORRECTION FOR INORG. P SETTLING RATE
NFLDOF = 1 0 (FT UNIT); 1 (OWENS RELATION); 2 (BANKS FOR LAKE)
0.00000 0.05000 0.25000 0.50000 (PRINTOUT TIMES)
-----Tidal boundary (water elevation) data-----
SINTIDE = 0 I6 Sinusoidal tide, 1= yes, 0= no
TIDEAMP = 0.0700 F10.4 Tidal Amplitude (only used if SINTIDE=1)
TIDEMWL = 0.2000 F10.4 Tidal Mean Water Level (only used if SINTIDE=1)
TIDEHR = 10.0000 F10.4 Tidal period (wavelength for sinusoidal tide, length of cycle
to repeat for non-sinusoidal tide) (hours)
TIDESTART=HIGH A4 Start sinusoidal tidal cycle at: high tide (HIGH), Rising
Mean Water Level (MWL+), Falling Mean Water Level (MWL-) or low tide (LOW)
PRETIDE = 0.0000 F10.4 Time before tidal boundary cycle is started. (hours)
NOPTS = 3 I6 Number of points specified for non-sinusoidal tide
NUMTDS = 10.0000 F10.4 Number of tidal cycles
time elevation (non-sinusoidal tide points on NOPTS lines below here F6.3 F8.3)
0.000 +0.070
0.050 +0.227
10.000 +0.227
time elevation (non-sinusoidal tide points on NOPTS lines below here F6.3 F8.3)
0.000 +0.070
0.050 +0.070
10.000 +0.070
-----Flow or velocity boundary data-----
FLOWTYPE = 0 I6 Type of Boundaries (0=Flow 1=Velocity)
FPHASE = 0.0500 F10.4 Time over which flow at boundary is introduced

```

```

0.0500    5.000    0.0500
-----Layer Domain Specifcation-----

```

- 1
- 2
- 3
- 4
- 5
- 6
- 7
- 8
- 9
- 10
- 11
- 12
- 13
- 14
- 15
- 16
- 17
- 18
- 19
- 20
- 21
- 22
- 23
- 24
- 25
- 26
- 27
- 28
- 29
- 30
- 31
- 32
- 33
- 34
- 35
- 36
- 37
- 38
- 39
- 40
- 41
- 42
- 43
- 44
- 45
- 46
- 47
- 48
- 49
- 50
- 51
- 52
- 53
- 54
- 55
- 56
- 57
- 58
- 59
- 60
- 61
- 62
- 63
- 64
- 65
- 66
- 67
- 68
- 69
- 70
- 71
- 72
- 73
- 74
- 75
- 76
- 77
- 78
- 79
- 80
- 81

263

APPENDIX B DETAILED DISCRETISATIONS

i) x - direction

$$\frac{\partial p}{\partial t} + \frac{\partial \beta p U}{\partial x} + \frac{\partial \beta p V}{\partial y} + gb \frac{\partial \xi}{\partial x} + \frac{gp\sqrt{p^2 + q^2}}{C^2 b^2} - \varepsilon \left[2 \frac{\partial^2 p}{\partial x^2} + \frac{\partial^2 p}{\partial y^2} + \frac{\partial^2 q}{\partial x \partial y} \right] - \Omega q - fW_x + \frac{b}{\rho} \frac{\partial}{\partial x} (p_a) = 0$$

ii) y - direction

$$\frac{\partial q}{\partial t} + \frac{\partial \beta q U}{\partial x} + \frac{\partial \beta q V}{\partial y} + gb \frac{\partial \xi}{\partial y} + \frac{gq\sqrt{p^2 + q^2}}{C^2 b^2} - \varepsilon \left[\frac{\partial^2 q}{\partial x^2} + 2 \frac{\partial^2 q}{\partial y^2} + \frac{\partial^2 p}{\partial x \partial y} \right] - \Omega p - fW_y + \frac{b}{\rho} \frac{\partial}{\partial y} (p_a) = 0$$

Taking the terms in sequence, and using the x-direction for the full expansion, the above equations can be discretised in time and space. X-direction discretisations are centred around $i+1/2, j$ and $n+1/2$. Y-direction discretisations are centred around $i, j+1/2$ and $n+1$.

Term 1

Equation 10.1: - Term 1 x-direction

$$\frac{\partial p}{\partial t} = \left(\frac{\mathbf{p}_{i+1/2,j}^{n+1} - p_{i+1/2,j}^n}{\Delta t} \right)$$

Equation 10.2: - Term 1 y-direction

$$\frac{\partial q}{\partial t} = \left(\frac{\mathbf{q}_{i,j+1/2}^{n+3/2} - q_{i,j+1/2}^{n+1/2}}{\Delta t} \right)$$

Term 2

Centred about $i+1/2, j$

Equation 10.3: - Term 2 x-direction

$$\begin{aligned} \frac{\partial \beta p U}{\partial x} &= \beta \left[\frac{\partial p U}{\partial x} \right] = \beta \left[\frac{(pU)_{i+1,j}^n - (pU)_{i,j}^n}{\Delta x} \right] \\ &= \beta \left[\frac{\frac{(p_{i+3/2}^n + p_{i+1/2}^n)}{2} \cdot \frac{(U_{i+3/2}^n + U_{i+1/2}^n)}{2} - \frac{(p_{i+1/2}^n + p_{i-1/2}^n)}{2} \cdot \frac{(U_{i+1/2}^n + U_{i-1/2}^n)}{2}}{\Delta x} \right] \\ &= \frac{\beta}{4\Delta x} \left[(p_{i+3/2}^n + p_{i+1/2}^n)(U_{i+3/2}^n + U_{i+1/2}^n) - (p_{i+1/2}^n + p_{i-1/2}^n)(U_{i+1/2}^n + U_{i-1/2}^n) \right] \end{aligned}$$

Equation 10.4: - Term 2 y-direction

$$\begin{aligned}
\frac{\partial \beta q U}{\partial x} &= \beta \left[\frac{\partial q U}{\partial x} \right] = \beta \left[\frac{(qU)_{i+1,j}^{n+1} - (qU)_{i,j}^{n+1}}{\Delta x} \right] \\
&= \beta \left[\frac{q_{i+1}^{n+1} \cdot \frac{(U_{i+3/2}^{n+1} + U_{i+1/2}^{n+1})}{2} - q_i^n \cdot \frac{(U_{i+1/2}^n + U_{i-1/2}^n)}{2}}{\Delta x} \right] \\
&= \frac{\beta}{2\Delta x} \left[q_{i+1}^n \cdot (U_{i+3/2}^n + U_{i+1/2}^n) - q_i^n \cdot (U_{i+1/2}^n + U_{i-1/2}^n) \right]
\end{aligned}$$

Term 3**Equation 10.5: - Term 3 x-direction**

$$\begin{aligned}
\frac{\partial \beta p V}{\partial y} &= \frac{\partial \beta U h V}{\partial y} = \frac{\partial \beta q U}{\partial y} \\
&= \beta \left[\frac{\partial q U}{\partial y} \right] = \beta \left[\frac{(qU)_{i+1/2,j+1/2}^n - (qU)_{i+1/2,j-1/2}^n}{\Delta y} \right] \\
&= \beta \left[\frac{\frac{(q_{i+1,j+1/2}^{n+1/2} + q_{i,j+1/2}^{n+1/2})}{2} \cdot U_{i+1/2,j}^n - \frac{(q_{i+1,j-1/2}^{n+1/2} + q_{i,j-1/2}^{n+1/2})}{2} \cdot U_{i+1/2,j}^n}{\Delta y} \right] \\
&= \frac{\beta}{2\Delta y} \left[(q_{i+1,j+1/2}^{n+1/2} + q_{i,j+1/2}^{n+1/2}) U_{i+1/2,j}^n - (q_{i+1,j-1/2}^{n+1/2} + q_{i,j-1/2}^{n+1/2}) U_{i+1/2,j}^n \right]
\end{aligned}$$

Equation 10.6: - Term 3 y-direction

$$\begin{aligned}
\frac{\partial \beta q V}{\partial y} &= \frac{\partial \beta U h V}{\partial y} = \frac{\partial \beta q U}{\partial y} \\
&= \beta \left[\frac{\partial q U}{\partial y} \right] = \beta \left[\frac{(qU)_{i+1/2,j+1/2}^n - (qU)_{i+1/2,j-1/2}^n}{\Delta y} \right] \\
&= \beta \left[\frac{\frac{(q_{i+1,j+1/2}^{n+1/2} + q_{i,j+1/2}^{n+1/2})}{2} \cdot U_{i+1/2,j}^n - \frac{(q_{i+1,j-1/2}^{n+1/2} + q_{i,j-1/2}^{n+1/2})}{2} \cdot U_{i+1/2,j}^n}{\Delta y} \right] \\
&= \frac{\beta}{2\Delta y} \left[(q_{i+1,j+1/2}^{n+1/2} + q_{i,j+1/2}^{n+1/2}) U_{i+1/2,j}^n - (q_{i+1,j-1/2}^{n+1/2} + q_{i,j-1/2}^{n+1/2}) U_{i+1/2,j}^n \right]
\end{aligned}$$

Centred about $i,j+1/2$

Eddy Viscosity Term

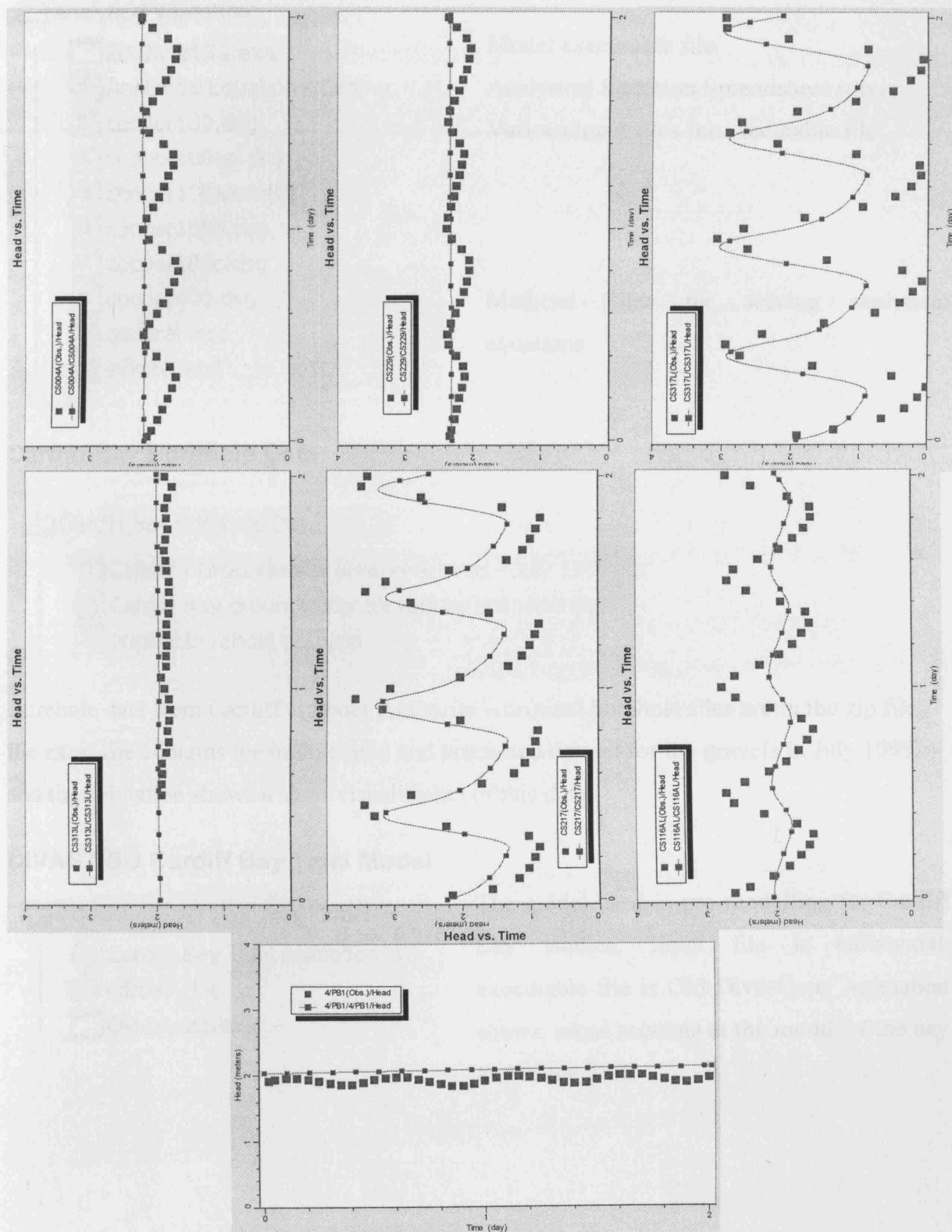
Centred around $i+1/2, j$

Equation 10.7: - Eddy Viscosity term

$$\begin{aligned}
 & \varepsilon \left[2 \frac{\partial^2 p}{\partial x^2} + \frac{\partial^2 p}{\partial y^2} + \frac{\partial^2 q}{\partial x \partial y} \right] \\
 &= \varepsilon \left[2 \frac{\partial^2 bU}{\partial x^2} + \frac{\partial^2 bU}{\partial y^2} + \frac{\partial^2 bV}{\partial x \partial y} \right] \\
 &= \varepsilon \left[\begin{aligned} & 2 \frac{b_{i+1/2,j} \left(\frac{U_{i+3/2} - U_{i+1/2}}{\Delta x} - \frac{U_{i+1/2} - U_{i-1/2}}{\Delta x} \right)}{\Delta x} + \\ & \frac{b_{i+1/2,j} \left(\frac{U_{i+1/2,j+1} - U_{i+1/2,j}}{\Delta y} - \frac{U_{i+1/2,j} - U_{i+1/2,j-1}}{\Delta y} \right)}{\Delta y} + \\ & \frac{b_{i+1/2,j} \left(\frac{V_{i+1,j+1/2} - V_{i+1,j-1/2}}{\Delta y} - \frac{V_{i,j+1/2} - V_{i,j-1/2}}{\Delta y} \right)}{\Delta x} \end{aligned} \right] \\
 &= \frac{\varepsilon b_{i+1/2,j}}{\Delta x^2} \left(2(U_{i+3/2,j} + U_{i-1/2,j}) - 6U_{i+1/2,j} + U_{i+1/2,j+1} + U_{i+1/2,j-1} + V_{i+1,j+1/2} - V_{i+1,j-1/2} - V_{i,j+1/2} + V_{i,j-1/2} \right)
 \end{aligned}$$

APPENDIX C INDIVIDUAL BOREHOLE PLOTS

Conductivity of 5×10^{-3} m/s






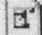
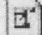
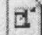




APPENDIX D APPENDIX CD

This appendix outlines the files available on the Appendix CD

Analytical Validation

Analytical Validation

-  2D Divast5G.exe
-  Analytical Equation - Cooper - ...
-  cooper100.dsg
-  cooper100aa.dsg
-  cooper100aaa.dsg
-  cooper100b.dsg
-  cooper100c.dsg
-  cooper400.dsg
-  general.mcd
-  infinite.mcd

Model executable file

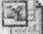


Analytical Equation Spreadsheet solver

Various input files for executable file

Mathcad Files for solving analytical equations

Cardiff Bay Borehole Data




Cardiff Bay Borehole Data

-  Cardiff - Groundwater level in Gravels - July 1999.xls
-  Cardiff Bay groundwater elevations animation.avi
-  original borehole data.zip

Borehole data from Cardiff Harbour Authority – original borehole files are in the zip file, the excel file contains the interpolated and processed dataset for the gravels in July 1999, and the animation shows a short visualisation of this data.

DIVAST-SG Cardiff Bay Tidal Model

DIVAST Cardiff Bay Tidal Model

-  Cardiff Bay Tidal Animation.avi
-  cdfbay.dat
-  Old Divast.exe




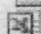
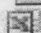




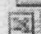

The model used in pre-modelling for Cardiff Bay studies. Input file is cdfbay.dat, executable file is Old Divast.exe. Animation shows cross sections at the mouth of the bay and in the Taff.

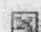







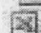
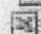

DIVAST-SG Cardiff Bay Model




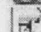


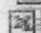
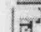

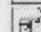

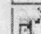
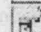
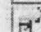
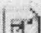
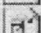

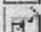
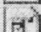
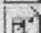

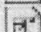

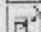
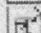
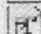
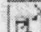
This section of the CD contains the DIVAST-SG model of Cardiff Bay. The executable file is Cardiff Bay DSG.exe. All the input files used in the study are included as *.dsg files – these are set-up to use the hotstart data saved as gtown500.hst (Grangetown is the geographical area under study, and the hotstart data was created after 500 hours). The models can be run again if desired, but the point data from the runs is also stored in the 'Data from Model Runs' folder. An animation of the model running is included as Cardiff Bay Optimal Animation.avi

DIVAST-SG Cardiff Bay Model

Data from Model Runs

-  taff01por10 point data.xls
-  taff01por20 point data.xls
-  taff01por30 point data.xls
-  taff01por40 point data.xls
-  taff02por10 point data.xls
-  taff02por20 point data.xls
-  taff02por30 point data.xls
-  taff02por40 point data.xls
-  taff004por10 point data.xls
-  taff004por20 point data.xls
-  taff004por30 point data.xls



-  taff004por40 point data.xls
-  taff005por10 point data.xls
-  taff005por20 point data.xls
-  taff005por30 point data2.xls
-  taff0005por30 point data.xls
-  taff005por30 point data.xls
-  taff005por40 point data.xls
-  taff0025por10 point data.xls
-  taff0025por20 point data.xls
-  taff0025por30 point data.xls
-  taff0025por40 point data.xls





-  528hrs.jpg
-  Cardiff Bay DSG.exe
-  Cardiff Bay Optimal Animation...
-  gtown500.dsg
-  gtown500.hst
-  macros.xls
-  rankings.xls
-  taff01por10.dsg
-  taff01por20.dsg
-  taff01por30.dsg
-  taff01por40.dsg
-  taff02por10.dsg
-  taff02por20.dsg
-  taff02por30.dsg
-  taff02por40.dsg
-  taff004por10.dsg
-  taff004por20.dsg
-  taff004por30.dsg
-  taff004por40.dsg
-  taff005por10.dsg
-  taff005por20.dsg
-  taff005por30.dsg
-  taff005por40.dsg
-  taff0025por10.dsg
-  taff0025por20.dsg
-  taff0025por30.dsg
-  taff0025por40.dsg

DIVAST-SG General Model and Input files

DIVAST-SG General Model and Input Files

Source Code

 divastsg.cmn
 DSG_Layer.for

 3D DivastSG 2D output.exe
 bar.dsg
 bar_nogw.dsg
 permeability grid sheet.xls

This section contains the general model for use in other studies. The source code is included as a fortran fixed format file along with a common file .cmn – this can be recompiled if desired with any Fortran compiler.

The executable file is called ‘3D DivastSG 2D output.exe’ meaning it is



















the full 3-D layered code but with only 2-D visualisation of model results (tecplot format).

The input files are those referred to in Chapter 5, ‘bar.dsg’ is the simple scenario discussed – and bar_nogw.dsg is an identical scenario but with the groundwater code portion switched off – essentially reverting the model to the old version of DIVAST.

‘permeability grid sheet.xls’ is a spreadsheet useful for creating the permeability and porosity matrix used in the input files to define the permeability and porosity in the domain.

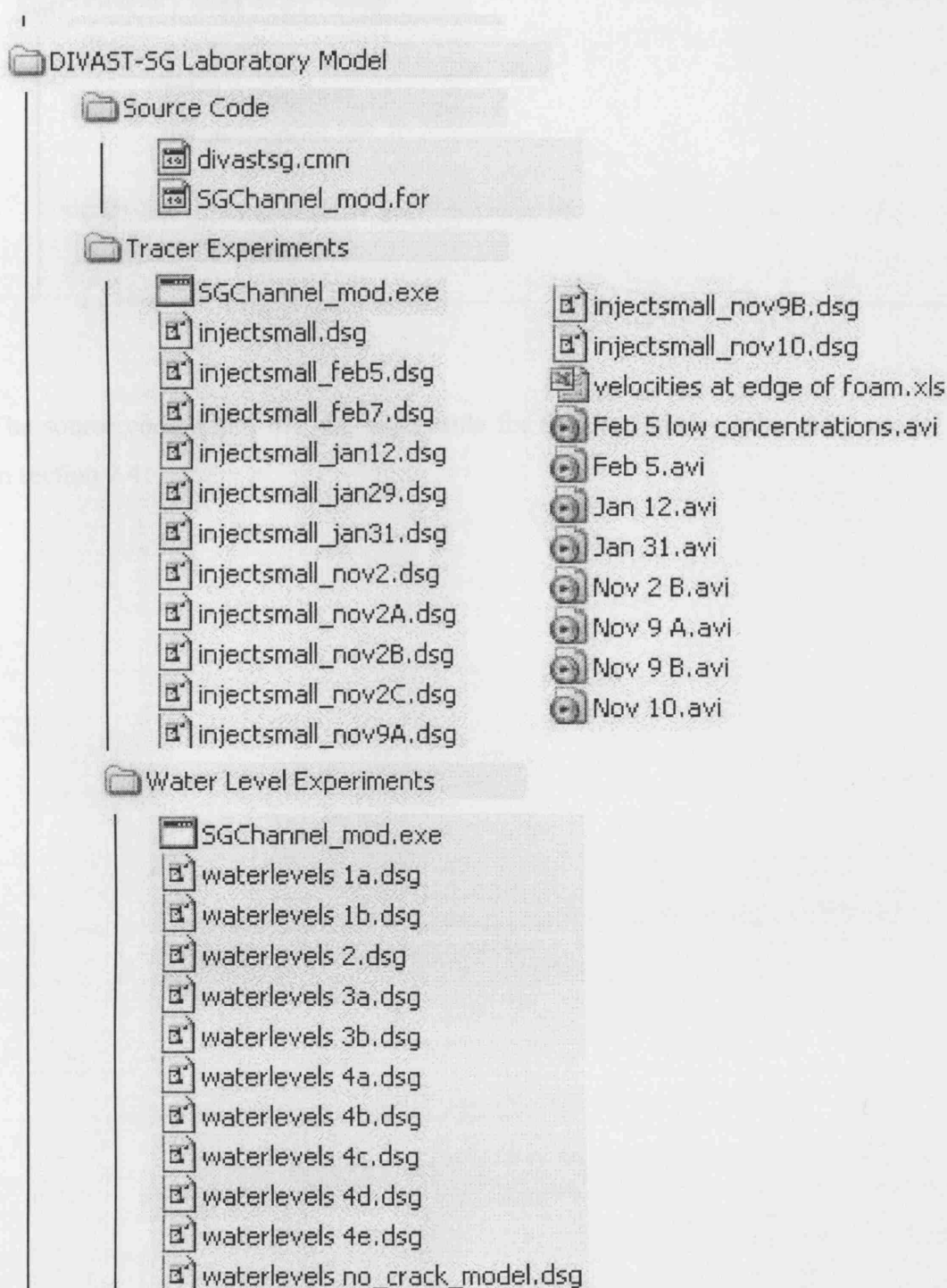
Laboratory Data

Laboratory Data

 feb 5 fluorometer 1.PRN	 jan31 log.txt
 feb 5 fluorometer 2.PRN	 jan 12 fluorometer 2.PRN
 feb 7 fluormeter 1.PRN	 jan 12 log.txt
 feb 7 fluorometer 2.PRN	 Nov 9 A log.txt
 feb 7 log.txt	 Nov 9 A.PRN
 jan29 fluorometer 1.PRN	 Nov 9 B log.txt
 jan29 fluorometer 2.PRN	 Nov 9 B.PRN
 jan29 log.txt	 Nov 10 log.txt
 jan31 fluorometer 2.PRN	 Tracer Experiments compiled.xls

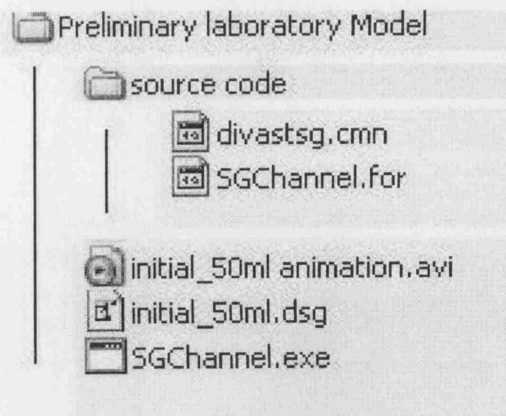
Fluorometer Data collected from the laboratory experiments is stored here, together with log files containing other details of each experiment. The data from the water level measurements is also stored here as ‘Water Level.xls’.

DIVAST-SG Laboratory Model



Input files for the tracer model runs and the water level model runs, along with several animations of tracer movement. Also, the source code for the channel model.

Preliminary Laboratory Model



The source code, input file and executable for the preliminary laboratory model discussed in section 7.4.

